OXIDATIVE METABOLISM OF EXOCYCLIC DNA ADDUCTS

By

Charles Gerhard Francesco Knutson

Dissertation

Submitted to the Faculty of the

Graduate School of Vanderbilt University

in partial fulfillment of the requirements

for the degree of

DOCTOR OF PHILOSOPHY

in

Biochemistry

May, 2008

Nashville, Tennessee

Approved:

Professor Lawrence J. Marnett

Professor F. Peter Guengerich

Professor David Cortez

Professor Jason D. Morrow

Professor Carmelo J. Rizzo

In memory of my grandfather, Dr. Leonard Joseph Michienzi, MD, PhD, MPH, who impressed upon me the value of education.

ACKNOWLEDGEMENTS

"Classes keep you in graduate school. Research gets you out," is but one of the many timeless tidbits of advice my advisor, Lawrence J. Marnett, passed along during my dissertation research. Of course, I am also grateful for his influence on the some of the finer points of my education, especially: introducing me to the wonderment of *live* World Wrestling Entertainment and Professional Bull Riding. More importantly, Larry's attention to detail, demand for excellence, persistent work ethic, and inquisitive mind projected an environment within his laboratory that helped bring out the best in my research. His procurement of our daily coffee was also much appreciated.

The committee advising my doctoral research was exceptional and their genuine interest in science was very encouraging. I am quite pleased to say that I have collaborated, in one way or another (on various projects), with each of my committee member's laboratories—a true testament to their collegial and supportive character. Therefore, I salute Fred P. Guengerich, Jason D. Morrow, Carmelo J. Rizzo and Dave Cortez for their leadership and guidance.

I am indebted to those who have directly contributed to specific areas of this dissertation. In particular, the contributions of three rotation students have found their way into several chapters. Dapo Akingbade keenly investigated several *in vitro* aspects of M_1G turnover and inhibition, in addition to some work with M_1dG and other structural analogs. Emily Rubinson characterized the products and kinetics of 1,N^2-ε-dG metabolism. Carly Anderson characterized the principal metabolite of heptanone-1,N^2-ε-Gua metabolism, and evaluated the turnover of other etheno adducts. Every

heteronuclear NMR spectrum (and several carbon and two-dimensional spectra) was obtained with the guiding-hand of Donald F. Stec, whose expertise enabled the collection of valuable structural information. Dave Hachey, Wade Calcutt and Dawn Overstreet, in one way or another, have assisted with training and/or the philosophical design of mass spectrometry experiments and analysis. By the same token, Phil Kingsley was a valuable resource within the laboratory to advise on the implementation and use of analytical instrumentation. Andy Vila provided training in the area of protein purification, and in exchange I provided the beer. Brenda Crews assisted with each animal experiment and helped teach me that animals are people too--or something like that. Andrew Felts was a valuable consultant during my remedial attempts at chemical synthesis. Several chemists within the Rizzo Laboratory provided purified reagents and substrates for use in chemical and enzymatic reactions. Thus, I am grateful to Hao Wang, Katya Petrova, and Ivan Kozekov for their contributions. Finally, I am indebted to three prior Marnett Laboratory members, who I have never met, that laid the foundations for my dissertation work: Michael Otteneder, J. Scott Daniels, and Muhammed Hashim.

Personnel within the Marnett Laboratory were generally of cheerful disposition and helped make each day a new adventure. Members of our DNA Damage group (Carol Rouzer, M. D. Kalam, Jozsef Szekely, Jennifer Stafford, and Leena Maddukuri) were particularly engaging. Melisssa Turman and Mary Konkle were students who also joined Larry's laboratory in the spring of 2004, and I am grateful for their friendship and enthusiasm for science over the years. Many others within the laboratory (past and present) have been influential including, but not limited to: Jeff Prusikiewicz, James West, Aaron Jacobs, and Robyn Richie.

Many involved in administration were there to ensure the vast majority of my time was spent in the laboratory and not fretting over employment/registration details. In particular I am grateful to Celeste Riley, Marlene Jayne, Anne Lara, Mary Veazey, Kakie Mashburn, Kathy Trisler, and Ellen Rochelle. Thank you for watching out for me, and thank you for assisting with all things administrative.

I am very fortunate to have a loving and supportive family; it starts at the top with my Grandparents. Margaret Knutson is a quite remarkable woman, who is inspiring, passionate, and sharp-minded. Leonard Michienzi, who passed away during the drafting of this manuscript, and his wife Shirley have been an inspiration to me. My parents, Mary Jo and Gerhard Knutson, are terrific role models and unwavering in their support. My brothers Eric, Andy, Ted, and Matt (and their families) throughout my existence have challenged me to do my very best—sometimes by brute force. Jim and Kate Vanden Eynden, my father- and mother-in-law, have been very welcoming and caring. I am also very grateful for my lovely wife, Sarah, who brings joy to my life and is a constant reminder to me of all that is good.

TABLE OF CONTENTS

LIST OF TABLES

LIST OF FIGURES

LIST OF ABBREVIATIONS

A	adenine
AMS	accelerator mass spectrometry
arg	arginine
B[*a*]P	benzo[*a*]pyrene
C	cytidine
^{14}C	carbon 14
Ci	curie
COSY	correlated spectroscopy
CO_2	carbon dioxide
CYP	cytochrome P450
dA	2′-deoxyadenosine
dC	2′-deoxycytidine
dG	2′-deoxyguanosine
DMF	dimethylformamide
DMSO	dimethylsulfoxide
dpm	disintegrations per minute
dT	2′-deoxythymidine
2,6-dioxo-M_1G	pyrimido[1,2-α]purin-2,6,10(3*H*)-trione
ERCC1	excision repair cross complimentary group 1
ESI	electrospray ionization
G	Guanine

GC-ECNCI	gas chromatography electron capture negative chemical ionization
H_2O_2	hydrogen peroxide
HMBC	heteronuclear multiple bond correlation
HPLC	high performance liquid chromatography
HPODE	hydroperoxyoctadecadienoic acid
HSQC	heteronuclear singe quantum coherence
iv	intravenous
LC	liquid chromatography
lys	lysine
M_1dG	3-(2-deoxy-β-D-*erythro*-pentofuranosyl)pyrimido[1,2-α]purin-10(3*H*)-one
M_1G	pyrimido[1,2-α]purin-10(3*H*)-one
MDA	malondialdehyde
MS	mass spectrometry
m/z	mass-to-charge
NER	nucleotide excision repair
$O_2^{\bullet-}$	superoxide anion
$^{\bullet}OH$	hydroxyl radical
γ-OH-PdG	1,N^2-8-OH-propanodeoxyguanosine
α-OH-PdG	1,N^2-6-OH-propanodeoxyguanosine
$ONOO^-$	peroxynitrite
ONOOH	peroxynitrous acid
8-oxo-dG	8-oxo-7,8-dihydrodeoxyguanosine

8-oxo-Gua	8-oxo-7,8-dihydroguanine
6-oxo-M_1dG	3-(2-deoxy-β-D-*erythro*-pentofuranosyl)pyrimido[1,2-α]purin-6,10(3*H*)-dione
6-oxo-M_1G	pyrimido[1,2-α]purin-6,10(3*H*)-dione
PFB-Br	pentafluorphenylbromine
PMSF	phenylmethanesulfonyl fluoride
PNP	purine nucleoside phosphorylase
PUFA	polyunsaturated fatty acid
ROS	reactive oxygen species
SPE	solid phase extraction
T	Thymine
*t*BDMS	*N*-methyl-*N*-*tert*-butyldimethylsilyl trifluoroacetamide
TFIIH	transcription factor IIH
XD	xanthine dehydrogenase
XO	xanthine oxidase
XOR	xanthine oxidoreductase
XP	xeroderma pigmentosum

CHAPTER I

INTRODUCTION

Exposure and Toxicity

Physicians and scientists have described the association between chemical exposure and toxicity in human populations for several hundred years. The Swiss physician, alchemist, and philosopher, Paracelsus, stated in the 1600s that, "all things are poison and nothing is without poison, only the dose permits something not to be poisonous" (*1*). Poisons of the 17th century are, in general, the toxic chemical and biological agents of today's generation. Even the enigmatic Paracelsus could not have imagined just how intensely the dose-response relationship of chemical agents would be investigated in today's field of chemical toxicology.

Correlations between exposure and cancer incidence were first observed in the 18th century. An English physician, John Hill, reported in his 1761 essay on the *Cautions against the immoderate use of snuff* an increased incidence of nasal cancer among individuals who partook in tobacco snuff (*2*). Hill stated, "If only five in a hundred ruined their constitutions by it [snuff], who shall be able to say, when he enters on the custom, whether he shall be one of the ninety-five who escape, or of the five that perish?" Another English physician, Percivall Pott, reported an increase incidence of scrotal cancer among chimney sweeps in the late 1700s. Young boys were typically recruited as chimney sweeps because their slender bodies enabled easier passage through the narrow chimneys. Children engaged in this labor without clothing to prevent them from getting

caught-up in the chimney. Naturally, the lack of clothing led to excessive contact with soot from the chimney. Baths were not taken regularly. Pott noted in his essay *Cancer Scroti* in 1775 that, "The disease in these people, seems to derive its origin from a lodgement of soot in the rugae of the scrotum" (*3*).

The mechanisms by which the complex mixtures of tobacco and soot elicited their toxic effects were eventually elucidated by investigators in the twentieth century. Exogenous compounds were found to be metabolically activated to reactive electrophiles that were capable of reacting with proteins and nucleic acids. Bioactivation became a common theme in the newly emerging field of chemical carcinogenesis (*4, 5*). Additionally, Avery's discovery of DNA as the inheritable, genetic material (*6*), and the description of its structure by Watson and Crick greatly advanced the field of cancer research (*7, 8*).

The polyaromatic hydrocarbon (PAH) benzo[*a*]pyrene (B[*a*]P), a component of soot and tobacco smoke) and other structurally related PAHs were the focus of research for many laboratories. Monooxygenase systems such as the cytochrome P450 (CYP) enzymes were found to play a key role in the metabolism of environmental compounds like the PAHs. Several metabolites of B[*a*]P were characterized. Of particular interest were the multiple epoxidation reactions of B[*a*]P resulting in the product 7,8-diol-9,10-epoxy-B[*a*]P, which was determined to be an ultimate carcinogen of B[*a*]P metabolism (**Figure 1**). The 7,8-diol-9,10-epoxy-B[*a*]P proved to be a potent electrophile and was found to react with DNA (principally, deoxyguanosine residues (dG)) to generate DNA adducts (*9*).

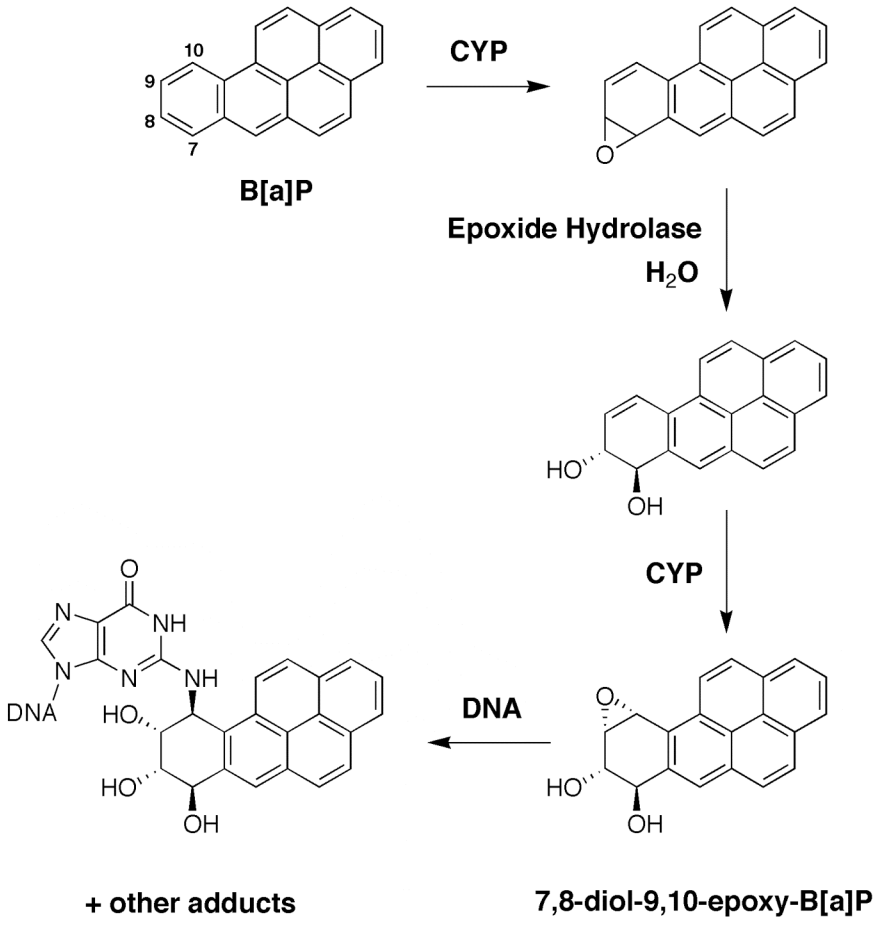

Figure 1. Metabolic activation of B[*a*]P to 7,8-diol-9,10-epoxy-B[*a*]P and its reaction with dG residues in DNA.

The concept that strong electrophiles were capable of modifying cellular macromolecules was an important advancement, and strengthened the association between environmental exposure and the onset of toxicity in human populations. When metabolic activation of exogenous chemicals led to modification of DNA, a vital link to cancer development was forged. However, it became increasingly apparent that exogenous carcinogens were not the only chemicals capable of modifying DNA. DNA

was found to undergo spontaneous depurination and deamination reactions, which produced abasic sites and mispairing in DNA (*10*). Additionally, work from the Ames Laboratory demonstrated the presence of oxidized bases, and correlated their occurrence with age and metabolic rates (*11, 12*). Later Randerath *et al.* demonstrated the presence of modifications on DNA from unknown sources (*13-16*). These observations suggested that an uncharacterized population of chemical agents was contributing to DNA damage in human populations. As a result, the field of chemical carcinogenesis shifted its focus, in part, to the production of reactive electrophiles and nucleophiles by cells and tissues within the body. These factors were described as endogenously produced chemical and biological agents, and were found in abundance during the inflammatory response.

Inflammation and cancer

In 1863 Rudolf Virchow hypothesized that inflammatory cells (leukocytes) were responsible for cancer development due to their ability to induce the proliferation of neighboring cells (*17, 18*). To date the strongest association between inflammation and carcinogenesis is seen with ulcerative colitis and the onset of colon cancer (*18*). In 1925 Burril B. Crohn detailed that inflammation recurrence in ulcerative colitis impacted nearly the entire digestive tract from anus to ceacum, and these effects were not due to a microorganism. He noted the most aggressive forms of ulcerative colitis were highly correlated with an outcome of malignancy (*19*). Decades of research have connected carcinoma development in ulcerative colitis to two main factors: the age of the individual when ulcerative colitis begins and the length of time the disease persists (*20, 21*). Other diseases of chronic inflammation have also revealed an increased incidence of cancer

development such as hepatitis C viral infection leading to hepatocellular carcinoma (*22*), and *Helicobacter pylori* infection leading to gastric cancer (*23*).

Reactive oxygen species

A uniting aspect of the chronic inflammatory response is the steady and persistent recruitment of activated macrophages to the site of inflammation. The presence and activity of these immune cells results in a constant barrage of chemical agents designed to eliminate pathogens. However, the non-specific release and reaction of these chemicals exposes host tissue to the same barrage of chemical damage **(Figure 2)**. Immune cells release large amounts of reactive oxygen species (ROS) in the form of superoxide anion ($O_2^{\bullet-}$), which dismutates to form H_2O_2. A more powerful oxidant, hydroxyl radical ($^{\bullet}OH$), can be produced in Fenton reactions from H_2O_2 in the presence of ferrous iron (Fe^{2+}) or other transition metals. Considered the most powerful endogenously produced oxidant, $^{\bullet}OH$ is extremely reactive and diffuses less than 5 molecular diameters before reacting (*24*).

Nitric oxide ($NO^{\bullet}$), an important signaling molecule, is released from activated macrophages following production by inducible nitric oxide synthase. $O_2^{\bullet-}$ and $NO^{\bullet}$ react rapidly forming peroxynitrite ($ONOO^-$) (*25*), which may undergo proton-catalyzed homolysis to $^{\bullet}OH$ and $NO_2^{\bullet}$ (*26-28*). The reported pK_a for $ONOO^-$ is 6.8, which suggests that at physiological pH a significant amount of $ONOO^-$ exists in the protonated state as peroxynitrous acid (ONOOH). ONOOH is direct oxidant and undergoes homolysis to $^{\bullet}OH$ and $NO_2^{\bullet}$ (*27, 29, 30*). $ONOO^-$ also reacts with CO_2 to form nitrosoperoxycarbonate ($ONO_2CO_2^-$), which is a reactive nitrogen species capable of additional oxidation and

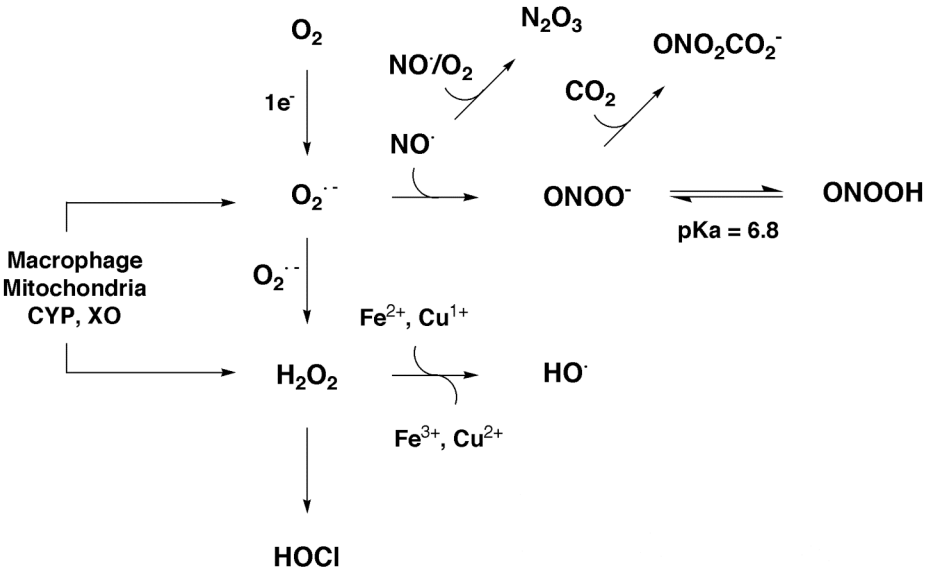

Figure 2. Generation of ROS from endogenous sources.

nitration reactions (*31, 32*). In addition to an abundance of ROS released from macrophages, the nitrosating agent N_2O_3 and the chlorinating agent HOCl are also produced, which are both capable of modifying cellular macromolecules (*30*).

The generation of ROS is not limited to the immune response. Humans are aerobic animals that utilize molecular oxygen and often release ROS as by products of cellular metabolism. Approximately 4-5% of the oxygen metabolized during cellular respiration is released as ROS (principally as $O_2^{\bullet -}$ via NADPH oxidase) (*33*), and peroxisomal metabolism significantly contributes to the production (and scavenging) of H_2O_2 in cells (*34*). ROS are also produced on membranes or within the cytosol by oxidative enzymes such as CYPs (*35, 36*), xanthine oxidase (XO) (*37*), and others (*38*).

High levels of ROS can lead to oxidative stress, which occurs when the cell's antioxidant defense is overmatched by an abundance of ROS, and results in radical reactions with cellular macromolecules such as DNA, lipid and protein. Modification of cellular components due to ROS exposure is broadly referred to as oxidative damage. Oxidative damage to protein is an important and emerging area of research, but it will not be discussed in detail. It should be noted, though, that protein damage produces altered protein structure and function, changes in cell signaling, gene transcription and may result in necrosis or apoptosis (*39*). Reactions of radicals with polyunsaturated fatty acids in the lipid bilayer results in lipid peroxidation, which is the non-enzymatic degradation of lipids producing multiple downstream products, many of which are potent electrophiles. Radical reactions with DNA can lead to strand breaks, oxidized bases and the production of electrophiles generated in close proximity to nucleic acids.

Lipid peroxidation

All known phospholipids in cell membranes contain an unsaturated fatty acid at the 2-position on the glycerol portion of the phospholipid head group. Many of these unsaturated lipids are polyunsaturated (linoleic acid, linolenic acid, arachidonic acid, etc.) **(Figure 3)**.

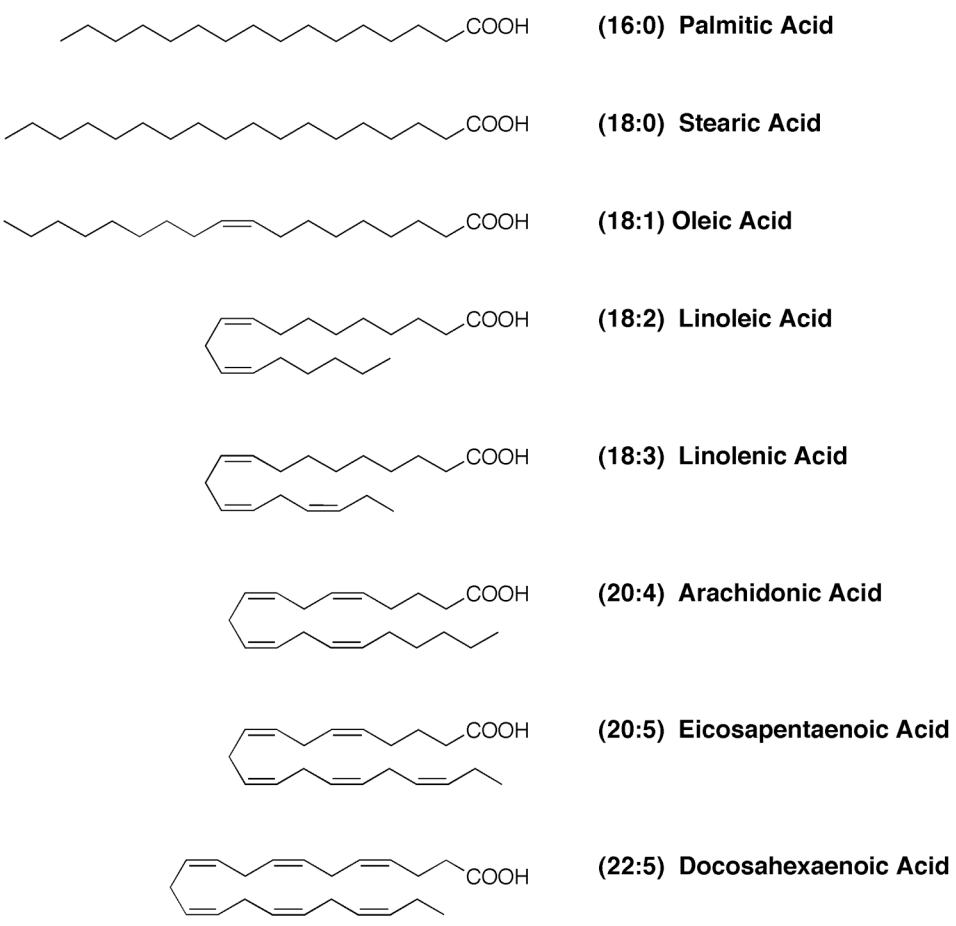

Figure 3. Common fatty acids found in biological membranes.

As with all free radical chain reactions, the autoxidation of polyunsaturated fatty acids (PUFAs) is described as a three-step process: initiation, propagation and termination **(Figure 4)**. Methylene hydrogens in between the double bonds (*bis*-allylic hydrogens) of PUFAs are the target of free-radical abstraction by ROS (initiation) **(Figure 5)**. The resulting carbon-centered radical is delocalized across adjacent double bonds as a pentadienyl radical that rapidly reacts with molecular oxygen to form peroxyl radicals. Peroxyl radicals may then abstract a *bis*-allylic hydrogen from a neighboring PUFA to form a lipid hydroperoxide and produce another carbon-centered radical (propagation) **(Figure 6)**. In this way, it is estimated that initiation of one PUFA peroxyl radical may propagate as many as 10 to 200 additional free radical reactions (depending on the degree of unsaturation in the lipid environment). Lipid peroxidation is terminated upon reaction of two radicals, forming a non-radical species (termination).

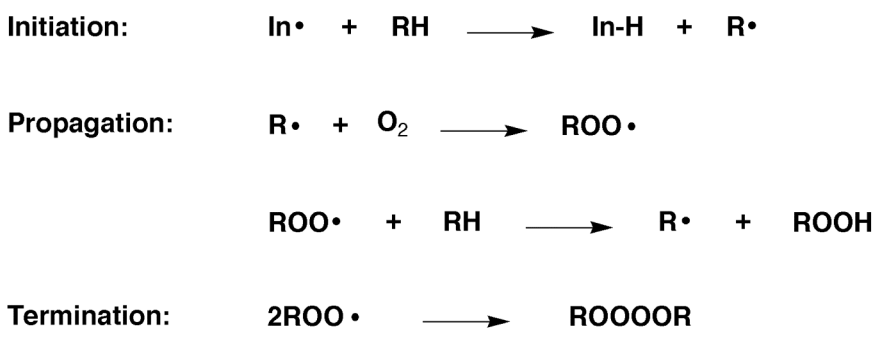

Figure 4. General mechanism of autoxidation.

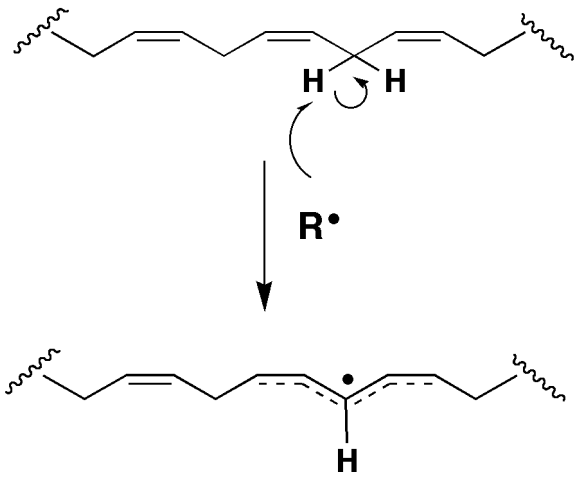

Figure 5. Initiation of lipid peroxidation occurs by radical abstraction of a *bis*-allylic hydrogen from a PUFA producing a carbon-centered pentadienyl radical.

A competing reaction for the peroxyl radical is intramolecular cyclization. This can occur when the oxidized PUFA contains three or more double bonds with an inner peroxyl radical (a peroxyl radical positioned between double bonds). The inner peroxyl radical may react with an unsaturated carbon center three atoms away producing an endoperoxide. The endoperoxide radical may react with oxygen, or initiate another intramolecular cyclization forming a bicyclic endoperoxide **(Figure 6)**. Products resulting from lipid peroxidation are numerous, and complex in regards to stereochemistry, with the abundance of products proportional to the degree of unsaturation.

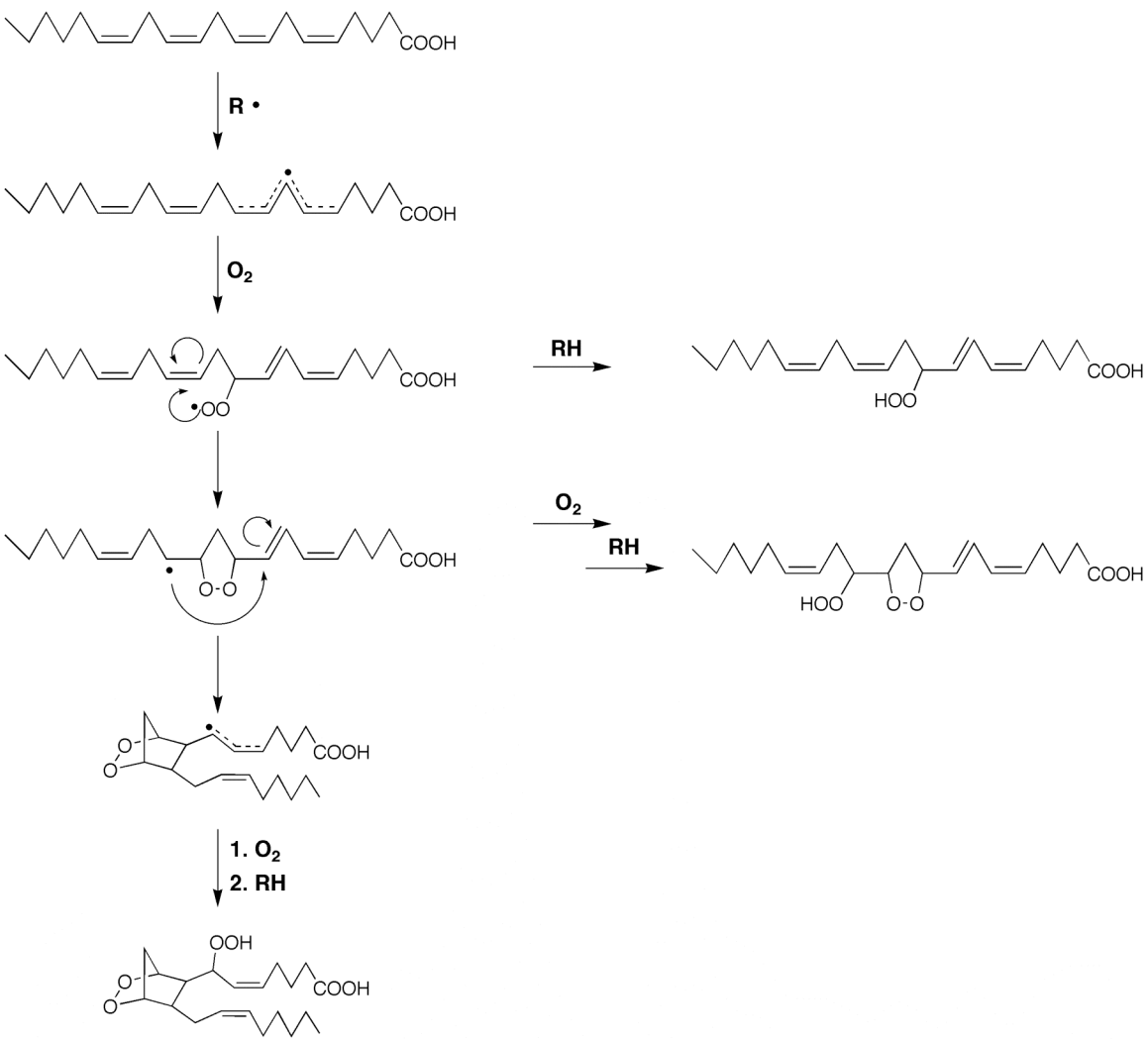

Figure 6. Autoxidation of arachidonic acid. Following initial hydrogen abstraction from C-7 on arachidonic acid, an inner peroxyl radical forms leading to the production of lipid hydroperoxides, endoperoxides, and bicyclic endoperoxides (Figure adapted from (*40*)).

The initial products derived from lipid peroxidation are subject to decomposition reactions, which may be facilitated by the presence of metals and other one electron donating species. The bicyclic endoperoxide and hydroperoxide products are of particular importance. Cyclic peroxides have been reported to undergo acid catalyzed ring scission across the endoperoxide to yield the three-carbon dialdehyde, malondialdehyde (MDA) **(Figure 7)** (*41*). MDA is also produced enzymatically from the endoperoxide-metabolizing enzyme thromboxane synthase (*42, 43*). MDA is an abundant product of lipid peroxidation and reactive with protein and DNA nucleosides (see discussion below).

Lipid hydroperoxides are produced from non-enzymatic lipid peroxidation reactions and as products of lipoxygenase and cyclooxygenase enzymes (*44-47*). The lipid hydroperoxides 9- and 13-hydroperoxy-octadecadieneoic acid (HPODE) are precursors to the production of several reactive bifunctional electrophiles. In the presence of Vitamin C or transition metals (Fe^{2+}, Cu^{1+}), 9- and 13-HPODE are decomposed to 4-hydroperoxy-2-nonenal, 4-oxo-2-nonenal, 4-hydroxy-2-nonenal, and 4,5-epoxy-2-decenal, among other products **(Figure 8)**; these compounds display varied reactivity with cellular macromolecules. Decomposition of other lipid hydroperoxides such as 5- and 15-hydroperoxyeicosatetraenoic acid (derived from arachidonic acid) also leads to a similar array of products (*48-50*). Several mechanisms for the decomposition of lipid hydroperoxides have been implicated, such as homolytic cleavage, autoxidation and Hock cleavage (*51-54*). Both 4-hydroperoxy-2-nonenal and 4-oxo-2-nonenal can be directly produced from lipid hydroperoxide decomposition of 13-HPODE (*51-53*). 4-Oxo-2-nonenal is also a dehydration product of 4-hydroperoxy-2-nonenal (*55*). 4-

Hydroxy-2-nonenal can form from the reduction of 4-oxo-2-nonenal, but is mainly produced from the reduction of 4-hydroperoxy-2-nonenal (*51, 53*).

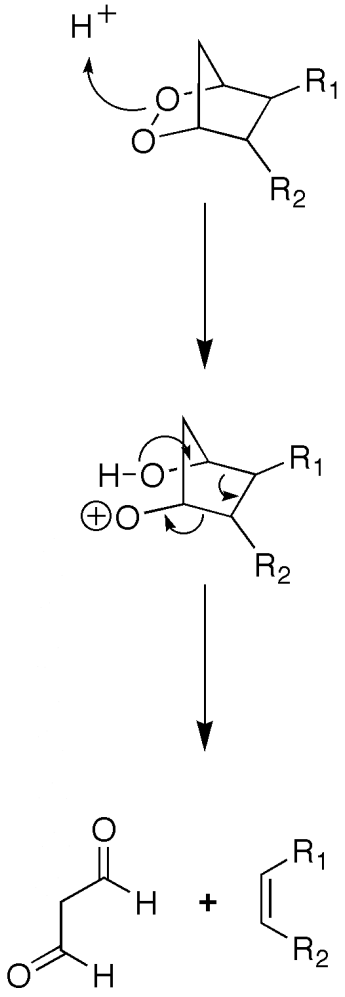

Figure 7. Beta-scission of a bicyclic endoperoxide to generate MDA.

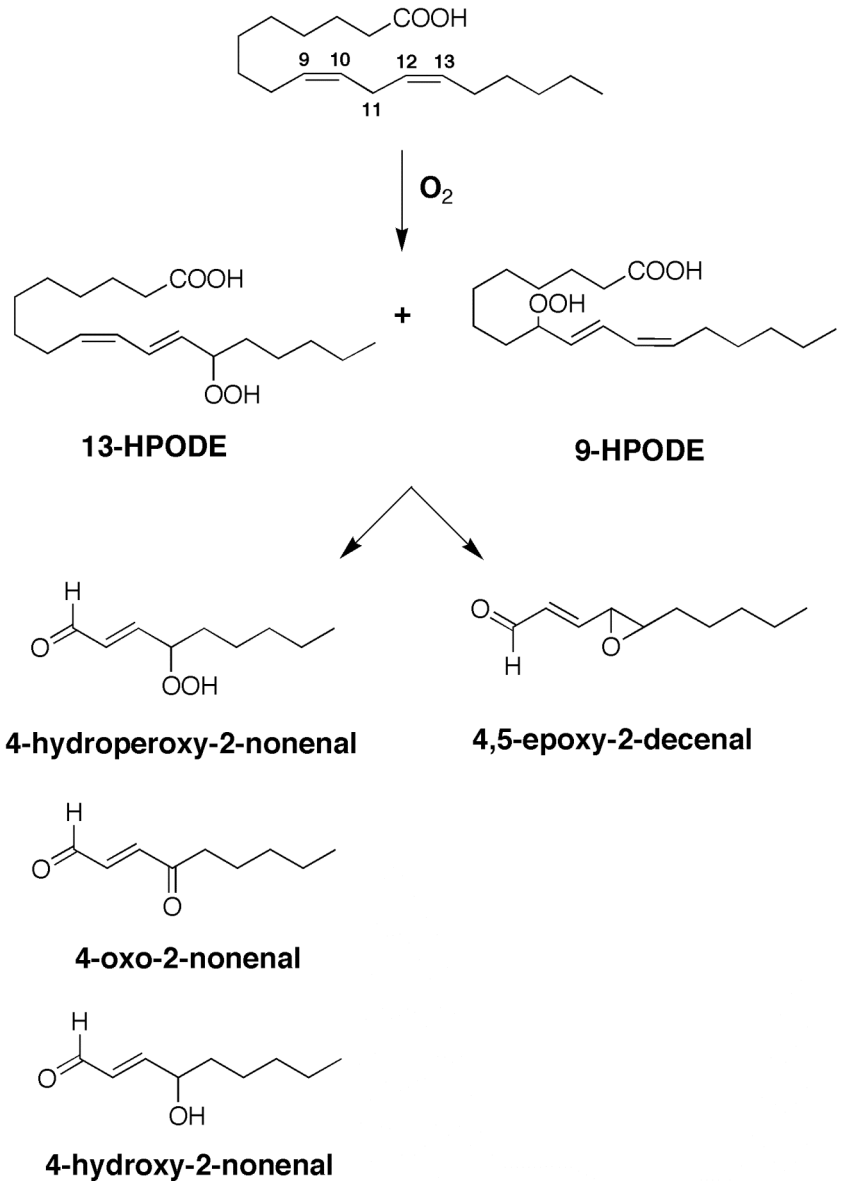

Figure 8. Non-enzymatic degradation of 9- and 13-HPODE. Production of reactive bifunctional electrophiles: 4-hydroperoxy-2-nonenal, 4-oxo-2-nonenal, 4-hydroxy-2-nonenal, and 4,5-epoxy-2-decenal.

Two other important bifunctional electrophiles produced during lipid peroxidation are acrolein and crotonaldehyde. These molecules are also environment contaminants, which arise during the combustion of organic material (*56, 57*). Acrolein and crotonaldehyde are 3- and 4-carbon α,β-unsaturated aldehydes, respectively, and their reactivity with cellular macromolecules is similar to 4-hydroxy-2-nonenal.

Deoxyribose peroxidation

ROS can initiate free radical reactions with the deoxyribose scaffold of DNA. Every hydrogen on the deoxyribose ring is subject to free radical-mediated abstraction and subsequent diffusion-limited reactivity with molecular oxygen. Each site of peroxidation leads to a separate and overlapping array of products. Following hydrogen abstraction on deoxyribose by ROS, a peroxyl radical is rapidly formed leading to additional intra- and intermolecular reactions, producing abasic sites and strand breaks. DNA strand breaks and abasic sites are thought to significantly contribute to the toxicity and mutagenicity induced by ROS. Several side-products derived from fragmentation of the deoxyribose ring are produced such as MDA, base propenal and base propenoate. These electrophiles, which are generated within DNA, have been characterized to react with nucleic acids.

Chemistry at the 4′-position of deoxyribose has been extensively studied due to the availability of reagents producing radical formation at this site (bleomycin, calicheamicin, $ONOO^-$, and Fe^{2+}-EDTA) (*58-61*). 4′-Free radical formation produces either an abasic site or a strand break with a free 3′-phosphoglycolate terminus. Fragmentation products derived from the deoxyribose moiety following a strand break

depend on the free radical initiator (*60*), and form either base propenal or MDA and a free base, which appear to be derived from separate mechanisms **(Figure 9)** (*61-63*).

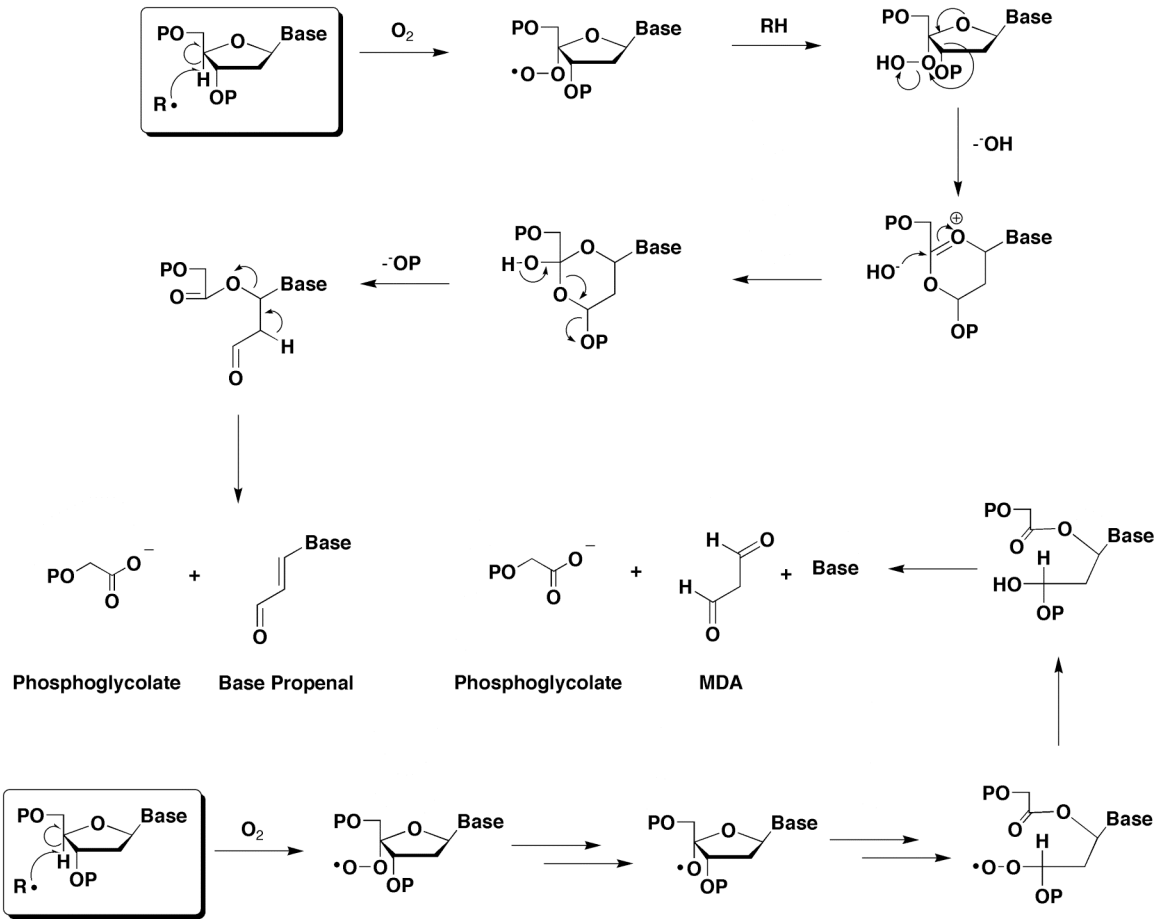

Figure 9. 4′-Autoxidation of deoxyribose. 4′-Autoxidation of deoxyribose leads to the production of a free phosphoglycolate with either a base propenal or MDA and the base (Figure adapted from (*63*)).

Assessing exposure to oxidative damage

Oxidative damage to membranes initiates lipid peroxidation to induce the formation of many highly reactive lipid electrophiles. These molecules can react with cellular nucleophiles to alter native function. Also produced from lipid peroxidation are a series of molecules known as the isoprostanes. Isoprostanes are non-enzymatic lipid oxidation products of arachidonic acid that are isomeric to the enzymatically produced prostaglandins (*64*). Cyclooxygenase imparts a *trans* orientation of the side chains on the bicyclic endoperoxide of the prostaglandin products. The isoprostanes are a racemic mix of diastereomer, but the alkyl side chains are predominantly in the *cis* orientation (*65*). Isoprostanes are byproducts of lipid peroxidation and are widely considered the best *in vivo* marker of oxidative stress (*66*). Increased isoprostanes levels have been correlated with several pathological conditions including atherosclerosis (*67*), Alzheimer's disease (*68*), and ischemia-reperfusion injury (*69, 70*), among others (*71, 72*). Additionally, they are strongly correlated with lipid peroxidation in animal models (*73, 74*). Despite their strong correlations to multiple pathologies, their appearance does not necessarily reflect genomic exposure to oxidative damage.

Since many endogenously produced nucleophiles and electrophiles that modify DNA are highly reactive, their direct detection is not feasible. Identifying end products of their reactions may be a useful approach to assessing their production. In the case of reactions with DNA, adducted DNA basesare often considered terminal products of reaction. Therefore, monitoring the levels of endogenously formed DNA adducts has been proposed as a means of assessing genomic exposure to oxidative damage (*75*).

Evaluating the formation of DNA adducts and their biological processing is an essential prerequisite to their use as a marker of exposure to endogenous sources of DNA damage.

Chemistry and Biology of MDA

MDA is an abundant product of lipid peroxidation, and one of the first products hypothesized to arise from the oxidation of lipids (*76-80*). MDA is a bifunctional electrophile with pH-dependent reactivity. At lower pH values (< 5), MDA displays similar reactivity to that of other bifunctional electrophiles produced from lipid peroxidation. At pH values above 5, MDA exists as an enolate ion and is considerably less reactive towards nucleophiles. Understanding the reactivity of MDA offers insight into the reactivity of a broad class bifunctional electrophiles derived from lipid and DNA peroxidation.

Cellular effects of MDA

MDA exists as the β-hydroxyacrolein tautomer in polar solvents (*81*) and forms an enolate at physiological pH (pK_a = 4.46) (*82*) **(Figure 10)**. Early studies on the biological consequences of MDA exposure demonstrated weak mutagenicity in bacteria and human cells, and MDA was found to be carcinogenic in mice (*83-86*). Acid hydrolysis of commercially available tetraalkoxypropanes was commonly performed as a means of producing MDA. Subsequent investigations revealed that the earlier mutagenesis studies were influenced by impurities present from the preparation of MDA from tetraalkoxypropanes. Marnett and Tuttle demonstrated that incomplete acid hydrolysis of tetraalkoxypropanes yielded side products (i.e., β-alkoxyacroleins) that

were 20 to 40 times more mutagenic than the conjugate base of β-hydroxyacrolein (*87*). Later, Basu and Marnett unequivocally demonstrated that pristine preparations of MDA were weakly mutagenic in bacteria (*88*), and topical exposures to mice demonstrated MDA was not carcinogenic (*89*). However, MDA was found to be carcinogenic in rats and mice upon administration by oral gavage (*90*).

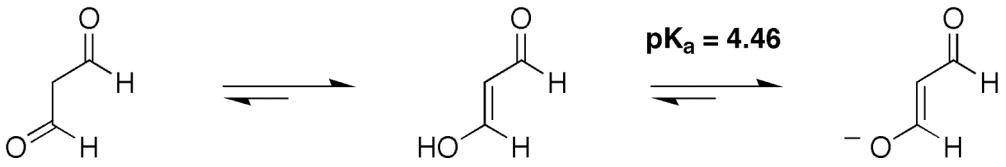

Figure 10. Tautomerization of MDA to β-hydroxyacrolein and pH-dependent formation of the enolate ion.

Further investigation into the mutagenicity of MDA-like molecules was undertaken using a structure-based approach with model electrophiles similar to β-hydroxyacrolein. Chemical substitutions were made at the β-position and the mutagenicity of each analog was evaluated with tester strains of bacteria. It was found that mutagenicity was related to the strength of the leaving group at the β-position: as the strength of the leaving increased, so did mutagenicity (β-chloroacrolein > di-γ-oxopropenal ether > β-(*p*-nitrophenoxy)-acrolein > β-benzoyloxyacrolein). Additionally, as the steric bulk of the β-substitution increased, without changing the electron withdrawing nature of the leaving group, the mutagenicity decreased (β-methoxyacrolein > β-ethoxyacrolein > β-isobutoxyacrolein) (*91*). It should be noted that substituting non-

ionizeable derivatives in place of the hydroxyl on β-hydroxyacrolein resulted in greater mutagenicity. Thus, it was implied that the negative charge carried by the conjugate base of β-hydroxyacrolein at physiological pH negatively impacted mutagenicity.

Chemical reactivity of MDA and β-substituted acroleins with nucleosides

Initial studies on the reactivity of MDA with DNA were performed by Brooks and Klammerth, who demonstrated that DNA treated with MDA (at pH 4.6 and not at pH 6.9) resulted in altered thermal decomposition profiles and resistance to deoxyribonuclease cleavage (*92*). Additionally, Reiss *et al.* found DNA treated with MDA at pH 4.6 exhibited a significant increase in fluorescence and enhanced absorbance at long wavelengths (~320 nm) (*93*). Reiss *et al.* also found that when reacted with MDA, adenine and guanine produced fluorescent products (*93*). Implicit in these results was the dependence of pH on reactivity, which demonstrated that β-hydroxyacrolein was much less reactive at pH values greater than 4.5 (*82*). These studies provided multiple lines of evidence, which suggested MDA was very reactive with DNA at low pHs leading to the formation of fluorescent modifications.

Early characterization of the reactivity of nucleosides with MDA and related structural analogs stemmed from work in the Leonard Laboratory. Moschel and Leonard found that dG reacted under acidic conditions with α-substituted MDA analogs, and produced fluorescent products exhibiting pyrimidopurinone structures (*94*). Subsequently, it was found that reactions of guanosine and dG under acidic conditions with MDA yielded two products: a pyrimidopurinone molecule (similar to that found by Moschel and Leonard), with one equivalent of MDA incorporated (*95-97*), and an

oxadiazabicyclononene-derivative (a pair of enantiomers), with two equivalents of MDA incorporated **(Figure 11)**. The MDA-dG derivatives were named based on the number of MDA equivalents added to dG (M_1dG = 1 equivalent and M_2dG = two equivalents added to dG). Reaction of MDA at neutral pH in the presence of a mixture of deoxynucleosides revealed dG was the most reactive (dG > 2′-deoxyadenosine (dA) > > 2′-deoxycytidine (dC)), but adducts were formed in low yields (< 1%) (*98*). A thymidine adduct was not observed (*98*).

Reaction of MDA with dA and dC was also investigated. Single and multimeric additions of MDA were observed with the deoxynucleosides (*99-102*). One equivalent of MDA added to the exocyclic amino group yielding oxopropenyl-derivatives: N^6-(3-oxo-1-propenyl)-dA (OPdA or M_1dA) and N^4-(3-oxo-1-propenyl)-dC (OPdC or M_1dC) **(Figure 11)**. Mulitmeric adducts arose from reactions of polymers derived from MDA *in situ* and were not the product of successive additions of MDA to the oxopropenyl-derivatives (*99-101*). The multimeric adducts are unlikely to form *in vivo*. Thus, the significance of their formation is currently unknown.

The reaction mechanism of β-substituted acroleins with dG was investigated using deuterium labeled β-(*p*-nitrophenoxy)-acrolein. The reaction was found to proceed via 1,2-addition of the exocyclic N^2-amino group to the aldehyde of the β-substituted acrolein, followed by cyclization on the ring nitrogen (N1). Cyclization was preceded by hydrolysis of the β-substituent forming a 3-oxo-1-propenyl intermediate on the exocyclic N^2 (*103*). The reaction mechanism was further explored in reactions of dG with a series base propenals (β-substituted acroleins derived from DNA peroxidation). Plastaras *et al.* observed that the extent of reactivity of β-substituted acroleins with dG was dependent on

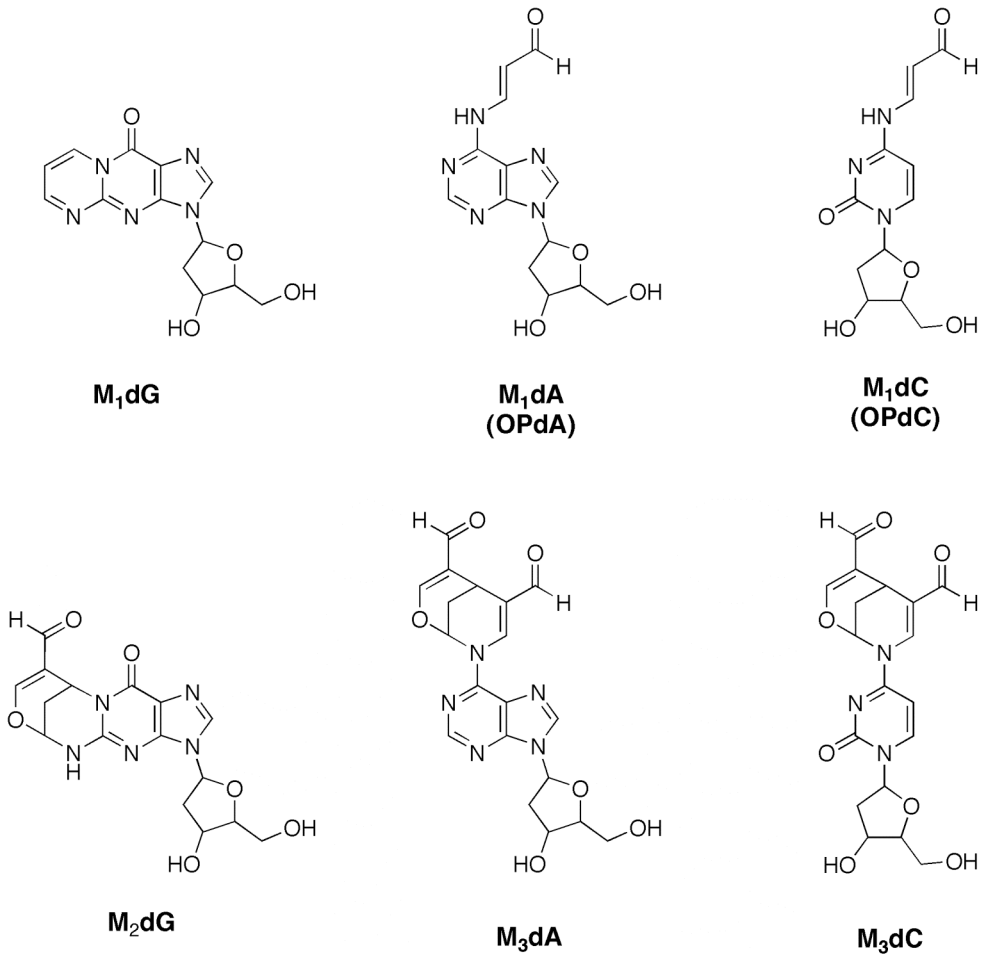

Figure 11. DNA adducts derived from MDA and related β-substituted acroleins.

the pK_a of the conjugate acid for the leaving group **(Figure 12)** (*104*). The order of reactivity observed in reactions of base propenals with dG was as follows: adenine propenal (9.8) > cytosine propenal (12.2) > thymine propenal (>13) > β-hydroxyacrolein (15.7) (pK_a values for the leaving groups in parenthesis). The use of the pK_a for β-hydroxyacrolein understates the reactivity of its conjugate base because β-hydroxyacrolein exists principally as an enolate ion at neutral pH. In the case of the MDA-enolate ion, the oxide is an exceptionally poor leaving group.

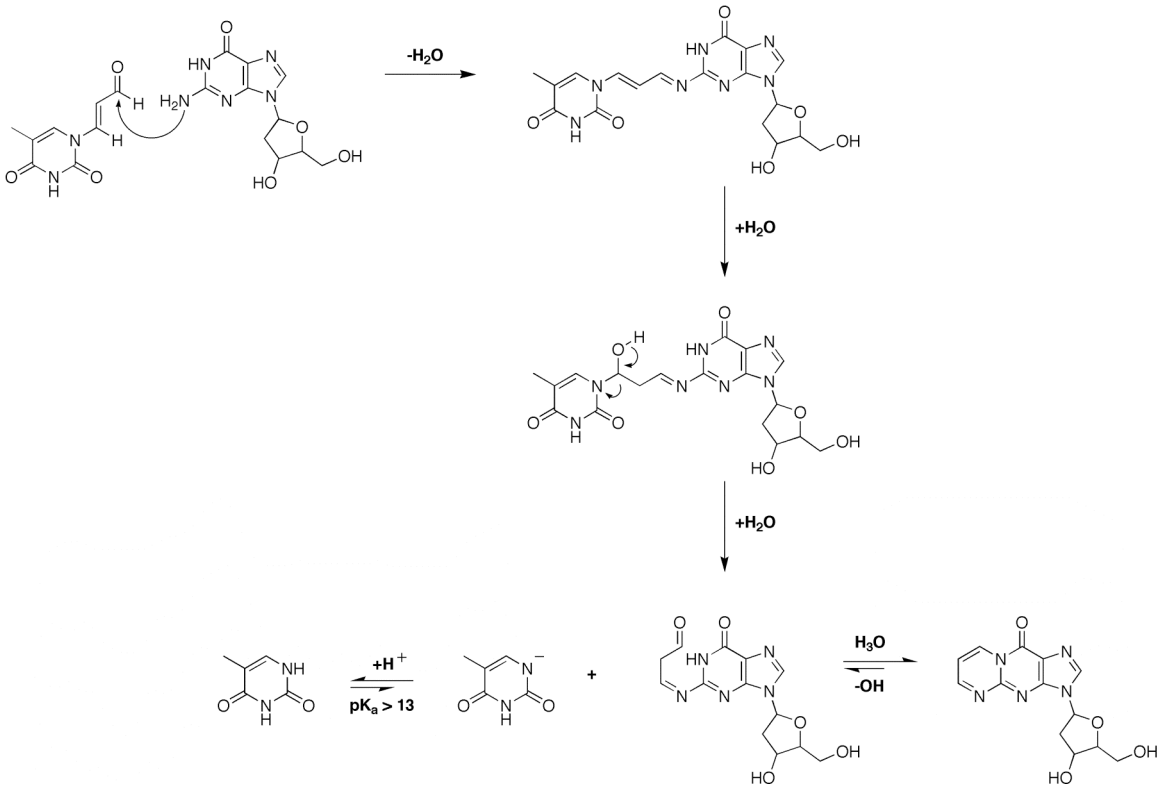

Figure 12. Reaction mechanism for the 1,2-addition of β-substituted acroleins (thymine propenal) with dG (Figure adapted from (*104*)).

Based on the reaction mechanism for β-hydroxyacrolein derivatives with dG, which followed 1,2-addition to the exocyclic N^2-amino group, it was hypothesized that the position of the N^2-atom within DNA may impact its reactivity towards model electrophiles (*105*). The N^2-position of dG is located in the minor groove and is involved in hydrogen bonding. Investigations into the DNA structural requirements leading to the formation of M_1dG revealed access of electrophiles (β-hydroxyacrolein, adenine propenal) to the minor groove was critical for reaction. Factors that limited access to the minor groove (high ionic strength, minor groove binding agents) reduced M_1dG formation, while factors that enhanced access to the minor grove (intercalating agents, major groove binders) increased M_1dG formation. Furthermore, single-stranded DNA was found to be more reactive than double-stranded DNA, implying that access to the exocyclic N^2-position of dG was critical for the formation of M_1dG. Considering M_1dG formation in the context of double stranded DNA, initial approach of an enolate ion may be affected by charge repulsion from the negatively charged phosphate backbone of DNA. Thus, at physiological pH the formation of M_1dG is likely to arise from neutral β-hydroxyacrolein analogs such as base propenal.

Two recent studies strongly support the hypothesis that base propenals are the principal reactants leading to M_1dG formation. Investigation by Zhou *et al.* demonstrated an increase in M_1dG levels *in vitro* when calf thymus DNA was exposed to reagents that promote base propenal formation (bleomycin or $ONOO^-$) and no change in M_1dG levels with reagents that principally produce MDA (Fe^{2+}-EDTA or γ-radiation) (*106*). Additionally, in bacterial cells an increase in M_1dG formation was dependent on $ONOO^-$ exposure (produces base propenal) but not seen following exposure to γ-radiation

(produces MDA) (*106*). Jeong and Swenberg made similar observations (*107*). In their study with uniformly ^{13}C-labeled DNA in the presence of H_2O_2 and Cu^{1+}, all M_1dG was derived from deoxyribose. The same results were obtained when the above incubation was supplemented with non-isotopically enriched oleic acid (18:1). Upon addition of non-isotopically enriched PUFAs the majority of M_1dG was derived from deoxyribose rather than lipid (*107*).

Stability of M_1dG: hydrolytic ring-opening and reaction with nucleophiles

Investigations on the aqueous stability of M_1dG revealed that the adduct was subject to hydrolytic ring opening in basic solutions resulting in the formation of 3-oxo-1-propenyl-moiety on the exocyclic N^2-position of dG (OPdG) (*108*). This structure was analogous to the OPdA and OPdC structures previously characterized as major reaction products of MDA with dA and dC, respectively. Further investigation into the mechanism of ring opening for M_1dG revealed that hydroxide ion added directly to C_8 of the exocyclic ring producing a transient carbinolamine, which rapidly ring-opened by breaking the C_8-N_9 bond (*109*) (**Figure 13**). A resulting negative charge remains on the purine nitrogen (N1) in the ring-opened state, which has a calculated pK_a of 6.9 (*110*). The negative charge on OPdG impacts further reactions with nucleophiles (see below). Ring opening of M_1dG is reversible, and OPdG is subject to a general-acid-catalyzed ring-closure. This reaction is biphasic with a fast protonation step (protonation of N1) and a slower dehydration step (*110*).

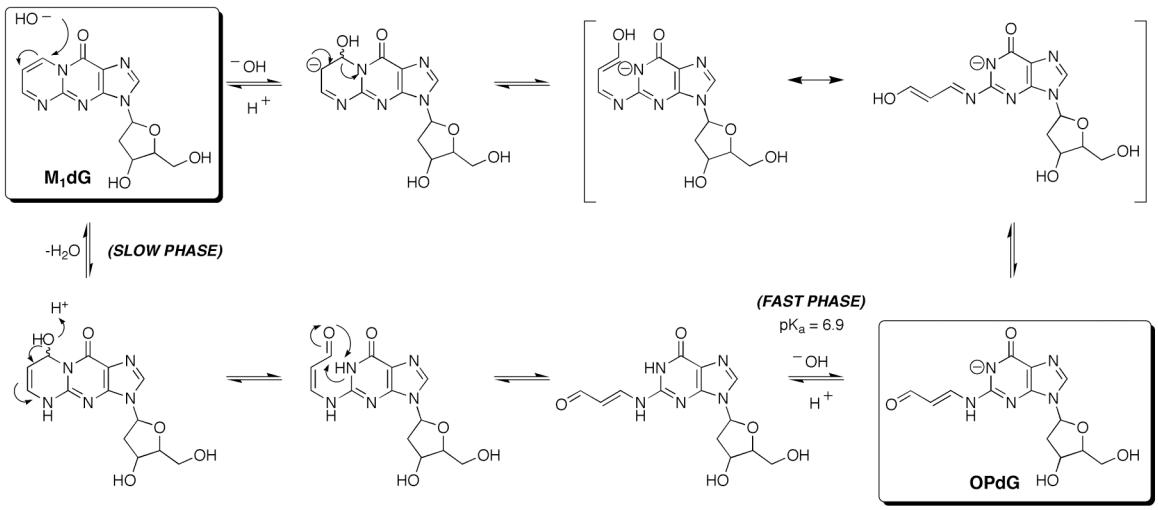

Figure 13. Hydrolytic ring opening of M_1dG to OPdG and general-acid-catalyzed ring-closure of OPdG to M_1dG.

The mechanism of M_1dG ring-opening is not limited to reactions with hydroxide. Other nucleophiles have been characterized to react with M_1dG such as amines, hydroxylamines, and hydrazines (*111-113*). These reactions principally occur by direct addition to C_8, but nucleophiles also may react with the free aldehyde of OPdG (*112, 113*) demonstrating that other oxopropenyl derivatives (OPdA, OPdC, base propenal, etc.) are subject to derivatization (*113*). Further investigation into the reactivity of M_1dG with oxidative enzymes will be discussed in Chapter 2.

In single-stranded oligonucleotides, M_1dG is present in the ring-closed form (*109*). Interestingly, in duplex DNA the conformation of M_1dG is sequence-dependent. When positioned opposite dC residues in double-stranded DNA, M_1dG ring opens to OPdG; however, when opposite dT residues, M_1dG remains as a pyrimidopurinone (*114, 115*). It has been hypothesized that duplex annealing is responsible for catalyzing ring opening to OPdG suggesting that the exocyclic N^4-amino group on the dC residue on the complimentary strand functions to activate water and direct the addition to C_8 of M_1dG

prior to stacking of the incoming nucleotides (*109*). Once positioned in DNA, OPdG extends into the minor grove where it may react with DNA-binding proteins and affect protein-DNA interactions. Of note, the minor grove is also the location where MDA and base propenals are believed to react with the N^2-amino group on dG residues for initial 1,2-addition to OPdG (*105*). Preliminary studies on the ability of M_1dG to disrupt protein-DNA interactions suggested the dynamic equilibrium of M_1dG and OPdG may impact protein-DNA interactions as witnessed by the impaired ability of restriction enzymes to cleave at consensus sites containing M_1dG (*116*).

Many DNA binding proteins are rich in basic amino acids such as lysine (lys), histidine (his) and arginine (arg), with the resulting net positive charge of these residues providing a means of associating with the negatively charged DNA helix. Amines are reasonable nucleophiles and have been characterized to react with M_1dG (*104, 111*). Therefore, to model the potential interactions of oxopropenyl-nucleoside adducts with DNA, reactions with *N*-α-acetyl-lys (a model nucleophile) were examined (*117*). The reaction of *N*-α-acetyl-lys with M_1dG produced a Schiff base adduct and was rapidly hydrolyzed at neutral pH (similar to what was seen upon reaction with tris-(hydroxymethyl)-aminomethane (Tris) (*111*)). The ring-opened OPdG, bearing a full negative charge on N1, did not react with *N*-α-acetyl-lys. To eliminate the effect of the negative charge on the reaction of *N*-α-acetyl-lys, OPdG was reacted with iodomethane to yield (N1-methyl)-OPdG and displayed an increase in the pK_a to 8.2. Removal of the negative charge resulted in enhanced reactivity of OPdG with *N*-α-acetyl-lys and produced a reversible, but stable, Schiff base conjugate ($t_{1/2}$ = 12 h). Based on these results, it was hypothesized that the other oxopropenyl deoxynucleoside adducts, OPdA

(pK_a = 10.0) and OPdC (pK_a = 10.5), which do not carry a negative charge at neutral pH, would form stable crosslinks in reactions with *N*-α-acetyl-lys. Subsequent reaction of either OPdA or OPdC with *N*-α-acetyl-lys demonstrated stable crosslinks with similar characteristics seen with (N1-methyl)-OPdG. These data suggest that the acidity of the oxopropenyl deoxynucleoside is a key determinant of its reactivity. Thus, under physiological conditions, one can reasonably assume that either OPdA or OPdC are the most likely MDA-modified oxopropenyl derivatives to react and form stable DNA-protein crosslinks.

M_1dG as a premutagenic lesion

Initial studies on the biological effects of MDA and β-substituted acroleins were performed in tester strains of the bacterium *Salmonella typhimurium*. These studies suggested MDA and β-substituted acroleins induced base pair substitutions and frameshift mutations (*83, 88, 91, 118*). More detailed sequence information on the mutagenicity of MDA was obtained by transforming MDA-modified single stranded phage DNA into *Escherichia coli.* Following replication of the viral genome, sequence analysis was performed which revealed base-pair substitutions (G → T, C → T, and A → G) and frameshift mutations (mainly single base additions occurring in runs of reiterated bases) (*119*). It is important to note from the data that specific types of adducts formed in these experiments cannot unequivocally be linked to their genetic consequences (i.e., it was unknown which adducts induced a particular mutation). However, the base-pair substitution data from latter experiment is suggestive of specific types of MDA-induced lesions (i.e., a G → T transversion would imply modification of G by MDA).

A significant advancement in the mutational analysis of M_1dG was made by Reddy and Marnett, who successfully incorporated the pyrimidopurinone ring adduct into an oligonucleotide (*108*). Shortly to follow was the ligation of these oligonucleotides into gapped duplex DNA for use in bacterial and mammalian cells. Initial reports from *E. coli* demonstrated that M_1dG, within the sequence context of 5′-GGT(M_1dG)TCCG-3′, was an efficient premutagenic lesion that induced base-pair substitutions ($M_1dG \rightarrow A \sim M_1dG \rightarrow T > M_1dG \rightarrow C$). No frameshift mutations were detected in this experiment, but the site-specific position of the adduct was not in a reiterated repeat sequence. However, M_1dG was found to be a strong block to replication, and when correcting for strand bias M_1dG was shown to have a mutation frequency of 18% (*120*).

VanderVeen *et al.* later demonstrated that the mutational spectrum of M_1dG was sequence dependent in both *E. coli* and mammalian cells (*121*). M_1dG was incorporated into one of several positions on a single-stranded vector within the context of a reiterated sequence (5′-GGTGTCCG$_1$CG$_2$CG$_3$CG$_4$GCATG-3′). Following sequence analysis of the replicated plasmids it was revealed that M_1dG induced mostly -2 and some -1 deletions (frameshift mutations). Base-pair substitutions were also found ($M_1dG \rightarrow A \sim M_1dG \rightarrow T > M_1dG \rightarrow C$). Insertion of M_1dG at position-3 resulted in the highest mutation frequency. A non-reiterative sequence (5′-GGT(M_1dG)TCCG-3′) used in mammalian cells produced no deletion mutants, which strongly implicated the sequence context of DNA in which M_1dG resides to be a determining factor for its mutational spectrum (*121*).

Repair mechanisms for M_1dG

The repair of M_1dG from genomic DNA is mediated by the nucleotide excision repair (NER) pathway. Bacterial cells deficient in NER display an increased mutation frequency compared to NER-competent cells when transformed with M13 vectors containing site-specifically positioned M_1dG (*120*). Similar results were observed in bacteria upon site-specific incorporation of propano-dG (PdG, tetrahydro-pyrimidopurinone-dG, which is a structural analog of M_1dG) using NER-deficient and proficient cells (*122*). Additionally, PdG was found to be a substrate for NER repair *in vitro* using recombinant bacterial repair proteins or mammalian cell extracts (*122*). Based on the close structural similarity between PdG and M_1dG, it appears likely that the NER pathway in mammalian cells also repairs M_1dG. Currently, there is no evidence supporting a role for base excision repair in the repair of M_1dG.

In eukaryotes, NER is carried-out by a complex network of proteins designed to identify and remove lesions from DNA. A more simplified complex of three proteins (UvrA, UvrB, and UvrC) is involved in prokaryotic NER. This repair mechanism is typically associated with the removal of large, bulky adducts such as intrastrand crosslinks, DNA-protein crosslinks and chemical modification by large molecules (B[*a*]P, cisplatin). However, NER is also involved with the repair of small lesions such as O^6-methyl-dG, 8-oxo-Gua, abasic sites, and the pyrimidopurinone adduct, M_1dG (*123-125*). Independent of the type of lesion present for NER-mediated excision, a similar cascade of molecular interactions occurs, which involves (1) recognition of the lesion, (2) unwinding of the DNA, (3) dual-incision around the lesion on the damaged strand, (4) removal of an oligonucleotide, (5) DNA synthesis, and (6) ligation (**Figure 14**).

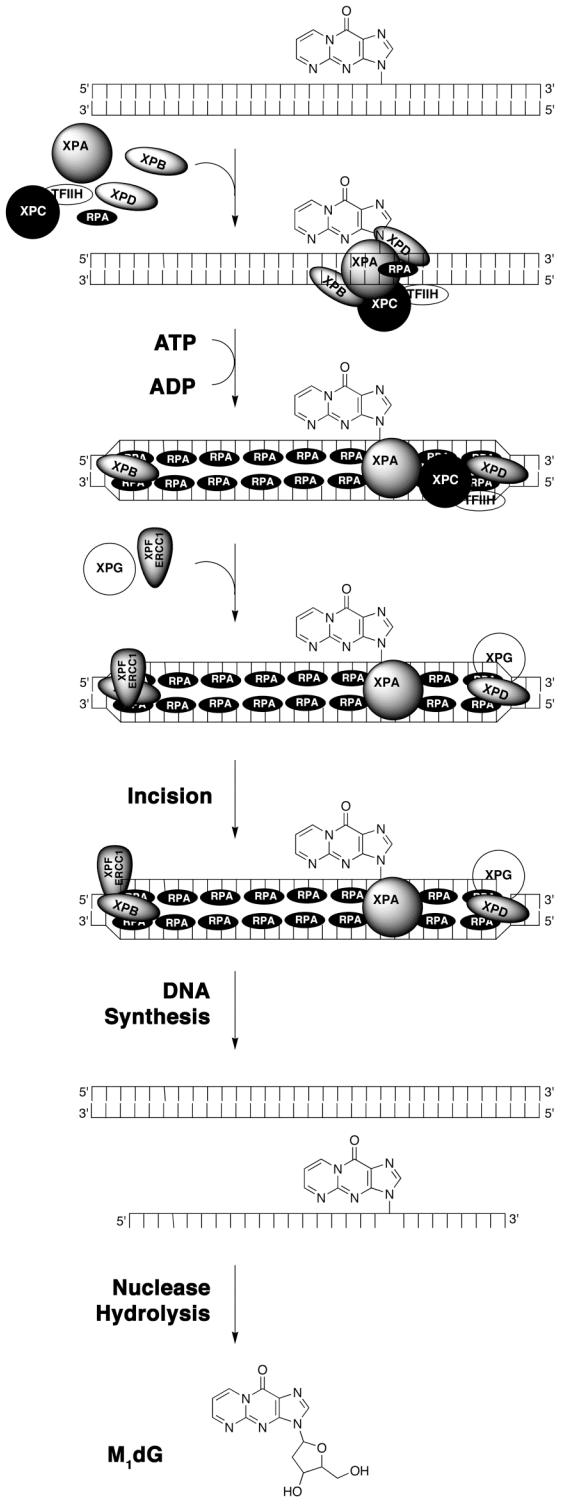

Figure 14. NER-dependent release of M_1dG from DNA in eukaryotes (Figure adapted from (*124*)).

In eukaryotes, the lesion is recognized by replication protein A (RPA), xeroderma pigmentosum-A (XPA), XPC-TFIIH (transcription factor IIH), XPB, and XPD, which assemble at the lesion site. In the presence of damage, the helix is unwound in an ATP-dependent process by XPB and XPD. XPG replaces XPC in the complex followed by the recruitment of XPF-ERCC1 (excision repair cross complementary group 1). The damaged strand is incised at the 3′-end by XPG and at the 5′-end by XPF-ERCC1. A 24-32 unit oligonucleotide is released and the gap is repaired by a DNA replication complex involving either polymerase δ or ε. DNA ligase then joins the newly synthesized DNA to the existing duplex (**Figure 14**) (*124*). Defects in any of the XP proteins A-G result in a genetic predisposition to cancer and neurological abnormalities. These defects are principally attributed to a reduced or abolished NER mechanism (*126*).

Of no small importance is the fate of the lesion-containing oligonucleotide produced from NER. Following removal from DNA, the oligonucleotide is subject to hydrolysis, which results in the formation of free deoxynucleosides. Thus, lesions repaired by NER are removed from cells in the form of deoxynucleosides.

Analytical assessment of DNA lesions

Characterizing the reactivity of MDA and related β-substituted acroleins with nucleosides and DNA *in vitro* is an important step towards understanding the chemical reactivity of these endogenously produced electrophiles. Relating adduct formation to a biological outcome (i.e., mutation) is also critical to understanding the consequences of DNA modification. Additionally, another very important factor to investigate is the level of DNA adduct formation *in vivo*. The ability to accurately quantify M_1dG levels may

offer a means of identifying changes in adduct levels across different populations and in relation to varied pathological conditions. Thus, assessing endogenous adduct levels may offer insight into the contribution of oxidative damage observed in genomic DNA. MDA and β-substituted acroleins have been characterized to form multiple nucleoside adducts. However, the principal adduct formed at physiological pH is M_1dG. Thus, the quantification of M_1dG has been the focus of research directed at assessing genomic exposure to oxidative damage.

Two main approaches exist for the analysis of DNA adducts in human populations: direct detection from genomic DNA and analysis of DNA adducts in biological waste products. Genomic DNA may be isolated from cells, hydrolyzed to individual nucleosides, purified, and quantified by various analytical techniques. This tactic requires access to cells, which may originate from tissue or blood. Analysis of this type is typically regarded as an invasive approach. Its main advantage is that it represents a very direct analysis technique (DNA adducts are associated with a specific tissue), but it is limited by access to the sample. The analysis of DNA adducts in biological waste products (urine, feces) represents non-invasive means of assessing DNA adduct levels. However, this approach represents an indirect method of analysis, since the true origin (tissue-specificity, dietary components, etc.) of the adduct is difficult to determine. However, the appearance of DNA adducts in urine is often attributed to their repair-dependent removal from DNA.

Analytical assessment of aflatoxin-N^7-Gua lesions

The best example of correlating urinary DNA adduct levels with carcinogen exposure is seen with the aflatoxin B_1 guanine adduct (aflatoxin-N^7-Gua). Aflatoxin B_1 is a fungal metabolite found in contaminated foods such as corn, peanuts, and soy beans that are risk factors for the development of hepatocellular carcinoma in humans (*127*). Absorption of aflatoxin B_1 from contaminated food leads to the metabolic activation of aflatoxin B_1 in the liver by CYPs to aflatoxin-B_1-8,9-oxide (*128, 129*). The *exo* stereoisomer reacts with dG residues in DNA to produce aflatoxin-N^7-dG (*129-132*). This adduct is unstable and undergoes depurination in DNA, and is released as the base adduct (aflatoxin-N^7-Gua), which is eliminated in urine (**Figure 15**) (*133*).

Treatment of rats with aflatoxin B_1 produces a dose-dependent increase in both the elimination of aflatoxin-N^7-Gua in the urine and the amount of aflatoxin-N^7-dG in genomic DNA (*133, 134*). No other urinary metabolites of aflatoxin B_1 were found to correlate with aflatoxin B_1 exposure. Similar observations were made from epidemiological studies in human populations at risk for dietary aflatoxin B_1 exposure. Population-based studies in China and West Africa have revealed strong associations between dietary intake of aflatoxin B_1 and the urinary elimination of aflatoxin-N^7-Gua (*135-138*). A 2- to 3-fold greater risk for developing hepatocellular carcinoma was observed with individuals who had aflatoxin-N^7-Gua in their urine (*139*). Additionally, individuals who test positive for hepatitis B are approximately 8 times more likely to develop hepatocellular carcinoma when exposed to dietary aflatoxin B_1 than non-infected individuals. In infected and non-infected individuals, strong correlations are observed between the urinary levels of aflatoxin-N^7-Gua and the onset of cancer (*139, 140*). Thus,

the elimination of DNA adducts in urine can be reflective of exposure to genotoxic chemicals and identify individuals at risk for cancer.

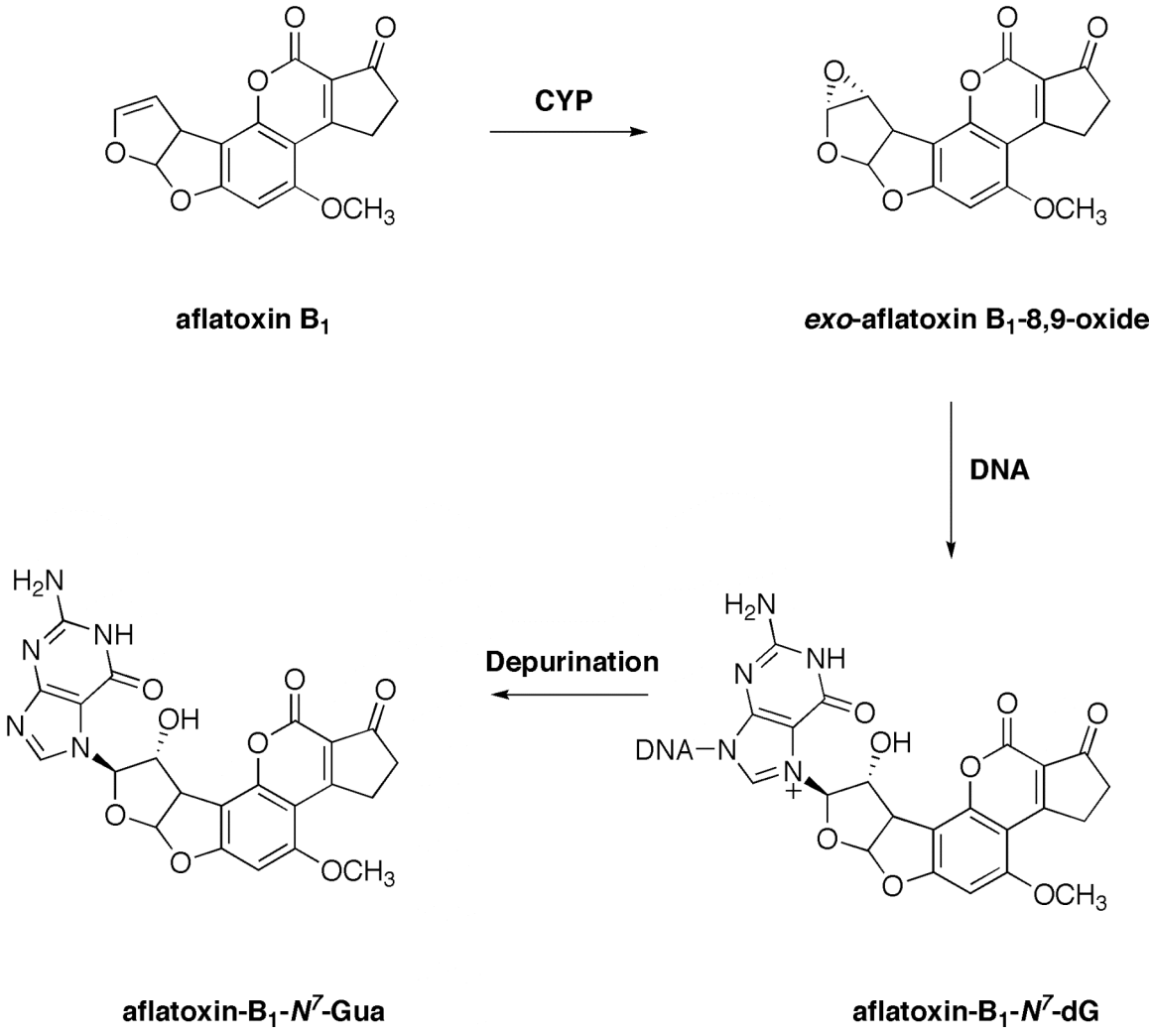

Figure 15. Generation of aflatoxin-B_1-N^7-Gua. Oxidaiton of aflatoxin B_1 produces *exo*-aflatoxin B_1-8,9-oxide, which reacts with dG residues in DNA to generate aflatoxin-B_1-N^7-dG. Aflatoxin-B_1-N^7-Gua spontaneously depurinates from DNA and is eliminated in the urine.

Analytical assessment of M_1dG lesions

Initial observations for the covalent modification of DNA by MDA were made by absorbance and fluorescence measurements (*93*). Seto *et al.* later determined by chromatographic separation that the bulk of the fluorescence produced in the reaction of MDA with DNA was not covalently bound to nucleic acid (> 70%), and only 6% of the material was attributed to M_1dG (*141*). The conjugated structure of M_1dG provides modest fluorescence (2% quantum yield) with an excitation maximum at 363 nm and an emission wavelength at 511 nm. Fluorescence measurements of M_1dG levels have been performed on DNA isolated from rat liver and in human urine, but the reported levels were quite high (*142-144*), presumably due to the inherent non-specificity of fluorescence detection within the context of a complex medium.

Mass spectrometry (MS) analysis offers an enhanced linear range of analytical detection and improved analyte selectivity when compared to fluorescence analysis. The selectivity is particularly evident upon coupling chromatographic separation to MS detection. An initial MS approach was undertaken to determine the level of M_1G (the free base of M_1dG) in human urine samples (*145*). M_1G is a putative product of DNA repair by DNA glycosylases and, therefore, may appear in urine following repair-dependent removal from DNA. This methodology utilized liquid chromatography-mass spectrometry analysis (LC-MS) and implemented the use of a di-deuterium labeled M_1dG internal standard ($[^2H_2]$-M_1dG). The use of an isotopically labeled internal standard in mass spectrometry analysis allows for corrections in recovery during sample work-up and provides a reference for quantitation. M_1G was enriched during the sample work-up by C18 solid phase extraction (SPE) and HPLC collection. Furthermore, the sample was

reacted with sodium borohydride to reduce the 5,6-double bond on the pyrimido ring to yield 5,6-dihydro-M_1G (**Figure 16**), which enhanced chemical ionization and improved chromatographic separation (*145, 146*). This method of analysis had a limit of sensitivity of 250 fmol (on column), but the level of M_1G in urine was below the limit of detection for the assay (< 500 fmol/mL).

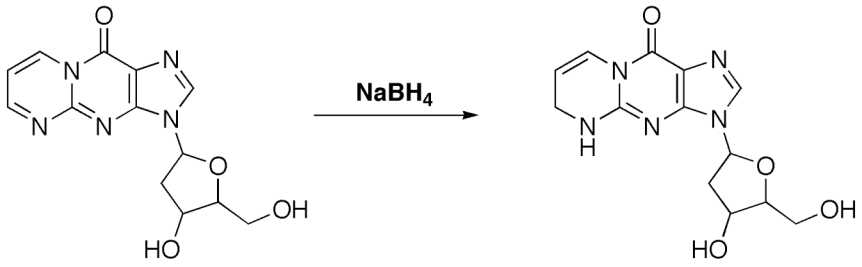

Figure 16. Reduction of M_1dG with sodium borohydride to yield 5,6-dihydro-M_1dG.

Further method development was undertaken to enhance the assay sensitivity with the purpose of evaluating the level of M_1dG in genomic DNA. Two similar assays were developed utilizing gas chromatography electron capture negative chemical ionization MS (GC-ECNCI-MS), which utilized the [$^2H_2$]-M_1dG internal standard (*147, 148*). One approach implemented sodium borohydride reduction to yield 5,6-dihydro-M_1dG, which was then successively derivatized, first with pentafluorphenylbromine (PFB-Br, to enhance ionization) and second with *N*-methyl-*N*-*tert*-butyldimethylsilyl trifluoroacetamide (*t*BDMS, to enhance GC mobility). Following several SPE clean-up

steps (and derivatizations), the resulting M_1G-PFB-BDMS derivative was then analyzed by GC-ECNCI-MS with a limit of detection of 30 fmol on column and revealed the presence of 5 adducts per 10^7 bases in rat liver (*147*). The second approach neither reduced M_1dG to 5,6-dihydro-M_1dG nor derivatized to the BDMS conjugate. Rather, a mild acid hydrolysis of the deoxynucleosides from rat liver was implemented to hydrolyze to the free purines and pyrimidines. These samples were then derivatized with PFB-Br, which produces a mixture of isomers at N1 and N3 of M_1G that are separable by GC. Implementing additional SPE steps during sample work-up enabled a limit of detection 3 adducts per 10^9 bases. Upon analysis of human liver DNA the level of endogenous M_1dG was found to be present at an average of 9 adducts per 10^7 bases (approximately 5400 adducts per cell) (*148*). This represented the first analytical evidence for the formation of lipid peroxidation-derived DNA adducts in healthy humans.

Immunochemical methodologies have been developed both to directly analyze M_1dG in ELISA assays and as an enrichment step prior to mass spectrometry analysis (*104, 105, 113, 149, 150*). The latter was implemented by Rouzer *et al.* and for use in the GC-ECNCI/MS and also adapted to a LC-MS/MS analysis using electrospray ionization (ESI) to analyze M_1dG in DNA isolated from leukocytes (*149*). Both analytical methods readily detected the presence of M_1dG in leukocyte DNA; however the GC-ECNCI/MS analysis proved to be more sensitive than the LC-MS/MS analysis. Interestingly, the level of M_1dG found in human leukocyte DNA was considerably lower than the level of M_1dG in human liver. Approximately 6 adducts per 10^8 bases were detected by GC-ECNCI-MS in human leukocytes.

More recently, Jeong and Swenberg have developed another method of analysis for the detection of M_1dG in DNA (*151*). Their approach takes advantage of the chemical reactivity of M_1dG in reactions with nucleophiles. M_1dG was derivatized with a dual-functionality reagent containing a biotin moiety linked to a hydroxylamine. When reacted with DNA the hydroxylamine portion adds directly to the ring-closed M_1dG to produce a stable oxime. The enhanced hydrophobicity of the biotin linker allows for greater fold-purity during SPE work-up, enhanced retention on a reverse phase C18 column, and lower background signal in the mass analyzer. This method also utilizes uniformly labeled [^{15}N]-DNA, with a known amount of M_1dG adducts, as an internal standard during sample work-up. The accuracy and precision of this assay is remarkable, with the calculated y-intercept for the calibration curve nearly passing through the origin. The observed LC-MS/MS limit of detection for M_1dG on column was between 200-500 amol. Based on 200 μg of DNA, 2 adducts per 10^8 bases can be reliably detected with this analysis. The application of this method to the analysis of rat tissue samples demonstrated M_1dG levels of approximately 1 to 4 adducts per 10^8 bases (*152*). This is currently the most accurate and precise method for the analysis of M_1dG in DNA.

A separate analytical approach was developed to probe for the presence of M_1dG in human urine. Since M_1dG is principally repaired by the NER machinery (rather than via DNA glycosylases) it was reasoned that the deoxynucleoside would be the most abundant form of the adduct in urine. Otteneder *et al.* utilized immunoaffinity capture to isolate M_1dG from urine, and sodium borohydride reduction to enhance ionization (*153*). 5,6-dihydro-M_1dG was analyzed by ESI positive ion LC-MS/MS analysis with a lower limit of detection of 50 fmol on column. In all urine samples analyzed, however, the

level of analyte was below the limit of detection. A modified analytical procedure was implemented by Hoberg *et al.*, who utilized atmospheric pressure chemical ionization in place of ESI during the analysis (*154*). This afforded an enhanced limit of sensitivity and lowered the limit of detection to 500 amol on column (a 100-fold improvement). Analysis of human urine samples revealed an M_1dG elimination rate of 12 fmol/kg/24 h (*154*).

The low rate of M_1dG elimination in human urine was unexpected. Other commonly monitored urinary DNA adducts such as 8-oxo-Gua and 8-oxo-dG are eliminated at rates of 2 nmol/kg/24 h and 0.4 nmol/kg/24 h, respectively (*155, 156*). There are several possibilities for the observed decreased elimination rate observed for M_1dG. Perhaps the most obvious possibilities are that M_1dG is formed at lower levels in DNA than 8-oxo-dG, or repaired at reduced rates. It is also possible that the amount of M_1dG observed in urine may be affected by alternative routes of metabolic processing following NER-dependent removal from DNA. Therefore, Otteneder *et al.* hypothesized that M_1dG may undergo biotransformation to alternative metabolic products prior to urinary elimination (*157*). Initial reports revealed that M_1dG was oxidized *in vitro* and *in vivo* to a novel metabolite, 6-oxo-M_1dG. Based on these initial observations a series of experiments were undertaken to determine the total metabolic profile of M_1dG. These studies will be the focus of Chapters 2, 3, and 4. The metabolic stability of M_1G (a putative product of base excision repair by DNA glycosylase) will be described in Chapter 5.

Other Major Endogenously Formed DNA Adducts

In addition to their reactivity with PUFAs, ROS also may react with other cellular macromolecules including protein and nucleic acids. These reactions are considered direct effects of ROS and produce oxidized nucleic acids. Alternatively, an abundant pool of secondary reaction products are derive from ROS-mediated lipid peroxidation reactions. Lipid peroxidation-derived bifunctional electrophiles also react with cellular nucleophiles throughout cell, and of particular interest are their reactions with nucleic acids. The bifunctional nature of many lipid peroxidation products provides two reactive centers. Addition reactions to pyrimidines and purines often produce exocyclic structures on nucleobases, which form across the Watson-Crick basepairing interface. Exocyclic rings are either 5- or 6-membered, with varying degree of saturation. These lesions are highly mutagenic and repaired by multiple mechanisms.

Oxidation of nucleosides by ROS

ROS can directly modify DNA bases, with hydroxyl radical thought to be the principal mediator of damage. dG is more susceptible to oxidation than other nucleosides due to its low oxidation potential (*158*). The primary product arising from direct oxidation of dG is 8-oxo-7,8-dihydrodeoxyguanosine (8-oxo-dG). 8-Oxo-dG is subject to additional oxidations and can ring open to a minor product, 2,6-diamino-5-formamidino-4-hydroxypyrimidine (*159*).

Direct oxidation of adenine is also targeted to the imidazole ring to produce 8-oxo-7,8-dihydrodeoxyadenosine (8-oxo-dA) (*159, 160*). Pyrimidine oxidation occurs across the 5,6-double bond to produce glycols (thymidine glycol, cytidine glycol) (*161*).

Oxidation of cytidine at the 5- and 6-positions commonly results in deamination of the exocyclic N^4 amino group producing uracil derivatives. In the case of thymidine, oxidation may also occur on the exocyclic methyl group **(Figure 17)** (*159, 160*). For a thorough overview of DNA base oxidation, the reader is referred to review articles by Burrows (*159*), Cadet (*160*), and Neeley (*162*).

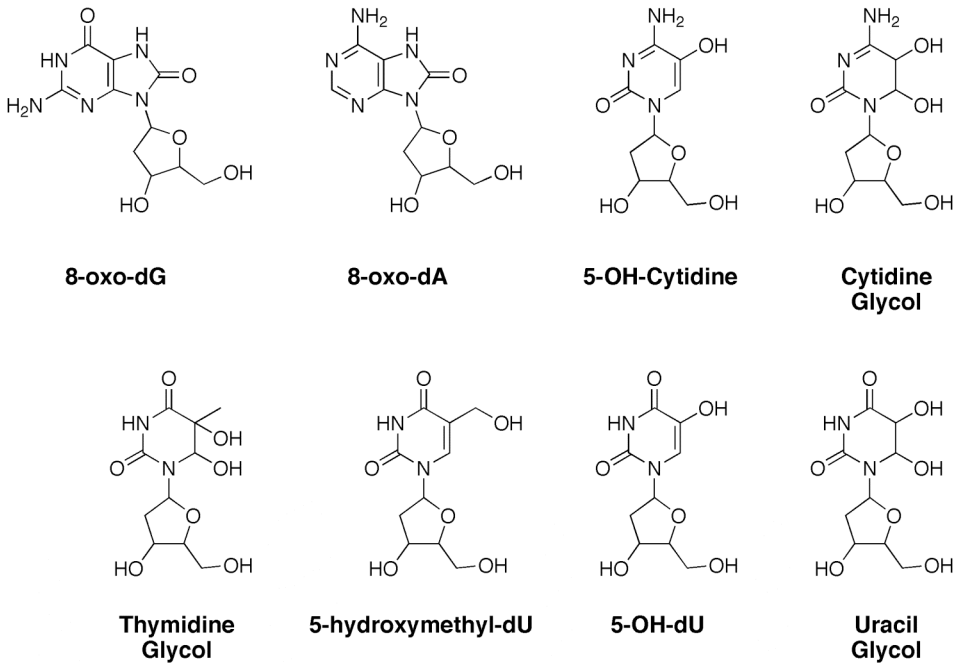

Figure 17. DNA adducts arising from direct oxidation of DNA by ROS.

Propano adducts

Acrolein is the prototype α,β-unsaturated aldehyde, which reacts across N^2 and N1 of dG to add three carbons and generate the exocyclic propano ring. The reaction

occurs via Michael addition of the olefin to either N1 or N^2 followed by 1,2-addition of the aldehyde to N^2 or N1, respectively. 1,N^2-8-Hydroxy-propanodeoxyguanosine (γ-OH-PdG) and 1,N^2-6-OH-PdG (α-OH-PdG) are the principal products with the former being the major isomer (**Figure 18**) (*163, 164*). Reaction of dG with crotonaldehyde produces a similar propano ring. However, addition occurs exclusively at the β-carbon of crotonaldehyde with N^2 of dG followed by reaction with the aldehyde at N1 yielding α-CH_3-γ-OH-PdG (**Figure 18)** (*164, 165*). 4-Hydroxy-2-nonenal addition to dG is identical to that seen for crotonaldehyde, resulting in the formation of α-hydroxyhexyl-γ-OH-PdG (**Figure 18**) (*166*). Reactions of crotonaldehyde and 4-hydroxy-2-nonenal with dG produce 4 diastereomers at the chiral centers (C_6 and C_8) of the propano ring. It is proposed that the stereochemistry of propano adducts affects their biological reactivity in the context of DNA (*167*).

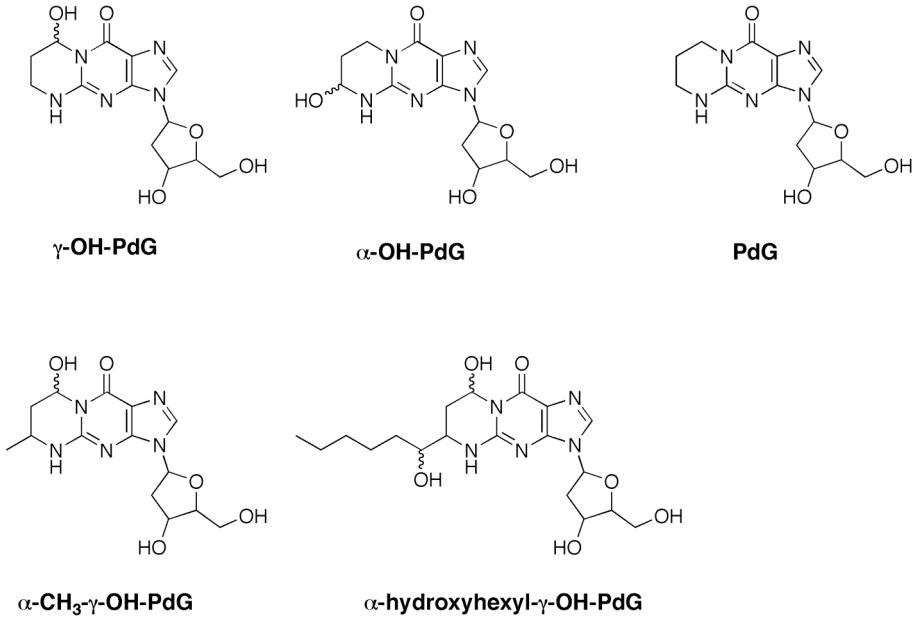

Figure 18. Propano DNA adducts of dG derived from lipid peroxidation products.

The propano ring is unsaturated and puckered in structure, which is distinctly different from the planar and aromatic character of the pyrimidopurinone ring of M_1dG. Like M_1dG, the propano rings derived from acrolein, crotonaldehyde, and 4-hydroxy-2-nonenal have been shown to ring open in duplex DNA (**Figure 19**) (*164, 168-170*). In the ring-opened state the extended oxopropyl side-chain may interact with neighboring nucleic acids and protein to form crosslinks. Several intra- and interstrand crosslinks have been identified for the propano adducts (*171-176*). The interchanging conformation of the propano adducts is believed to contribute to the broad array of genetic mutation exhibited by these adducts (*177-181*).

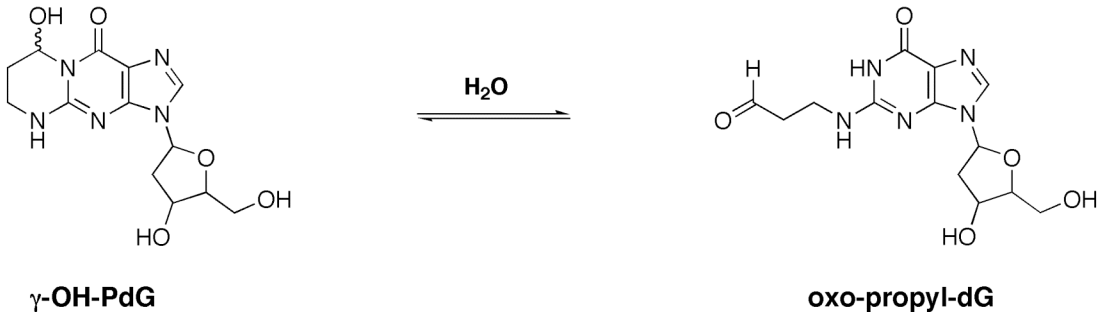

γ-OH-PdG **oxo-propyl-dG**

Figure 19. Hydrolytic ring opening of γ-OH-PdG to 3-oxo-1-propyl-dG.

Etheno adducts

The addition of two carbons across the exocyclic and ring nitrogens of dA, dG and dC produces an etheno bridge. Etheno addition grants fluorescent properties to the nucleosides. Originally, etheno adducts were the synthetic target of Leonard and colleagues, who were interested in obtaining fluorescent nucleotide derivatives to probe

for the biological activity and structure of nucleotide-containing enzymes and tRNA molecules (*182-184*). Some of the reagents commonly used to synthesize etheno adducts were found to be mutagens, such as chloroacetaldehyde (*185*). Chloroacetaldehyde was identified as a metabolite of the industrial contaminant, vinyl chloride (*186*). Later 1-chlorooxirane (another metabolite of vinyl chloride) was found to be more reactive with DNA than chloroacetaldehyde (*187*). Further study into the metabolism and reactivity of other alkyl halides revealed many of these molecules were either directly damaging to DNA or underwent metabolic transformation to reactive electrophiles capable of modifying DNA; etheno DNA adducts were an abundant and important product of their reactivity.

Four etheno adducts arise from exposure to alkyl halides: 1,N^6-ε-dA, 1,N^2-ε-dG, N^2-3-ε-dG, and 3,N^4-ε-dC (**Figure 20**). However, etheno adducts have also been found in genomic DNA of humans and animals in the absence of exposure to alkyl halides (*188-190*). Therefore, it was reasoned that etheno adducts must also have an endogenous origin. Based on previous work demonstrating the reactivity of substituted 2,3-epoxy-aldehydes (*191, 192*), Sodum and Chung demonstrated the formation of 1,N^2-ε-dG upon reacting dG with an epoxide derived from 4-hydroxy-2-nonenal (2,3-epoxy-4-hydroxy-nonenal) (*193*). El Ghissassi *et al.* later found that transition metal-mediated decomposition of microsomes supplemented with arachidonic acid in the presence of dA and dC led to the production of etheno adducts 1,N^6-ε-dA and 3,N^4-ε-dC (*194*). They hypothesized a similar mechanism for etheno adduct formation (*194*). However, it was later demonstrated that formation of 2,3-epoxy-4-hydroxy-nonenal in cells was unlikely (*195*).

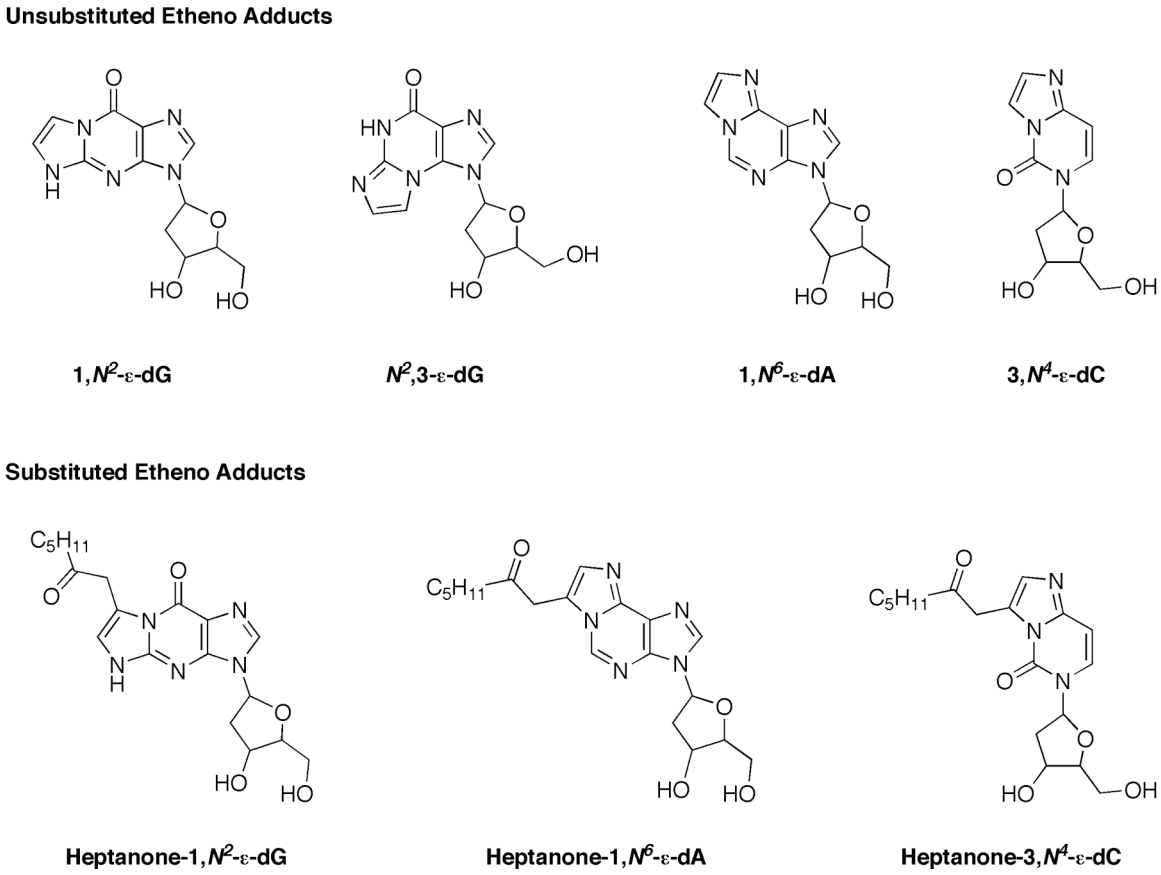

Figure 20. Unsubstituted and substituted etheno adducts.

Another mechanism of etheno adduct formation was proposed by Lee and Blair (*196, 197*). Lee and Blair in addition to Schneider and Brash have identified several highly reactive bifunctional electrophiles produced from the transition metal-mediated decomposition of lipid hydroperoxides (**Figure 8**) (*51-53*). Both 4-hydroperoxy-2-nonenal and 4,5-epoxy-2-decenal were characterized to react with dG and dA to form two unsubstituted etheno adducts, 1,N^6-ε-dA and 1,N^2-ε-dG (*196, 197*). The proposed

mechanism of addition by 4-hydroperoxy-2-nonenal proceeds by 1,2-addition of the exocyclic *N*-amino group to the aldehyde, followed by intramolecular cyclization to an epoxide intermediate, which either decomposes directly or sequentially dehydrates to the etheno product (**Figure 21**) (*196*).

Substituted etheno adducts have also been characterized from the addition of lipid peroxidation products to nucleosides. Reactions of 4-oxo-2-nonenal with dG, dA, and dC produce substituted etheno adducts containing a heptanone chain extended from the etheno carbon proximal to the ring nitrogen (**Figure 20**) (*198-200*). 4-Oxo-2-nonenal appears to be most reactive with dC (*200, 201*). This type of reaction is indicative of 1,2-addition of the exocyclic *N*-amino group to aldehyde followed by intramolecular cyclization on the ring nitrogen (**Figure 22**). Other substituted etheno adducts have been characterized in reactions of nucleic acids with lipid peroxidation products (*50, 202, 203*).

Etheno addition forms across the Watson-Crick base-pairing surface, and all etheno adducts that have been investigated exhibit miscoding properties. Etheno adducts are mutagenic in bacterial and mammalian cells (*188, 204-209*), and they mainly yield base-pair substitutions. Unlike the propano and pyrimidopurinone adducts, the etheno adducts are not subject to ring-opening; although, etheno adducts may react under basic or acidic conditions to produce hydrated derivatives (*210*).

Etheno adducts have been analyzed in the DNA and urine of animals and humans. 1,N^6-ε-dA is found in human liver DNA at levels of 0.2 – 3.0 per 10^8 bases and 1,N^6-ε-Ade has been quantified in human urine at levels of 40 – 3000 pg/mL (*189, 211, 212*). 3,N^4-ε-dC was found in human liver DNA at levels of 0.8 – 3.0 per 10^8 bases. In human

urine, 3,N^4-ε-Cyd is reported to be present at 0.6 – 3.0 ng/kg/mg creatinine and 3,N^4-ε-dC at concentrations of 0.0 – 800 pM (*213, 214*). The genomic levels of 1,N^2-ε-dG have been determined in rat liver at levels of 50 per 10^8 bases (*215*); however, the genomic and urinary levels of 1,N^2-ε-dG and 1,N^2-ε-Gua have escaped detection in humans. The levels of substituted etheno adducts have not been reported in urine samples. However, heptanone-1,N^2-ε-dG and heptanone-3,N^4-ε-dC have been found in mouse intestine at levels of 6 – 18 per 10^8 bases and 1 – 10 per 10^8 bases, respectively (*216*).

The repair mechanisms for the unsubstituted etheno adducts are unknown. However, NER is likely to be involved. Each unsubstituted etheno adduct is subject to base excision repair by DNA glycosylases. 1,N^6-ε-dA is repaired by alkylpurine-DNA-*N*-glycosylase in mammalian cells (*217, 218*), as is 1,N^2-ε-dG (*217, 219*). N^2,3-ε-dG is a substrate for 3-methyl-adenine DNA glycosylase (*220*), and 3,N^4-ε-dC is removed by the mismatch specific thymine-DNA glycosylase (*221-223*). Glycosylases catalyze the hydrolytic removal of the adducted base from the DNA helix and leave an apurinic/apyridinic site. The remaining abasic site is nicked, removed, filled in by a polymerase, and re-ligated to the helix (*224*). Cleavage products formed by glycosylase action are, therefore, released from DNA as base adducts. The metabolic stability of etheno adducts will be evaluated in Chapter 6.

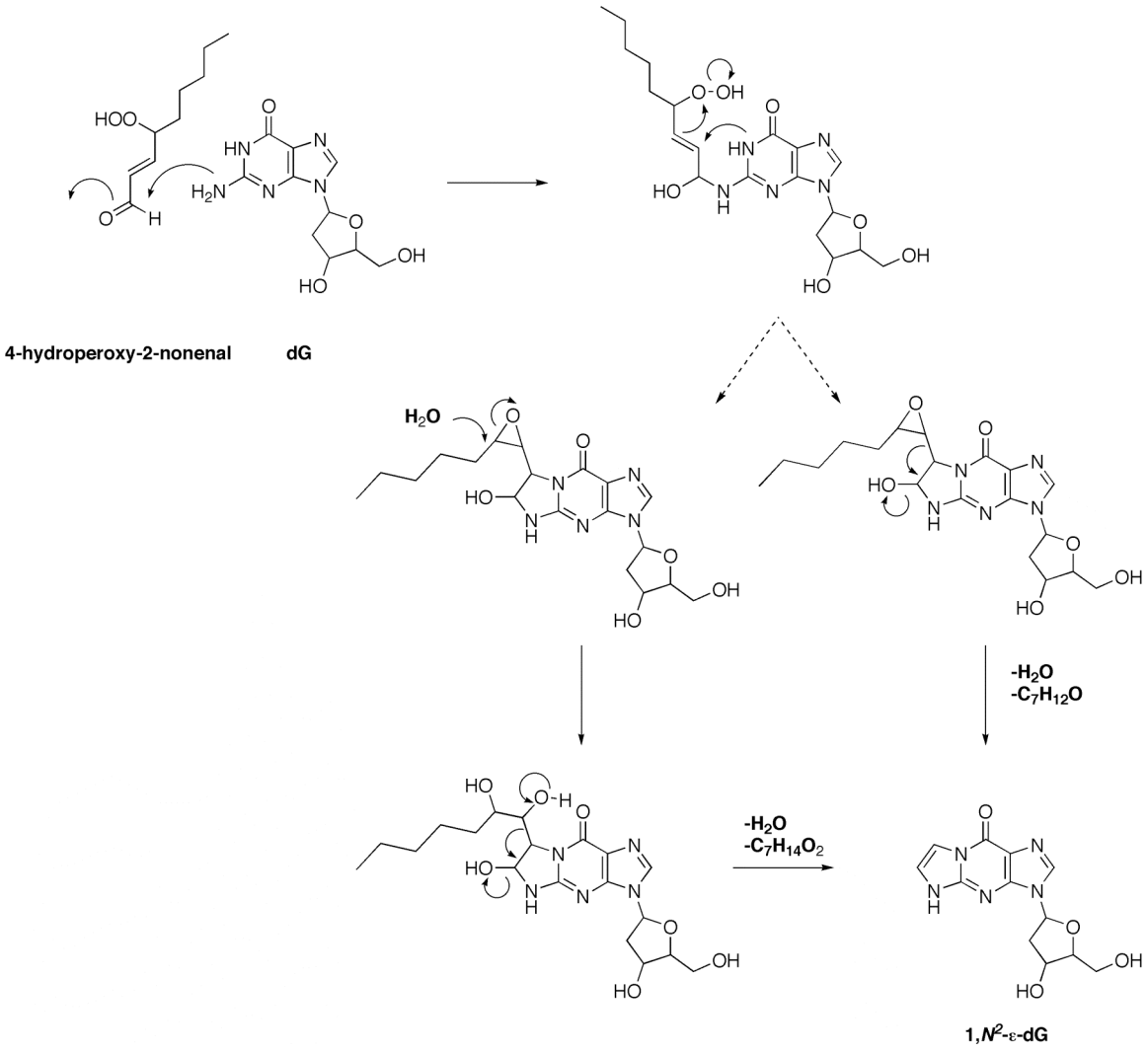

Figure 21. Proposed mechanism of formation for 1,N^2-ε-dG from reaction of 4-hydroperoxy-2-nonenal with dG (Figure adapted from (*196*)).

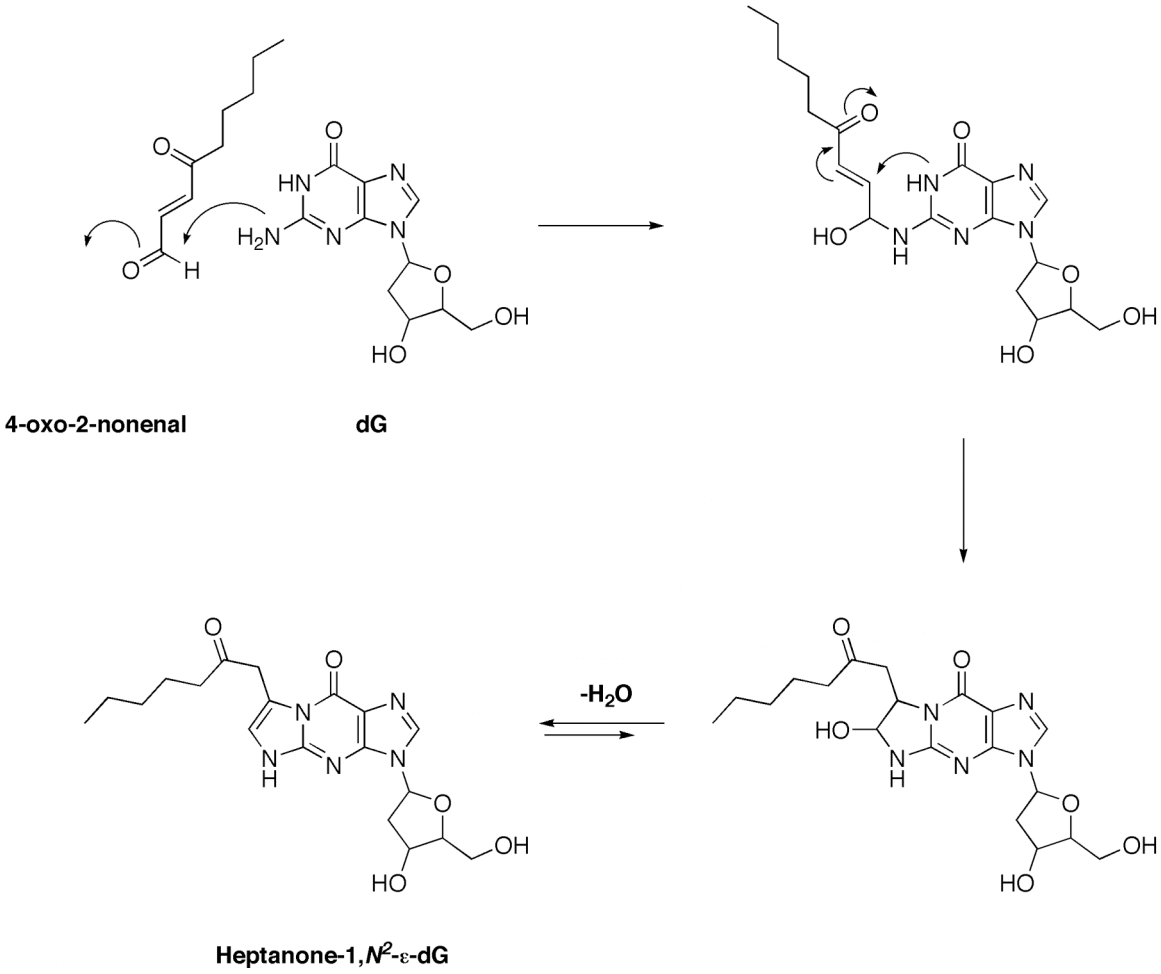

Figure 22. Proposed mechanism of formation for heptanone-1,N^2-ε-dG from reaction of 4-oxo-2-nonenal with dG (Figure adapted from (*199*)).

Dissertation Aims

The goal of this dissertation is to address the hypothesis that endogenously formed DNA adducts are subject to oxidative metabolism. Particular emphasis will be placed on defining the *in vitro* and *in vivo* metabolism of M_1dG. Chapter 2 will evaluate the enzymology and kinetics of M_1dG metabolism in the rat. In Chapter 3 a definitive evaluation of the metabolism and elimination of M_1dG in the rat will be reported by the use of carbon-14 labeled M_1dG. The metabolism and elimination of M_1dG at near-physiological levels will be addressed in Chapter 4 by the use of accelerator mass spectrometry. Evaluation of the *in vitro* and *in vivo* metabolism of free base, M_1G, will be discussed in Chapter 5. Chapter 6 will address the metabolism of other structural analogs of M_1dG and M_1G.

CHAPTER II

METABOLISM OF M_1dG *IN VITRO* AND *IN VIVO*

Summary

M_1dG is an endogenous DNA adduct arising from the reaction of dG with the lipid peroxidation product, MDA, or the DNA peroxidation product, base propenal. M_1dG is mutagenic in bacteria and mammalian cells and is present in genomic DNA of healthy human beings. It is also detectable at low levels in the urine of healthy individuals, which may make it a useful biomarker of DNA damage linked to oxidative stress. We investigated the possibility that the low urinary levels of M_1dG reflects metabolic conversion to others derivatives. M_1dG was rapidly removed from plasma ($t_{1/2}$ = 10 min) following intravenous (iv) administration to rats. A single urinary metabolite was detected and identified as 6-oxo-M_1dG by mass spectrometry, NMR spectroscopy, and independent chemical synthesis. 6-Oxo-M_1dG was generated *in vitro* by incubation of M_1dG with rat liver cytosol. Experiments with chemical inhibitors *in vitro* and *in vivo*, in addition to studies with partially purified enzymes, suggested that xanthine oxidoreductase (XOR) and aldehyde oxidase (AO) are involved in the oxidative metabolism. M_1dG was also metabolized by three separate human liver cytosol preparations indicating 6-oxo-M_1dG is a likely metabolite in humans. This represents the first report of the oxidative metabolism of an endogenous DNA adduct and raises the possibility that other endogenous DNA adducts are metabolized by oxidative pathways.

6-Oxo-M_1dG may be a useful biomarker of endogenous DNA damage associated with inflammation, oxidative stress, and certain types of cancer chemotherapy.

Introduction

M_1dG is an adduct found at varying levels in genomic DNA of rodents and humans (*149, 152, 225*). It is derived from the lipid peroxidation product, MDA, or the DNA peroxidation product, base propenal (**Figure 23**) (*58, 96*). M_1dG is miscoding when assayed by *in vitro* DNA replication and is mutagenic in bacterial and mammalian cells (*120, 121, 226*). It induces base pair substitutions (M_1dG→T and M_1dG→A) and frameshift mutations in reiterated sequences (e.g., CG_n) when shuttle vectors containing a site-specific lesion are replicated in COS-7 cells (*227*). Genetic and biochemical experiments indicate that M_1dG is removed by NER in both bacterial and mammalian cells (*120, 122*).

As a prerequisite for preclinical, clinical, and population-based studies of the factors that contribute to the production of M_1dG, we are developing assays to quantify the adduct in urine. We recently described a highly sensitive and specific analytical method based on immunoaffinity purification and LC-MS/MS analysis (*154*). Application of this technique reveals that M_1dG is detectable in the urine of healthy human volunteers in amounts corresponding to 10-20 fmol/kg/24 h (*154*). These values are several orders of magnitude lower than the levels reported for another oxidative DNA lesion, 8-oxo-dG (~400 pmol/kg/24 h) (*155, 156*). The lower levels of M_1dG may reflect lower levels in genomic DNA, less efficient repair, or differential processing before excretion. Previous studies have established that DNA adducts from xenobiotics

(ethylene dibromide) or drugs that are based on nucleobases (O^6-benzylguanine, allopurinol) are metabolized by hydrolytic processing to mercapturic acids or by oxidation, respectively (*228, 229*). However, no reports suggest that endogenous DNA lesions are metabolized following repair. We report here that M_1dG is oxidized in rats to a novel 6-oxo derivative and that enzymes of the purine salvage pathway appear to play a role. Based on *in vitro* and *in vivo* experiments with chemical inhibitors and with partially purified enzymes, both XOR and AO were found to be involved in the metabolic processing of M_1dG. Several other endogenously formed exocyclic adducts are structurally similar to M_1dG. This suggests the possibility that other endogenous DNA lesions may be metabolized after they are repaired and that an additional, as yet unaccounted for, population of adducts may exist in urine that could serve as biomarkers of endogenous DNA damage.

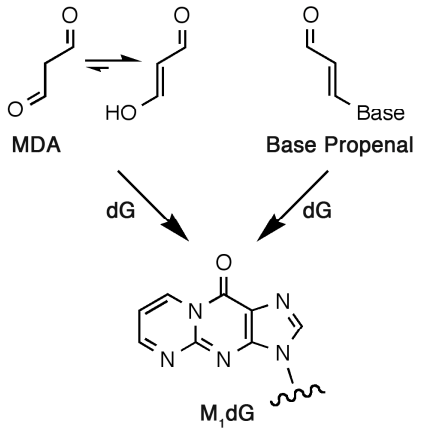

Figure 23. Endogenous formation of M_1dG from MDA or base propenal. M_1dG is produced from the reaction of dG with either the lipid peroxidation product, MDA, or the DNA peroxidation product, base propenal.

Experimental Procedures

Chemicals and reagents

All chemicals were obtained from commercial sources and used as received. Solvents were of HPLC grade purity or higher. M_1dG was synthesized as described (*230*). Human liver cytosol preparations were purchased from BD Bioscience (Woburn, MA). Rat liver cytosol was prepared by established methods (*231*) or purchased from BD Bioscience (Woburn, MA), Xenotech (Lenexa, KA), or InvitroTechnologies (Baltimore, MA). Bovine XO (from buttermilk) was obtained from CalBiochem (La Jolla, CA). HPLC separations were performed using a Waters 2695 autosampler and binary pump with a Waters 2487 dual wavelength UV detector. LC-MS/MS spectra were obtained on a Finnigan TSQ 7000 instrument .

Administration of M_1dG to rats

Animal protocols were performed under approval of Vanderbilt University and in accordance with the Institutional Animal Care and Use Committee policies. Male Sprague Dawley rats (225-250 g) uncatheterized or catheterized in the femoral and jugular veins were obtained from Charles River Laboratories (Wilmington, MA) and housed in shoebox cages. Animals were transferred to metabolism cages prior to dosing and allowed to feed *ad libitum* throughout the experiment. The dosing solution was prepared in sterile saline solution and administered in the jugular vein of catheterized rats at 2 mg/kg in approximately 0.5 mL of total volume. The dose was delivered over 45 s and the catheter was flushed with 0.4 mL of sterile heparinized saline. A portion of whole

blood (0.5 mL) was removed at intervals (0.17, 0.33, 0.5, 1, 2, 4, 6, and 24 h) post-dose from the femoral vein and placed on ice. To maintain constant circulatory volume, 0.5 mL of heparinized saline was injected following blood draws. Plasma was separated by centrifugation and removed. Urine was collected over intervals (pre-dose, 0-4, 4-6, 6-16, and 16-24 h). A standard curve was prepared by spiking known concentrations of M_1dG into whole blood obtained from unaltered, male Sprague Dawley rats and processed as above. All samples were stored at -80 °C until sample work-up.

Sample work-up and analysis

A sample of urine (0.4 mL) was extracted by adding 0.8 mL ethanol followed by 0.8 mL chloroform. Following vigorous mixing, the phases were separated by centrifugation. The organic layer was removed, and the remaining aqueous layer was extracted with an additional 0.8 mL chloroform. The organic layers were pooled, dried under nitrogen, and reconstituted in potassium phosphate (0.2 M, pH 7.5). Plasma (0.15 mL) was diluted to 0.25 mL with 0.2 M potassium phosphate, pH 7.5, and processed as above. Samples (10 μL) were loaded onto a Phenomenex Luna C18(2) column (2.0 x 250 mm, 5 μm) (Torrence, CA) equilibrated with 90% solvent A (0.5% formic acid in H_2O) and 10% solvent B (0.5% formic acid in methanol) at a flow rate of 0.3 mL/min. The solvent was programmed as follows: a linear gradient from the starting solvent to 20% B in 10 min, holding at 20% B for 10 min increasing to 80% B in 0.1 min, holding for 5 min, decreasing to 10% B in 0.1 min, and re-equilibrating at initial conditions for 5 min. Eluting compounds were detected by UV absorbance at 254 nm or by liquid chromatography/mass spectrometry (LC/MS). Positive ion ESI was employed with the

following parameters: spray voltage = 4.5 kV; capillary temperature = 200 °C; sheath gas = 60 psi; CID pressure = 2.3 mTorr (nitrogen gas); and 15 eV collision energy. Samples were analyzed by selected reaction monitoring, which followed the neutral loss of deoxyribose from M_1dG (*m/z* = 304.3 → 188.3). The method was adapted to scan for the presence of an additional oxygen atom in the pyrimidopurinone ring by scanning eluting peaks for the transition *m/z* 320.3 → 204.3.

Co-administration of allopurinol and M_1dG to rats

Six male Sprague Dawley rats (225-250 g) catheterized in the femoral and jugular veins were obtained from Charles River Laboratories (Wilmington, MA) and housed in shoebox cages. M_1dG dosing solution (5 mg/mL) was prepared in sterile saline solution and administered via the jugular vein catheter in approximately 0.4 mL of total volume and delivered over 45 s. Allopurinol dosing solution (10 mg/mL) was prepared in sterile saline solution, to which was added one equivalent of sodium hydroxide to bring the allopurinol into solution, and administered via the jugular vein catheter in approximately 0.4 mL of total volume and delivered over 45 s. Upon arrival animals either received an iv dose of allopurinol (n = 3) or vehicle control (saline solution, n = 3). This dosing procedure was repeated after 24 h. Animals were transferred to metabolism cages prior to M_1dG dosing and allowed to feed *ad libitum* throughout the experiment. One h prior to M_1dG dosing, animals either received a final administration of either allopurinol or vehicle control dosing solution. M_1dG dosing solution was administered via the jugular vein catheter in approximately 0.4 mL of total volume. Following administration of M_1dG a portion of whole blood (0.5 mL) was removed at intervals (0.17, 0.33, 0.5, 1, 2,

4, 6, and 24 h) from the femoral vein post-dose and placed on ice. To maintain constant circulatory volume, 0.5 mL of heparinized saline was injected following blood draws. Plasma was separated by centrifugation and removed. Urine was collected over intervals (pre-dose, 0-4, 4-8, 8-24, and 24-30 h). A standard curve was prepared by spiking known concentrations of M_1dG into whole blood obtained from unaltered, male Sprague Dawley rats and processed as above. All samples were stored at -80 °C until sample work-up.

Analytical analysis of *in vivo* allopurinol co-administration samples

A sample of urine (0.4 mL) was extracted by adding 0.8 mL ethanol followed by 0.8 mL chloroform. Following vigorous mixing, the phases were separated by centrifugation. The organic layer was removed, and the remaining aqueous layer was extracted with an additional 0.8 mL chloroform. The organic layers were pooled, dried under nitrogen and reconstituted in potassium phosphate (0.2 M, pH 7.5). Plasma (0.15 mL) was diluted to 0.25 mL with 0.2 M potassium phosphate, pH 7.5, and processed as above. Samples (10 μL) were loaded onto a Phenomenex (Torrence, CA) Luna C18(2) column (2.0 x 250 mm, 5 μm) equilibrated with 90% solvent A (0.5% formic acid in H_2O) and 10% solvent B (0.5% formic acid in methanol) at a flow rate of 0.3 mL/min. The solvent was programmed as follows: a linear gradient from the starting solvent to 20% B in 10 min, holding at 20% B for 10 min, increasing to 80% B in 0.1 min, holding for 5 min, decreasing to 10% B in 0.1, min and re-equilibrating at initial conditions for 5 min. Eluting compounds were detected by UV absorbance at 254 nm or by LC/MS. Positive ion ESI was employed with the following parameters: spray voltage = 4.5 kV; capillary temperature = 200 °C; sheath gas = 60 psi; CID pressure = 2.3 mTorr (nitrogen

gas); and 15 eV collision energy. Samples were analyzed by selected reaction monitoring, which followed the neutral loss of deoxyribose from M_1dG (*m/z* = 304.3 → 188.3). The method was adapted to scan for the presence of an additional oxygen atom in the pyrimidopurinone ring by scanning eluting peaks for the transition *m/z* 320.3 → 204.3.

Biochemical synthesis of the M_1dG metabolite

Rat liver cytosol (20 mL solution of 20 mg protein/mL) was incubated with 10 mg of M_1dG and allowed to react to completion. The reaction was monitored by HPLC (conditions described below) and terminated by the addition of one volume of acetonitrile to precipitate the protein. The resulting mixture was centrifuged and the supernatant was lyophilized overnight. The residue was reconstituted in water and applied to a preconditioned C18 solid phase extraction column (Waters Oasis® HLB), which was washed twice with water and eluted with methanol. The purified sample was evaporated to dryness and analyzed by NMR. ^{1}H-NMR (300 MHz, D_2O): δ 8.71 (d, 1H *J* = 8 Hz, H_8), 8.13 (s, 1H, H_2), 6.4-6.3 (m, 2H, H_7 and H_1'), 4.61 (m, 1H, H_3'), 4.05 (m, 1H, H_4'), 3.73 (m, 2H, H_5', H_5''), 2.85-2.51 (m, 2H, H_2', H_2''). ^{13}C-NMR (500.13 MHz, D_2O): δ 84.3 ($C_{1'}$), 109.5 (C_7), 116.6 (C_{10a}), 135.4 (C_8), 140.1 (C_2), 149.8 (C_6), 150.4 (C_{3a}), 154.5 (C_{10}) and 168.8 (C_{5a}).

Chemical synthesis of 3-(2-Deoxy-β-D-erythropentofuranosyl)-pyrimido[1,2-*f*]purine-6,10(3*H*,5*H*)-dione (6-oxo-M_1dG)

Ethyl 2-amino-9-(2-deoxy-β-D-erythropentofuranosyl)-6,9-dihydro-6-oxo-1H-purine-1-acrylate. dG hydrate was dried in an Abderhalden apparatus overnight at 78 °C

under vacuum. A mixture of anhydrous dG (134 mg, (0.5 mmol), K_2CO_3 (104 mg, 0.75 mmol), and ethyl *cis*-3-bromoacrylate (135 mg, 0.75 mmol) in anhydrous *N,N*-dimethylformamide (DMF, 10 mL) was added to a flame-dried round bottom flask and stirred overnight at 64 °C. HPLC analysis of the reaction mixture showed that nearly all of the dG had been consumed. The mixture was cooled to room temperature, filtered, and the filtrate was concentrated under high vacuum. In general, the crude product was used in the next step without further purification. A portion of the product was purified by C18 reversed-phase HPLC for characterization.. ^{1}H NMR (CD_3OD): d 8.00 (s, 1H), 7.56 (d, J = 14.4 Hz, 1H), 6.61 (d, J = 14.4 Hz, 1H), 6.27 (t, J = 6.9 Hz, 1H), 4.52 (m, 1H), 4.19 (q, J = 7.2 Hz, 2H), 4.00 (m, 1H), 3.75 (m, 2H), 2.68 (m, 1H), 2.35 (m, 1H), 1.27 (t, J = 7.2 Hz, 3H).

3-(2-Deoxy-β-D-erythropentofuranosyl)-pyrimido[1,2-f]purine-6,10(3H,5H)-dione (6-oxo-M_1dG). The crude acrylate (*vide supra*) was suspended in anhydrous methanol (4 mL). Sodium methoxide (0.5 mmol, 1 mL of a 0.5 M solution in methanol) was added dropwise to the stirred suspension, resulting in a clear solution. HPLC analysis showed the completed conversion of the starting material after stirring at room temperature for 1 h. The reaction mixture was neutralized by the addition of acetic acid (30 mL, 0.5 mmol) and evaporated under reduced pressure. The residue was dissolved in a 1:1 mixture of methanol and water (0.5-1 mL) and purified on a BIOTAGE® system using a C18 reversed-phase column (C18HS 12+M) with a linear gradient from 0% to 20% acetonitrile in water to give the desired product (71 mg, 44 % yield from dG). The proton NMR spectrum was identical to that of the biochemically synthesized metabolite from rat liver cytosol described above.

Liver cytosol incubations and analysis

All sample preparation was performed on ice at 4 °C. The final incubation conditions for the kinetic determinations contained rat liver cytosol (5 mg/mL), varied concentrations of M_1dG (20, 40, 50, 60, 80, 100, 120, 200, 400, or 800 μM), and 0.4% DMSO in 0.2 M potassium phosphate buffer, pH 7.4. The final incubation conditions for the inhibition studies were performed with rat liver cytosol (5 mg/mL) or human liver cytosol (5 mg/mL), 370 μM M_1dG, 160 μM inhibitor (allopurinol or menadione), and 0.4% DMSO in 0.2 M potassium phosphate, pH 7.4. The inhibitors were diluted in DMSO. IC_{50} determinations were performed with rat liver cytosol (5 mg/mL), 370 μM M_1dG, with inhibitor (allopurinol, menadione, raloxifene) adjusted to logarithmic intervals between 1 nM and 500 μM. The buffer contained 0.4% DMSO in 0.2 M potassium phosphate (pH 7.4). In all experiments reagents were equilibrated to 37 °C for 5 min, initiated by the addition of substrate, and terminated after 60 min by the addition of two volumes of ice-cold ethanol. Samples were then extracted twice with two volumes of chloroform. The extracts were evaporated under nitrogen, reconstituted in 0.2 M potassium phosphate, pH 7.4, and analyzed by HPLC as described above. Samples from the kinetic determination were analyzed for M_1dG content by comparison to a standard curve prepared by spiking known concentrations of M_1dG into rat liver cytosol solutions (5 mg/mL) followed immediately by termination, extraction, and analysis. Percent inhibition of inhibitors was determined in reference to 0 and 60 min standards. V_{max}, K_m, and IC_{50} values were calculated with Prism software (Version 4.0c) using nonlinear regression one-site binding and one-site competition models, respectively. All experiments were performed in triplicate.

Bovine XO incubations and analysis

Purified bovine XO from buttermilk (CalBiochem) was used for *in vitro* incubations. All sample preparation was performed on ice at 4 °C. The final incubation conditions for the kinetic determinations contained XO (0.05 mg/mL) and varied concentrations of M_1dG (10, 25, 50, 100, 200, 350, 500, 600, 700, or 800 μM) in 0.2 M potassium phosphate (pH 7.8). IC_{50} determinations were performed with XO (0.05 mg/mL), 370 μM M_1dG, and allopurinol adjusted to logarithmic intervals between 1 nM and 500 μM in a 0.2 M potassium phosphate (pH 7.8). In all experiments reagents were equilibrated to 37 °C for 5 min, initiated by the addition of substrate, and terminated after 30 min by the addition of 100 μL ice-cold methanol, vortexed, and placed on ice. Samples (300 μL) from each incubation were transferred to separate vials and centrifuged at 200,000 g for 20 min at 4 °C. Aliquots (200 μL) were removed and placed into autosampler vials for analysis by HPLC with UV detection. Samples from the kinetic determination were quantified based on substrate consumption in reference to an M_1dG standard curve. The standard curve was prepared by spiking known concentrations of M_1dG into XO solutions (0.05 mg/mL) on ice previously spiked with 100 μL methanol and processed as above. Percent inhibition during IC_{50} analysis was determined in reference to 0 and 30 min standards. V_{max}, K_m, and IC_{50} values were calculated with Prism software (Version 4.0c) using nonlinear regression one-site binding and one-site competition models, respectively. All experiments were performed in triplicate.

Purification of XOR and AO from rat liver

The purification of XOR and AO was based on several literature references (*232-238*). Approximately 100 g of liver were excised from anesthetized Sprague Dawley rats, pooled, and homogenized in 50 mM potassium phosphate, pH 7.8, containing 0.2 mM phenylmethanesulfonyl fluoride (PMSF). The homogenate was spun at 500 g for 10 min to remove nuclei and cell debris. The remaining supernatant was heated gradually to 55 °C and maintained at 55 °C for 10 min. The solution was then centrifuged at 10,000 g for 3 h. The supernatant was removed and brought to 60% saturation with ammonium sulfate and allowed to stir overnight. This solution was then centrifuged at 10,000 g for 30 min. The supernatant was discarded and the pellet was dissolved in a minimum amount of 100 mM potassium phosphate, pH 7.8, and centrifuged at 250,000 g for 3 h. The remaining supernatant was then concentrated with an Amicon filtration device to 5% total volume twice and applied to a ceramic hydroxyapatite column (CHT, BioRad, 2.6 x 30 cm) equilibrated in 100 mM potassium phosphate (pH 7.8). The column was washed with 3 column volumes of 100 mM potassium phosphate, pH 7.8, and the retained protein was eluted with a linear gradient of 100 to 400 mM potassium phosphate, pH 7.8 over 2 column volumes. Fractions were collected and analyzed for AO and XOR activity as described above. Fractions containing AO and XOR activity were pooled separately, concentrated, and buffer-exchanged into 100 mM Tris-HCl, pH 7.8, with 0.001 M EDTA and applied separately to a MonoQ anion exchange column (GE Healthcare, 1.6 x 10 cm) equilibrated in 100 mM Tris-HCl (pH 7.8) containing 0.001 M EDTA. The column was washed with 3 column volumes of equilibration buffer and eluted with a linear gradient of 0.0 to 0.5 M NaCl in equilibration buffer. Fractions containing AO and XOR activity

were pooled separately. AO fractions were exchanged into 0.1 M Tris-glycine, pH 9.0, containing 0.001 M EDTA and applied to a Benzamidine-Sepharose 6B affinity column (GE Healthcare, 1.6 x 10 cm) equilibrated in 0.1 M Tris-glycine containing 0.001 M EDTA (pH 9.0). The column was eluted with 50 mM *p*-aminobenzamidine dissolved in equilibration buffer. XOR containing fractions were exchanged into 0.1 M potassium phosphate, pH 7.8, containing 0.001 M EDTA and loaded onto a HiTrap Sephadex 200 gel filtration column (GE Healthcare, 1.6 x 60 cm). Fractions containing XOR activity were pooled and saved.

Analytical analysis of protein samples

Column fractions (~100 μL) were incubated with 200 μM M_1dG at 37 °C in 0.2 M potassium phosphate, pH 7.4, for 60 min and terminated with 2x volume of ethanol. The samples were extracted into chloroform (2x volume) and separated by centrifugation. The organic layer was removed and the remaining aqueous layer was extracted with an additional 2x volume of chloroform. The organic layers were pooled, dried under nitrogen, and reconstituted in potassium phosphate (0.2 M, pH 7.4). Samples (20 μL) were loaded onto a Phenomenex (Torrence, CA) Luna C18(2) column (4.6 x 250 mm, 5 μm) equilibrated with 90% solvent A (0.5% formic acid in H_2O) and 10% solvent B (0.5% formic acid in methanol) at a flow rate of 1.0 mL/min. The solvent was programmed as follows: a linear gradient from the starting solvent to 20% B in 10 min, holding at 20% B for 10 min, increasing to 80% B in 0.1 min, holding for 5 min, decreasing to 10% B in 0.1 min, and re-equilibrating at initial conditions for 5 min. Eluting compounds were detected by UV absorbance at 254 nm.

Activity assays

XOR activity was assessed by monitoring the conversion of xanthine to uric acid at 295 nM (ε_{295} 95000 $M^{-1}cm^{-1}$) in 0.1 M potassium phosphate, pH 7.8, at room temperature. AO activity was assessed by monitoring the disappearance of 4-(dimethylamino)-cinnamaldehyde at 398 nM (ε_{398} 30500 $M^{-1}cm^{-1}$) in 0.1 M potassium phosphate, pH 7.8, at room temperature.

Results

Administration of M_1dG to rats

Sprague Dawley rats, cannulated in the femoral and jugular veins, were obtained commercially and housed in metabolic cages during the course of the experiment. M_1dG (2 mg/kg) was administered iv in the jugular vein and whole blood was drawn at intervals from the femoral vein. Additionally, urine was collected over the time-course of the study to monitor the excretion of M_1dG. Plasma and urine extracts were separated by reversed-phase HPLC and eluting peaks were detected by either UV absorbance or positive ion ESI LC-MS/MS. M_1dG in plasma samples was analyzed by selective reaction monitoring following the neutral loss of deoxyribose from M_1dG (*m/z* 304.3 → 188.3) and quantified against a standard curve.

Figure 24 displays the time-course of M_1dG disappearance from plasma following iv administration. M_1dG was rapidly removed from plasma with a half-life of approximately 10 min. Parallel analysis of urine samples revealed that the disappearance of M_1dG was not solely accounted for by rapid elimination of M_1dG in the urine.

Approximately 80% of the total excreted M_1dG was recovered during the first 4 h of urine collection (**Figure 24, inset**) and M_1dG was detectable as long as 24 h after administration.

The rapid disappearance of M_1dG from plasma suggested it was rapidly distributed to tissue and subject to biotransformation. Urine and plasma samples were probed for the presence of metabolites containing an additional oxygen atom by performing HPLC with selected reaction monitoring of *m/z* 320.3 → 204.3. **Figure 25** displays a representative profile from a urine extract collected from 0 to 4 h following administration of M_1dG. A single peak that eluted shortly after M_1dG was detected. UV profiles from pre-dose urine showed nearly identical background traces to those from the dosed samples, with the exception of peaks eluting at 12.8 and 13.5 min (corresponding to M_1dG and the putative metabolite, respectively). The putative metabolite was also observed in plasma one h following administration. M_1dG was stable in urine and did not exhibit conversion to the putative metabolite on standing for up to 24 h. Attempts to discover additional metabolites in the urine samples were unsuccessful. For example, treatment with β-glucuronidase yielded neither M_1dG nor the later eluting product, suggesting that neither of these compounds was a substrate for glucuronidation *in vivo*.

Oxidation of M_1dG *in vitro*

These *in vivo* studies suggested M_1dG was subject to oxidation prior to excretion. In an attempt to characterize the pathway(s) responsible for metabolism, M_1dG was incubated with liver microsomal and cytosol fractions prepared from Sprague Dawley rats. Microsomal fractions failed to metabolize M_1dG either in the absence or presence

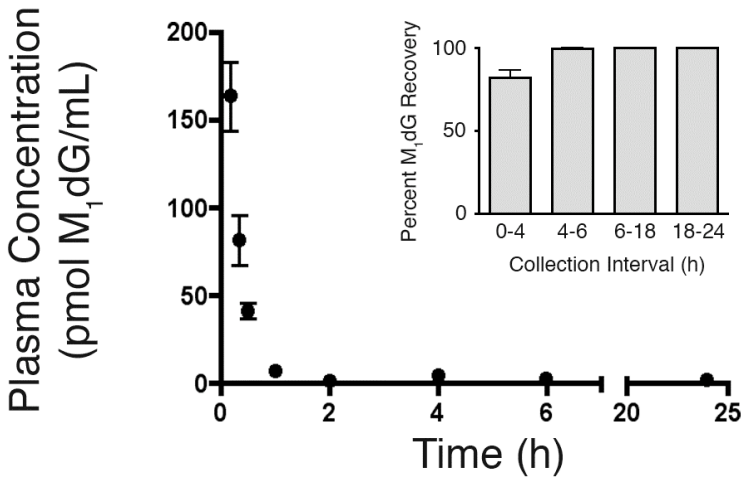

Figure 24. Time-course of M_1dG disappearance from plasma following iv administration. M_1dG (2 mg/kg) was administered to male Sprague Dawley rats (n = 3). Quantification was performed by LC-MS/MS with selected reaction monitoring of M_1dG following the *m/z* transition of 304.3 → 188.3. *Inset,* the time-course for appearance of M_1dG in urine following iv administration of M_1dG (n = 3).

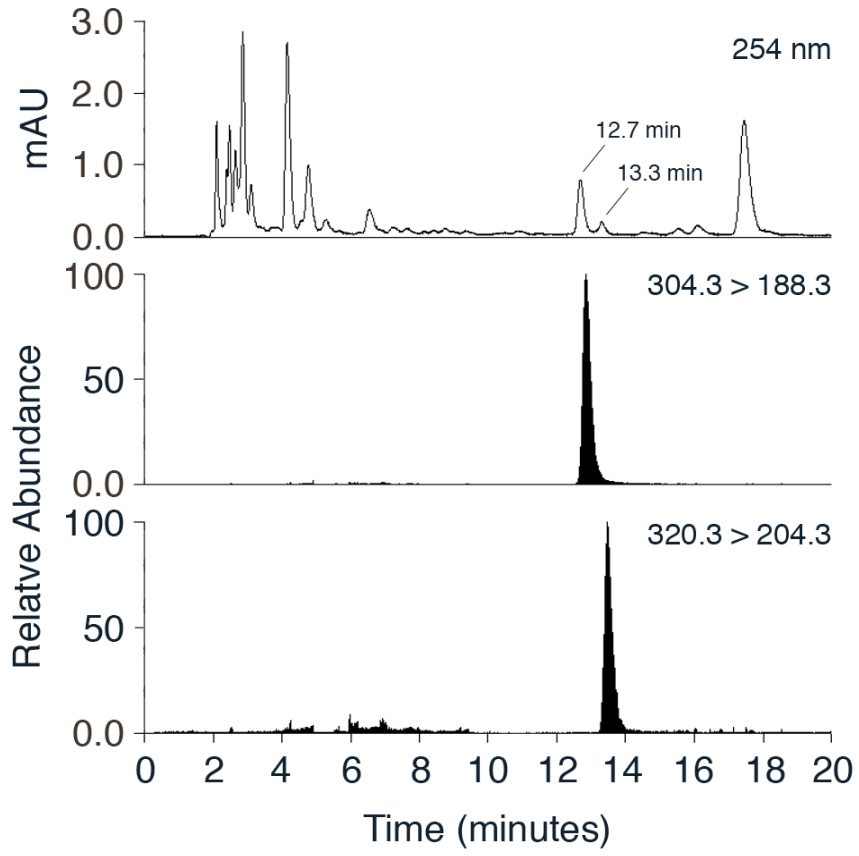

Figure 25. LC-UV and LC–MS/MS analysis of urine from rats treated with M_1dG. M_1dG (2 mg/kg) was administered to Sprague Dawley and urine collected from 0 – 4 h. M_1dG was monitored by the transition *m/z* 304.3 → 188.3 and the putative oxidized metabolite by the transition *m/z* 320.3 → 204.3.

of NADPH. However, cytosolic fractions rapidly converted M_1dG to a single product that exhibited an HPLC retention time and mass spectrum identical to the product detected in urine. Metabolite formation was dependent on substrate concentration, protein concentration, and the time of incubation. Oxidation of M_1dG by rat liver cytosol exhibited a K_m of 370 μM and a V_{max} of 104 pmol/min/mg protein (**Figure 26,** Top). **Figure 26 (**Bottom**)** displays the M_1dG concentration-dependence of product formation. There was a close correspondence between the concentration-dependence of M_1dG consumption and that for product formation. The latter demonstrated a K_m of 330 μM.

Biochemical synthesis of the M_1dG metabolite

To identify the product of *in vitro* enzymatic oxidation, 20 mL of concentrated rat liver cytosol (20 mg/mL) was incubated with 10 mg of M_1dG, and oxidation allowed to proceed to completion. The metabolite was purified and dissolved in D_2O for NMR analysis. A small amount of unreacted M_1dG was apparent in the ^{1}H-NMR spectrum of the purified product (**Figure 27**). Detection of the singlet at 8.13 ppm in the product spectrum, corresponding to the H_2 proton, indicated that oxidation had not occurred on the imidazole ring. By comparison to the M_1dG spectrum it was apparent that only two of the three pyrimido ring protons (H_6, H_7, H_8) remained in the product spectrum indicating that oxidation had occurred in this ring. The doublets at 8.71 and 6.35 ppm were coupled (confirmed by a COSY experiment), indicating the presence of a double bond conjugated to a carbonyl group. This implied oxidation at either the 6- or 8-position of the pyrimidopurinone ring. ^{13}C-NMR revealed a shift of the peak corresponding to C_6 (162 ppm) in the M_1dG spectrum and appearance of a new peak at 149.8 ppm in the

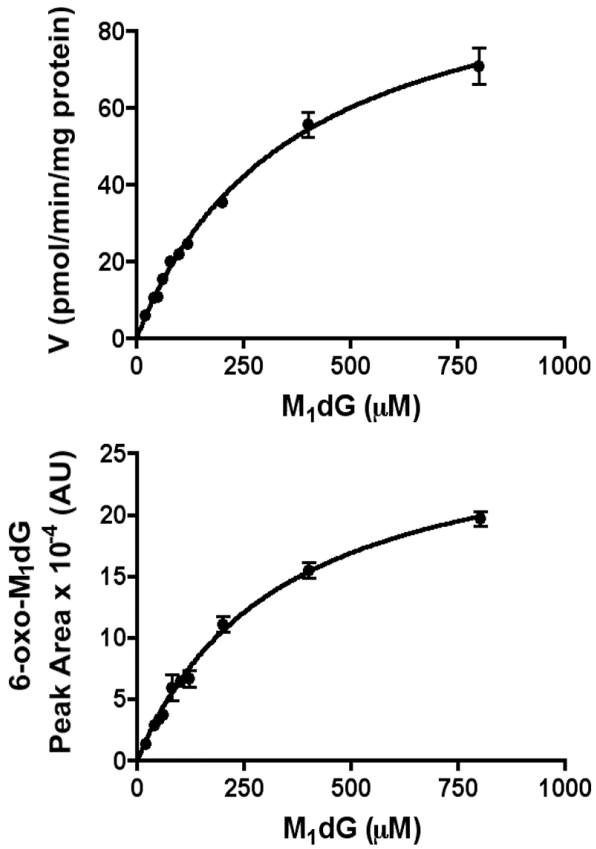

Figure 26. Concentration dependence of M_1dG oxidation by rat liver cytosol. (Top) M_1dG consumption; (Bottom) M_1dG metabolite formation. Incubations were conducted for 60 min with rat liver cytosol (5 mg protein/mL) prepared from male Sprague Dawley rats. M_1dG consumption was calculated by reference to a standard curve (K_m = 370 μM and V_{max} = 104 pmol/min/mg protein) whereas product formation was based on peak area production (K_m of 330 μM).

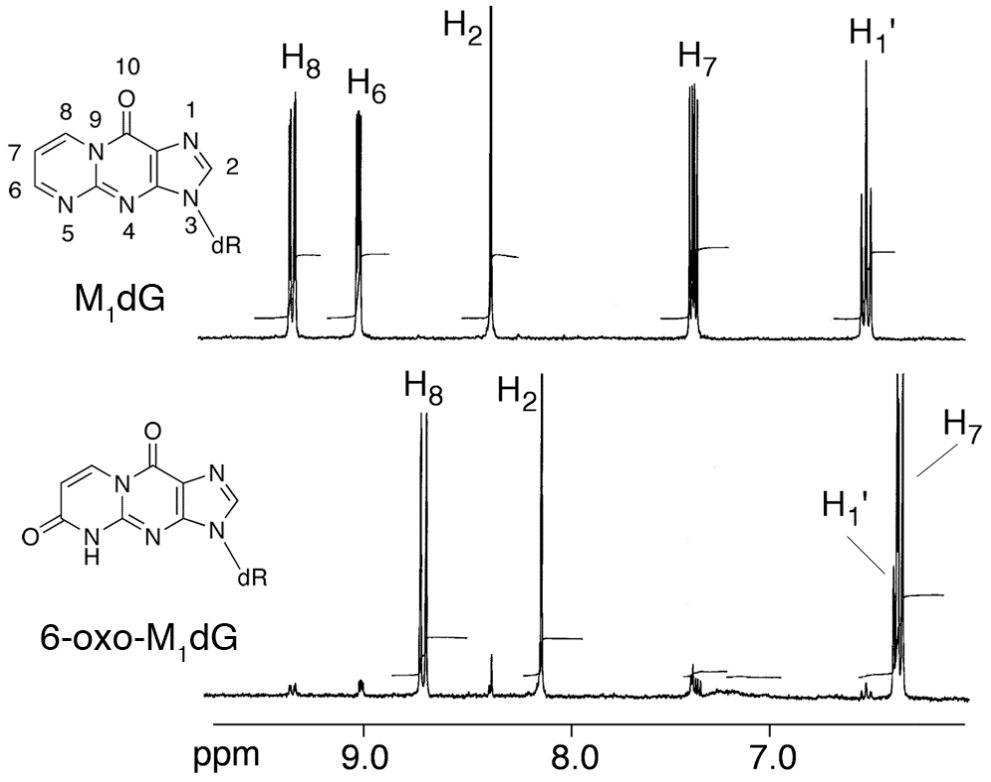

Figure 27. ^{1}H-NMR spectrum of M_1dG (top) and the M_1dG metabolite prepared using rat liver cytosol (bottom).

product spectrum. A heteronuclear multiple bond correlation (HMBC) NMR experiment identified strong, three-bond proton-carbon correlations between the proton assigned as H_8 and carbons C_{4a}, C_6, and C_{10}, which enabled the assignment of the structure as 6-oxo-M_1dG (**Figure 28**).

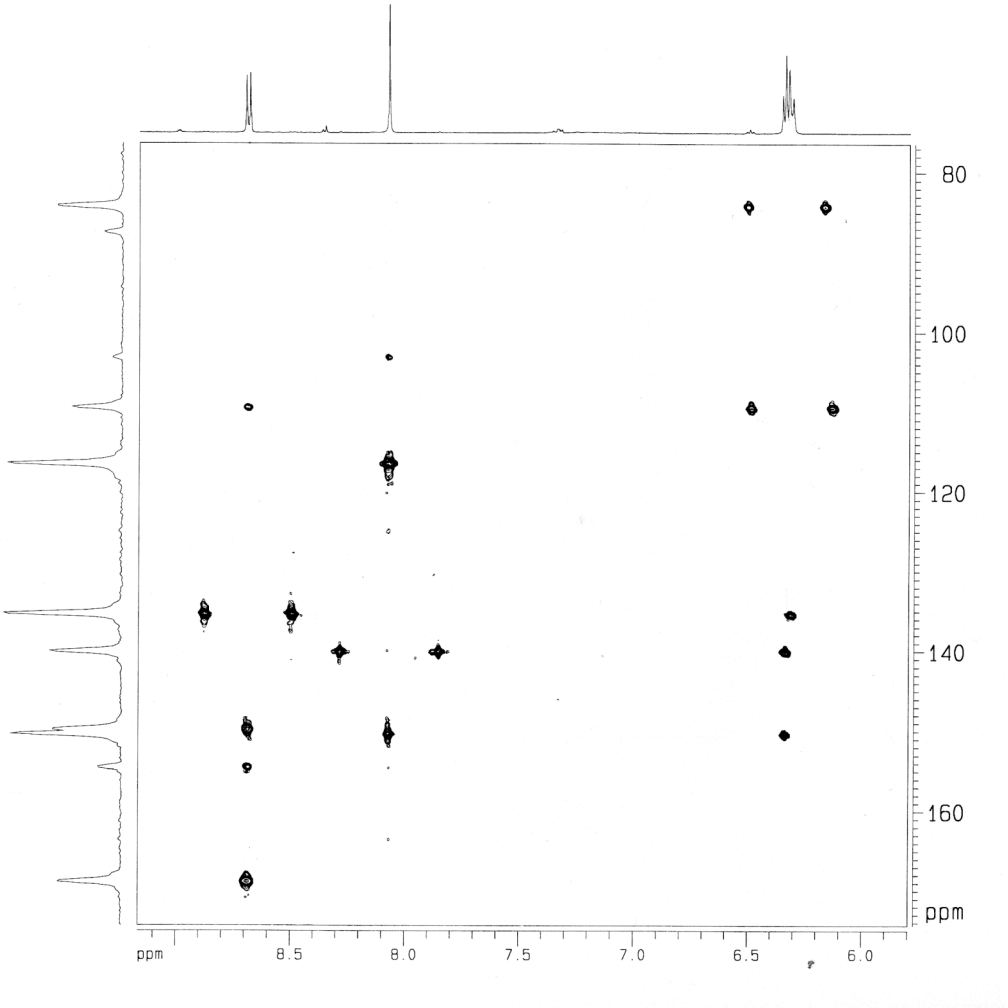

Figure 28. HMBC spectrum of the M_1dG metabolite prepared from rat liver cytosol.

Chemical synthesis of 6-oxo-M_1dG

To confirm the assigned structure of the metabolite, a synthesis of 6-oxo-M_1dG was designed and executed (**Figure 29**). 3-Bromo-ethylacrylate was reacted with dG under basic conditions, producing N1-ethyl-3-carboxyethenyl-dG. Subsequent treatment with sodium methoxide to promoted double bond isomerization and lactam formation by intramolecular cyclization. The synthesized product displayed identical mass, UV, and NMR spectra to the biochemically produced metabolite, and the two co-chromatographed by reversed-phase HPLC. These results unambiguously identified the major *in vitro* metabolite of M_1dG as 6-oxo-M_1dG. The mass spectrum and chromatographic behavior of synthetic 6-oxo-M_1dG were identical to those of the *in vivo* M_1dG metabolite.

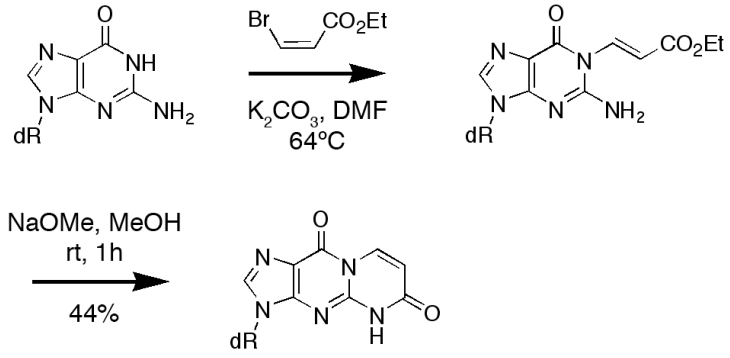

Figure 29. Chemical synthesis of 6-oxo-M_1dG. Reaction of dG in the presence of a mild base (K_2CO_3) with 3-bromo-ethylacrolate leads to the formation of a dG-propenoic ethyl ester intermediate, which undergoes cyclization upon addition of NaOMe to produce 6-oxo-M_1dG.

Inhibition of M_1dG metabolism *in vitro* in rat liver cytosol

In an attempt to provide a preliminary characterization of the enzymes responsible for M_1dG oxidation, incubations with separate lots of cytosol prepared from 3 strains of rats (Sprague Dawley, Fischer, Wistar) were conducted in the presence of allopurinol (160 μM) or menadione (160 μM) to inhibit XOR or AO, respectively (**Figure 30**). All rat liver cytosol lots were incubated at 5 mg/mL with 370 μM M_1dG for 60 min, and each lot produced 6-oxo-M_1dG. The extent of metabolism varied between preparations (20-55% consumption), and each lot displayed varied sensitivities to the inhibitors (5-90% inhibition). Menadione inhibited metabolism, in some instances, while in other cases it stimulated metabolism. XOR is a single gene product that exists as a dehydrogenase (XD) under physiological conditions (*239*). *Ex vivo* manipulations of the enzyme leads to irreversible proteolytic cleavage or reversible oxidation (formation of disulfides), generating the oxidase form (XO) (*240, 241*). Both forms of the enzyme are catalytically competent and capable of using molecular oxygen as a terminal electron acceptor; although, XO is more efficient that XD at utilizing O_2 (*242*). XD can use NAD^+, which increases the efficiency of catalysis. NAD^+ has no effect on XO turnover (*242*). Menadione and other quinones can be reduced by flavoproteins such as XO during the oxidation of reducing substrates (*243*), thereby stimulating oxidation (*244*). Preliminary evaluation of rat liver cytosol did not reveal enhanced metabolism in the presence of NAD^+, suggesting the oxidase form is responsible for the oxidation of M_1dG in the liver cytosols evaluated.

Rat liver cytosol lot 5 was chosen for further *in vitro* characterization of M_1dG metabolism by performing an IC_{50} determination with allopurinol. Co-administration of

increasing concentrations of allopurinol in the presence of M_1dG (370 μM) revealed an IC_{50} value of 120 nM. Of interest, the inhibition of M_1dG metabolism was not complete, as noted by the inability to completely inhibit 6-oxo-M_1dG formation at saturating concentrations of allopurinol (**Figure 31A**).

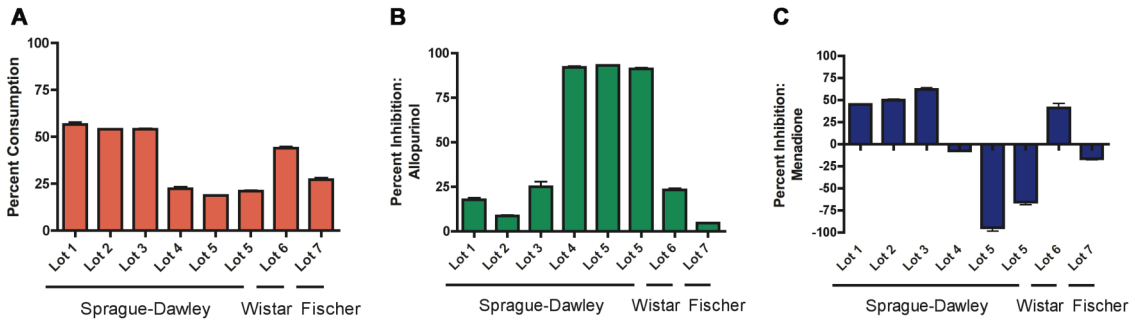

Figure 30. Investigation of M_1dG metabolism with several lots of rat liver cytosol. (A) Percent metabolism of M_1dG (370 μM) incubated in different lots of rat liver cytosol (5 mg/mL for 60 min). (B) Percent inhibition of M_1dG metabolism co-incubated with allopurinol (160 μM, inhibitor of XOR) in different lots of rat liver cytosol (5 mg/mL for 60 min with 370 μM M_1dG). (C) Percent inhibition of M_1dG metabolism co-incubated with menadione (160 μM, inhibitor of AO) in different lots of rat liver cytosol (5 mg/mL for 60 min with 370 μM M_1dG).

The contribution of AO to the production of 6-oxo-M_1dG in rat liver cytosol lot 4 was confounded by the observed stimulatory effects, thereby masking any inhibition of AO. To mitigate the stimulatory effects of menadione observed in the metabolism of M_1dG we selected an alternative inhibitor of AO. Raloxifene was recently characterized as an inhibitor AO in human liver cytosol (*245*). Mild inhibition of 6-oxo-M_1dG production was observed in rat liver cytosol in the presence of raloxifene. However, in the presence of saturating concentrations of allopurinol (40 μM) and increasing concentrations of raloxifene the production of 6-oxo-M_1dG was almost completely

inhibited (**Figure 31B**), and an IC_{50} of 4 μM was determined. Thus, preliminary *in vitro* data implicated XOR as the major enzyme contributing to the oxidation of M_1dG in rat liver cytosol.

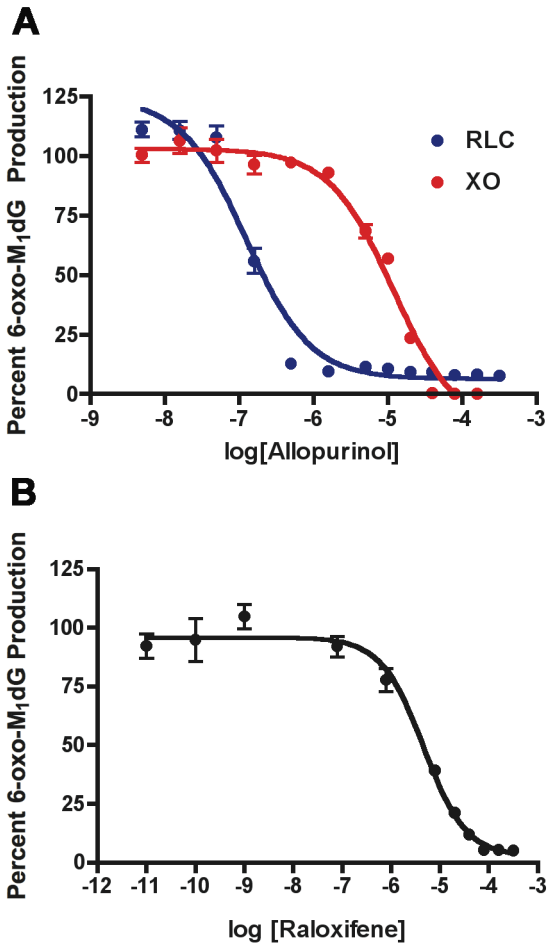

Figure 31. IC_{50} determinations in rat liver cytosol and purified XO with allopurinol or raloxifene using M_1dG as a substrate. (A) Using M_1dG (370 μM) as substrate, IC_{50} values were determined based on 6-oxo-M_1dG inhibition with increasing concentrations of allopurinol in rat liver cytosol (blue) or purified XO (red). (B) Using M_1dG (370 μM) as a substrate, IC_{50} values were determined based on 6-oxo-M_1dG inhibition in the presence of 40 μM allopurinol and increasing concentrations of raloxifene in rat liver cytosol.

Metabolism of M_1dG *in vitro* with purified XO

Based on results obtained from rat liver cytosol incubations, which suggested the involvement of XOR and AO in the metabolism of M_1dG, we further investigated the role of XOR using purified XO from cow's buttermilk. 6-oxo-M_1dG production was dependent on substrate consumption and linearized with respect to time and protein concentration. XO was found to be efficient at metabolizing M_1dG (V_{max} = 0.044 μmol min^{-1} mg XO^{-1}, K_m = 186 μM) and produced a single product, 6-oxo-M_1dG. 6-Oxo-M_1dG production in XO was completely inhibited by allopurinol (IC_{50} = 12 μM) (**Figure 31A**).

Co-administration of allopurinol and M_1dG in the rat

Based on our *in vitro* observations in rat liver cytosol and with purified XO, we set out to determine the *in vivo* contribution of XOR to M_1dG metabolism. Allopurinol is a specific, tight binding inhibitor of XOR *in vitro* (*228, 246*). Co-administration of allopurinol with other therapeutics can be used as an index of XOR activity *in vivo* (*247, 248*). Therefore, we monitored the effect on allopurinol on the metabolism of M_1dG in the rat. Six male Sprague Dawley rats were obtained from Charles River Laboratories with catheters surgically implanted in the femoral and jugular veins. The animals were housed in shoebox cages and allowed to feed *ad libitum* prior to experimentation. Upon arrival allopurinol was administered iv through the jugular vein (10 mg/kg) to a subset of animals (n = 3) and repeated at 24 h intervals prior to the dosing of M_1dG (*249, 250*). Animals not receiving allopurinol (n = 3) were administered a vehicle dose (saline solution) at the same intervals. Allopurinol (or vehicle control) was then administered to

1 h prior to dosing with M_1dG (5 mg/mL). Whole blood and urine were collected over the course of the experiment and analyzed by LC-MS/MS for the presence of M_1dG and 6-oxo-M_1dG. (**Figure 32**) shows the plasma time-course of M_1dG and 6-oxo-M_1dG during the first 2 h. Animals pretreated with allopurinol showed a marketed increase in plasma M_1dG levels as well as a substantial decrease in plasma 6-oxo-M_1dG levels in comparison to control animals. Analysis of urine samples (**Figure 33**) demonstrated a 4- to 5-fold increase in the M_1dG levels found in the urines of animals pretreated with allopurinol during the 0 to 4 h collection.

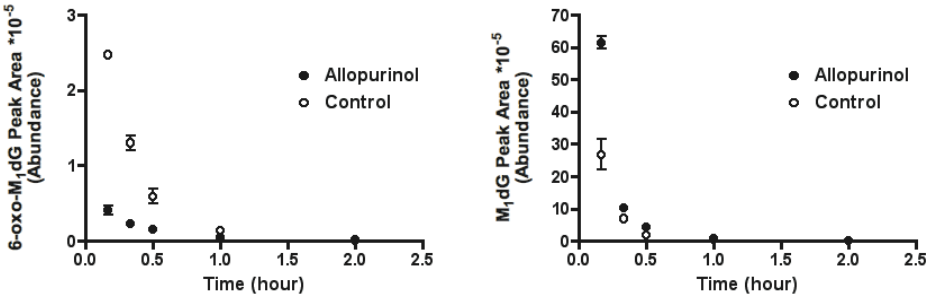

Figure 32. LC-MS/MS analysis of plasma 6-oxo-M_1dG and M_1dG levels following iv administration of M_1dG. Sprague Dawley rats were pretreated with allopurinol (●) or vehicle control (○) prior to iv administration of M_1dG (5 mg/kg).

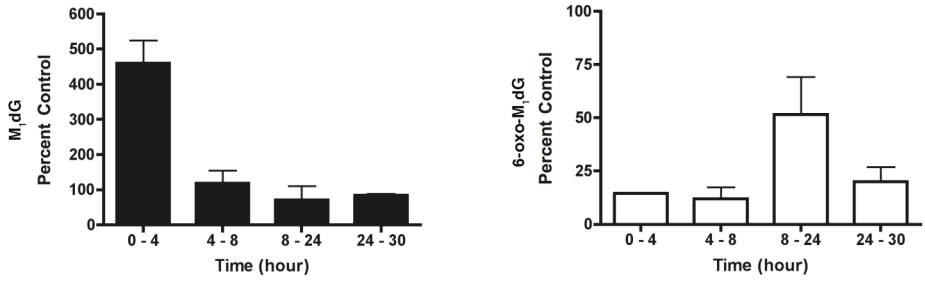

Figure 33. Percent recovery of M_1dG and 6-oxo-M_1dG in urine following iv administration of M_1dG. Sprague Dawley rats were pretreated with allopurinol or vehicle control prior to iv administration of M_1dG (5 mg/kg). Percent M_1dG (■) and 6-oxo-M_1dG (□) in reference to vehicle control was determined by LC-MS/MS analysis.

Metabolism of M_1dG *in vitro* in human liver cytosol

Three separate human liver cytosol preparations (HG23, HK27, and HG64) were obtained from commercial sources and evaluated for their ability to oxidize M_1dG in the presence or absence of either allopurinol or menadione (**Figure 34**). All 3 preparations oxidized M_1dG to 6-oxo-M_1dG but the variation in activities was significant. Some inhibition of oxidation was observed in the presence of allopurinol but greater inhibition was observed with menadione. This suggests that AO as well as XOR plays a significant role in the metabolism of M_1dG in humans. Further experiments are necessary to more completely characterize the enzymology of metabolism of M_1dG in humans, but our results indicate that human liver cytosols are capable of catalyzing M_1dG oxidation in a fashion qualitatively similar to rat liver cytosols.

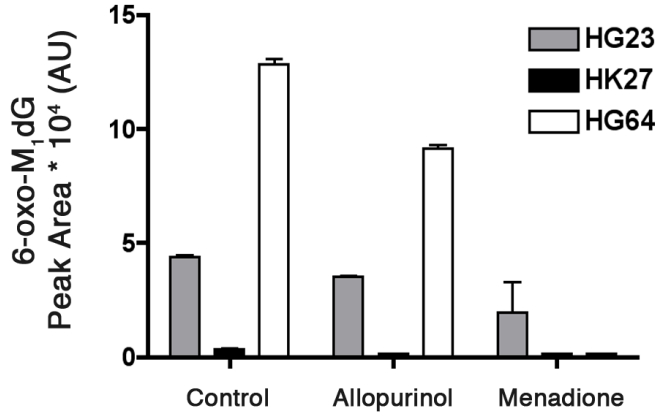

Figure 34. Oxidation of M_1dG by human liver cytosol. M_1dG (370 μM) was incubated with 3 separate preparations of human liver cytosol (5 mg/mL, 60 min): HG23 (gray), HK27 (black), and HG64 (white).

Enrichment of XOR and AO from rat liver

We continued our investigation of M_1dG metabolism in the rat by enriching XOR and AO activity from rat liver through a series protein purification steps. We based our study on several literature procedures for the purification of XOR and AO from biological matrices. XOR was originally purified by in 1939 (*232*). Subsequent revision and modifications to the general protocol have been assembled over the years (*233, 235, 238*). AO was first purified in 1962 (*234*), and more recently modified (*236-238*).

Following heat denaturation and ammonium sulfate precipitation, separation on the ceramic hydroxyapatite column allowed for the resolution of AO activity from XOR activity (**Figure 35**) and quickly associated M_1dG metabolism with both the AO and the XOR containing fractions. Following separate applications on the MonoQ resin the AO and XOR containing fractions were further purified. Each sample was pooled (separately) and targeted for purification by separate affinity chromatography steps.

XOR can be further purified by affinity chromatography on resin derivatized with folic acid. Preparation of the folate affinity matrix was carried out as previously described (*235*). However, XOR did not bind to the folate resin. The reason for the lack of XOR interaction with the folate resin was unknown, but likely resulted from incomplete derivatization of the affinity matrix. The XOR fractions from rat liver were then purified by gel filtration on a HiTrap Sephadex 200 column to approximately 25% purity. Further purification of AO activity by affinity chromatography on benzamidine sepharose was unsuccessful. The overall purification of XOR and AO from rat liver resulted in 24-fold purification for XOR (**Table 1**) and 5-fold purification for AO (**Table 2**).

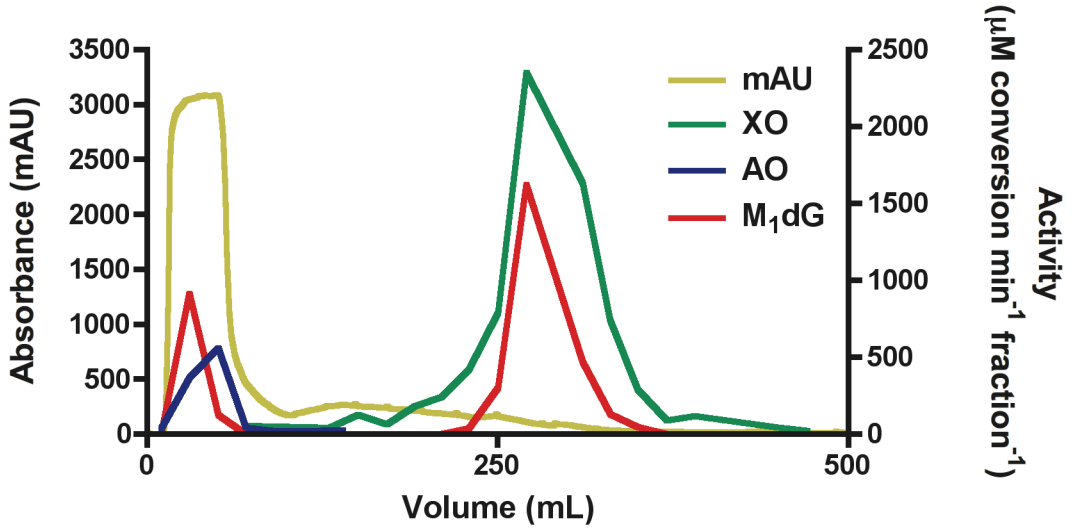

Figure 35. Elution of XOR and AO (from rat liver homogenate) on a hydroxyapatite column. Protein was eluted from a hydroxyapatite column by an increasing gradient of potassium phosphate, pH 7.8 (100 – 400 mM). Protein absorbance (gold), XOR activity (green), AO activity (blue) and M_1dG metabolism (red) was monitored from eluting fractions**.** XOR activity was assessed by UV, monitoring conversion of xanthine to uric acid (ε_{295} 95000 M^{-1} cm^{-1}). AO activity was assessed by UV, monitoring the disappearance of 4-dimethylamino-cinnamaldehyde (ε_{398} 30500 M^{-1} cm^{-1}). M_1dG activity was assessed by HPLC-UV in reference to buffer control.

Table 1. XOR purification from rat liver homogenate: Unit Activity = 1 μmol xanthine consumed min^{-1}.

Step	*Volume*	*Protein*	*Activity*	*Specific Activity*	*Purification*	*Recovery*
	mL	*mg*	*Units*	*Units/mg*	*Fold*	*%*
$(NH_4)SO_4$	9.2	500	30,000	61	1.0	100
CHT	8.0	3.5	5,200	190	3.1	17
Mono Q	3.2	1.1	1,600	1500	24	5

Table 2. AO purification from rat liver homogenate: Unit Activity = 1 μmol 4-(dimethylamino)-cinnamaldehyde consumed min^{-1}.

Step	*Volume*	*Protein*	*Activity*	*Specific Activity*	*Purification*	*Recovery*
	(mL)	*(mg)*	*Units*	*Units/mg*	*Fold*	*%*
$(NH_4)SO_4$	9.2	500	12,000	24	1.0	100
CHT	9.0	280	7,500	27	1.1	62
Mono Q	4.2	7.9	960	120	5.0	8

Discussion

Considerable effort has been expended to develop biomarkers of DNA damage for use in human clinical and population-based studies as well as in animal investigations. Quantification of repaired adducts in urine represents a particularly attractive approach. Various methodologies have been described for quantification of alkylated deoxynucleosides and nucleobases, oxidized deoxynucleosides and nucleobases, polycyclic hydrocarbon-derived adducts, aflatoxin-derived adducts, and *cis*-Pt-derived adducts (*251*). The oxidized guanine adducts 8-oxo-Gua and 8-oxo-dG have been reported to be present in the urine of healthy human donors at levels of ~2 nmol/kg/24 h and 0.4 nmol/kg/24 h, respectively (*155, 156*). Attempts to quantify M_1dG indicated that it is present at much lower concentrations in human urine, raising the possibility that it is metabolized prior to excretion (*154*).

In the present study, we report that M_1dG is rapidly oxidized following iv administration to rats. The sole product was 6-oxo-M_1dG; neither evidence for multiple oxidations was observed nor was there any evidence for the production of glucuronide conjugates. However, we cannot definitively rule out the possibility for the formation of additional metabolites or alternative routes of biological processing *in vivo* (i.e., biliary elimination). The extent of metabolism could not be rigorously determined, but it was estimated that approximately 20% to 30% of the exogenously administered M_1dG was converted to the metabolite, 6-oxo-M_1dG, *in vivo*. The incomplete conversion of M_1dG to 6-oxo-M_1dG implies that oxidative metabolism is not the sole reason for the low levels of M_1dG in human urine. However, such a conclusion may be premature because the level of M_1dG administered was likely higher than the steady-state level produced from

DNA following repair. Thus, the percentage conversion of M_1dG to 6-oxo-M_1dG may be greater under physiological conditions than the percentage conversion observed in the present experiments. It is also important to consider the possibility that other unknown factors besides oxidative metabolism (e.g., enterohepatic recycling of M_1dG or alternative pathways of DNA repair) are responsible for the low endogenous levels in urine.

The structure of 6-oxo-M_1dG was elucidated by mass spectrometry and NMR spectroscopy (proton and carbon) and confirmed by independent chemical synthesis. Oxidation of M_1dG to 6-oxo-M_1dG was catalyzed by cytosolic preparations of both rat and human liver indicating that this is a metabolic pathway common to both species. Based on *in vitro* and *in vivo* experiments with chemical inhibitors and partially purified enzymes, both XOR and AO were identified in the metabolism of M_1dG. During the purification of rat liver homogenate only fractions that corresponded to XOR and AO displayed M_1dG metabolism. Thus, it appears unlikely that other enzymes are involved in the production of 6-oxo-M_1dG. Additionally, there was no evidence for oxidation of M_1dG by CYPs in liver microsomal preparations.

Comparing inhibition results between human and rat liver cytosols suggested AO played a more significant role in the metabolism of M_1dG in human liver cytosol than in rat liver cytosol. XOR was involved in both species. The precise role of AO in the production of 6-oxo-M_1dG in rat liver cytosol was slightly confounded by the stimulatory effect of menadione (although, not seen in human liver cytosol incubations). Substituting raloxifene for menadione effectively inhibited 6-oxo-M_1dG in rat liver cytosol. When both allopurinol and raloxifene were co-incubated with rat liver cytosol 6-oxo-M_1dG

production nearly eliminated. It should be noted that the relative amount of AO to XOR activity in Sprague Dawley rat liver cytosol is low. Other species, such as guinea pig and rabbit, often contain higher ratios of AO to XOR (*252*). Therefore, the total contribution of AO towards the metabolism of M_1dG may be underestimated in these studies with rat liver cytosol.

The role of XOR *in vivo* in the rat appears to be significant. Pretreating animals with allopurinol prior to dosing with M_1dG resulted in a considerable reduction in 6-oxo-M_1dG plasma levels and concomitant increase in M_1dG plasma levels. Recovery data in urine also demonstrated the effect of XOR inhibition on 6-oxo-M_1dG production as marked by a 5-fold decrease in metabolite recovery. The total inhibition of M_1dG was not observed following allopurinol pre-treatment of rats, which would suggest either incomplete inhibition of XOR or the involvement of additional enzymes, such as AO. It is important to note that the role of allopurinol on other possible aspects of M_1dG metabolism (disposition, transport, etc.) is unknown. Allopurinol is a commonly used in the clinic to treat individuals with gout, or other forms of hyperuricemia. When evaluating urinary levels of M_1dG and 6-oxo-M_1dG in human populations, it may be important to consider those individuals taking therapeutic regiments of allopurinol, as it may alter their elimination of M_1dG.

Prior studies have demonstrated that alkylated adducts, polycyclic hydrocarbon adducts, and aflatoxin adducts are stable *in vivo* whereas the chemotherapeutic agent O^6-benzylguanine is oxidized (*133, 229, 253, 254*). The position of oxidation of O^6-benzylguanine is the 8-position of the imidazole ring, which is different than the site of oxidation on M_1dG. The pyrimido ring of M_1dG has been previously demonstrated to be

highly reactive to nucleophiles and hydride reducing agents so the present observations indicate it is also subject to oxidation (*109, 112, 153*). It will be interesting to elucidate the mechanism of enzyme-catalyzed oxidation.

Our findings raise the possibility that other DNA adducts from endogenous sources are oxidized or otherwise metabolized following repair-dependent removal from the genome or from mitochondrial DNA. 8-Oxo-dG appears to be stable to metabolism and recent reports have demonstrated the presence of another endogenous adduct, 1,N^6-ε-Ade and its nucleobase (1,N^6-ε-dA), in urine (*255*). However, a growing number of endogenous adducts have been formed in *in vitro* experiments that contain an exocyclic ring that blocks the Watson-Crick base-pairing region (*165, 197, 200, 256*). It will be important to determine the metabolic fate of these lesions as part of any attempt to develop convenient biomarkers suitable for clinical or population-based studies.

CHAPTER III

[^{14}C]M_1dG METABOLISM IN THE RAT

Summary

Endogenously occurring damage to DNA is a contributing factor to the onset of several genetic diseases including cancer. Monitoring urinary levels of DNA adducts is one approach to assess genomic exposure to endogenous damage. However, metabolism and alternate routes of elimination have not been considered as factors that may limit the detection of DNA adducts in urine. We recently demonstrated that the peroxidation-derived dG adduct, M_1dG, is subject to enzymatic oxidation *in vivo* resulting in the formation of a major metabolite, 6-oxo-M_1dG. We now report, based on the administration of [^{14}C]M_1dG to Sprague Dawley rats that 6-oxo-M_1dG is the principal metabolite of M_1dG *in vivo* representing 45% of the total administered dose. When [^{14}C]6-oxo-M_1dG was administered to Sprague Dawley rats, 6-oxo-M_1dG was recovered unchanged (>97% stability). These studies also revealed that M_1dG and 6-oxo-M_1dG are subject to biliary elimination. Additionally, both M_1dG and 6-oxo-M_1dG exhibited a long residence time following administration (>48 h), and the major species observed in urine at late collections was 6-oxo-M_1dG.

Introduction

M_1dG is an endogenous pyrimidopurinone adduct formed by the reaction of dG with MDA, a product of enzymatic and non-enzymatic lipid peroxidation reactions, or

base propenal, a DNA peroxidation product (*42, 58, 96-98, 106, 107, 257*). This adduct is mutagenic in bacteria and mammalian cells (*88, 120, 121, 258*) and is a substrate for NER (*120, 122*). It is also one of the first endogenously occurring DNA damage products to be detected in DNA of healthy humans (*148*). Prior attempts to quantify the levels of M_1dG in human urine demonstrated an excretion rate of 12 fmol/kg/24 h (*154*). The rate of M_1dG elimination in rats could not be determined, since the levels were below the limit of detection for the analytical method (*153*). The low rate of elimination in human populations and the absence of observed material in the urine of rats led us to hypothesize that factors such as metabolism (oxidation, conjugation, etc.) or alternative routes of elimination may limit the appearance of M_1dG in urine.

We recently demonstrated that M_1dG is subject to oxidative metabolism in the rat to a principal metabolite, 6-oxo-M_1dG (*157*). However, the total recovery and extent of metabolism in these studies could not definitively be determined. To unambiguously monitor the metabolism and elimination of M_1dG *in vivo*, we synthesized M_1dG containing carbon-14 incorporated into the purine ring for use in animal studies. This tracer allowed us to quantitatively monitor the metabolism and elimination of M_1dG and its principal metabolite, 6-oxo-M_1dG, in the rat. The results of this investigation are described herein.

Experimental Procedures

Chemicals and reagents

All chemicals were obtained from commercial sources and used as received. Solvents were of HPLC grade purity or higher. [8-^{14}C]-2′-dG ([^{14}C]dG) was purchased from Sigma (St. Louis, MO). Purified bovine XO was purchased from CalBiochem (La Jolla, CA). Catheterized male Sprague Dawley rats were obtained from Charles River Laboratories (Wilmington, MA). HPLC-UV βRAM separations were performed on a Waters 2695 autosampler and binary pump with a Waters 2487 dual wavelength UV detector (Milford, MA) and an IN/US Systems Model 2 βRAM (Tampa, FL). Liquid scintillation counting was performed with a Beckman LS 6500 Multi-Purpose Scintillation Counter (Fullerton, CA).

Chemical synthesis of [^{14}C]M_1dG

[^{14}C]M_1dG synthesis was carried out as previously described (*259*). Briefly, [^{14}C]dG was obtained from Sigma-Aldrich (0.2 mCi, 55 mCi/mmol) as a solution in ethanol: water (1:1). Iodoacrolein was freshly prepared from ethyl *cis* 3-iodoacrylate as previously described and dissolved in anhydrous DMF (*260*). Freshly prepared iodoacrolein was analyzed by [^{1}H]-NMR and determined to be >95% pure. [^{14}C]dG (0.2 mCi, 1 mg) was diluted with excess ethanol and evaporated to dryness under reduced pressure. The remaining residue was dissolved in DMF (0.4 mL) in the presence of 1.5 equivalents, K_2CO_3 and heated to 65 °C. To this solution, 1 equivalent of freshly prepared iodoacrolein was added each h over 5 h of reaction (**Figure 36**). The resulting

solution was evaporated under reduced pressure and dissolved in 1.0 mL of 0.01 M potassium phosphate. The mixture was purified by HPLC using a Phenomenex Luna C18(2) column (250 x 4.6 mm, 5 μm) equilibrated with 100% solvent A (0.01 M potassium phosphate, pH 7.8) at a flow rate of 1.0 mL/min. The following gradient elution was applied: 100% solvent A with 0% solvent B (methanol) for 5 min followed by a linear increase to 20% B over 30 min, holding at 20% B for 5 min, increasing to 85% B in 1 min, holding at 85% B for 5 min, decreasing to 0% B in 1 min and re-equilibrating at initial conditions for 5 min. Fractions corresponding to M_1dG (~35 min) were collected, pooled and concentrated to a minimal volume. Purity was assessed by HPLC-UV with βRAM detection. The radiochemical purity was assessed to be >95%, with a minor impurity of residual [^{14}C]dG. A final yield of 15% was obtained. ESI MS: *m/z* 306.4.

Chemical synthesis of [^{14}C]6-oxo-M_1dG

A solution of [^{14}C]M_1dG was diluted in 0.6 mL of 0.1 M potassium phosphate, pH 7.8, and allowed to incubate with 2 Units of purified bovine XO for 1 h; after which an additional 2 Units was added and allowed to incubate for an additional h (**Figure 36**). The resulting solution was purified by HPLC as described for [^{14}C]M_1dG. Fractions containing [^{14}C]6-oxo-M_1dG (~26 min) were collected, pooled and concentrated to a minimal volume. The resulting sample exhibited >99% radiochemical purity and final yield of 10% was obtained. ESI MS: *m/z* 322.4.

Administration of [^{14}C]M_1dG and [^{14}C]6-oxo-M_1dG to male Sprague Dawley rats

Animal protocols were performed under the approval of Vanderbilt University and in accordance with the Institutional Animal Care and Use Committee policies. Male Sprague Dawley rats (225 – 250 g) with catheters surgically implanted into the jugular vein and bile duct were obtained from Charles River Laboratories and housed in shoebox cages. Prior to the experiment the animals were transferred into metabolism cages and allowed to feed *ad libitum*. The dosing solution was prepared in sterile saline solution, administered through the jugular vein over 45 s in an approximate volume of 0.4 mL, and flushed with 0.4 mL of sterile heparinized saline. Four animals were used in each experiment (2 animals with and 2 animals without bile catheters). [^{14}C]M_1dG was dosed at 22 μCi/kg (123 μg/kg) and [^{14}C]6-oxo-M_1dG was dosed at 15 μCi/kg (83 μg/kg) in separate experiments. All animals were housed in metabolism cages throughout the duration of the experiment to collect urine and feces over the following intervals: Pre-dose, 0-4, 4-8, 8-12, 12-16, 16-20, 20-24, 24-32, 32-40, 40-48, and 48-64 h. Bile was also collected (from 2 animals) as outlined above; although, the first interval was broken down as follows: 0-0.5, 0.5-1, 1-2, and 2-4 h. All samples were collected into pre-tared tubes and weighed following the collection interval to determine the mass of sample collected (feces was first dried on the bench top). All samples were stored at -20 °C until analysis.

Radiochemical analysis of biological samples

Biological samples were processed as suggested by PerkinElmer. Urine (0.1-1.0 mL) and bile (0.1 – 0.3 mL) samples were added directly to 10 mL of Pico-Fluor™ 40 and

analyzed by liquid scintillation counting (10 min counts). Fecal samples were dried on the bench top for a minimum of 24 h. The fecal material was broken into small pieces, mixed, and approximately 20 mg of feces (dry weight) was transferred to scintillation vials (n = 4) and re-hydrated with 0.2 mL of water. To each sample 0.5 mL of Soluene®-350 was added, mixed, and heated to 40 °C for 1.5 h. A 0.5 mL aliquot of isopropanol was added and swirled, followed by drop-wise addition of 0.2 mL H_2O_2. The resulting mixture was heated to 40 °C for 2 h, cooled, and 10 mL of Hionic-Fluor™ scintillation cocktail was added. Samples were stored in the dark for a minimum of 36 h prior to analysis by liquid scintillation counting (10 min counts). Urine and bile samples were profiled by HPLC-UV with βRAM detection, and centrifuged at 200,000 g for 1 h prior to analysis. Injections (0.025 – 0.3 mL) were made onto a Phenomenex Luna C18(2) column (250 x 4.6 mm, 5 μm) equilibrated with 100% solvent A (0.5% formic acid in H_2O) at a flow rate of 1.0 mL/min. The following gradient elution was applied: 100% solvent A with 0% solvent B (0.5% formic acid in methanol) for 5 min followed by a linear increase to 20% B over 30 min, holding at 20% B for 5 min, increasing to 85% B in 1 min, holding at 85% B for 5 min, decreasing to 0% B in 1 min and re-equilibrating at initial conditions for 5 min. Column eluent first passed through the UV detector (254 nm) and onto the βRAM, where it mixed with IN-FLOW™ 2:1 (IN/US Systems) at a ratio of 1:1.1 (HPLC eluent: cocktail), and was analyzed in 0.5 mL flow cell with a dwell time of 0.2 s.

LC-MS/MS analysis of biological samples

Tandem mass spectrometry employing selected reaction monitoring was used to verify the molecular ions attributed to the main source or radioactivity in the biological samples. Approximately 500 – 1000 dpm were analyzed per injection. Urine and bile samples were diluted to an approximate concentration of 50,000 dpm/mL and injected onto a Phenomenex Luna C18(2) column (250 x 2.0 mm, 5 μm) equilibrated with 100% solvent A (0.5% formic acid in H_2O) at a flow rate of 0.3 mL/min. The following gradient elution was applied: 100% solvent A with 0% solvent B (0.5% formic acid in methanol) for 5 min followed by a linear increase to 20% B over 30 min, holding at 20% B for 5 min, increasing to 85% B in 1 min, holding at 85% B for 5 min, decreasing to 0% B in 1 min and re-equilibrating at initial conditions for 5 min. A ThermoElectron Quantum triple-quadrupole instrument with an electrospray source operated in positive ion mode was used during the analysis. The following instrument parameters were set: spray voltage 4.3 kV; capillary temperature = 250 °C; sheath gas = 33 psi; auxiliary gas = 25; source CID off; collision pressure 1.5 mTorr.

Results

Recovery of [^{14}C]M_1dG

[^{14}C]M_1dG was synthesized from [^{14}C]dG in a reaction with iodoacrolein in the presence of a mild base (K_2CO_3) (**Figure 36**) (*259*). The material was purified by HPLC and the radiochemical purity was determined to be >95% (**Figure 37**). A small amount (<5%) of unreacted starting material ([^{14}C]dG) was observed in the dosing solution.

[^{14}C]M_1dG was diluted in sterile saline solution and administered iv (22 μCi/kg, 123 μg/kg) to male Sprague Dawley rats (n = 4) via catheters surgically implanted in the jugular vein. Two animals contained additional catheters surgically implanted into the bile duct. The animals were housed in metabolism cages throughout the duration of the experiment to collect urine, feces, and bile (where applicable). The collected biological samples were analyzed for total radioactivity by liquid scintillation counting and the data are summarized in **Table 3**. Approximately 50% of the radioactivity was recovered in the urine of both bile-catheterized and non-bile-catheterized animals. Greater than 90% of the urinary recovery was collected during the first 8 h (**Figure 38**). The remaining radioactivity was recovered in the feces of non-bile-catheterized animals and in the bile of bile-catheterized animals (**Figure 38**).

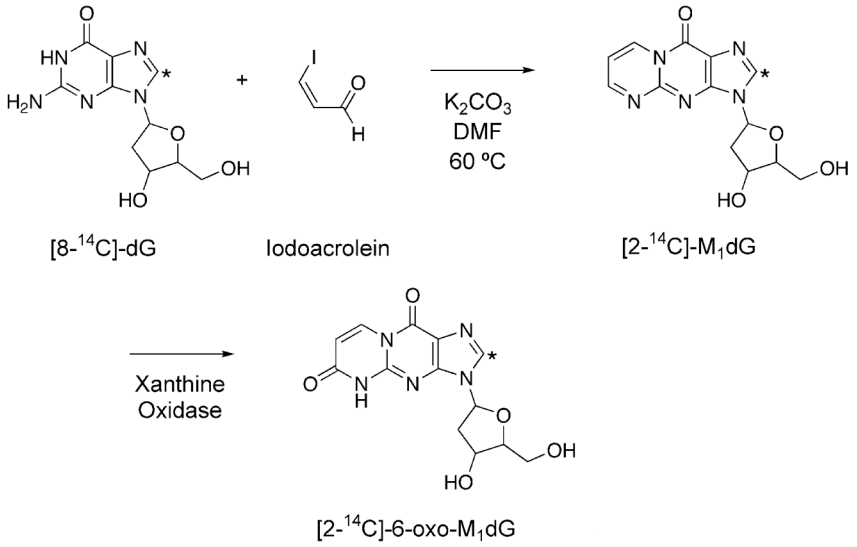

Figure. 36. Chemical synthesis of [^{14}C]M_1dG and [^{14}C]6-oxo-M_1dG. The convention used for numbering the atoms of exocyclic dG adducts labels the 8-position of dG as the 2-position of the exocyclic dG adduct.

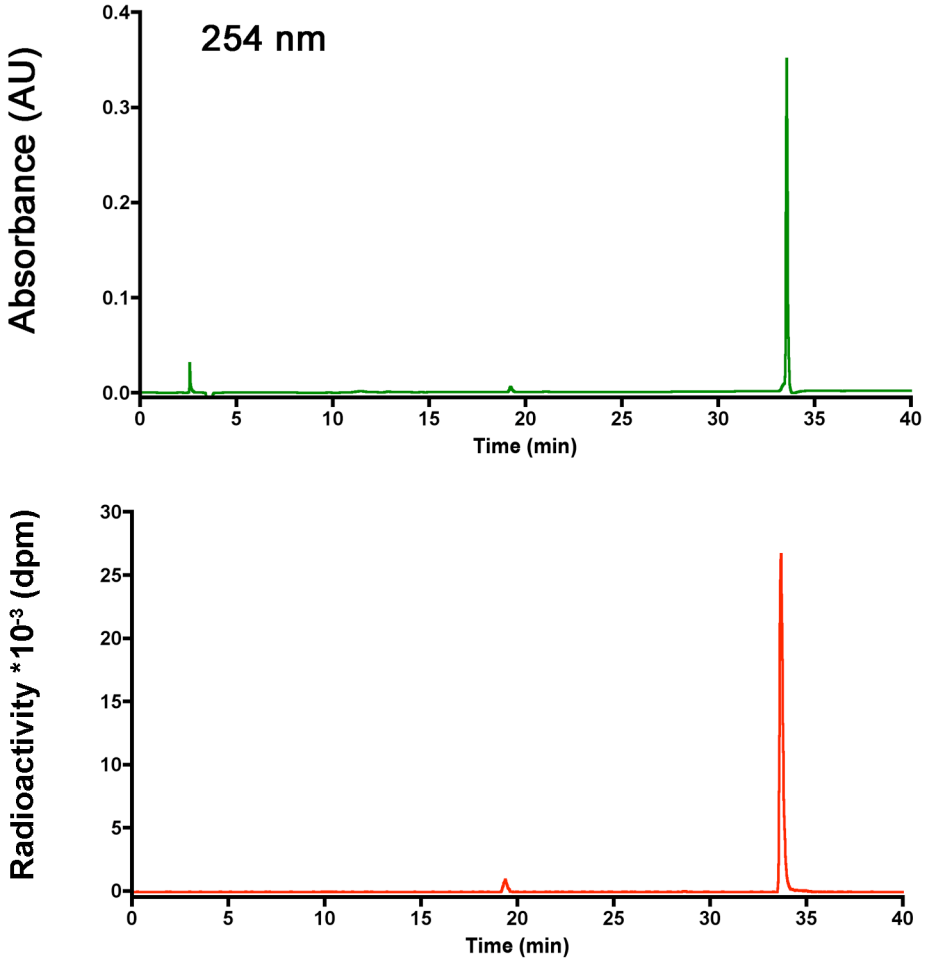

Figure 37. HPLC-UV and HPLC-βRAM analysis of the [^{14}C]M_1dG dosing solution. (Top) HPLC-UV analysis at 254 nm and (Bottom) radiochemical analysis with βRAM detection.

Table 3. Total radioactivity recovered following administration of [^{14}C]M_1dG. [^{14}C]M_1dG (22 μCi/kg) was administered iv to male Sprague Dawley rats with (n = 2) or without (n =2) surgically implanted bile catheters.

	Bile Catheter	No Bile Catheter
Dose (μCi)	4.95 ± 0.15	5.65 ± 0.05
Urine	2.92 ± 0.38	3.00 ± 0.38
Feces	0.14 ± 0.03	2.45 ± 0.36
Bile	2.52 ± 0.01	*NA*
Recovery (%)	113.8 ± 10.8	96.2 ± 12.3

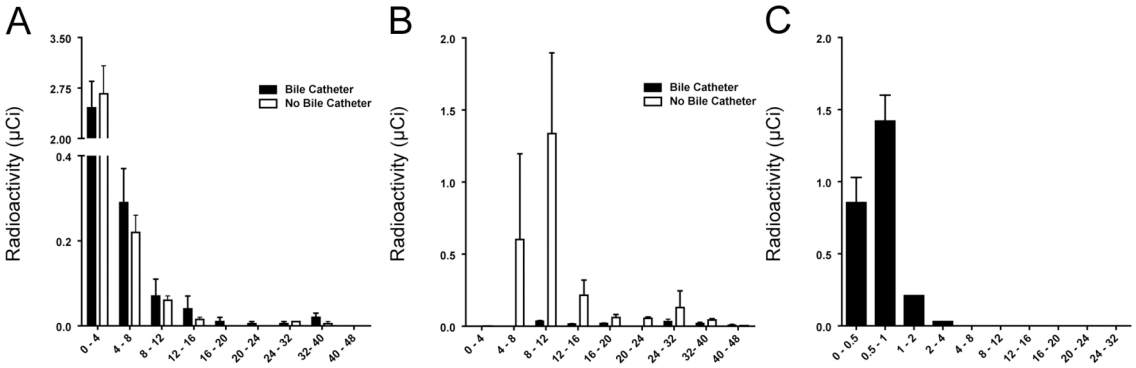

Figure 38. [^{14}C]Recovery following administration of [^{14}C]M_1dG. Male Sprague Dawley rats were dosed iv with [^{14}C]M_1dG (22 μCi/kg) and housed in metabolism cages to collect urine, bile and feces during the experiment. A, [^{14}C]Recovery in urine from bile-catheterized and non-bile-catheterized animals. B, [^{14}C]Recovery in feces from bile-catheterized and non-bile-catheterized animals. C, [^{14}C]Recovery in bile from bile-catheterized animals.

Analysis of [^{14}C]M_1dG metabolism in urine and bile

Urine and bile samples were profiled by HPLC with radiochemical detection. Representative chromatograms from urine and bile are shown in **Figure 39**. The urine profiles from both the bile-catheterized and non-bile-catheterized rats were identical. The major metabolite observed in all radiochemical profiles eluted with the authentic retention time for 6-oxo-M_1dG, and accounted for 20% of the radioactivity recovered in urine. The analysis of bile samples revealed that 70% of the radioactivity in bile was attributed to the metabolite, 6-oxo-M_1dG. Selected reaction monitoring analysis of these samples revealed the expected transitions for M_1dG (*m/z* 306.4 → 190.4) and 6-oxo-M_1dG (*m/z* 322.4 → 206.4), thereby confirming their identity. The bile and urine HPLC profiles demonstrated that 90% of the recovered radioactivity could be attributed to the combination of M_1dG and 6-oxo-M_1dG. The remaining 10% of the radioactivity was distributed among 5 distinct peaks in the radiochemical profiles; part of which (~5%) was attributed to the [^{14}C]dG in the dosing solution. Thus, metabolites other than 6-oxo-M_1dG collectively accounted for <6% of the total radioactivity. 6-Oxo-M_1dG accounted for 45% of the total recovered radioactivity.

Analysis of late time-point urine collections (post 24 h) from both non-bile-catheterized and bile-catheterized animals suggested 6-oxo-M_1dG was present at the same or higher abundance than M_1dG (**Figure 40**). This was especially apparent in the LC/MS-MS analysis of the bile-catheterized animals where the radioactivity present in the sample could almost entirely be attributed to 6-oxo-M_1dG.

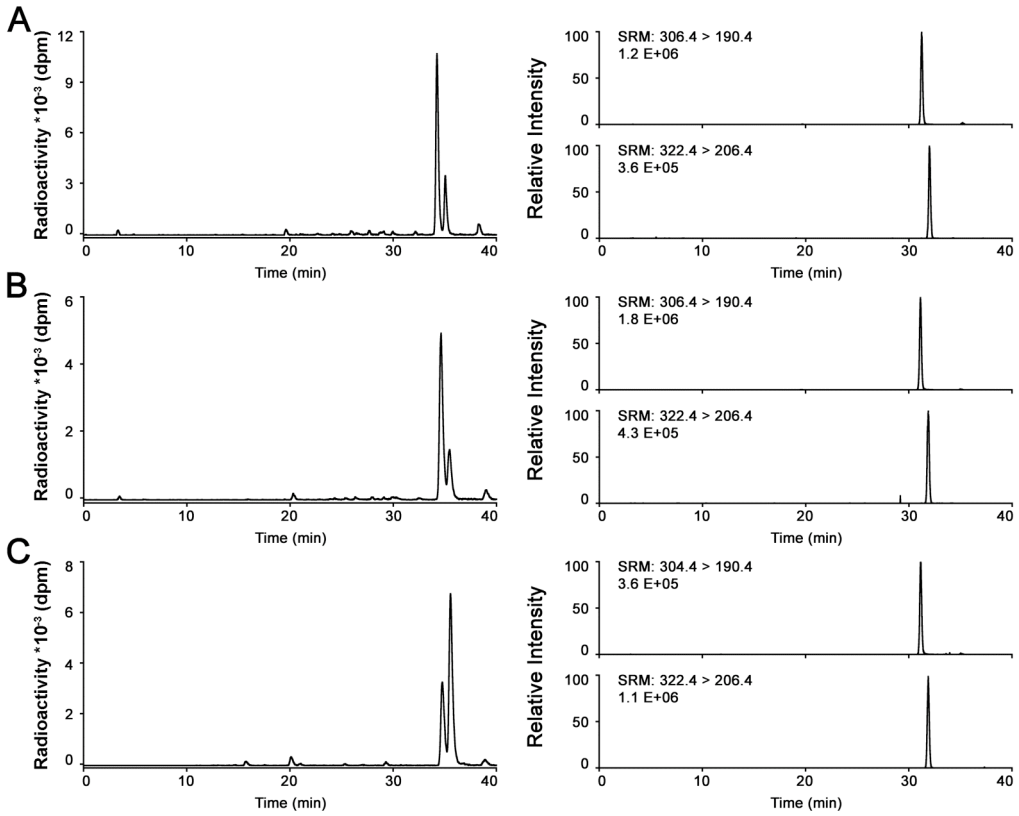

Figure 39. HPLC-radiochemical and -MS/MS profiles of urine and bile samples following administration of [^{14}C]M$_1$dG. Male Sprague Dawley rats received a single iv dose of [^{14}C]M$_1$dG (22 μCi/kg). A, Representative urine sample (0-4 h) from a non-bile-catheterized animal was profiled by radiochemical detection and separately by LC-MS/MS using selected reaction monitoring following the transitions for the parent molecule M$_1$dG (*m/z* 306.4 → 190.4) and the principal metabolite, 6-oxo-M$_1$dG (*m/z* 322.4 → 206.4). B, Representative urine sample (0-4 h) from a bile-catheterized animal was profiled by radiochemical detection and separately by LC-MS/MS using selected reaction monitoring following the transitions for the parent molecule M$_1$dG (*m/z* 306.4 → 190.4) and the principal metabolite, 6-oxo-M$_1$dG (*m/z* 322.4 → 206.4). B, a representative bile sample (0-0.5 h) from a bile-catheterized animal was profiled by radiochemical detection and separately by LC-MS/MS using selected reaction monitoring following the transitions for the parent molecule M$_1$dG (*m/z* 306.4 → 190.4) and the principal metabolite, 6-oxo-M$_1$dG (*m/z* 322.4 → 206.4).

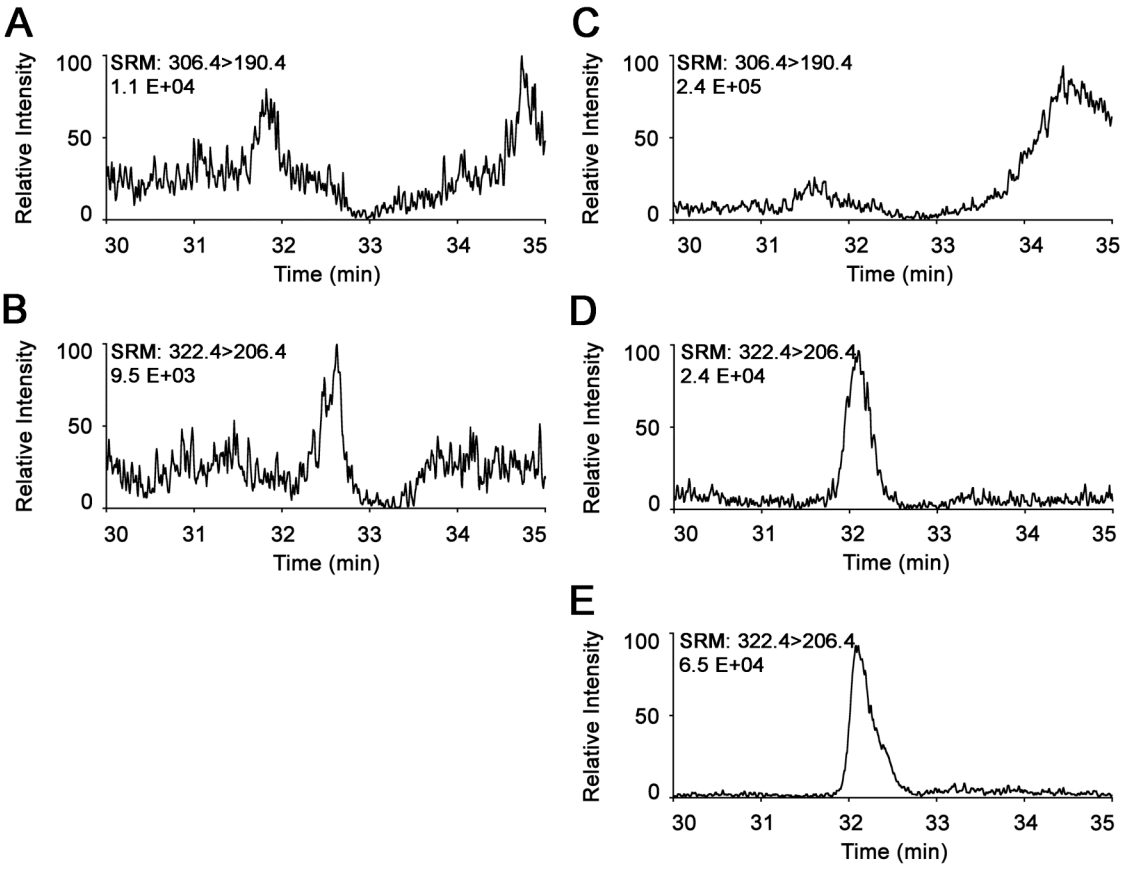

Figure 40. Analysis of late time-point urine samples following administration of either [^{14}C]M_1dG or [^{14}C]6-oxo-M_1dG. LC-MS/MS analysis of a 32-40 h urine sample from a non-bile-catheterized rat monitoring the transitions for: A, [^{14}C]M_1dG (*m/*z 306.4 → 190.4) and B, [^{14}C]6-oxo-M_1dG (*m/*z 322.4 → 206.4). LC-MS/MS analysis of a 32-40 h urine sample from a bile-catheterized rat monitoring the transition for: C, [^{14}C]M_1dG (*m/*z 306.4 → 190.4) and D, [^{14}C]6-oxo-M_1dG (*m/*z 322.4 → 206.4). E, LC-MS/MS analysis of a 32-40 h urine sample from a non-bile-catheterized rat monitoring the transition of [^{14}C]6-oxo-M_1dG (*m/*z 322.4 → 206.4) following an iv dose of [^{14}C]6-oxo-M_1dG.

Recovery of [^{14}C]6-oxo-M_1dG

Based on the long residence time of the [^{14}C]M_1dG dose and the significant conversion of M_1dG to 6-oxo-M_1dG, we continued experiments to study the metabolism and elimination of the principal metabolite, 6-oxo-M_1dG. We hypothesized that 6-oxo-M_1dG would have significant biliary clearance, and a long residence time similar to the parent molecule, M_1dG. Furthermore, this experiment would clarify the ultimate source of the minor metabolites observed in the [^{14}C]M_1dG study (i.e., derived from M_1dG or 6-oxo-M_1dG).

[^{14}C]6-Oxo-M_1dG was prepared from [^{14}C]M_1dG (described above) by enzymatic oxidation at the 6-position of the pyrimido ring with purified bovine XO (**Figure 36**). The material was purified by HPLC and exhibited radiochemical purity of >99% (**Figure 41**). Freshly prepared [^{14}C]6-oxo-M_1dG was diluted in sterile saline solution and administered iv (15 μCi/kg, 83 μg/kg) to male Sprague Dawley rats (n = 4) via the jugular catheter. Two animals also contained catheters surgically implanted into the bile duct. The animals were housed in metabolism cages throughout the duration of the experiment to collect urine, feces, and bile (where available) at intervals. All samples were collected into pre-tared tubes and weighed following collection to determine the mass of sample collected. The biological samples were processed by liquid scintillation counting (**Figure 42**) and the results from the elimination data are summarized in **Table 4**. The non-bile-catheterized rats eliminated 30 ± 5% of the dose in the urine, while 70 ± 5% was recovered in the feces. In bile-catheterized animals, 45 ± 7% was recovered in urine, 1% in feces, and 54 ± 2% in bile.

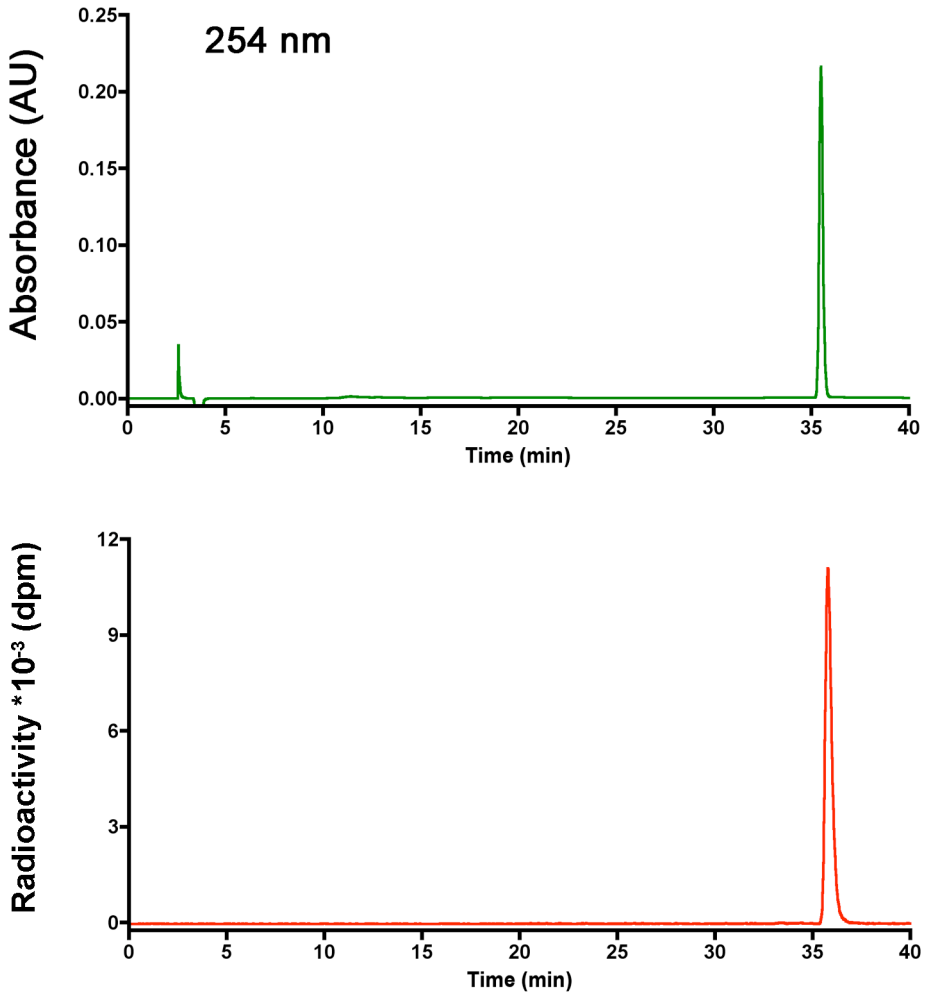

Figure 41. HPLC-UV and HPLC-βRAM analysis of the [^{14}C]6-oxo-M$_1$dG dosing solution. (Top) HPLC-UV analysis at 254 nm and (Bottom) radiochemical analysis with βRAM detection.

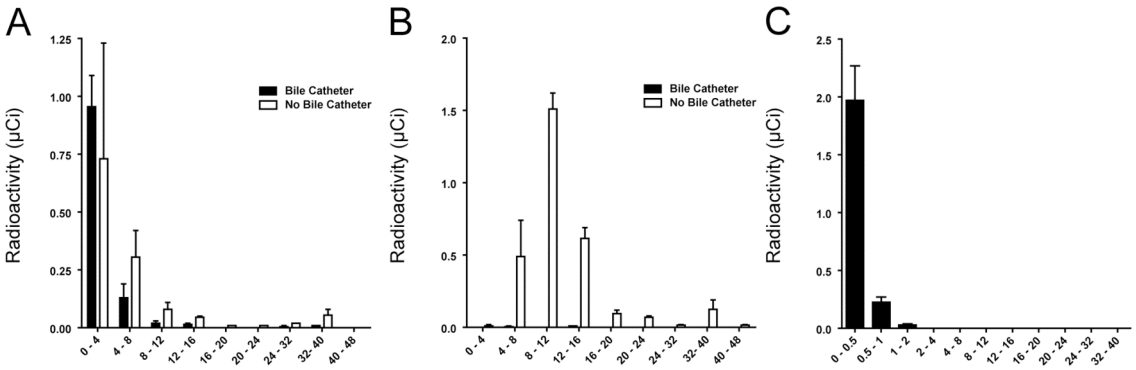

Figure 42. [^{14}C]Recovery following administration of [^{14}C]6-oxo-M$_1$dG. Male Sprague Dawley rats were dosed iv with [^{14}C]6-oxo-M$_1$dG (15 μCi/kg) and housed in metabolism cages to collect urine, bile and feces during the experiment. A, [^{14}C]Recovery in urine from bile-catheterized and non-bile-catheterized animals. B, [^{14}C]Recovery in feces from bile-catheterized and non-bile-catheterized animals. C, [^{14}C]Recovery in bile from bile-catheterized animals.

Table 4. Total radioactivity recovered following administration of [^{14}C]6-oxo-M$_1$dG. [^{14}C]6-Oxo-M$_1$dG (15 μCi/kg) was administered iv to male Sprague Dawley rats with (n = 2) or without (n =2) surgically implanted bile catheters.

	Bile Catheter	No Bile Catheter
Dose (μCi)	3.5 ± 0.05	4.15 ± 0.05
Urine	1.84 ± 0.26	1.25 ± 0.39
Feces	0.03 ± 0.01	2.90 ± 0.16
Bile	2.22 ± 0.34	*NA*
Recovery (%)	114.6 ± 4.5	101.2 ± 15.2

Analysis of [^{14}C]6-oxo-M_1dG metabolism in urine and bile

In all HPLC radiochemical profiles, the principal peak observed eluted with the retention time of 6-oxo-M_1dG (**Figure 43**). No significant secondary metabolites of 6-oxo-M_1dG were observed during any collection interval. Therefore, 6-oxo-M_1dG was determined to be metabolically stable (>97%) and not subject to further metabolism *in vivo*. These data suggest that the minor metabolites observed in the [^{14}C]M_1dG study arose directly from M_1dG and did not represent further metabolism of 6-oxo-M_1dG.

[^{14}C]6-Oxo-M_1dG also exhibited significant biliary clearance (as seen in the [^{14}C]M_1dG study), which suggested 6-oxo-M_1dG was absorbed by the liver and subject to transport into bile. As seen in the [^{14}C]M_1dG study, [^{14}C]6-oxo-M_1dG also exhibited a long residence time (>48 h) following iv administration. The identity of 6-oxo-M_1dG was verified by selected reaction monitoring analysis of the late time-point urine collections (**Figure 40**).

Discussion

The endogenous peroxidation-derived DNA adduct, M_1dG, was recently found to undergo metabolism *in vivo* to a single, oxidized metabolite, 6-oxo-M_1dG (157). Our laboratory has now performed definitive *in vivo* analysis of the metabolism and excretion of M_1dG and its major metabolite, 6-oxo-M_1dG, by the incorporation of stable carbon-14 tracers into these molecules. Male Sprague Dawley rats with (n = 2) and without (n = 2) bile catheters were dosed iv with [^{14}C]M_1dG at 22 μCi/kg (123 μg/kg). Approximately 50% of the administered dose was recovered in the urine while the remainder was recovered in the feces and bile (**Figure 38**). 6-Oxo-M_1dG accounted for 45% of the

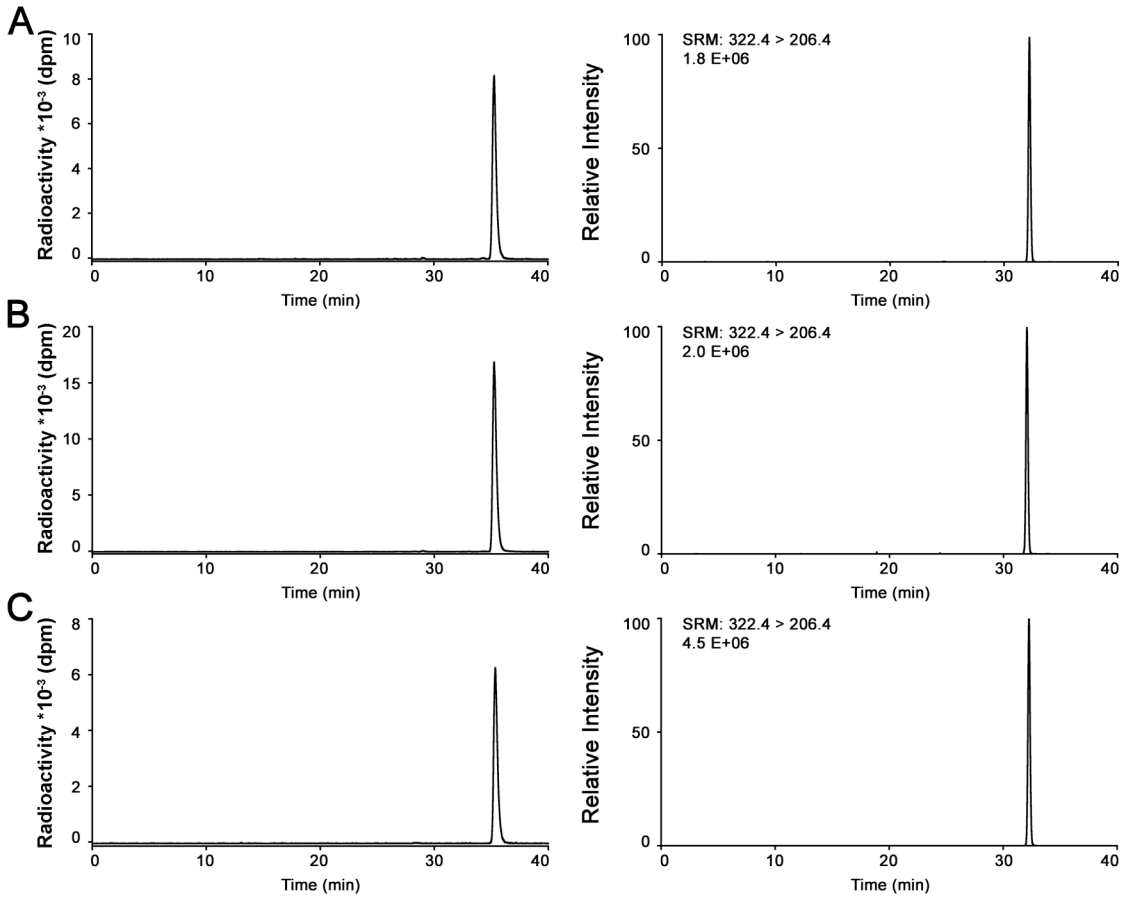

Figure 43. HPLC-radiochemical and -MS/MS profiles of urine and bile samples following administration of [^{14}C]6-oxo-M$_1$dG. Male Sprague Dawley rats received a single iv dose of [^{14}C]6-oxo-M$_1$dG (15 μCi/kg). A, Representative urine sample (0-4 h) from a non-bile-catheterized animal was profiled by radiochemical detection and separately by LC-MS/MS using selected reaction monitoring selected reaction monitoring following the transition for 6-oxo-M$_1$dG (*m/z* 322.4 → 206.4). B, Representative urine sample (0-4 h) from a bile-catheterized animal was profiled by radiochemical detection and separately by LC-MS/MS using selected reaction monitoring following the transition for 6-oxo-M$_1$dG (*m/z* 322.4 → 206.4). C, Representative bile sample (0-0.5 h) from a bile-catheterized animal was profiled by radiochemical detection and separately by LC-MS/MS using selected reaction monitoring following the transitions for 6-oxo-M$_1$dG (*m/z* 322.4 → 206.4).

recovered radioactivity. The significant conversion of M_1dG to 6-oxo-M_1dG prompted additional metabolism and elimination studies on the metabolite. Upon dosing [^{14}C]6-oxo-M_1dG (15 μCi/kg, 83 μg/kg), 30 ± 6% of the radioactivity was recovered in the urine while 71 ± 6% was excreted in the feces of non-bile-catheterized animals. Rats containing bile catheters deposited 45 ± 7% of the radioactivity into the urine, 54 ± 2% into the bile, and 1% into the feces. Profiling bile and urine samples revealed that the metabolite, [^{14}C]6-oxo-M_1dG, was cleared unchanged (>97%) with no significant metabolism to secondary metabolites.

The simplicity of M_1dG metabolism and elimination is noteworthy (**Figure 44**). A single metabolite is formed that is neither conjugated nor further metabolized. In our study, 6-oxo-M_1dG represents a significant contribution (45% of the total dose) in the overall mass balance of M_1dG. It was previously hypothesized that depurination reactions may give rise to the free base, M_1G, as an alternate metabolic pathway (*261*); however, no accumulation of this compound or its metabolites was observed in our analysis. Furthermore, our investigation of 6-oxo-M_1dG metabolism revealed that it was exceptionally stable *in vivo* (>97%) and not metabolized to additional products. It should be noted that 6-oxo-M_1dG contains a possible Michael acceptor on the pyrimido ring (at C_8), but no evidence for nucleophilic addition or conjugation (glutathione addition) was observed in the recovered samples.

Considering that the main metabolite of M_1dG is a singly oxidized species, the extent to which M_1dG and 6-oxo-M_1dG were cleared through biliary excretion was unexpected. The iv administration of M_1dG and 6-oxo-M_1dG and subsequent appearance of these products in bile and feces strongly suggests the role of transporters in the

disposition of M_1dG and 6-oxo-M_1dG *in vivo*. Nucleosides and nucleoside derivatives are reported substrates for transport proteins, such as organic anion transporters (*262*) and the concentrative Na^+-dependent (CNT) and equilibrative Na^+-independent nucleoside transporters (ENT) (*263*). Indeed, ENT isoforms appear to be involved in nucleoside transport into hepatocytes (*264*), whereas the CNT isoforms are expressed along the bile canalicular membrane and are likely involved in biliary transport (*265*). It would be interesting to evaluate their involvement in DNA adduct disposition in future studies.

The notion that DNA adducts were subject to biliary elimination was first suggested by the work of Wang and Hecht (*266*). Following an iv administration of N^7,C-8 *N*-nitrosopyrrolidine guanine adduct to F344 rats, 52.2% of the administered radioactivity was recovered in the urine. Ninety percent of the urinary radioactivity was attributed to the parent molecule. The remaining 47.8% of the radioactivity was either retained in the animal or cleared through the biliary elimination pathway. However, neither biliary elimination nor fecal elimination was measured in their study. It is tempting to speculate that either the N^7,C-8 *N*-nitrosopyrrolidine guanine adduct was a direct substrate for biliary transport or that the adduct underwent metabolism that rendered the molecule a substrate for transport into bile. Our findings, in addition to those of Wang and Hecht, suggest that disposition of adducts may be a key limiting factor in the analysis of urinary DNA adducts and their metabolites.

The amount of M_1dG administered in our study (approximately 31 μg per animal) was lower than our previous investigation (approximately 500 μg per animal) (*157*). However, the administered dose is still higher than the anticipated physiological levels of M_1dG in the rat (*154*). Administration of μg levels of M_1dG and 6-oxo-M_1dG in these

studies was necessary to obtain a reliable mass balance and metabolite profile from which to proceed with future physiological determinations.

Administration of [^{14}C]M_1dG and [^{14}C]6-oxo-M_1dG resulted in rapid elimination of the administered material in the first 4 h, followed by an extended slow release of the remaining dose. During the LC-MS/MS analysis of late time-point urine collections from the [^{14}C]M_1dG administration study, we observed that 6-oxo-M_1dG was as abundant or more abundant than the parent molecule M_1dG. Considering the likely involvement of transporters in the disposition of M_1dG, it remains possible that transport may afford an effectively high concentration at the site of metabolism to facilitate the production of 6-oxo-M_1dG even at low concentrations. Inspection of the relative urinary elimination rate for M_1dG and 6-oxo-M_1dG suggests this increase cannot simply be explained by a slower rate of elimination for 6-oxo-M_1dG, since the elimination profiles for M_1dG and 6-oxo-M_1dG are nearly identical. Ongoing efforts in our laboratory are directed towards assessing the contribution of 6-oxo-M_1dG to the overall levels of M_1dG in human and animal studies.

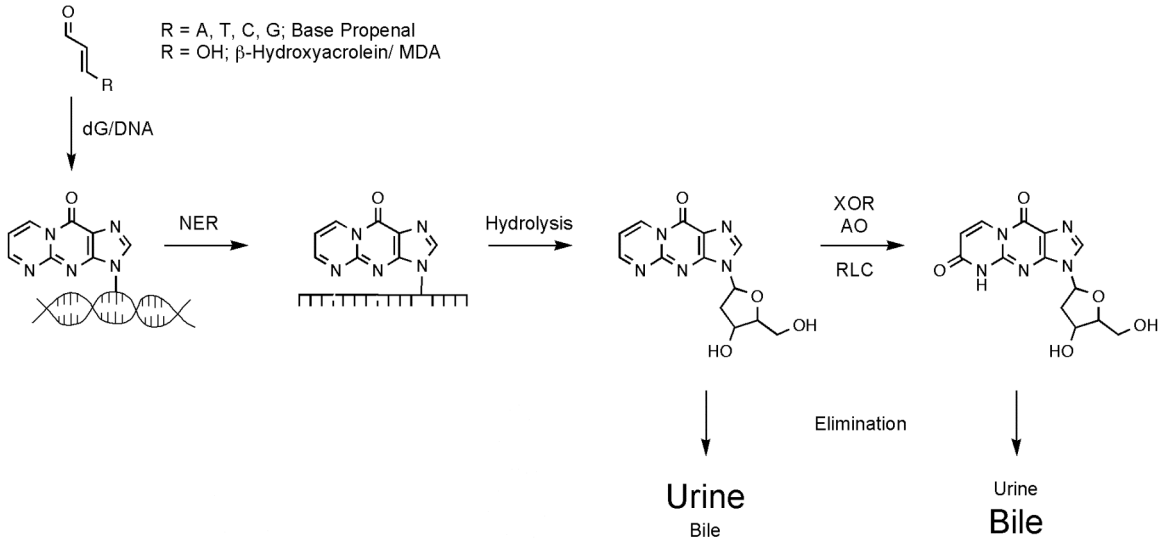

Figure 44. Metabolic processing of M_1dG. RLC, rat liver cytosol.

CHAPTER IV

ANALYSIS OF [^{14}C]M_1dG METABOLISM IN THE RAT BY ACCELERATOR MASS SPECTROMETRY

Summary

Our laboratory is investigating the *in vitro* and *in vivo* metabolic processing of endogenously formed DNA adducts as a means of evaluating candidate urinary biomarkers. In particular, we have focused our studies on the metabolism and disposition of the peroxidation-derived pyrimidopurinone dG adduct, M_1dG, and its principal metabolite, 6-oxo-M_1dG. We now report the metabolic processing of M_1dG at concentrations 4 to 8 orders of magnitude lower in concentration than previously analyzed, by the use of accelerator mass spectrometry analysis. Administration of 2.0 nCi/kg [^{14}C]M_1dG resulted in 49% of the ^{14}C recovered in urine whereas 51% was recovered in feces. In urine samples, approximately 40% of the ^{14}C corresponded to the metabolite, 6-oxo-M_1dG. Following iv administration of 0.5 and 54 pCi/kg [^{14}C]M_1dG, approximately 25% of the urinary recovery corresponded to the metabolite, 6-oxo-M_1dG. Thus, upon administration of trace amounts of M_1dG, a significant percentage of 6-oxo-M_1dG was produced suggesting that 6-oxo-M_1dG may be a useful urinary marker of exposure to endogenous oxidative damage.

Introduction

Results from *in vitro* and *in vivo* metabolism experiments have demonstrated that M_1dG is subject to enzymatic oxidation to the metabolite, 6-oxo-M_1dG (*157*). *In vivo*

radiochemical tracer studies performed with [^{14}C]M_1dG revealed that following iv administration, 45% of the isotope was recovered as the metabolite, 6-oxo-M_1dG (*267*). 6-Oxo-M_1dG accounted for 20% of the total radioactivity in the early time-point urine samples; however, at late time-points, there was an approximate equal ratio of M_1dG to 6-oxo-M_1dG. The increase in observed metabolism was unexpected given the calculated K_m for M_1dG metabolism *in vitro* in rat liver cytosol is 370 μM (*157*). Additionally, since endogenously formed adducts are produced in very low amounts, we were curious to know if M_1dG would be metabolized when administered at very low quantities, which might approximate physiological levels. To address this question, we employed nCi and pCi dosing procedures with [^{14}C]M_1dG and monitored metabolism and elimination. Analysis of biological samples from these studies was possible by the use of accelerator mass spectrometry (AMS).

Experimental Procedures

Chemicals and reagents

All chemicals were obtained from commercial sources and used as received. Solvents were of HPLC grade purity or higher. [^{14}C]dG was purchased from Sigma (St. Louis, MO). [^{14}C]M_1dG was synthesized as previously described (*259*). HPLC-UV separations were performed with either a Waters 2695 autosampler and binary pump or a Waters 1585 binary pump and 717plus autosampler, and a Waters 2487 dual wavelength UV detector (Milford, MA).

Administration of [^{14}C]M_1dG to Sprague Dawley rats

Animal protocols were performed under approval of Vanderbilt University and in accordance with the Institutional Animal Care and Use Committee policies. Male Sprague Dawley rats (225-250 g), with vascular catheters surgically implanted in the jugular vein were obtained from Charles River Laboratories (Wilmington, MA) and housed in shoebox cages. Animals were transferred to metabolism cages prior to dosing and allowed to feed *ad libitum* throughout the experiment. The [^{14}C]M_1dG dosing solution (>99% pure) was prepared in sterile saline to the desired specific activity (3.0 dpm/μL, 0.1 dpm/μL and 0.001 dpm/μL) and administered via the jugular catheter in approximately 0.3 mL of total volume over 45 s. All doses were followed by 0.4 mL of sterile heparinized saline to flush the catheters.

One cohort of four animals was used for the 2.0 nCi/kg (11 ng/kg) dosing. Three animals received the [^{14}C]M_1dG dosing solution (3.0 dpm/μL), and 1 animal received a vehicle control (sterile saline). Urine was collected over intervals (pre-dose, 0-4, 4-8, 8-12, 12-16, 16-20, and 20-24 h). All samples were stored at –20 °C following collection.

A second cohort of 4 animals was used for the 0.5 pCi/kg (3.0 pg/kg) and 54 pCi/kg (300 pg/kg) studies. Three animals received the 0.5 pCi/kg [^{14}C]M_1dG dosing solution (0.001 dpm/μL), and 1 animal received the vehicle control (saline). After 12 h, the animals were removed from the metabolism cages and returned to shoebox cages overnight. Metabolism cages were thoroughly washed following the 0.5 pCi/kg dose. Approximately 24 h after receiving the 0.5 pCi/kg dose, the same 3 experimental animals received 54 pCi/kg [^{14}C]M_1dG dosing solution (0.1 dpm/μL) and the same control animal

received a vehicle administration (saline). Urine was collected over intervals (pre-dose, 0-2 and 2-4, and 4-8). All samples were stored at –20 °C.

Fecal samples were dried on the bench top overnight. All pellets from a given time-point were pooled, placed in a sealable plastic bag, crushed with a rubber mallet, and stored at -20°C. For AMS analysis, fecal samples were weighed, diluted in 1 N NaOH, and stored at -20 °C.

HPLC fraction collection

Urine samples were centrifuged for 10 min at 14,000 g. Supernatants were removed and directly injected onto a Phenomenex Luna C18(2) column (4.6 x 250 nm, 5 μm) equilibrated with 90% solvent A (10 mM potassium phosphate in H_2O, pH 7.8) and 10% solvent B (methanol) at a flow rate of 1.0 mL/min. The solvent was programmed as follows: a linear gradient from the equilibration conditions to 20% B in 10 min, holding at 20% B for 10 min, increasing to 90% B in 0.1 min, holding for 5 min, decreasing to 10% B in 0.1 min and re-equilibrating to initial conditions. Standards applied to this gradient eluted at 12.7 min (6-oxo-M_1dG) and 15.8 min (M_1dG). Standards spiked into blank urine samples demonstrated slight shifts in retention to 11.5 min (6-oxo-M_1dG) and 15.7 min (M_1dG). 300 μL injections were made for the 2.0 nCi/kg study and 200 μL injections were made for the 54 pCi/kg and 0.5 pCi/kg studies. Fractions were collected from 10.5 min to 12.5 min for 6-oxo-M_1dG and from 15 to 17 min for M_1dG. Samples were evaporated to dryness under a stream of nitrogen in a heated water bath and stored at -20 °C.

AMS analysis

AMS analyses were conducted at the MIT BEAMS Laboratory using the instrument and procedures described elsewhere (*268-271*). Urine samples and fecal extracts were diluted as required to bring the total carbon and ^{14}C concentrations within the dynamic range of the AMS system and analyzed without further processing. HPLC fractions were reconstituted with appropriate measured volumes of H_2O. Aliquots of urine, fecal, and HPLC samples (1.50 μL) were absorbed into pellets of packed CuO powder that had previously been exposed for 30 min to an atmosphere of O_2 at 720 °C. After drying briefly in a vacuum oven, the sample-loaded CuO pellets in their holders were transferred to a laser-induced combustion interface for subsequent AMS analysis. Each run of samples was organized to include quantitation standards (0.0030 dpm/μL) and blanks (1 μg/μL albumin). Quantitation was performed by integrating peaks produced in the continuous trace of ^{14}C detector count rate vs. time generated during operation of the combustion interface, which produces and delivers the CO_2 of combustion to the AMS ion source, and taking the product of the sample:standard peak area ratio multiplied by the standard concentration as the concentration of the sample. All samples were analyzed in duplicate.

Results

nCi dosing of [^{14}C]M_1dG

[^{14}C]M_1dG was synthesized and purified as previously described (*259, 267*). The purified material was diluted in sterile saline to a specific activity of 3.0 dpm/μL for a

final dosing load of 2.0 nCi/kg. The resulting solution was administered to male Sprague Dawley rats via a catheter surgically implanted in the jugular vein. Three animals received [^{14}C]M_1dG dosing solution, while a fourth animal received a vehicle control (saline). Animals were housed in metabolism cages to collect urine and feces at intervals over the course of the experiment.

Urine and fecal samples were subject to AMS analysis for total [^{14}C]recovery (**Table 5**). Forty-nine percent of the recovered ^{14}C was found in urine while 51% was found in feces. Approximately 84% of the urinary radioactivity was collected in the first 4 h and isotope was observed out to 24 h of collection (**Figure 45**). This elimination profile was very similar to the previously observed time-course from the μCi dosing of [^{14}C]M_1dG (*267*). No ^{14}C was detected in any biological samples from the vehicle control animal at levels measurably above the background levels (standard isotopic abundance) of ^{14}C present in biological samples.

To determine the contribution of M_1dG and 6-oxo-M_1dG to the total ^{14}C content in the urine samples fraction collection analysis was performed. Urine samples were injected directly onto a C18 HPLC column and fractions corresponding to either M_1dG or 6-oxo-M_1dG were collected (**Figure 46A**). The collected fractions were then analyzed by AMS (**Figure 46B**). The average observed ratio of M_1dG to 6-oxo-M_1dG over the 24-h collection was 1.4:1, which demonstrated 40% of the urinary radioactivity corresponded to 6-oxo-M_1dG. The mean [^{14}C]recovery from fraction analysis was 82% with a standard deviation of 12%.

Table 5. Total [^{14}C]recovery in urine and feces following administration of 2.0 nCi/kg [^{14}C]M_1dG to male Sprague Dawley rats (n = 3).

	AMS Analysis
Dose (dpm)	1027.00 ± 25.51
Urine	584.11 ± 91.10
Feces	603.97 ± 29.01
Recovery (%)	115.70 ± 3.67

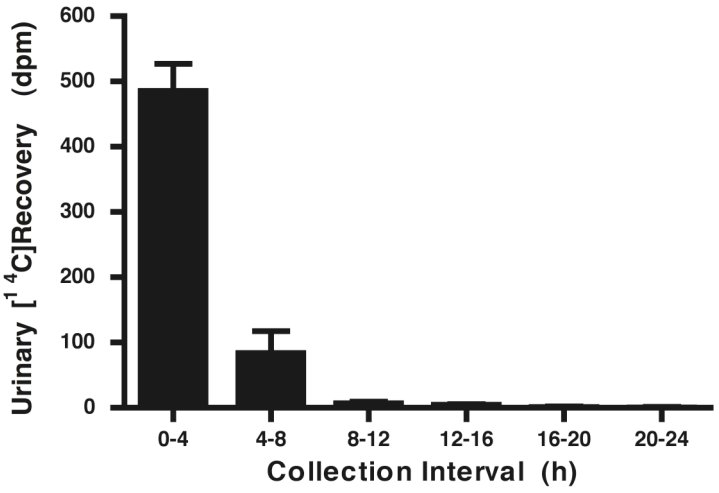

Figure 45. [^{14}C]Recovery in urine following administration of 2.0 nCi/kg [^{14}C]M_1dG to male Sprague Dawley rats (n = 3).

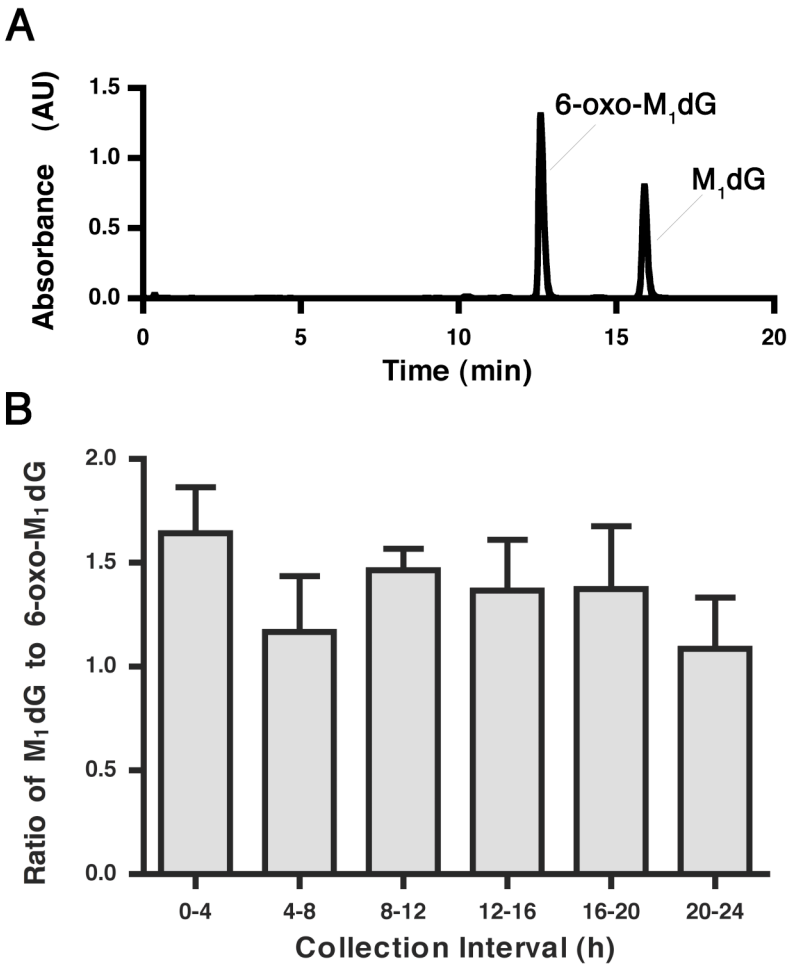

Figure 46. Fraction collection analysis of 6-oxo-M_1dG and M_1dG in rat urine. (A**)** Reverse phase HPLC separation of M_1dG and 6-oxo-M_1dG standards on a C18 column with a potassium phosphate, pH 7.8, and methanol gradient. **(**B**)** Ratio of M_1dG to 6-oxo-M_1dG in rat urine over time following administration of 2.0 nCi/kg [^{14}C]M_1dG to male Sprague Dawley rats (n = 3).

pCi dosing of [^{14}C]M_1dG

Based on our [^{14}C]M_1dG nCi dosing results we lowered the dose to our AMS limit of detection for ^{14}C in urine. We formulated dosing solutions at 0.001 and 0.1 dpm/μL for a final dosing load of 0.5 and 54 pCi/kg, respectively. Three male Sprague Dawley rats were dosed first at 0.5 pCi/kg [^{14}C]M_1dG via catheters surgically implanted into the jugular vein. A fourth animal received vehicle (saline) control. The animals were housed in metabolism cages during the course of the experiment to collect urine at intervals. After 12 h, the animals were removed from the metabolism cages and placed into standard shoebox cages. The same animals were returned to metabolism cages and again dosed at 54 pCi/kg with [^{14}C]M_1dG (n = 3) or vehicle control (n = 1) approximately 24 h following the 0.5 pCi/kg injection. Urine was collected at intervals during the experiment.

Total ^{14}C content in urine samples was assessed directly by AMS analysis. The urinary data from the 54 pCi/kg dosing is summarized in **Figure 47**; approximately 42% of the administered ^{14}C was recovered in urine. Direct AMS analysis of urine samples from the 0.5 pCi/kg dose did not offer significant signal above background, and no total urinary [^{14}C]recovery could be determined. Significant ^{14}C enrichment was observed in all fractions following HPLC purification. Analyte was detected in some urine samples following AMS analysis of the 0.5 pCi/kg samples, albeit at a low signal-to-noise. Only samples that displayed a signal-to-noise ≥ 3 were considered in this analysis. The average observed ratio of M_1dG to 6-oxo-M_1dG was approximately 3:1 following administration at either 54 pCi/kg or 0.5 pCi/kg [^{14}C]M_1dG (**Table 6**), which implies 25% of the total ^{14}C was recovered as 6-oxo-M_1dG following administration of M_1dG at

the AMS limit of detection. The mean [^{14}C]recovery from fraction analysis performed on the 54 pCi/kg urine samples was 55% with a standard deviation of 20%. A similar decrease in recovery was observed with late time-point urine collections in the nCi dosing study. Recoveries of nearly 86-99% were obtained during the first 8 h of collection and recoveries of 56-78% were obtained during the final 8 h of collection following administration of 2.0 nCi/kg M_1dG. Thus, due to the very low analyte levels, the lower recovery was attributed to non-specific loss.

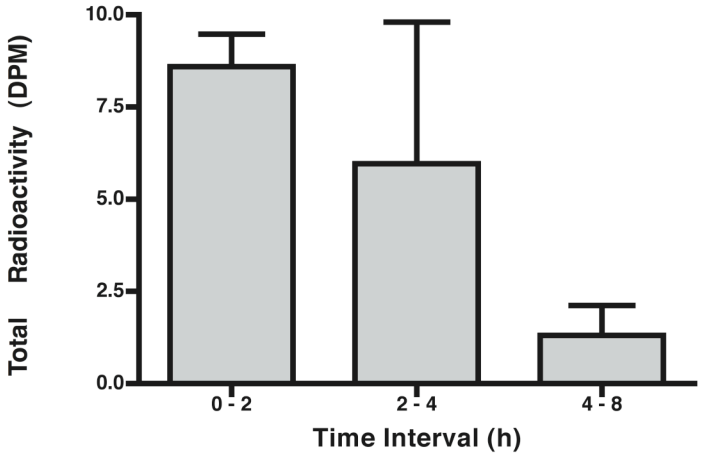

Figure 47. [^{14}C]Recovery in urine following administration of 54 pCi/kg [^{14}C]M_1dG to male Sprague Dawley rats (n = 3).

Table 6. Percent of [^{14}C]M_1dG converted to [^{14}C]6-oxo-M_1dG in urine following administration of 0.5 pCi/kg or 54 pCi/kg [^{14}C]M_1dG to male Sprague Dawley rats (n = 3).

	Collection Interval (h)	Percent 6-oxo-M_1dG
54 pCi/kg	0 – 2	24.5 ± 3.0
	2 – 4	26.1 ± 2.4
0.5 pCi/kg	0 – 2	25.4 ± 10.5
Mean & Standard Deviation		25.4 ± 5.9

Discussion

^{14}C-Incorporation for use in metabolism and elimination studies provides unambiguous tracking of the isotopically labeled molecule. Analysis of ^{14}C is most frequently performed by measurement of radioactivity. The use of ^{14}C in DNA adduct analysis has been limited, principally due to the poor yields in synthesis, coupled to the need of sufficient amounts of material for traditional liquid scintillation counting. The advent of AMS analysis has greatly reduced the required isotope levels for experimental analysis, by altering the mode of detection from decay counting to mass analysis (*271*). Our study suggests that less than 1000 dpm per animal are required for sound *in vivo* metabolism and elimination studies involved in evaluating candidate urinary biomarkers. Results from this type of analysis provide, at a minimum, recovery and elimination data; and when coupled to fraction collection analysis offers an estimation of percent metabolism of the administered material. Thus, AMS analysis may be applicable to

many toxicology problems and significantly impact the development and evaluation of biomarkers.

The use of a ^{14}C radiochemical tracer stably incorporated into M_1dG for use *in vivo* in rats has allowed us to investigate the metabolic processing at very low adduct concentrations. Analysis was performed at the limit of detection by AMS measurements. Our findings revealed that when [^{14}C]M_1dG was administered at 0.5 and 54 pCi/kg (approximately 750 fg and 75 pg per animal, respectively) approximately 25% of the urinary ^{14}C was recovered as 6-oxo-M_1dG. Interestingly, when [^{14}C]M_1dG was administered at 2.0 nCi/kg (approximately 2.5 ng per animal) approximately 40% of the urinary ^{14}C was recovered as 6-oxo-M_1dG. Total ^{14}C elimination was determined following 2.0 nCi/kg dosing and revealed that 49% of the recovered ^{14}C appeared in urine and 51% was found in feces.

The observed contribution of 6-oxo-M_1dG to the total M_1dG in rat urine approximated our previous estimations based on ^{14}C content (*267*). The fact that 25-40% of the administered [^{14}C]M_1dG was recovered from urine as 6-oxo-M_1dG in the present studies strongly suggests that M_1dG metabolism is likely to occur under physiological conditions of M_1dG production. A prior estimate of the M_1dG elimination rate in human urine demonstrated the adduct was eliminated at 12 fmol/kg/24 h (*154*). This elimination rate corresponds to approximately 3.6 pg/kg/24 h. Our administration of [^{14}C]M_1dG at 0.5 and 54 pCi/kg (750 fg and 75 pg, respectively) brackets the anticipated daily physiological clearance of M_1dG. The rate of elimination for M_1dG in the rat has not been determined. However, if we assume the average elimination rate to be similar in

rats as observed in humans, then based on the elimination of 30 mL of urine per day, a total clearance of 100 fg may be anticipated in the rat.

It should be noted that our discussion of the percent conversion to 6-oxo-M_1dG following nCi and pCi dosing is limited to urinary analysis. Prior studies have shown that biliary elimination is a key route of excretion for 6-oxo-M_1dG (*267*). Following administration of 6-oxo-M_1dG to Sprague Dawley rats, 55-70% of the dose was cleared in either bile or feces. And following administration of M_1dG to Sprague Dawley rats, 70% of the dose cleared in bile corresponded to 6-oxo-M_1dG. If we apply the same biliary conversion to the nCi and pCi dosing studies, then greater than 50% of the administered material in the current studies would have been converted to 6-oxo-M_1dG. This represents a significant portion of the total M_1dG.

The reasons for the observed differences in percent conversion at different dosing levels are unknown. However, several factors may have influenced the outcome. First, while all animals investigated were Sprague Dawley rats, it is possible that small changes in expression of enzymes that either metabolize or transport M_1dG might affect the percent conversion between cohorts. XOR and AO have been implicated in M_1dG metabolism, and decreased expression or activity of these enzymes could decrease the production of 6-oxo-M_1dG. Alternatively, an increase or decrease in expression of transport proteins that affect the disposition of M_1dG or 6-oxo-M_1dG may alter the observed ratio of M_1dG and 6-oxo-M_1dG in rat urine.

A second possibility for decreased conversion of M_1dG to 6-oxo-M_1dG may be related to enzyme efficiency. Based on the calculated K_m for M_1dG metabolism in rat liver cytosol (370 μM) (*157*), *in vivo* metabolism at very low concentrations may not be

expected. However, at doses as low as 750 fg, a clear conversion to 6-oxo-M_1dG was observed. It is possible that at the lower level of administration (0.5 pCi/kg and 54 pCi/kg) the effective concentration at the site of metabolism was not sufficient to promote turnover at saturating conditions. Thus, a decrease in the percent conversion may be observed at lower levels of abundance.

Based on these and prior experiments, it is clear that iv administered M_1dG is taken up, and likely accumulates, in the liver. The physiological explanation for this is unknown, but it is reasonable to assume that transport proteins are involved in the disposition of M_1dG and 6-oxo-M_1dG. The result of this process leads to oxidative metabolism of exogenously administered M_1dG, even at concentrations that approach the analytical limit of sensitivity by AMS. Thus, there exists a distinct possibility that metabolism occurs at the projected rates of M_1dG formation in animals and humans. Our laboratory is currently developing analytical methods to probe for the appearance of M_1dG and 6-oxo-M_1dG in human elimination products.

CHAPTER V

M_1G METABOLISM *IN VITRO* AND *IN VIVO*

Summary

Oxidative damage is considered a major contributing factor to genetic diseases including cancer. Our laboratory is evaluating endogenously formed DNA adducts as genomic biomarkers of oxidative injury. Recent efforts have focused on investigating the metabolic stability of adducts *in vitro* and *in vivo*. Here, we demonstrate that the base adduct, M_1G, undergoes oxidative metabolism *in vitro* in rat liver cytosol (K_m = 105 μM and V_{max}/K_m = 0.005 min^{-1} mg^{-1}) and *in vivo* when administered iv to male Sprague Dawley rats. LC-MS analysis revealed 2 metabolites containing successive additions of 16 amu. One- and two-dimensional NMR experiments showed oxidation occurred first at the 6-position of the pyrimido ring forming 6-oxo-M_1G, then at the 2-position of the imidazole ring yielding 2,6-dioxo-M_1G. Authentic 6-oxo-M_1G was chemically synthesized and observed to undergo metabolism to 2,6-dioxo-M_1G in rat liver cytosol (K_m = 210 μM and V_{max}/K_m = 0.005 min^{-1} mg^{-1}). Allopurinol partially inhibited M_1G metabolism (75%) and completely inhibited 6-oxo-M_1G metabolism in rat liver cytosol. These inhibition studies suggest XOR is the principal enzyme acting on M_1G in rat liver cytosol and the only enzyme that converts 6-oxo-M_1G to 2,6-dioxo-M_1G. Both M_1G and 6-oxo-M_1G are better substrates (5-fold) for oxidative metabolism in rat liver cytosol than the deoxynucleoside, M_1dG. Alternative repair pathways or biological processing of

M_1dG makes the fate of M_1G of interest as a potential marker of oxidative damage *in vivo*.

Introduction

Many endogenously produced exocyclic ring adducts are substrates for base excision repair (*30*). Some adducts are subject to multiple repair pathways (i.e., 8-oxo-dG is repaired by base excision repair and presumably NER machinery (*125, 272*)). Etheno adducts bearing structural similarity to M_1dG (e.g., 1,N^2-ε-dG, 1,N^6-ε-dA, and 3,N^4-ε-dC) are substrates for DNA glycosylases (*217-219, 221, 273, 274*). The structural resemblance between M_1dG and the etheno adducts might suggest that similar, yet unknown, repair pathways are also involved in the repair of M_1dG. Emerging discoveries regarding induction of base excision repair enzymes *in vivo* in response to stress has made alternate routes of repair of particular interest (*275, 276*).

Our laboratory recently demonstrated that M_1dG was oxidized to 6-oxo-M_1dG in rats and that XOR and AO were the likely enzymes responsible (*157*). M_1dG oxidation was detected in rat and human liver cytosol and was in purified bovine XO. In all cases, 6-oxo-M_1dG was the sole product and there was no evidence for oxidation on the imidazole ring. This was surprising because the imidazole ring is the primary site for chemical oxidation on dG, and a site for oxidation on xanthine by XOR. The present report describes the *in vitro* and *in vivo* oxidation of the base, M_1G, a putative product of repair in M_1dG-containing DNA by glycosylase action (**Figure 48**). Results from our metabolism studies on M_1G show that it is a better substrate for enzymatic oxidation than M_1dG. Furthermore, its initial oxidation product, 6-oxo-M_1G, is susceptible to further

oxidation on the imidazole ring. When administered to Sprague Dawley rats, M_1G and both of the oxidized metabolites were excreted in urine. Thus, a family of oxidized metabolites may serve as biomarkers of M_1dG formation in genomic DNA.

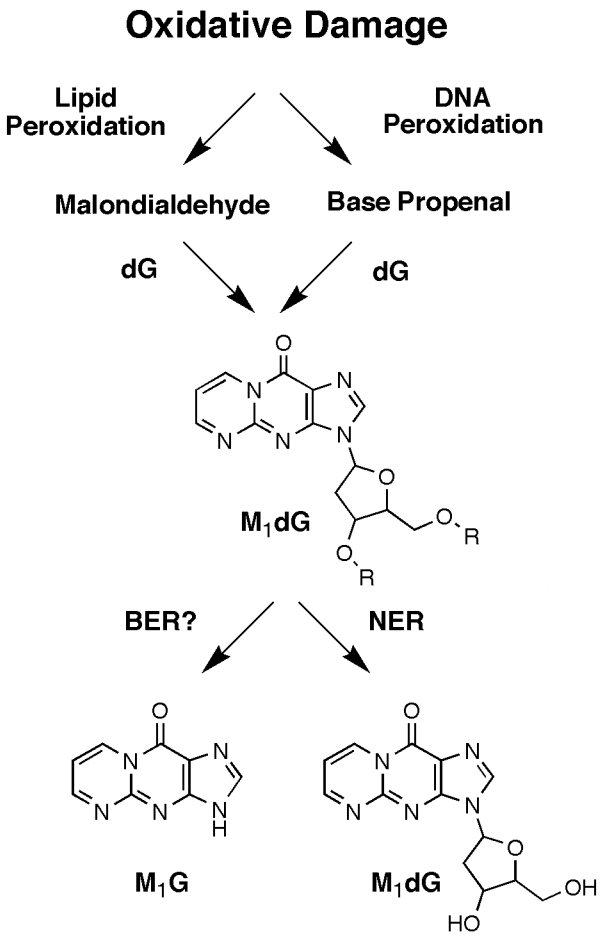

Figure 48. Formation of M_1dG from endogenous sources and possible routes of release from DNA.

Experimental Procedures

Chemicals and reagents

All chemicals were obtained from commercial sources and used as received. Solvents were of HPLC grade purity or higher. M_1G was synthesized as previously described (*230*). Rat liver cytosol was prepared by established methods (*231*). Purified bovine XO was purchased from CalBiochem (La Jolla, CA). HPLC-UV separations were performed on a Waters 2695 autosampler and binary pump with a Waters 2487 dual wavelength UV detector (Milford, MA). LC-MS/MS spectra were obtained on a ThermoFinnigan LCQ Deca-XP Ion Trap (San Jose, CA) with an inline Agilent 1100 series dual binary pump (Santa Clara, CA). Synthetic chemicals were purified by flash chromatography on a Biotage SP1 Instrument (Uppsala, Sweden).

M_1G treatment of rats

Animal protocols were performed under approval of Vanderbilt University and in accordance with the Institutional Animal Care and Use Committee policies. Male Sprague Dawley rats (225-250 g) with vascular catheters surgically implanted in the femoral and jugular veins were obtained from Charles River Laboratories (Wilmington, MA) and housed in shoebox cages. Animals were transferred to metabolism cages prior to dosing and allowed to feed *ad libitum* throughout the experiment. The M_1G dosing solution (5 mg/kg) was prepared in sterile saline and administered in the jugular catheter in approximately 0.5 mL of total volume over 45 s and flushed with 0.4 mL of sterile

heparinized saline. Urine and feces were collected over intervals (pre-dose, 0-4, 4-6, 6-10, and 10-24 h). All samples were stored at -80 °C until sample work-up.

Sample work-up and analysis

A sample of urine (25% of the total collected volume) was extracted by adding 2x volumes ethanol followed by 2x volumes chloroform and mixed vigorously. The phases were separated by centrifugation, the bottom organic layer was removed, and the remaining aqueous layer was extracted again with 2x volume of chloroform. The organic layers were pooled, dried under nitrogen, and reconstituted in potassium phosphate (0.2 M, pH 7.8). Samples (10 μL) were loaded onto a Phenomenex Luna C18(2) column (2.0 x 250 mm, 5 μm, Torrence, CA) equilibrated with 90% solvent A (0.5% formic acid in H_2O) and 10% solvent B (0.5% formic acid in methanol) at a flow rate of 0.3 mL/min. The solvent was programmed as follows: a linear gradient from equilibration conditions to 20% B in 10 min, holding at 20% B for 10 min, increasing to 80% B in 0.1 min, holding for 5 min, decreasing to 10% B in 0.1 min and, re-equilibrating to initial conditions. Eluting compounds were detected by LC/MS. Positive ion ESI was employed with the following parameters: spray voltage = 4.0 kV; capillary temperature = 325 °C; sheath gas = 52 psi; tube lens offset = 46 V; auxiliary gas = 56. Samples were analyzed by selected-ion monitoring.

Liver cytosol incubations

All sample preparations were performed at 4 °C. The final incubation conditions for the kinetic determinations contained 5 mg/mL rat liver cytosol, varied concentrations

of either M_1G (0.5, 10, 25, 50, 100, 150, 200, and 250 μM) or 6-oxo-M_1G (5, 20, 40, 60, 80, 100, 150, 200, 400, 600, and 900 μM) and 0.4% DMSO in 0.2 M potassium phosphate (pH 7.8). IC_{50} determinations were carried out in 0.2 M potassium phosphate (pH 7.8), and 5 mg/mL rat liver cytosol at the calculated K_m for each substrate (M_1G = 105 μM and 6-oxo-M_1G = 210 μM). The inhibitors were diluted in DMSO (0.4% total reaction volume). Reagents were equilibrated to 37 °C for 5 min and the reaction initiated by addition of substrate. Reactions were terminated after 60 min by adding 2 volumes of ice-cold ethanol, vortexed, and extracted twice with 2 volumes of chloroform. The extracts were evaporated under nitrogen, reconstituted in H_2O, and analyzed by HPLC-UV. Extraction of M_1G from rat liver cytosol into ethanol: chloroform resulted in a 60 to 70% recovery from rat liver cytosol incubations. Samples were separated on a Phenomenex Luna C18(2) column (4.6 x 250 nm, 5 μm) equilibrated with 90% solvent A (0.5% formic acid in H_2O) and 10% solvent B (0.5% formic acid in methanol) at a flow rate of 1.0 mL/min. The solvent was programmed as follows: a linear gradient from the equilibration conditions to 20% B in 10 min, holding at 20% B for 10 min, increasing to 80% B in 0.1 min, holding for 5 min, decreasing to 10% B in 0.1 min, and re-equilibrating to initial conditions. Samples from the kinetic determinations were quantified in reference to a standard curve prepared by spiking known concentrations of either M_1G (0.5. 25, 50, 100, 200, 300 μM) or 6-oxo-M_1G (5, 50, 100, 300, 500, 700, 900 μM) into 5 mg/mL rat liver cytosol solutions followed immediately by termination, extraction, and analysis as outlined above. Extraction of M_1G from rat liver cytosol into ethanol: chloroform resulted in a 40 to 50% recovery from rat liver cytosol incubations. All incubations and standards were performed in triplicate. The IC_{50} values were

calculated based on inhibition of substrate consumption (M_1G) or product production (2,6-dioxo-M_1G) in reference to the vehicle (DMSO) control. V_{max}/K_m and IC_{50} values were calculated with Prism software (Version 4.0c) using a nonlinear regression one-site binding and one-site competition models, respectively.

Biochemical synthesis of M_1G metabolites

M_1G was incubated at 250 μM in purified bovine XO (0.1 U) and allowed to react for 60 min. Incubations were pooled in a separatory funnel and mixed with 100 mL of ethanol, followed by 100 mL chloroform and shaken vigorously. The bottom organic layer was removed and the extraction was repeated a second time. The organic layers were pooled, dried with magnesium sulfate, and evaporated to dryness. The remaining residue was dissolved in HPLC-grade H_2O and purified by semi-preparative HPLC on a Phenomenex Luna C18(2) column (10 x 250, 10 μm). Isocratic elution (5 mL/min, 95:5 (H_2O: methanol), containing 0.5% formic acid) provided baseline resolution for eluting peaks: M_1G (~20 min), 6-oxo-M_1G (~24 min), and 2,6-dioxo-M_1G (~30 min). Each peak was collected, pooled, and extracted as above (twice with 2x volume ethanol/chloroform, pooled, dried and evaporated). The remaining product was attached to a vacuum pump to remove residual formic acid carried over from HPLC mobile phase. Samples were dissolved in d_6-DMSO and analyzed on a 400 MHz NMR.

Pyrimido[1,2-f]purin-6,10(3H,5H)-dione (6-oxo-M_1G). ^{1}H-NMR (400 MHz, d_6-DMSO): δ 8.64 (d, 1H, J = 8 Hz, H_8), 8.06 (s, 1H, H_2), 6.21 (m, 1H, J = 8 Hz, H_7). ESI-MS *m/z*: 204.3.

Pyrimido[1,2-f]purin-2,6,10(1H,3H,5H)-trione (2,6-dioxo-M_1G). ^{1}H-NMR (400 MHz, d_6-DMSO): δ 10.73 (s, 2.5H, N_1/N_3-H), 8.56 (d, 1H, *J* = 8 Hz, H_8), 6.18 (m, 1H, *J* = 8 Hz, H_7). ^{1}H-NMR (400 MHz, d_6-DMSO with D_2O): δ 8.57 (d, 1H, *J* = 8 Hz, H_7), 6.20 (m, 1H, *J* = 8 Hz, H_7). ESI-MS *m/z*: 220.3.

Chemical synthesis of pyrimido[1,2-f]purin-6,10(3H,5H)-dione (6-oxo-M_1G). 6-Oxo-M_1dG synthesis was carried out as described with minor modifications (*157*). The resulting product, 6-oxo-M_1dG, was purified by reversed phase chromatography on a C-18 Biotage cartridge (25+S). The pooled fractions were subjected to acid hydrolysis (0.1 N HCl for 60 min) and re-purified on a C-18 Biotage cartridge. The resulting product was analyzed by LC-MS and NMR spectroscopy to confirm the structure. ^{1}H-NMR (400 MHz, d_6-DMSO): δ 8.62 (d, 1H, *J* = 8 Hz, H_8), 8.04 (s, 1H, H_2), 6.18 (d, 1H, *J* = 8 Hz, H_7). ESI-MS *m/z*: 204.3.

HMBC analysis of M_1G-M1 (6-oxo-M_1G). HMBC experiments were acquired using an 11.7 T Oxford magnet equipped with a Bruker DRX console operating at 500.13 MHz and a 5 mm cryogenically cooled NMR probe. J_1(C-H) filtered HMBC experiments were acquired using a 2048 x 256 data matrix, a J_1(C-H) value of 9 Hz for detection of long range couplings resulting in an evolution delay of 55ms, J_1(C-H) filter delay of 145 Hz (34 ms) for the suppression of one-bond couplings, a recycle delay of 1.5 s and 64 scans per increment. The HMBC data was processed using a p/2 shifted squared sine window function and displayed in magnitude mode.

Saturation transfer NMR analysis of M_1G-M1 (6-oxo-M_1G). Routine (black trace) and saturation transfer (red trace) ^{1}H-NMR experiments were acquired using a 9.4 T Oxford magnet equipped with a Bruker AV-I console operating at 400.13 MHz.

Experimental conditions for standard 1H-NMR experiments included 12 ppm spectral sweep width, recycle delay of 1.5 s and 16 number of scans. Experimental parameters for the saturation transfer experiment included a 6 ppm spectral window, 8k data points and 1.5 s recycle delay. Saturation was achieved using presaturation with a normal Bruker presaturation pulse program.

Results

Metabolism of M_1G in rat liver cytosol

Based on our previous studies with M_1dG, we began our investigation of M_1G metabolism with liver cytosol. We hypothesized that M_1G would undergo metabolism in a manner qualitatively similar to that of M_1dG and that XOR and AO would be involved in the metabolism. To test these hypotheses, we performed incubations in the presence of characteristic inhibitors of XOR and AO (allopurinol and menadione, respectively). Chemically synthesized M_1G was incubated at 50 μM in rat liver cytosol (5 mg/mL) for varied times (0, 15, 30, and 60 min). Allopurinol and menadione (160 μM) were also added to selected reactions and stopped after 30 min. Metabolism of M_1G was monitored by reversed phase HPLC coupled to UV detection, which allowed for the separation and detection of incubation products. This analysis demonstrated a time-dependant decrease in M_1G peak area (**Figure 49**) throughout the duration of the incubation. The HPLC product profile revealed the appearance of a single metabolite (M_1G-M1) following 15 min of incubation. Further analysis revealed the appearance of a second metabolite (M_1G-M2) after 30 min of incubation and continued production of both metabolites at 60

min. Allopurinol co-incubation resulted in the total inhibition of metabolism, whereas the menadione-containing sample exhibited an increase in total metabolism (**Figure 49**) as seen for M_1dG (*157*) and other XOR substrates (*245, 277*). The HPLC-UV traces did not reveal any additional peaks associated with M_1G metabolism in the presence or absence of inhibitors. Subsequent analysis of the incubation mixtures by LC-MS revealed successive additions of 16 amu to M_1G, which resulted in the following increases: M_1G (*m/z* = 188.3) → M_1G-M1 (*m/z* = 204.3) → M_1G-M2 (*m/z* = 220.3) (**Figure 50)**.

Identification of M_1G metabolites

As suggested by our *in vitro* observations in rat liver cytosol, M_1G was investigated for its ability to undergo metabolism in incubations containing purified bovine XO. M_1G was rapidly oxidized by purified XO producing both M_1G-M1 and M_1G-M2 (**Figure 50**); therefore, purified bovine XO served as a platform to generate the metabolites for purification. The reaction was scaled up to 50 mL of total reaction volume and divided into separate 5 mL incubations. M_1G was incubated at a concentration of 250 μM and allowed to react for 60 min. Incubations were pooled, extracted, purified by semi-preparative HPLC, and analyzed on a 400 MHz NMR.

Preliminary ^{1}H-NMR analysis of M_1G-M1 (*m/z* = 204.3) revealed a spectrum rather similar to the previously characterized 6-oxo-M_1dG (**Figure 51**). The appearance of correlated peaks at 8.64 ppm (doublet) and 6.21 ppm (multiplet) suggested oxidation on the pyrimido ring, since the singlet assigned as H_2 (8.06 ppm) remained in the spectrum. Further NMR studies by HMBC analysis clearly revealed three-bond couplings of the proton assigned as H_8 to C_{4a}, C_6 and C_{10} (**Figure 52**). To verify the assignment

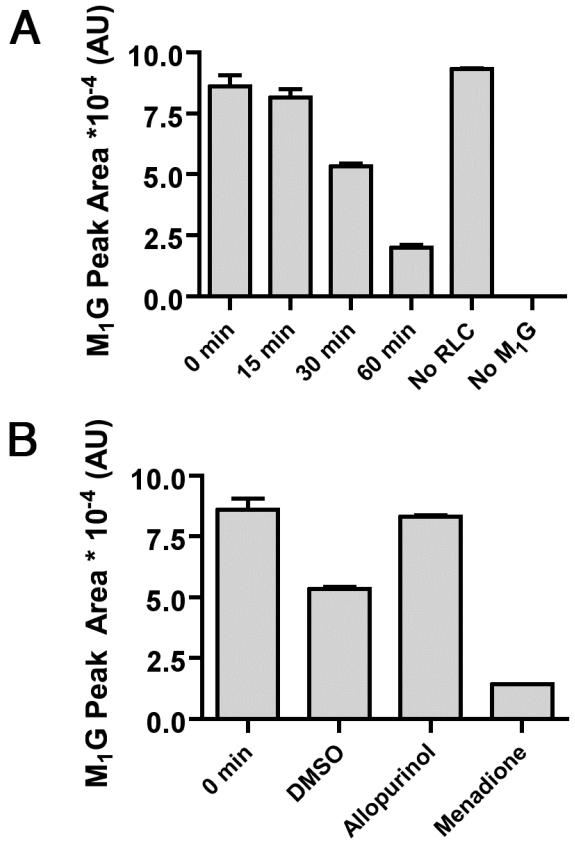

Figure 49. Time-course of M_1G consumption in rat liver cytosol and the effect of allopurinol and menadione on M_1G metabolism. All samples were incubated at 37 °C with 5 mg/mL rat liver cytosol and 50 μM M_1G. (A) Time-dependent decrease in M_1G peak area following incubation in rat liver cytosol. (B) Effect of vehicle (DMSO), allopurinol, and menadione on M_1G consumption after 30 min of incubation in rat liver cytosol.

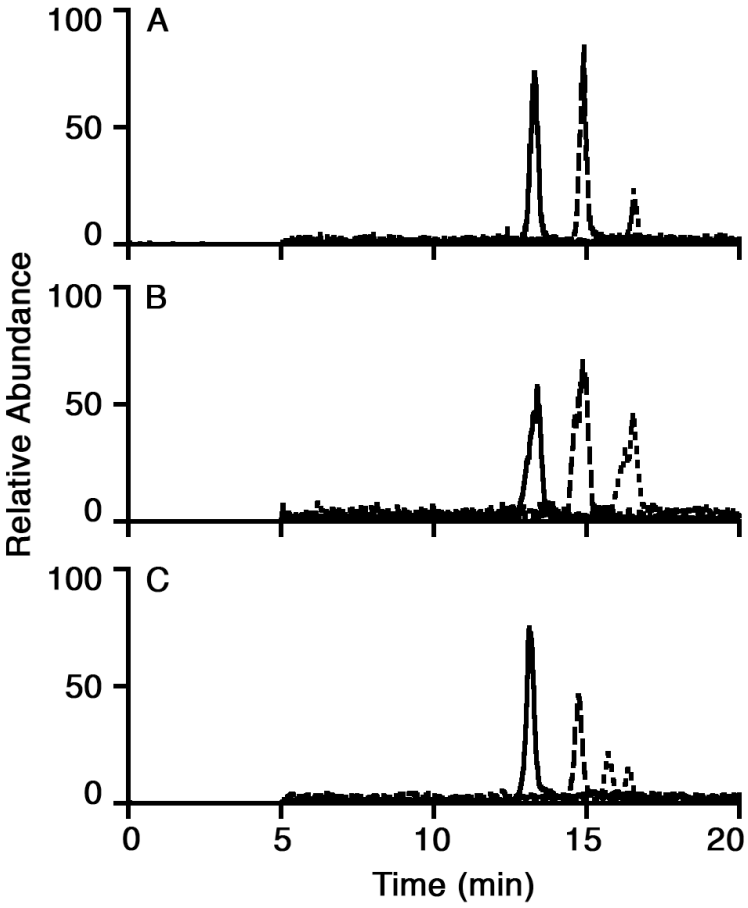

Figure 50. LC/MS chromatograms from *in vitro* and *in vivo* metabolism of M_1G. Samples were analyzed by selected-ion monitoring of *m/z* = 188.3 (—), 204.3 (---) and 220.3 (···). LC/MS profiling of *in vitro* incubations with rat liver cytosol (A) and bovine XO (B) revealed the successive additions of 16 amu to the parent ion M_1G (*m/z* = 188.3). (C) LC/MS analysis of urine collected from male Sprague Dawley rats that received iv M_1G (5 mg/kg).

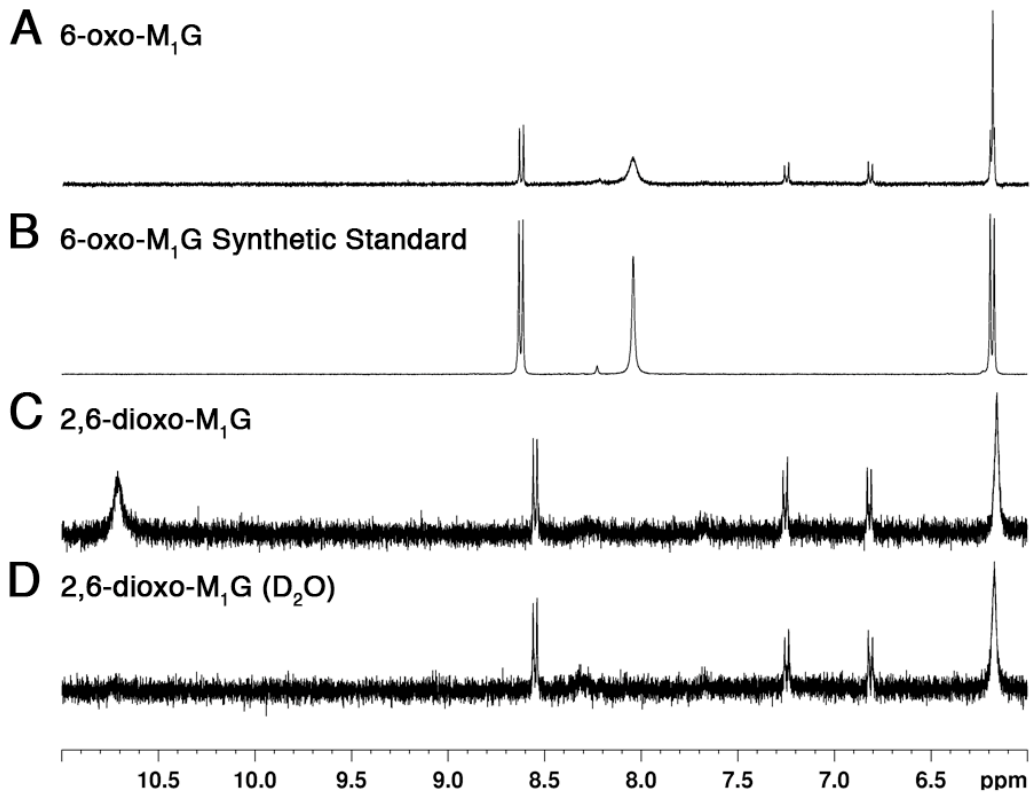

Figure 51. ^{1}H-NMR of M_1G metabolites derived from biochemical or chemical synthesis. All samples were analyzed on a 400 MHz NMR in d_6-DMSO. (A) 6-oxo-M_1G was biochemically synthesized with bovine XO and (B) generated through chemical sythesis. (C) 2,6-dioxo-M_1G was biochemically synthesized with bovine XO. (D) Addition of D_2O to the 2,6-dioxo-M_1G sample resulted in the loss of the chemical shift at 10.73 ppm indicating an exchangeable proton.

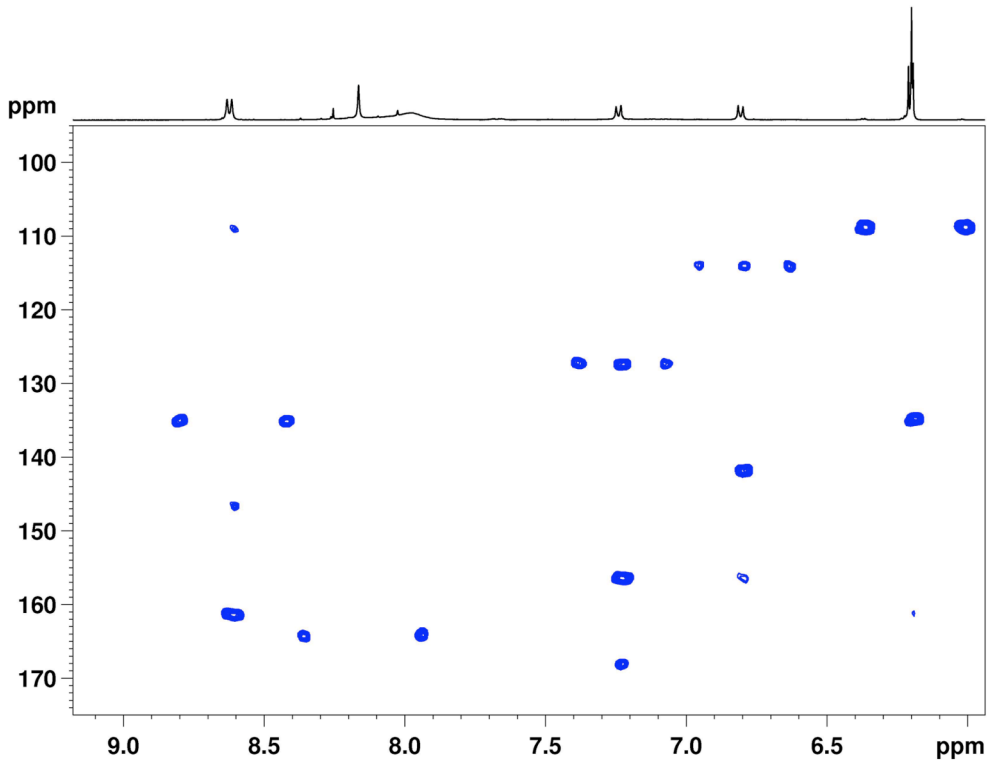

Figure 52. HMBC spectrum of biochemically synthesized 6-oxo-M_1G (M_1G-M1).

of this structure, an authentic standard of 6-oxo-M_1G was synthesized. The synthetic standard displayed identical spectral properties to M_1G-M1 (**Figure 51**). Together, these data confirmed the structure of M_1G-M1 as 6-oxo-M_1G.

The peaks appearing at 7.27 and 6.84 ppm in the biochemically purified 6-oxo-M_1G spectrum were determined to arise from impurities in the sample. This was confirmed by HMBC (**Figure 52**) and saturation transfer experiments (**Figure 53**). The HMBC revealed no three-bond couplings of these peaks to corresponding nuclei in the carbon spectrum, while the saturation transfer experiment determined these peaks did not arise from a chemical equilibrium (i.e., equilibrium between the amide and imin-ol about C_6 and N_5 on the pyrimido ring). Furthermore, no trace of these peaks was observed in the authentic standard of 6-oxo-M_1G. Therefore, the peaks at 7.27 and 6.84 ppm were reasoned to be impurities derived from the purification process. The observed singlet at 6.21 ppm also appeared to be an impurity overlapping the signal from the H_7 doublet. However, its designation was not identified completely due to the overlap (this was also observed with the M_1G-M2 sample, see below).

^{1}H-NMR analysis of M_1G-M2 (*m/z* = 220.3) identified correlated peaks at 8.56 ppm (doublet) and 6.18 ppm (singlet) suggesting that the C_7 and C_8 protons remained on the pyrimido ring. Notably, the singlet at 8.06 ppm from the 6-oxo-M_1G spectrum was not present in the M_1G-M2 sample, and a new singlet arose downfield at 10.73 ppm (**Figure 51**). The downfield peak appearance and the disappearance of the singlet at 8.06 ppm are consistent with oxidation at C_2. The addition of D_2O to the sample resulted in the disappearance of the peak at 10.73 ppm suggesting that this is an exchangeable proton (**Figure 51**). Oxidation at C_2 on the imidazole ring of 6-oxo-M_1G is similar to oxidation

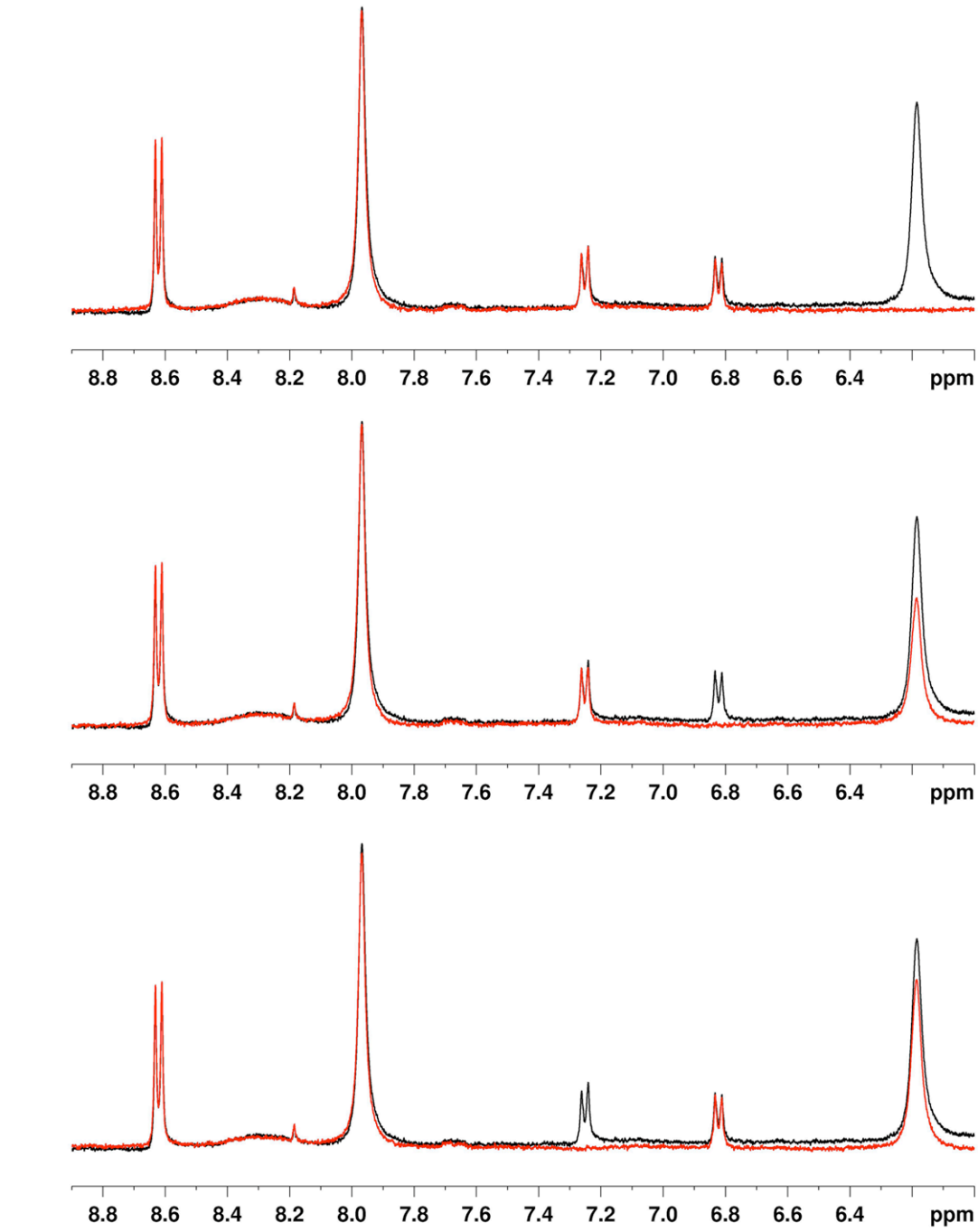

Figure 53. Saturation transfer ^{1}H-NMR spectra of biochemically synthesized 6-oxo-M_1G.

at C_8 on dG in the formation of 8-oxo-dG. 8-Oxo-dG was used as a reference when assigning the positions of oxidation on M_1G. The oxidation of dG at C_8 led to the appearance of a downfield peak at 10.75 ppm (in d_6-DMSO) attributed to the N_7-proton (*278*). Therefore, the chemical shift of 10.73 ppm was assigned to N_1/N_3-H's and the structure of M_1G-M2 was assigned as 2,6-dioxo-M_1G.

Peak impurities were also found in the 2,6-dioxo-M_1G spectrum. Most notable was the appearance of the singlet at 6.18 ppm, which also appeared in the spectrum of the biochemically synthesized 6-oxo-M_1G. In the 2,6-dioxo-M_1G spectrum, the singlet was likely overlapping with the doublet attributed to the H_7 proton at 6.18 ppm, which was inferred from the correlation seen in the 2D ^{1}H-NMR analysis. The amount of material in the 2,6-dioxo-M_1G was low, and some impurity signals were evident.

In vivo administration of M_1G to male Sprague Dawley rats

To determine whether the enzymatic oxidations could occur *in vivo*, male Sprague Dawley rats were dosed iv with 5 mg/kg M_1G. The animals (n = 3) were housed in metabolic cages to collect urine and feces over the course of the experiment. Urine samples were extracted, chromatographed on a reversed phase column and analyzed by LC-MS using selected ion monitoring. The parent compound (M_1G, *m/z* = 188.3) and the metabolites 6-oxo-M_1G (*m/z* = 204.3) and 2,6-dioxo-M_1G (*m/z* = 220.3) were monitored on separate channels of the same run. Analysis of the *in vivo* urine samples revealed molecular ions corresponding to M_1G (7.9 min), 6-oxo-M_1G (8.9 min), and 2,6-dioxo-M_1G (9.9 min). The molecular ions displayed identical retention times as the *in vitro*-generated metabolites from XOR and rat liver cytosol incubations (**Figure 50**), and the

authentic standard for M_1G and 6-oxo-M_1G. The *in vivo* samples contained a background peak with a molecular ion of 220.3 (*m/z*) that eluted at 9.4 min. This peak also appeared in pre-dose and late time-point urine samples and did not correlate with 2,6-dioxo-M_1G production.

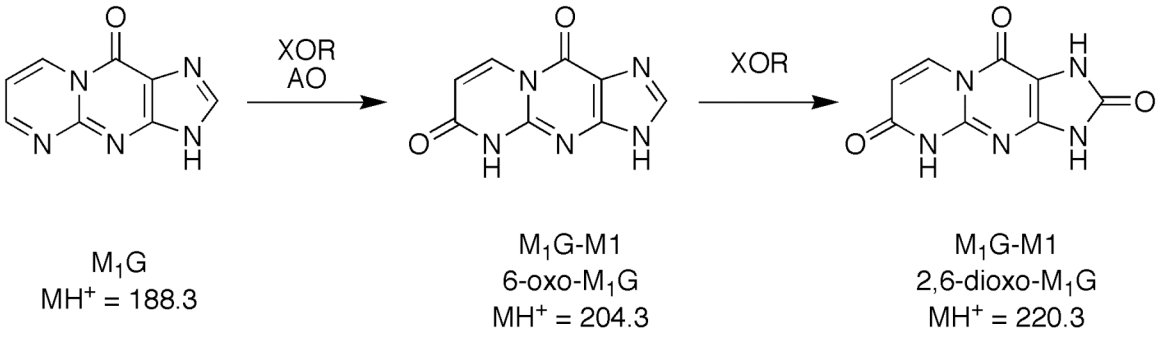

Figure 54. Sequential metabolism of M_1G to 6-oxo-M_1G and 2,6-dioxo-M_1G.

Kinetic determinations in rat liver cytosol with M_1G and 6-oxo-M_1G

Following the characterization of the M_1G metabolites (**Figure 54**), an investigation into their rates of formation was undertaken *in vitro* with rat liver cytosol. Our preliminary data suggested M_1G consumption in rat liver cytosol lead to the production of 6-oxo-M_1G, which then underwent an additional oxidation to 2,6-dioxo-M_1G. Based on inhibition experiments, XOR appeared to be involved in the metabolism.

M_1G consumption was dependent on protein concentration and time of incubation in rat liver cytosol. At 5 mg/mL rat liver cytosol, M_1G consumption was linear out to 60 min of incubation. The kinetic determinations were performed by incubating M_1G at varied concentrations for 60 min in the presence of 5 mg/mL rat liver cytosol. The resulting products were extracted, separated by reversed phase chromatography, and analyzed by UV absorbance. M_1G consumption was quantified by reference to a standard curve that was prepared by spiking known concentrations of M_1G into rat liver cytosol and terminating the reaction at time-zero. This was followed by extraction and analysis identical to the incubated samples.

Figure 55 shows the velocity vs. substrate concentration (v vs. [S]) plot for the consumption of M_1G. The K_m was calculated to be 105 μM and the V_{max} at 126 pmol min^{-1} mg^{-1}. The total peak area of metabolites (both 6-oxo-M_1G and 2,6-dioxo-M_1G peak areas) vs. [S] was also plotted (**Figure 55**) to determine a K_m of 118 μM, which was in good agreement with that for substrate consumption. A plot of the peak areas for each metabolite vs. [S] (**Figure 55**) revealed that as the M_1G concentration increased, the ratio of 2,6-dioxo-M_1G to 6-oxo-M_1G decreased. This suggested M_1G is capable of out-competing 6-oxo-M_1G at concentrations at or above its K_m in rat liver cytosol.

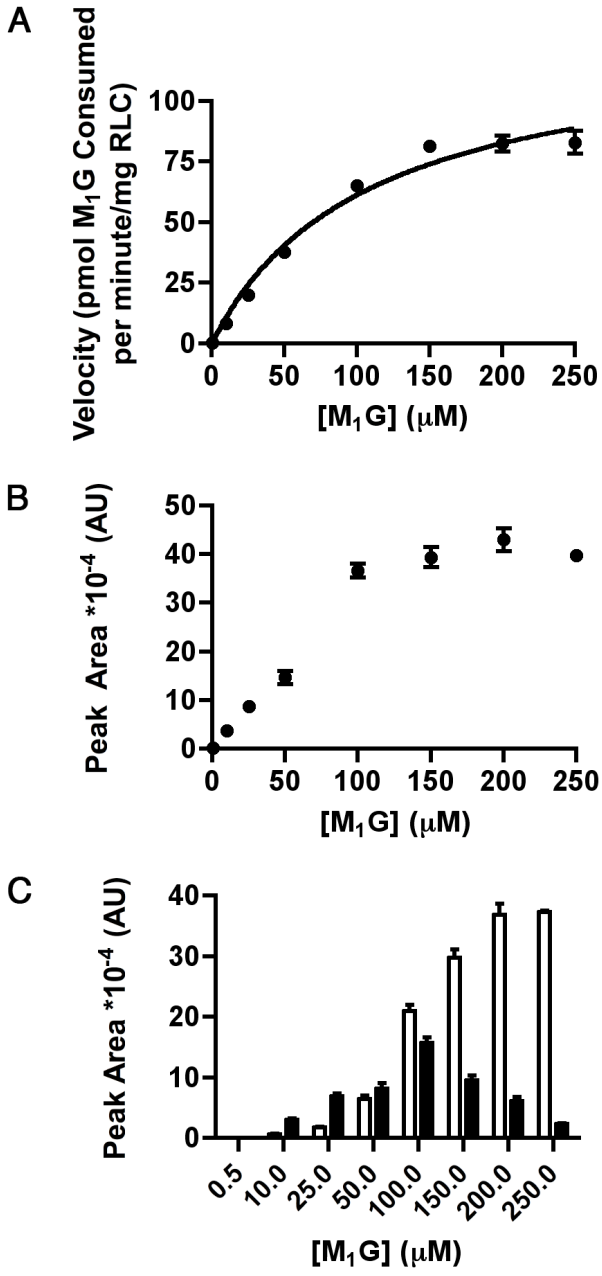

Figure 55. Kinetic determinations for M_1G consumption in rat liver cytosol. (A) M_1G was incubated in rat liver cytosol (5 mg/mL at 37 °C for 60 min) and quantified by reference to a standard curve. The data was analyzed by non-linear regression and fit to a one-site binding model: K_m = 105 μM and V_{max} = 126 pmol min^{-1} mg^{-1} (V_{max}/K_m = 0.005 min^{-1} mg^{-1}). (B) Plot of total metabolite peak area (both 6-oxo-M_1G and 2,6-dioxo-M_1G) vs. [S] (K_m = 118 μM). (C) Plot of peak areas vs. [M_1G] for 6-oxo-M_1G (□) and 2,6-dioxo-M_1G (■).

Since the exact concentration of enzyme(s) in the rat liver cytosol was unknown, the relative catalytic efficiency for turnover was calculated by dividing the V_{max} by the K_m and normalizing the total protein concentration. Performing this analysis on the above data yielded a V_{max}/K_m of 0.005 min^{-1} mg^{-1} for M_1G consumption in rat liver cytosol. An additional *v* vs. [S] determination of M_1G consumption was also performed in a separate preparation of rat liver cytosol, which yielded a K_m of 79 μM, a V_{max} of 84 pmol min^{-1} mg^{-1} and a V_{max}/K_m of 0.004 min^{-1} mg^{-1}. The relative catalytic efficiencies of the turnover were in good agreement, while the K_m and V_{max} were not. This likely reflects the differences in makeup between the two separate preparations of rat liver cytosol. Therefore, one may imply the relative amounts of XOR and AO (and any other enzyme that may be involved) in each preparation vary to a degree, resulting in altered kinetic parameters.

Kinetic determinations were also performed on the transformation of 6-oxo-M_1G to 2,6-dioxo-M_1G in rat liver cytosol. Synthetic 6-oxo-M_1G was synthesized and used in *v* vs. [S] determinations. The incubations and analyses were performed as described for M_1G. Based on substrate consumption, a K_m for 6-oxo-M_1G was calculated at 210 μM and a V_{max} at 257 pmol min^{-1} mg^{-1}. The V_{max}/K_m was 0.005 min^{-1} mg^{-1}, which was the same value calculated for M_1G consumption in rat liver cytosol. Therefore, it appears that both substrates are equally efficient in their turnover; however, M_1G possesses a higher apparent affinity (lower K_m) for the active site(s). This would allow M_1G to out-compete 6-oxo-M_1G at concentrations at or above the K_m for M_1G consumption, which was observed in the product profile from the M_1G kinetic determinations.

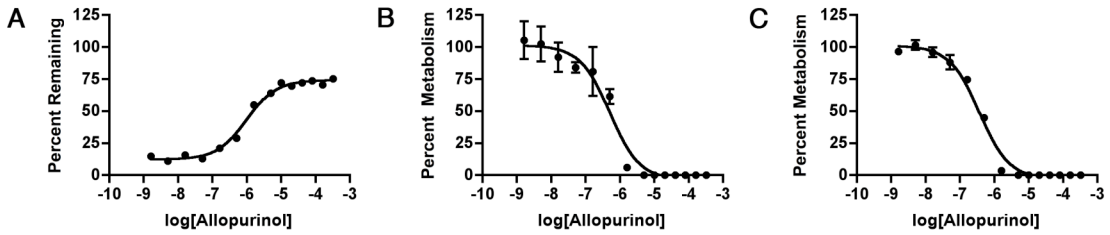

Figure 56. IC_{50} determinations in rat liver cytosol with allopurinol using M_1G and 6-oxo-M_1G as substrates. (A) Using M_1G as a substrate, IC_{50} values were determined based on substrate (M_1G) consumption (960 nM) and (B) inhibition of 2,6-dioxo-M_1G production (500 nM). (C) Using 6-oxo-M_1G as a substrate, the IC_{50} value was determined based on inhibition of 2,6-dioxo-M_1G production (360 nM).

IC_{50} determinations with allopurinol in rat liver cytosol

IC_{50} determinations were performed using varied concentrations of allopurinol in rat liver cytosol in the presence of M_1G and 6-oxo-M_1G. All substrates were incubated at their predetermined K_m. The percent inhibition was measured by inhibition of substrate consumption or product production. These studies attempted to demonstrate the involvement of XOR and AO in the metabolism of M_1G and 6-oxo-M_1G. An IC_{50} determination was first carried out with allopurinol using M_1G as a substrate. The amount of M_1G consumption at each concentration of allopurinol was determined based on peak area absorbance of M_1G and referenced to the vehicle control (no allopurinol) for percent consumption. Based on the inhibition of substrate consumption, an IC_{50} of 960 nM was determined (**Figure 56**). At saturating concentrations of allopurinol (> 20 μM), 25% of the M_1G was still consumed. This implied an additional enzyme(s) other than XOR metabolized M_1G (presumably AO). Analysis of the product profile revealed two findings. First, no correlation existed between 6-oxo-M_1G production and allopurinol

concentration (i.e., IC_{50} determination based on the inhibition of 6-oxo-M_1G production could not be determined). Second, at saturating concentrations of allopurinol (> 20 μM), there was incomplete inhibition of 6-oxo-M_1G and total inhibition of 2,6-dioxo-M_1G production (IC_{50} = 500 nM). Together, these data suggested that XOR catalyzed the conversion of M_1G to both 6-oxo-M_1G and 2,6-dioxo-M_1G, whereas the remaining enzyme activity, presumably AO, only converted M_1G to 6-oxo-M_1G.

Following these results, the IC_{50} was then determined with allopurinol using 6-oxo-M_1G as a substrate. The amount of 2,6-dioxo-M_1G produced at each concentration of allopurinol was determined based on peak area absorbance and referenced to the vehicle control (no allopurinol) for percent inhibition. This resulted in an IC_{50} determination of 360 nM. These data confirmed that at saturating concentrations of allopurinol (> 10 μM), no 2,6-dioxo-M_1G was produced and further implied that XOR, and not AO, was the enzyme that acted on 6-oxo-M_1G *in vitro*. In a separate set of experiments, we investigated the contribution of AO to the metabolism of M_1G in rat liver cytosol. Samples were incubated in the presence of M_1G (105 μM) and a saturating concentration of allopurinol (40 μM). To these reactions, increasing concentrations of menadione were added to generate an IC_{50} curve. A dose-dependent decrease in M_1G metabolism was observed with increasing concentrations of menadione (IC_{50} = 5 μM), which resulted in total inhibition of both 6-oxo-M_1G and 2,6-dioxo-M_1G formation at saturating concentrations of menadione (>300 μM).

The IC_{50} with allopurinol was also calculated with the M_1dG. The kinetic determinations for M_1dG conversion to 6-oxo-M_1dG in rat liver cytosol were determined previously (*157*). Upon co-incubation of M_1dG (370 μM) with increasing concentrations

of allopurinol, an IC_{50} of 120 nM was determined. It should be noted that at saturating concentrations of allopurinol (> 5 μM); the 6-oxo-M_1dG production was minimized, but not completely inhibited. This suggests that AO is also contributing to the enzymatic oxidation of M_1dG in rat liver cytosol.

Discussion

DNA adducts arise directly from, and downstream of, exposure to endogenously produced ROS. In the absence of repair, these adducts may lead to mutations (point and frameshift), strand breaks, arrest in cell division, and induction of apoptosis. Successful repair of adducts leads to their removal from genomic DNA; thus, averting these deleterious effects. Little is known about the fate of DNA adducts following their release from DNA. Our results suggest that exposure of DNA adducts to endogenous oxidative enzymes results in metabolism (oxidation) of the adducts. Oxidative metabolism of both deoxynucleoside-containing (*157*) and base adducts have now been observed.

The base adduct, M_1G, underwent sequential oxidative metabolism *in vitro* in rat liver cytosol to two separate metabolites – 6-oxo-M_1G and 2,6-dioxo-M_1G. The production of each metabolite was also seen *in vivo* upon iv administration of M_1G to male Sprague Dawley rats. M_1G, 6-oxo-M_1G, and 2,6-dioxo-M_1G were all excreted in the urine, suggesting that these metabolites may be suitable for evaluation as urinary biomarkers under physiological conditions. The kinetic parameters of M_1G and 6-oxo-M_1G metabolism were evaluated in rat liver cytosol. These studies demonstrated that M_1G has a lower K_m than 6-oxo-M_1G in rat liver cytosol, but each are metabolized with the same relative efficiency (V_{max}/K_m = 0.005 min^{-1} mg^{-1}). In comparison to M_1dG, both

M_1G and 6-oxo-M_1G are better substrates (V_{max}/K_m for M_1dG = 0.001 min^{-1} mg^{-1}) and exhibited a lower K_m (**Table 7**).

Table 7. Kinetic and IC_{50} determinations for M_1G, 6-oxo-M_1G and M_1dG in rat liver cytosol. [a]IC_{50} determined based on inhibition of M_1G consumption. [b]IC_{50} determined based on inhibition of 2,6-dioxo-M_1G production with M_1G as a substrate. [c]Values taken from Otteneder *et al.* (*157*).

Table 1. Kinetic and IC_{50} determinations for M_1G, 6-oxo-M_1G and M_1dG in Rat Liver Cytosol.

Substrate	K_M	V_{max}	V_{max}/K_M	IC_{50}
	μM	*pmol min^{-1} mg^{-1}*	*min^{-1} mg^{-1}*	*nM*
M_1G	105	126	0.005	960[a]
				500[b]
6-oxo-M_1G	210	257	0.005	360
M_1dG	370[c]	104[c]	0.001	120

M_1G, 6-oxo-M_1G, and M_1dG all appear to undergo oxidative metabolism by similar enzymes; namely XOR and AO. In rat liver cytosol, approximately 75% of the M_1G metabolism (and all of the 6-oxo-M_1G metabolism) can be attributed to XOR, as gauged by allopurinol inhibition. It should be noted that the relative amount of AO to XOR activity in Sprague Dawley rat liver cytosol is low. Other species, such as guinea pig and rabbit, often contain higher ratios of AO to XOR (*252*). Therefore, the total contribution of AO towards the metabolism of M_1G, 6-oxo-M_1G, and M_1dG may be underestimated in these studies.

The metabolism of each substrate is inhibited by co-incubation with allopurinol in rat liver cytosol. Co-incubation of menadione, in the absence of allopurinol, resulted in the stimulation of metabolism for each substrate (*157*). This phenomenon of XO

stimulation by menadione was first observed by Mahler *et al.* (*243*), continues to appear in the literature (*234, 245, 277*), and is seen in the metabolism of M_1dG (*157*). Stimulation by menadione was mitigated when saturating concentrations of allopurinol were used. Thus, this effect can be attributed to the stimulation of XO metabolism. When saturating concentrations of allopurinol were co-incubated with increasing concentrations of menadione, the ability of rat liver cytosol to metabolize M_1G was abolished (IC_{50} = 5 μM).

Under physiological conditions, XOR is believed to exist as a dehydrogenase (XD) (*239*). Ex-vivo manipulations of the enzyme leads to irreversible proteolytic cleavage, or reversible oxidation (formation of disulfides), generating the oxidase form (*240, 241*). Both forms of the enzyme are catalytically competent and capable of using molecular oxygen as a terminal electron acceptor; although, XO is more efficient that XD at utilizing O_2 (*242*). XD can use NAD^+, which increases the efficiency of catalysis, and has no effect on XO (*242*). Preliminary evaluation of rat liver cytosol did not reveal enhanced metabolism in the presence of NAD^+, suggesting the oxidase form is responsible for the oxidation of M_1dG, M_1G, and 6-oxo-M_1G in the liver cytosols evaluated.

The enzymatic conversion of M_1G to two separate, oxidized metabolites is unique to the free base, and not observed in metabolism studies with the deoxynucleoside, M_1dG. Furthermore, the sites of metabolism on M_1G are similar to the sites of oxidation on hypoxanthine, which is converted to xanthine, which is then oxidized to uric acid by XOR. Hypoxanthine oxidation occurs first at the 2-position on the pyrimidine ring (analogous to the 6-position on the pyrimido ring of M_1G) and subsequently on the 8-

position of the imidazole ring (analogous to the 2-position on the imidazole ring of M_1G). Further metabolism of 6-oxo-M_1dG on the imidazole ring is likely prevented by the steric hindrance from the deoxyribose moiety.

When exogenously administered to male Sprague Dawley rats (5 mg/kg), M_1G was oxidized *in vivo*, and the principal metabolite (based on relative ionization) appeared to be 6-oxo-M_1G with 2,6-dioxo-M_1G less abundant. These results were in agreement with the *in vitro* data, which suggested that at high concentrations M_1G could out-compete 6-oxo-M_1G, thus minimizing the amount of 2,6-dioxo-M_1G produced. One may expect the ratio of 2,6-dioxo-M_1G to 6-oxo-M_1G to increase *in vivo* when lower concentrations of M_1G are present. However, the sensitivity at later time-points during this analysis was too low to reliably address this hypothesis. When low concentrations of M_1G were incubated with rat liver cytosol, a near complete conversion of M_1G to 2,6-dioxo-M_1G was observed (**Figure 57**), which would suggest that upon physiological generation of M_1G *in vivo*, 2,6-dioxo-M_1G may be the main species observed.

The main route for repair of M_1dG residues in genomic DNA appears to be the NER pathway. Despite the fact that the base excision repair and DNA glycosylase enzymes have never been definitively associated with M_1dG repair *in vitro*, one cannot rule out the involvement of these repair pathways *in vivo*. Considering the high degree of structural similarity between M_1dG and the etheno adducts, it seems likely that a DNA glycosylase may catalyze the removal of M_1G from DNA.

The concept that repaired DNA adducts may undergo metabolism prior to urinary excretion has been previously investigated (*266*). Wang and Hecht evaluated the *in vivo* stability of the *N*-nitrosopyrrolidine (NPYR) guanine adduct, 2-amino-6,7,8,9-tetrahydro-

9-hydroxypyrido[2,1-*f*]purin-4(3*H*)-one (N^7,C8-NPYR-Gua), by ip administration of [^{14}C]-labeled N^7,C8-NPYR-Gua to male F-344 rats. Results from this study demonstrated that approximately 52% of the dose was recovered in the urine following 48 h of collection. HPLC with radioflow analysis revealed than 90% of the urinary radioactivity was recovered as the parent molecule (N^7,C8-NPYR-Gua), while the other 10% was distributed across several minor peaks – suggestive of metabolism. Neither the fate of the remaining 48% of the administered radioactivity, nor the identity of the peaks in the urine profile was commented on by the investigators. It seems likely that N^7,C8-NPYR-Gua was eliminated in the feces and that N^7,C8-NPYR-Gua underwent significant biliary uptake into the bile (as either the parent molecule or as a metabolite(s)). These data demonstrate that exogenously administered adducts are subject to metabolism *in vivo*, with elimination presumably proceeding through multiple pathways.

These studies demonstrate that in addition to deoxynucleoside adducts, purine base adducts are subject to metabolism following repair *in vivo* (*157, 266*). In the case of M_1G, the base is a better substrate for enzymatic oxidation than the deoxynucleoside (M_1dG). Endogenous lesions are subject to multiple repair pathways. Following repair, these adducts are exposed to membrane-bound and cytosolic enzymes. Structural analogs of M_1G and M_1dG, and other exocyclic ring adducts are likely candidates to undergo metabolism *in vitro* and *in vivo*. Therefore, a yet undiscovered population of biomarkers may exist to assess exposure to oxidative damage *in vivo*.

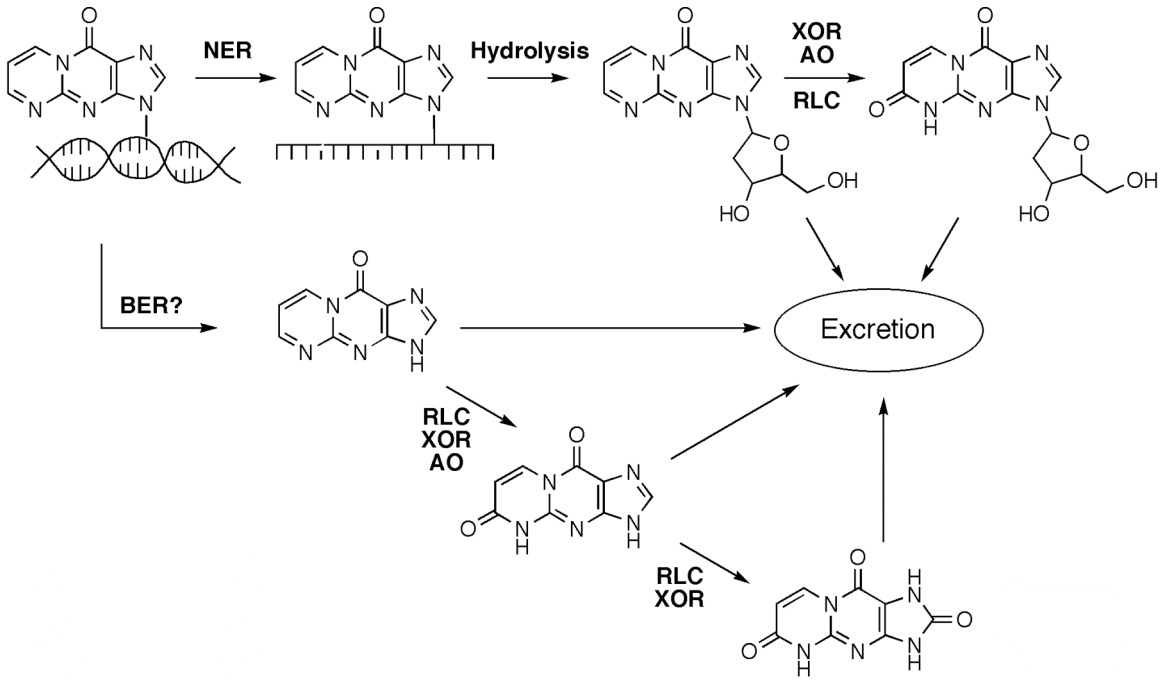

Figure 57. Metabolic processing of M_1dG. BER, base excision repair; RLC, rat liver cytosol.

CHAPTER VI

METABOLISM OF ETHENO AND PROPANO ADDUCTS *IN VITRO*

Summary

Non-invasive strategies for the analysis of endogenous DNA damage are of interest for the purpose of monitoring *in vivo* exposure to biologically produced chemicals. We have focused our research on the peroxidation-derived pyrimidopurinone dG adduct, M_1dG, and factors that may effect its appearance in urine. Recent studies have demonstrated that both M_1dG and its free base M_1G are subject to oxidative metabolism *in vitro* and *in vivo*. In fact, the base is a better substrate for *in vitro* metabolism than the deoxynucleoside (~ 5-fold). This observation suggests structurally similar exocyclic base adducts maybe good candidates for oxidative metabolism. We investigated several endogenously occurring etheno adducts (1,N^2-ε-Gua, 1,N^6-ε-Ade, 3,N^4-ε-Cyd, heptanone-1,N^2-ε-Gua) and their corresponding deoxynucleosides for metabolism *in vitro*. Both 1,N^2-ε-Gua and heptanone-1,N^2-ε-Gua underwent oxidative metabolism *in vitro* in incubations with rat liver cytosol. Heteronuclear NMR experiments revealed oxidation occurred on the imidazole ring for each substrate. Additional experiments with structural analogs of M_1G (5,6-dihydro-M_1G and PGua) suggested the aromatic nature of the exocyclic ring effects oxidation. Our analysis revealed tertiary heterocyclic imine carbons are targeted for oxidation. Additionally, the deoxynucleoside adducts 1,N^2-ε-dG and 1,N^6-ε-dA are subject to phosphorolysis by purine nucleoside phosphorylase (PNP) in rat liver. Together these data suggest that

multiple exocyclic adducts undergo metabolism *in vitro* in rat liver cytosol to oxidized and phosphorolyzed products—in some instances in succession. The multiple pathways of biotransformation produce an array of products from exocyclic DNA adducts. Thus, our data suggests the metabolic processing of exocyclic adducts should be considered as part of development projects designed to non-invasively quantify their *in vivo* levels.

Introduction

The endogenous DNA lesion, M_1dG, is derived from reactions of the lipid peroxidation product, MDA, or the DNA peroxidation product, base propenal (*42, 58, 96-98, 106, 107, 257*). M_1dG, is miscoding in bacteria and humans producing mainly M_1dG → T transversions and M_1dG → A transitions (*88, 119-121, 258*). When site-specifically incorporated into a reiterated repeat sequence (5′-CG_r-3′) M_1dG induces frameshift mutations (*121*). Genetic and biochemical evidence suggests that M_1dG is released from by NER (*120, 122*), which results in the formation of the free deoxynucleoside, M_1dG, following repair. The free base, M_1G, is a putative product of base excision repair by glycosylase action. However, no evidence suggests the role of base excision repair in the release of M_1G from DNA, which is surprising since several structurally similar etheno adducts (1,N^2-ε-Gua, N^2,3-ε-Gua, 1,N^6-ε-Ade, 3,N^4-ε-Cyd) are reported substrates for DNA glycosylases (*217-223*).

Our laboratory has recently described the metabolic processing of M_1dG and M_1G (*157, 261, 267*). M_1dG undergoes a single oxidation on the 6-position of the pyrimido ring to 6-oxo-M_1dG whereas M_1G undergoes successive oxidations: first at the 6-position and then on the 2-position of the imidazole ring to produce 6-oxo-M_1G and 2,6-dioxo-

M_1G, respectively. It was interesting to observe oxidation on the imidazole ring with M_1G, which was not observed with M_1dG, indicating the steric bulk of the deoxyribose affects the site of oxidation. Comparing the turnover of M_1dG, M_1G, and 6-oxo-M_1G in rat liver cytosol demonstrated that the bases were better substrate for oxidation than the deoxynucleoside (~5-fold). Based on these observations, we hypothesized that other exocyclic adducts were likely to undergo oxidation, with the imidazole ring being a likely target for oxidation. Due to the higher apparent turnover of the M_1G bases, we targeted our investigation to base adducts that are released from DNA by glycosylase action. Furthermore, we undertook a structure activity relationship with several analogs of M_1dG to determine structural requirements for the oxidation of exocyclic adducts.

Experimental Procedures

Chemicals and Reagents

All chemicals were obtained from commercial sources and used as received. Solvents were of HPLC grade purity or higher. M_1dG, 6-oxo-M_1dG, 5,6-dihydro-M_1dG and PdG were synthesized as previously described (*116, 259*). 1,N^2-ε-Gua (*183*), 1,N^6-ε-Ade (*184*), and 3,N^4-ε-Cyd (*182, 279*) were synthesized by established methods. Liver cytosols were prepared by established methods (*231*). Bovine XO from buttermilk was obtained from CalBiochem (La Jolla, CA). PNP was purchased from Sigma (St. Louis, MO). HPLC separations were performed on a Waters 2695 autosampler and binary pump with a Waters 2487 dual wavelength UV detector. LC-MS/MS and LC-MS^n spectra were obtained on either ThermoElectron Quantum or LTQ instruments.

Liver cytosol incubations and analysis

1,N^2-ε-Gua. All sample preparation was performed on ice at 4 °C. The final incubation conditions for the kinetic determinations contained 5 mg/mL rat liver cytosol, varied concentrations of 1,N^2-ε-Gua (10, 25, 50, 75, 100, 150, 250, 500, 750 μM) dissolved in 0.1 N NaOH, and 0.4% DMSO in 0.8 M potassium phosphate (pH 7.6). IC_{50} determinations were carried out in 0.8 M potassium phosphate (pH 7.6) and 5 mg/mL rat liver cytosol at the calculated K_m for 1,N^2-ε-Gua (85 μM) with varied concentrations of allopurinol (320, 160, 50, 16, 5, 1.6, 0.5, 0.016, 0.005, 0.0016, 0.0 μM). The inhibitor was diluted in DMSO (0.4% total reaction volume). Reagents were equilibrated to 37 °C for 5 min and the reaction was initiated by the addition of substrate. Reactions were terminated after 30 min by adding 0.5 mL ice cold ethanol, vortexed, and extracted twice with 2x volume chloroform. The extracts were evaporated under nitrogen, and reconstituted in 0.1 N NaOH for the kinetic determinations and H_2O for the IC_{50} determinations. The extraction of 1,N^2-ε-Gua from rat liver cytosol in ethanol/chloroform resulted in a 70 to 80% recovery from rat liver cytosol incubations. Samples were separated on a Phenomenex Luna C18(2) column (4.6 x 250 nm, 5μ) equilibrated with 95% solvent A (0.5% formic acid in H_2O) and 5% solvent B (0.5% formic acid in methanol) at a flow rate of 1 mL/min. The solvent was programmed as follows: a linear gradient from the starting solvent to 30% B in 15 min, increasing to 80% B in 0.1 min, holding for 5 min, decreasing to 5% B in 0.1 min, and re-equilibrating at initial conditions for 5 min. Eluting compounds were detected by UV absorbance at 285 nm. Samples from the kinetic determinations were quantified in reference to a standard curve prepared by spiking known concentrations of 1,N^2-ε-Gua (2.5, 5, 50, 100,

250, 500, 750 μM) into 5 mg/mL rat liver cytosol solutions, followed immediately by termination, extraction, and analysis as outlined above. All incubations and standards were performed in triplicate. The IC_{50} values ere calculated on the basis of the inhibition of 1,N^2-ε-Gua consumption in reference to the vehicle (DMSO) control. V_{max}/K_m and IC_{50} values were calculated with Prism software (Version 4.0c) using nonlinear regression one-site binding and one-site competition models, respectively.

1,N^2-ε-dG, 3,N^4-ε-dC, and 3,N^4-ε-Cyd. All sample preparation was performed on ice at 4 °C. The final incubation conditions contained 5 mg/mL rat liver cytosol, 100 μM of either 1,N^2-ε-dG, 3,N^4-ε-dC, or 3,N^4-ε-Cyd dissolved in 0.1 M potassium phosphate (pH 7.4). Inhibitors (allopurinol, menadione) were dissolved in DMSO with final incubation concentration of 160 μM (0.4% DMSO in the reaction). Reagents were equilibrated to 37 °C for 5 min and the reaction was initiated by addition of substrate. Reactions were terminated at intervals (0, 15, 30, and 60 min) by adding 0.5 mL ice cold ethanol, vortexed, and extracted twice with 2x volume chloroform. The extracts were evaporated under nitrogen and reconstituted in 0.1 M potassium phosphate, pH 7.4, for HPLC-UV and -MS/MS analysis. 1,N^2-ε-dG samples were separated as described above for 1,N^2-ε-Gua. 3,N^4-ε-dC, or 3,N^4-ε-Cyd were separated on a Phenomenex Luna Phenyl-Hexyl column (4.6 x 250 nm, 5μ) equilibrated with 90% solvent A (20 mM ammonium acetate, pH 7.0, in H_2O) and 10% solvent B (20 mM ammonium acetate, pH 7.0, in methanol) at a flow rate of 1.0 mL/min. The solvent was programmed as follows: a linear gradient from the starting solvent to 50% B in 10 min, decreasing to 10% B in 0.1 min and holding at initial conditions for 5 min. Eluting compounds were detected by UV absorbance at 254 and 285 nm. All incubations were prepared in triplicate.

1,N^6-ε-Ade and 1,N^6-ε-dA. All sample preparation was performed on ice at 4 °C. The final incubation conditions contained 5 mg/mL rat liver cytosol, 40 μM 1,N^2-ε-dA or 1,N^2-ε-Ade dissolved in 0.1 M potassium phosphate, pH 7.4, or 0.1 M Tris-HCl, pH 7.4 buffers. Reagents were equilibrated to 37 °C for 5 min and the reaction initiated by the addition of substrate. Reactions were terminated at intervals (0, 5, 15, 30, and 60 min) by adding 0.5 mL ice cold ethanol, vortexed, and extracted twice with 2x volume chloroform. The extracts were evaporated under nitrogen and reconstituted in 0.1 M potassium phosphate, pH 7.4, for HPLC-UV and -MS/MS analysis. The extraction of 1,N^2-ε-dA and 1,N^2-ε-Ade from rat liver cytosol into ethanol/chloroform resulted in a 70-80% recovery. Samples were separated on a Phenomenex Synergi POLAR-RP column (2.0 x 150 nm, 4μ) equilibrated with 98% solvent A (0.5% formic acid in H_2O) and 2% solvent B (0.5% formic acid in methanol) at a flow rate of 0.3 mL/min. The solvent was programmed as follows: a linear gradient from the starting solvent to 40% B in 10 min, holding at 40% B for three min, decreasing to 2% B in 0.1 min and holding at initial conditions for 7 min. Eluting compounds were detected by UV absorbance at 254 and 275 nm. All incubations were prepared in triplicate.

Heptanone-1,N^2-ε-Gua and heptanone-1,N^2-ε-dG. All sample preparation was performed at room temperature. The final incubation conditions for reactions contained 5 mg/mL rat liver cytosol, and 50 μM of either heptanone-1,N^2-ε-Gua or heptanone-1,N^2-ε-dG in 0.2 M potassium phosphate (pH 7.8). Inhibitors (allopurinol, menadione, raloxifene) were dissolved in DMSO to a final incubation concentration of 160 μM (0.4% DMSO in the reaction). Reagents were equilibrated to 37 °C for 5 min and the reaction was initiated by addition of substrate. Reactions were terminated at intervals (0, 15, 30,

and 60 min) by adding 0.5 mL ice-cold ethanol, vortexed, and put on ice. The samples were extracted twice with 2x volume chloroform. The organic layer was evaporated under nitrogen and reconstituted in methanol for HPLC-UV and -MS/MS analysis. Extraction of heptanone-1,N^2-ε-Gua and heptanone-1,N^2-ε-Gua metabolite from rat liver cytosol into ethanol/chloroform resulted in a >90% recovery. Samples were separated on a Phenomenex Luna C18(2) column (4.6 x 250 nm, 5μ) equilibrated with 70% solvent A (0.5% formic acid in H_2O) and 30% solvent B (0.5% formic acid in methanol) at a flow rate of 1 mL/min. The solvent was programmed as follows: a linear gradient from the starting solvent to 70% B in 20 min, increasing to 90% B in 0.1 min, holding for 5 min, decreasing to 30% B in 0.1 min, and re-equilibrating at initial conditions for 5 min. Eluting compounds were detected by UV absorbance at 300 nm. All incubations and standards were performed in triplicate.

5,6-Dihydro-M_1dG, 5,6-dihydro-M_1G, PdG, PGua, γ-OH-PdG, and α-OH-PdG. All sample preparation was performed on ice at 4 °C. The final incubation conditions contained 5 mg/mL rat liver cytosol and 200 μM substrate dissolved in 0.1 M potassium phosphate (pH 7.4). Reagents were equilibrated to 37 °C for 5 min and the reaction initiated by the addition of substrate. Reactions were terminated at intervals (0, 20, 40, and 60 min) by adding 0.1 mL ice cold methanol, vortexed, and centrifuged at 200,000 g for 30 min. Supernatants were removed and analyzed directly by HPLC-UV analysis. Samples were separated on a Phenomenex Luna C18(2) column (4.6 x 250 nm, 5μ) equilibrated with 90% solvent A (0.5% formic acid in H_2O) and 10% solvent B (0.5% formic acid in methanol) at a flow rate of 1.0 mL/min. The solvent was programmed as follows: a linear gradient from the starting solvent to 20% B in 10 min, holding at 20% B

for 10 min, increasing to 85% B in 0.1 min, holding at 85% B for 5 min, decreasing to 10% B in 0.1 min, and holding at initial conditions for 5 min. Eluting compounds were detected by UV absorbance at 254 nm. All incubations were prepared in triplicate.

Incubations of 1,N^2-ε-Gua with purified XO

All sample preparation was performed on ice at 4 °C. The final incubation conditions for the kinetic determinations contained 0.10 units XO/mL (CalBiochem, La Jolla, CA), varied concentrations of 1,N^2-ε-Gua (10, 25, 50, 75, 100, 150, 250, 500, 750 μM), and 0.4% DMSO in 0.8 M potassium phosphate (pH 7.6). Reagents were equilibrated to 37 °C for 5 min and the reaction was initiated by the addition of the substrate. Reactions were terminated after 15 min by adding 0.5 mL ice cold ethanol, vortexed, and extracted twice with 2x volume chloroform. The extracts were evaporated under nitrogen, and reconstituted in 0.1 N NaOH. Samples were separated on a Phenomenex Luna C18(2) column (4.6 x 250 nm, 5μ) equilibrated with 95% solvent A (0.5% formic acid in H_2O) and 5% solvent B (0.5% formic acid in methanol) at a flow rate of 1 mL/min. The solvent was programmed as follows: a linear gradient from the starting solvent to 30% B in 15 min, increasing to 80% B in 0.1 min, holding for 5 min, decreasing to 5% B in 0.1 min, and re-equilibrating at initial conditions for 5 min. Eluting compounds were detected by UV absorbance at 285 nm. Samples from the kinetic determinations were quantified in reference to a standard curve prepared by spiking known concentrations of 1,N^2-ε-Gua (2.5, 5, 50, 100, 250, 500, 750 μM) into 0.10 units/mL XO solutions, followed immediately by termination, extraction, and analysis as outlined above. All incubations and standards were performed in triplicate.

V_{max}/K_m values were calculated with Prism software (Version 4.0c) using nonlinear regression one-site binding and one-site competition models, respectively.

Incubations of 1,N^6-ε-dA with purified human PNP

All sample preparation was performed on ice at 4 °C. The final incubation conditions contained 100 μM 1,N^6-ε-dA dissolved in 0.1 M potassium phosphate (pH 7.4) buffer and varied amounts of PNP (0.05, 0.1, 0.25 and 0.75 Units/mL). The specific activity of PNP was 18 U/mg. Reagents were equilibrated to 37 °C for 5 min and the reaction was initiated by the addition of substrate. Reactions were terminated at intervals (0, 5, 15, and 30 min) by adding 0.5 mL ice cold ethanol, vortexed, and extracted twice with 2x volume chloroform. The extracts were evaporated under nitrogen and reconstituted in 0.1 M potassium phosphate, pH 7.4, for HPLC-UV analysis. Samples were separated on a Phenomenex Synergi POLAR-RP column (2.0 x 150 nm, 4μ) equilibrated with 98% solvent A (0.5% formic acid in H_2O) and 2% solvent B (0.5% formic acid in methanol) at a flow rate of 0.3 mL/min. The solvent was programmed as follows: a linear gradient from the starting solvent to 40% B in 10 min, holding at 40% B for 3 min, decreasing to 2% B in 0.1 min and holding at initial conditions for 7 min. Eluting compounds were detected by UV absorbance at 254 and 275 nm. All incubations were prepared in duplicate.

LC-MS/MS analysis

Following sample work-up as noted above, selected samples were analyzed by LC-MS/MS analysis. The previously described gradients (see above) were adapted to

lower flow rates (0.3 mL/min) for sample analysis. Eluting compounds were analyzed on either ThermoElectron LTQ or Quantum instruments. Positive ion ESI LC-MS/MS or LC-MS^n were performed with the following general parameters: spray voltage = 4.2 eV; capillary temperature = 275 °C; sheath gas = 60 psi; source CID off; with varied collision energies.

Biochemical synthesis of metabolites

1,N^2-ε-Gua metabolite. 1,N^2-ε-Gua (2 mg) was incubated with 5 mL of concentrated rat liver cytosol (13.6 mg/mL) and allowed to proceed to completion. The reaction mix was centrifuged at 10,000 g for 15 min to pellet protein and the supernatant was injected directly onto the HPLC. Fractions corresponding to the 1,N^2-ε-Gua metabolite were pooled, evaporated under reduced pressure and dissolved in DMSO-d_6 for NMR analysis.

Heptanone-1,N^2-ε-Gua metabolite. Heptanone-1,N^2-ε-Gua (1 mg) was reacted in 30 mL of concentrated gerbil liver cytosol and allowed to proceed to completion. 15 mL of ethanol was added to the reaction mix and centrifuged at 10,000 g for 15 min to precipitate protein. An additional 15 mL of ethanol was added to the supernatant and the mixture was extracted twice with 50 mL chloroform. The organic layers were pooled and evaporated under reduce pressure. The remaining residue was re-dissolved in methanol and directly injected onto the HPLC. Fractions corresponding to the heptanone-1,N^2-ε-Gua metabolite were collected, evaporated under reduced pressure and dissolved in d_6-DMSO for NMR analysis.

NMR analysis of 1,N^2-ε-Gua and heptanone-1,N^2-ε-Gua metabolites

NMR experiments were acquired using a 14.0 T Bruker magnet equipped with a Bruker AV-II console operating at 600.13 MHz. All spectra were acquired in 2.5 mm NMR tubes using a Bruker 5 mm TCI cryogenically cooled NMR probe. Chemical shifts were referenced internally to acetone (7.1 ppm), which also served as the ^{2}H lock solvent. For 1D ^{1}H NMR, typical experimental conditions included 32K data points, 13 ppm sweep width, a recycle delay of 1.5 s, and 32-256 scans depending on sample concentration. For 2D ^{1}H-^{1}H COSY, experimental conditions included 2048 x 512 data matrix, 13 ppm sweep width, recycle delay of 1.5 s and 4 scans per increment. The data was processed using squared sinebell window function, symmetrized, and displayed in magnitude mode. Multiplicity-edited heteronuclear single quantum coherence (HSQC) experiments were acquired using a 1024 x 256 data matrix, a J(C-H) value of 145 Hz which resulted in a multiplicity selection delay of 34 ms, a recycle delay of 1.5 s and 16 scans per increment along with GARP decoupling on ^{13}C during the acquisition time (150 ms). The data was processed using a π/2 shifted squared sine window function and displayed with CH/CH_3 signals phased positive and CH_2 signals phased negative. J_1(C-H) filtered HMBC experiments were acquired using a 2048 x 256 data matrix, a J(C-H) value of 9 Hz for detection of long range couplings resulting in an evolution delay of 55ms, J_1(C-H) filter delay of 145 Hz (34 ms) for the suppression of one-bond couplings, a recycle delay of 1.5 s, and 128 scans per increment. The HMBC data was processed using a π/2 shifted squared sine window function and displayed in magnitude mode.

Results

Metabolism of 1,N^2-ε-Gua in rat liver cytosol

1,N^2-ε-Gua is released from DNA by the alkylpurine-DNA-*N*-glycosylase in mammalian cells (*217, 219*). The base adduct 1,N^2-ε-Gua is structurally very similar to the pyrimidopurinone adduct, M_1G, which is oxidatively metabolized *in vitro* and *in vivo*. 1,N^2-ε-Gua and M_1G differ only by one carbon in the exocyclic ring (**Figure 58**). To investigate whether 1,N^2-ε-Gua was also a substrate for oxidative metabolism we performed *in vitro* experiments in rat liver cytosol. Profiling the reaction extracts by HPLC with UV detection demonstrated a time-dependent decrease of 1,N^2-ε-Gua and the appearance of a new peak eluting shortly after 1,N^2-ε-Gua. Positive ion ESI LC-MS analysis of the later eluting peak revealed a *m/z* of 192.1, which suggested the incorporation of an oxygen atom. No additional products were observed in the MS- or UV-spectra. MS^n experiments were carried out on the putative metabolite, which displayed similar fragmentation patterns to 1,N^2-ε-Gua, except for the addition of 16 amu, which was apparent with the base peak and with some fragments. 1,N^2-ε-Gua metabolite production was inhibited by allopurinol, an inhibitor of XOR, and not by menadione or raloxifene, inhibitors of AO, which suggested the involvement of XOR in the oxidation of 1,N^2-ε-Gua.

Further investigation into the turnover of 1,N^2-ε-Gua revealed a K_m of 84 μM and a V_{max} of 105 pmol min^{-1} mg^{-1} (K_m/V_{max} = 0.005 min^{-1} mg^{-1}) (**Figure 59**). These calculated values are very close to what was observed with M_1G metabolism in rat liver cytosol (K_m = 105 μM, V_{max}/K_m = 0.005 min^{-1} mg^{-1} (*261*)). IC_{50} determinations of

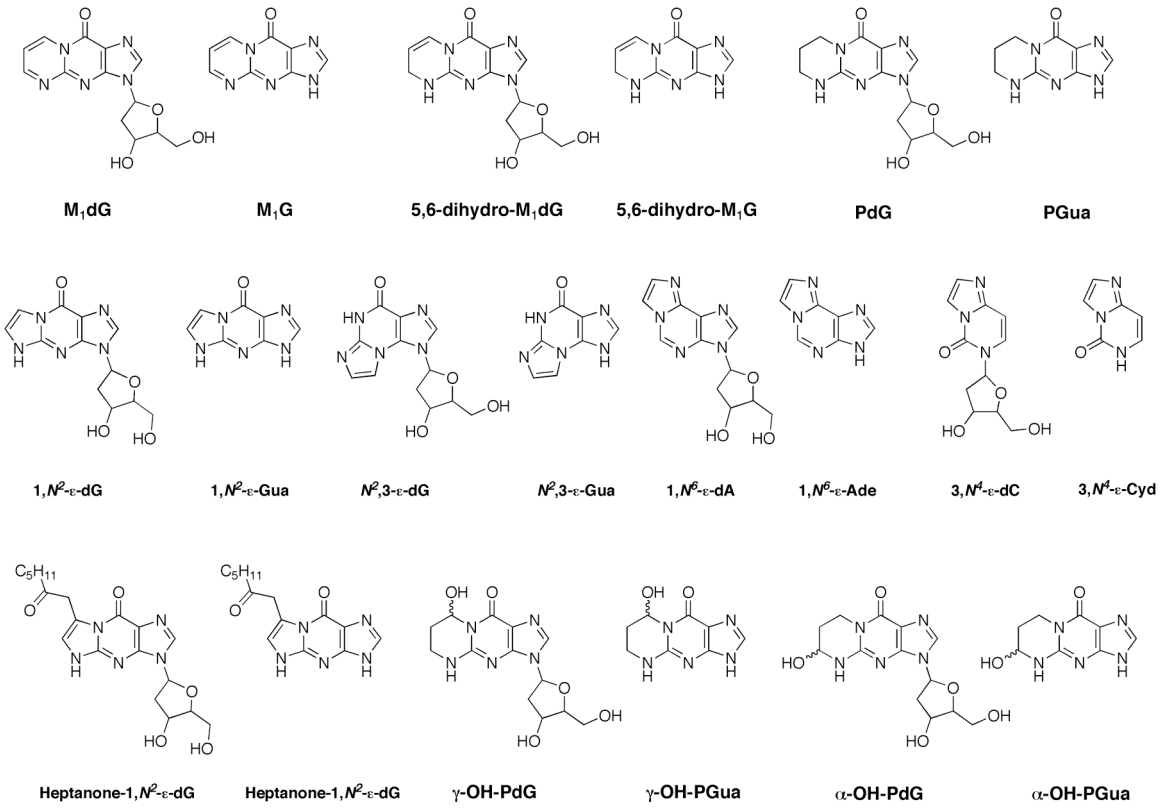

Figure 58. Structures of endogenous exocyclic DNA adducts and structural analogs of M_1dG.

1,N^2-ε-Gua metabolism with allopurinol revealed complete inhibition of metabolite production at saturating concentrations of allopurinol in rat liver cytosol (IC_{50} of 1.4 μM) (**Figure 60**).

Metabolism of 1,N^2-ε-Gua with purified XO

The complete inhibition of 1,N^2-ε-Gua metabolism by allopurinol suggested XOR was the only enzyme involved in the metabolism of 1,N^2-ε-Gua. To verify this observation, *in vitro* metabolism of 1,N^2-ε-Gua was performed using by purified bovine XO. XO efficiently metabolized 1,N^2-ε-Gua demonstrating a K_m of 108 μM and V_{max} of 10.1 μmol min^{-1} mg XO^{-1} (**Figure 61**).

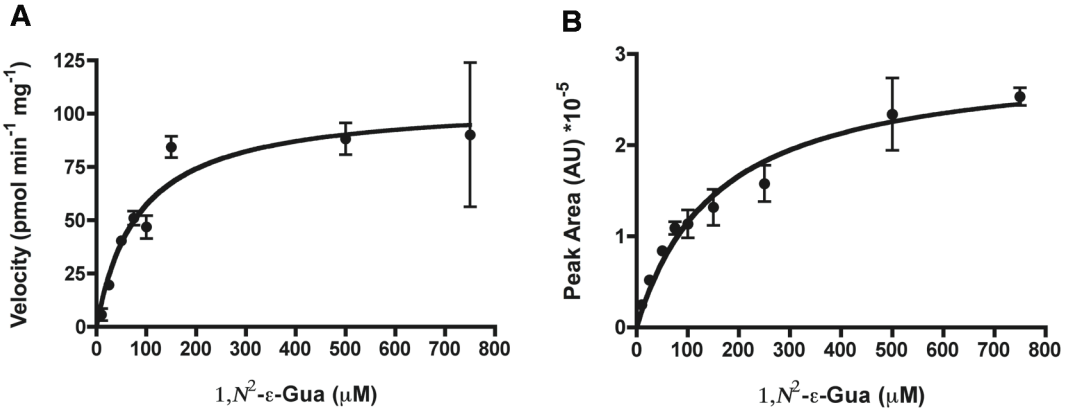

Figure 59. Concentration dependence of 1,N^2-ε-Gua oxidation in rat liver cytosol. (A) 1,N^2-ε-Gua consumption. (B) 1,N^2-ε-Gua metabolite formation. 1,N^2-ε-Gua consumption was calculated by reference to a standard curve (K_m = 84 μM and V_{max} = 105 pmol min^{-1} mg^{-1}) whereas product formation was based on the peak area production of the 1,N^2-ε-Gua metabolite (K_m = 156 μM).

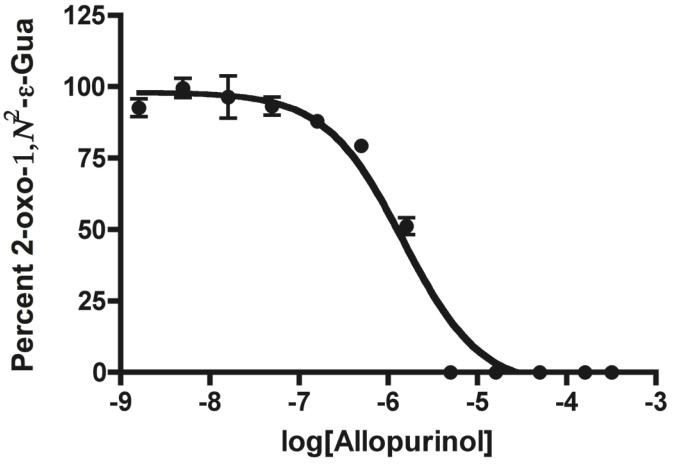

Figure 60. IC_{50} determination in rat liver cytosol with allopurinol using 1,N^2-ε-Gua as a substrate. Using 1,N^2-ε-Gua (84 μM) as a substrate, IC_{50} values were determined based on 1,N^2-ε-Gua metabolite inhibition with increasing concentrations of allopurinol in rat liver cytosol (IC_{50} = 1.4 μM).

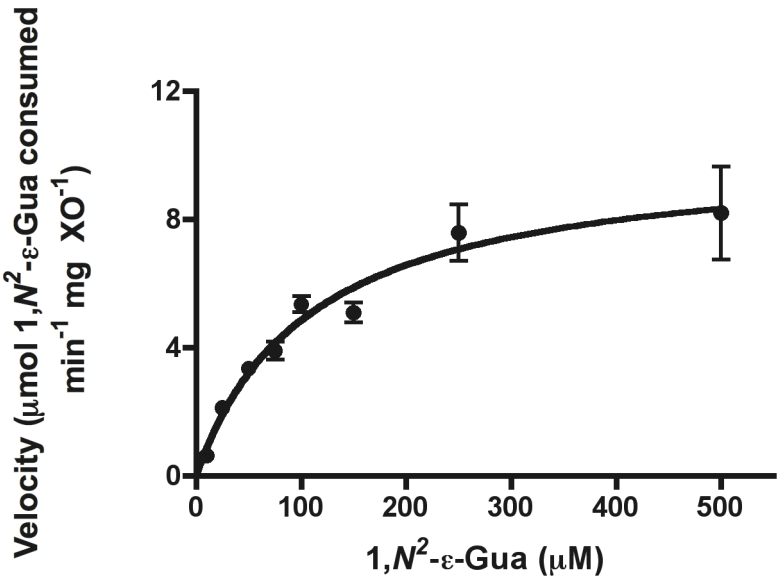

Figure 61. Concentration dependence of 1,N^2-ε-Gua oxidation in purified XO. 1,N^2-ε-Gua consumption was calculated by reference to a standard curve (K_m = 108 μM and V_{max} = 10.1 μmol min^{-1} mg XO^{-1}).

Biochemical synthesis of 1,N^2-ε-Gua metabolite

To identify the product of 1,N^2-ε-Gua metabolism in rat liver cytosol we biochemically synthesized the metabolite with concentrated rat liver cytosol and purified the product by fraction collection from an HPLC. The product was concentrated and dissolved in d_6-DMSO for NMR analysis. Comparison of the ^{1}H-NMR spectra for 1,N^2-ε-Gua and the metabolite revealed an absence of the singlet corresponding to H_2 (7.8 ppm) from the imidazole ring, while two correlated doublets remained from the etheno ring for H_7 (d, 1H, 7.6 ppm) and H_6 (d, 1H, 7.4 ppm) (*210*). This was confirmed by the HSQC spectrum, which demonstrated the metabolite only contained CH protons. If oxidation had occurred on the etheno ring, the adjacent carbon to the site of oxidation would have been reduced to CH_2. HMBC analysis revealed three-bond couplings for H_7 and H_6 to C_{4a} (145 ppm) confirming oxidation had not occurred on the etheno ring, but on the imidazole ring yielding 2-oxo-ε-Gua (**Figure 62**).

Metabolism of 1,N^2-ε-dG in rat liver cytosol

The observed metabolism of 1,N^2-ε-Gua in rat liver cytosol led us to investigate the metabolism of the deoxynucleoside, 1,N^2-ε-dG. We were curious to know if oxidation would occur on the imidazole ring of the etheno adduct containing deoxyribose. Identical incubation conditions to 1,N^2-ε-Gua metabolism studies were carried out using 1,N^2-ε-dG in rat liver cytosol. The deoxynucleoside adduct did not undergo oxidation. However, LC-UV and LC-MS analysis of the reaction mixture indicated 1,N^2-ε-dG was consumed over time, producing a new chromatographic peak eluting with an identical retention time and mass spectrum for the base, 1,N^2-ε-Gua.

Furthermore, the newly produced 1,N^2-ε-Gua was converted to the oxidized product, 2-oxo-ε-Gua. There was no evidence to support direct oxidation of the deoxynucleoside. These data suggested 1,N^2-ε-dG was subject to depurination in rat liver cytosol, and the product of this conversion was then subject to oxidation (**Figure 63**).

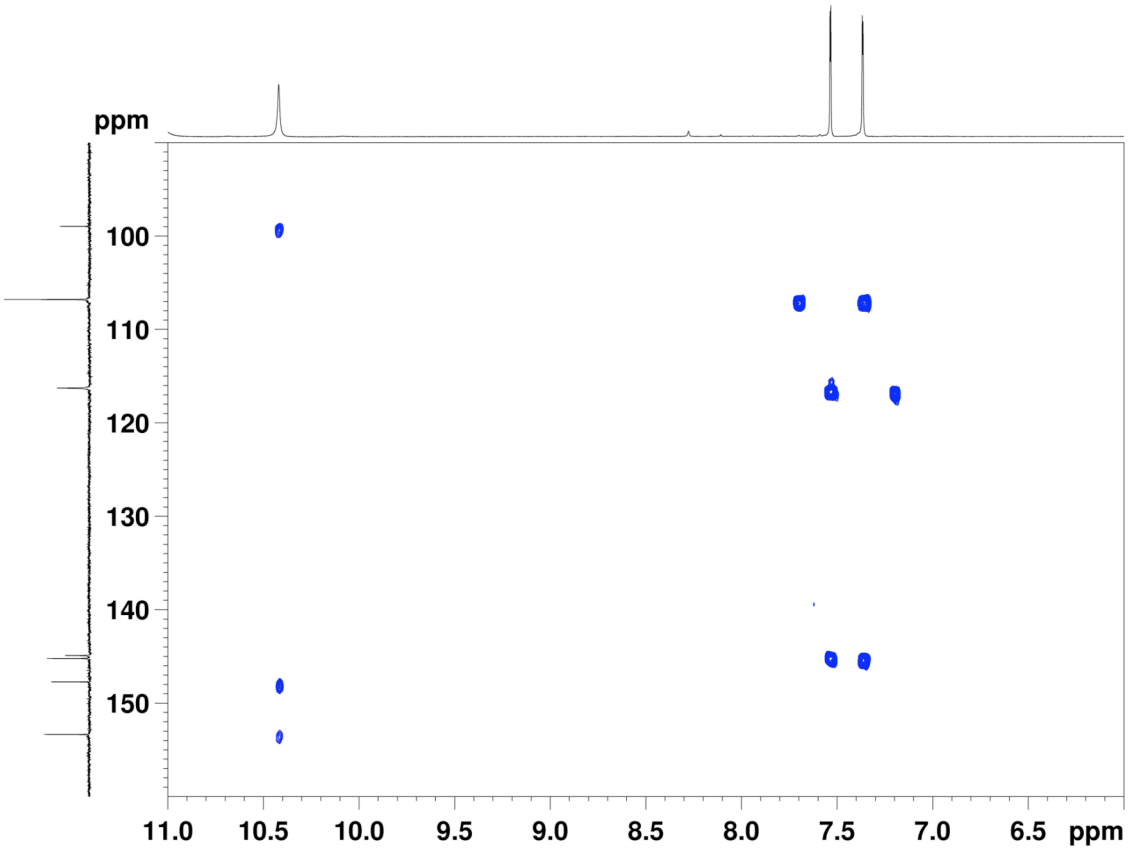

Figure 62. HMBC spectrum of the 1,N^2-ε-Gua metabolite from rat liver cytosol.

Depurination was not observed with M_1dG metabolism *in vitro* in rat liver cytosol or *in vivo* in the rat (*157, 267*). Results with 1,N^2-ε-dG suggest the involvement of an additional pathway for exocyclic adduct metabolism. PNP is an enzyme involved in the purine salvage pathway, which carries out the phosphorolysis of 6-oxo-purine nucleosides and deoxynucleosides (guanosine, inosine, dG and deoxyinosine) to their corresponding bases (Gua and xanthine). The enzyme uses inorganic phosphate ($H_2PO_4^-$) as a co-substrate and produces (deoxy)ribose-1-phosphate in addition to the base. PNP is expressed in rat liver (*280, 281*). The observed cleavage of 1,N^2-ε-dG to 1,N^2-ε-Gua suggests the involvement of PNP in rat liver cytosol metabolism.

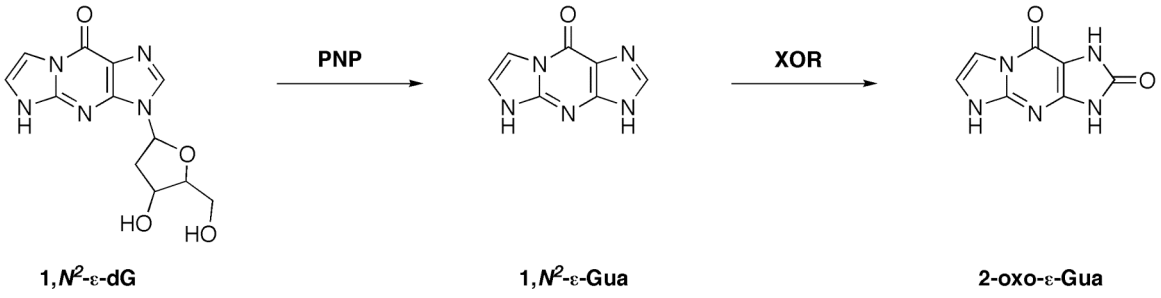

Figure 63. Conversion of 1,N^2-ε-dG to 2-oxo-ε-Gua in rat liver cytosol.

Metabolism of heptanone-1,N^2-ε-Gua in rat liver cytosol

Two exocyclic base adducts (M_1G and 1,N^2-ε-Gua) have been characterized to undergo oxidation on the imidazole ring. Presence of the deoxyribose moiety on the imidazole portion of the base prohibits this oxidation. As a corollary, we were curios to know what effects etheno ring substituents would have on imidazole oxidation. To address this question we investigated the endogenously produced heptanone-1,N^2-ε-dG, which contains a heptanone sidechain extending off of C_7 on the etheno ring (**Figure 58**) (*199*). We performed *in vitro* metabolism experiments in rat liver cytosol with heptanone-1,N^2-ε-dG and its corresponding base, heptanone-1,N^2-ε-Gua. The deoxynucleoside was stable in rat liver cytosol, and was neither a substrate for oxidation nor phosphorolysis. However, the base adduct heptanone-1,N^2-ε-Gua was subject to metabolism. Profiling the reaction mixtures by LC-MS/MS revealed a new peak eluting shortly after heptanone-1,N^2-ε-Gua, which contained an addition of 16 amu to the parent mass. The use of chemical inhibitors suggested the involvement of XOR because co-incubation with allopurinol inhibited metabolism, but co-incubation with menadione and raloxifene did not. Limitations in analyte solubility precluded concentration-dependent kinetic determinations in rat liver cytosol.

Biochemical synthesis of the heptanone-1,N^2-ε-Gua metabolite

Heptanone-1,N^2-ε-Gua was reacted to completion in concentrated gerbil liver cytosol, extracted, and purified by reverse phase HPLC. HPLC fractions containing the metabolite were pooled, evaporated to dryness, dissolved in d_6-DMSO, and analyzed by NMR. The HSQC and HMBC experiments enabled identification of the metabolite as 2-

oxo-heptanone-ε-Gua (**Figures 64 & 65**). H_6 (s, 1H, 7.1 ppm, C_6 at 116 ppm) was evident in the HSQC spectrum and showed a 2-bond correlation to C_7 (119 ppm) and a 3-bond correlation to C_{4a} (146 ppm) in the HMBC spectrum. $H_{1'}$ (s, 2H, 4.1 ppm, $C_{1'}$ at 39 ppm) was evident in the HSQC spectrum and exhibited two-bond correlations to C_7 (119 ppm) and C2′ (206 ppm) and a three-bond coupling to C_6 (116 ppm) in the HMBC. The 3-bond coupling from H_6 to $C_{1'}$ was not observed, however. Direct comparison of the metabolite spectra to the heptanone-1,N^2-ε-Gua spectra was inconclusive. Several additional chemical shifts were observed in the starting material, which were an artifact of the sample work-up, and attributed to the equilibrium between heptanone-1,N^2-ε-Gua and the hemiacetal (**Figure 22**) (*199*).

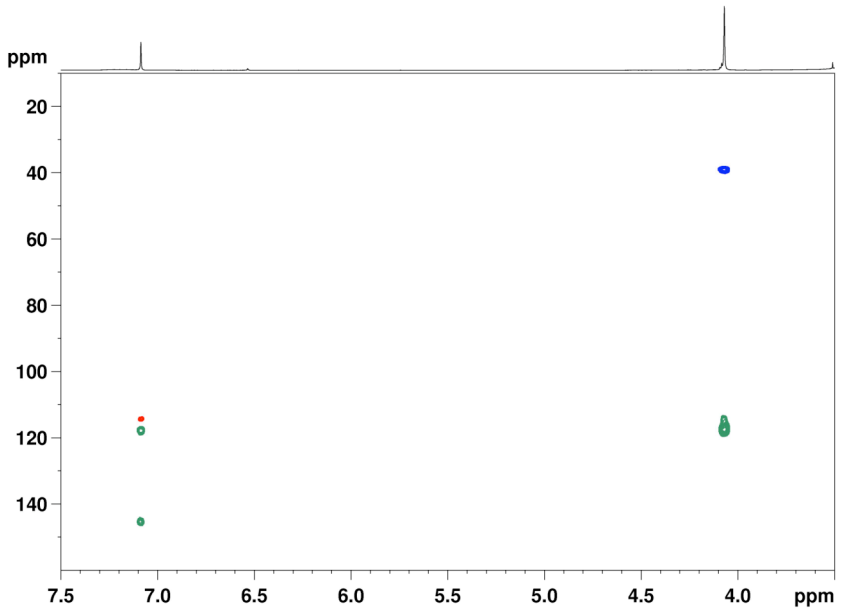

Figure 64. Overlay of the HSQC and HMBC spectra of the heptanone-1,N^2-ε-Gua metabolite from rat liver cytosol. HMBC (Green), HSQC-CH (red), HSQC-CH_2 (blue)**.**

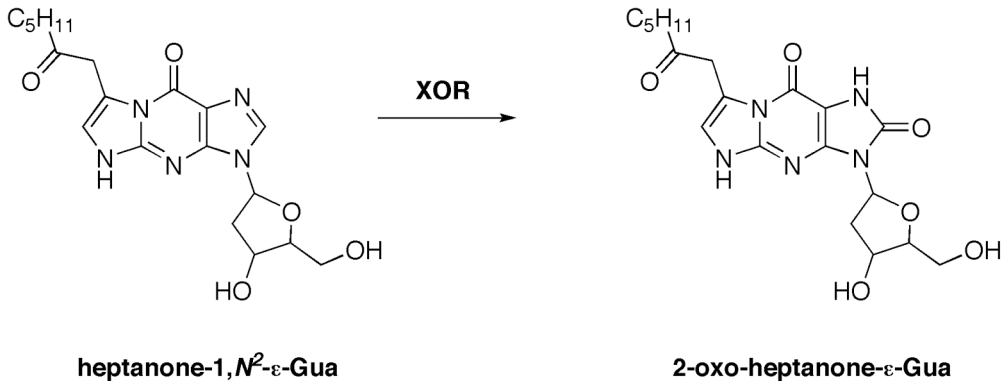

Figure 65. Conversion of heptanone-1,N^2-ε-Gua to 2-oxo-heptanone-ε-Gua in rat and gerbil liver cytosol

Investigation of 3,N^4-ε-dC, 3,N^4-ε-Cyd, 1,N^6-ε-dA, and 1,N^6-ε-Ade metabolism

Several exocyclic adducts of dG have been characterized to undergo oxidation in rat liver cytosol. One of these adducts, 1,N^2-ε-dG, is also a substrate for phosphorolysis. 3,N^4-ε-dC and 1,N^6-ε-dA are etheno adducts of dC and dA (**Figure 58**), respectively, with proposed routes of endogenous formation (*196, 197*). Each of these adducts are released from DNA by glycosylase action as the corresponding base adducts, 3,N^4-ε-Cyd (*221-223*) and 1,N^6-ε-Ade (*217, 218*). The exocyclic etheno ring for these molecules is structurally similar and contains a heterocyclic imine extending from a quaternary carbon on the base, which is a pyrimidine in the case of 3,N^4-ε-Cyd and purine for 1,N^6-ε-Ade. Each base adduct was investigated for metabolism in rat liver cytosol and neither was found to be metabolized.

The corresponding deoxynucleoside adducts 3,N^4-ε-dC and 1,N^6-ε-dA were also investigated for their stability in rat liver cytosol. The reaction mixtures were profiled by positive ion ESI LC-MS/MS and neither of these adduct was found to be oxidized *in vitro*. However, 1,N^6-ε-dA underwent a time-dependent decrease in total peak area, with a corresponding increase of an early eluting peak, which displayed a *m/z* of 162.1. The

appearance of *m/z* 162.1 was not detected in control incubations. The early eluting peak corresponded to the protonated molecular ion for the base (1,N^6-ε-Ade) suggesting that 1,N^6-ε-dA underwent phosphorolysis. The product of 1,N^6-ε-dA metabolism demonstrated an identical retention time to a 1,N^6-ε-Ade standard and co-chromatographed when the incubation extract was spiked with 1,N^6-ε-Ade. Identical observations were made using 1,N^6-ε-adenosine in incubations with rat liver cytosol.

PNP uses $H_2PO_4^-$ as a co-substrate. To investigate the role of PNP in the metabolism of 1,N^6-ε-dA we performed incubations using either potassium phosphate or Tris-HCl buffers. In the absence of phosphate, the production of 1,N^6-ε-Ade was diminished (**Figure 66**). 1,N^6-ε-dA was also incubated in reactions with purified PNP (from human) using potassium phosphate buffer. Phosphorolysis of 1,N^6-ε-dA was dependent on protein and time (**Figure 67**), providing evidence that 1,N^6-ε-dA is a substrate for human PNP (**Figure 68**).

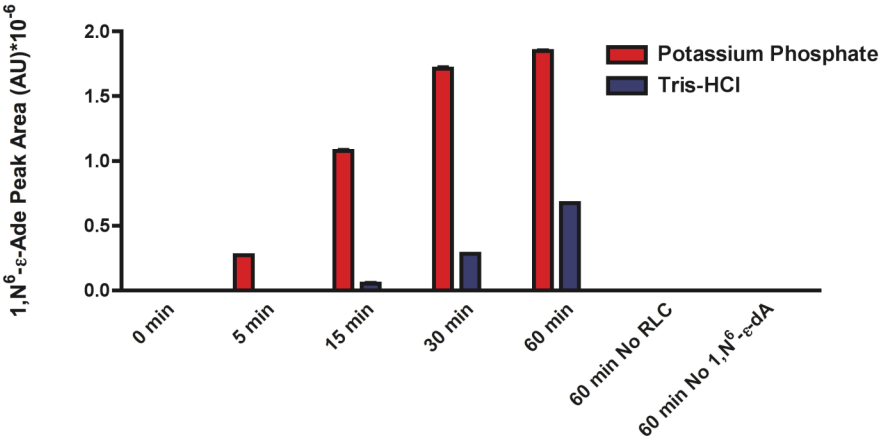

Figure 66. Conversion of 1,N^6-ε-dA to 1,N^6-ε-Ade in rat liver cytosol in potassium phosphate or Tris-HCl buffers.

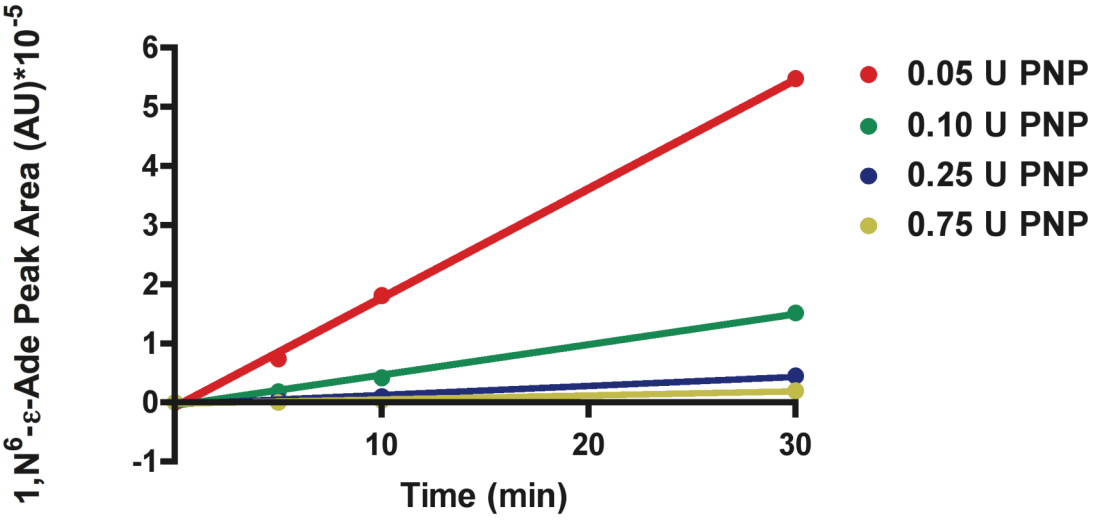

Figure 67. Phosphorolysis of 1,N^6-ε-dA to 1,N^6-ε-Ade with purified PNP from human blood.

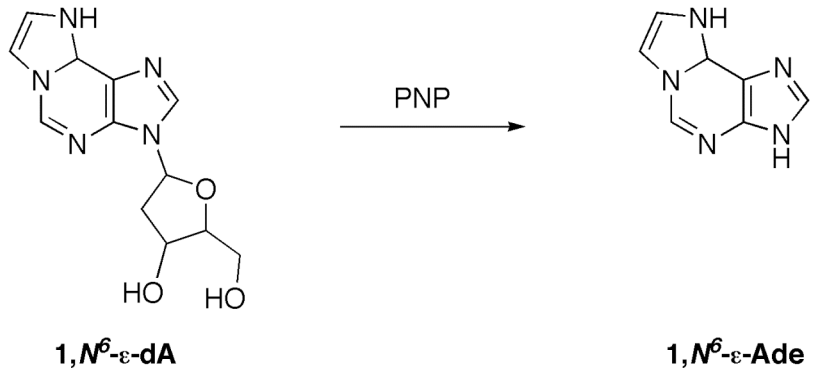

Figure 68. Conversion of 1,N^6-ε-dA to 1,N^6-ε-Ade with rat liver cytosol and PNP.

Metabolism of M_1dG analogs in rat liver cytosol

To lend further insight into the structural requirements for the metabolic processing of exocyclic adducts in rat liver cytosol, we investigated the metabolic stability of several pyrimidopurinone-dG analogs of M_1dG and M_1G (**Figure 58**). The partially reduced pyrimido analogs 5,6-dihydro-M_1dG and 5,6-dihydro-M_1G, and fully reduced analogs PdG and PGua have previously been used to mimic the biological activity of M_1dG in several genetic and biochemical investigations (*116, 122, 282, 283*). γ-OH-PdG and α-OH-PdG are endogenous adducts produced from reactions of acrolein with dG (*163, 164*). These dG modifications impart different electronic and structural effects on the exocyclic ring. For example, the pyrimido ring is planar and aromatic, while the propano ring is puckered and un-conjugated. This series of dG adducts are approximately the same size as the pyrimidopurinone adducts, so the exocyclic propano ring should not preclude access to the active sites of XOR, AO, or PNP.

All investigations on the metabolism of the deoxynucleoside structural analogs revealed no indication of either oxidative metabolism or phosphorolysis. To our surprise none of the base adducts were oxidized. It appears that planar and electron-rich exocyclic ring structures, in part, are a structural requirement for oxidation and phosphorolysis in rat liver cytosol *in vitro*.

Discussion

Non-invasive analysis of endogenously occurring DNA damage is of interest for use in clinical and animal studies. Our findings on the metabolism and elimination of M_1dG suggests that the metabolic processing of exocyclic DNA adducts may impact the

ability to detect deoxynucleoside and base adducts in biological matrixes (*157, 261, 267*). We propose that it is important to consider the possibility of metabolism prior to the development of analytical methods designed to evaluate endogenous levels of adducts. Our recent study was designed to determine structural features of exocyclic adducts that led to metabolism. We based our investigation on small changes in the pyrimido ring of dG that imparted alterations to size and conjugation as well as the addition of substituents.

In total, our findings demonstrate that oxidative metabolism can occur on either the exocyclic ring, as seen with M_1dG and M_1G, or the imidazole ring, as seen with M_1G, 1,N^2-ε-Gua and heptanone-1,N^2-ε-Gua. Both deoxynucleosides and bases are subject to oxidation, with the base adducts being better substrates. When conjugated to the base, deoxyribose appears to prohibit oxidation on the imidazole ring. Additionally, the metabolic processing is not limited to oxidation, as deoxynucleosides and nucleosides may also be phosphorolyzed to the corresponding base adducts. We did not observe oxidative metabolism with dA, Ade, dC, or Cyd etheno adducts, but this does not preclude others derivatives of dA, Ade, dC, or Cyd from metabolic processing.

There are multiple reports on the structural determinants of XOR and AO substrate specificity and inhibition (*284-293*). In general, substrates are nitrogen-containing heterocycles, and the enzyme-mediated oxidation is targeted to electropositive carbons, which lie adjacent to ring nitrogens (*293*). Our observations with exocyclic adducts are consistent with these observations.

In series of chemical and biochemical experiments, Leonard *et al.* demonstrated XOR-mediated metabolism with several modified purine structures that are structurally

similar to the pyrimido and etheno adducts of dG (Gua) and dA (Ade) (**Figure 69**) (*287, 288*). Inserting a benzene ring in between the imidazole and pyrimidine rings of and 6-oxo-purine (hypoxanthine) yielded several "stretched-out" purine analogs. *lin*-Benzoxanthine is similar to M_1G; however, for M_1G the benzene ring is attached to the pyrimidine opposite the imidazole ring. Using bovine XO, Leonard *et al.* demonstrated successive oxidations of *lin*-benzohypoxanthine to uric acid-like molecules. This is analogous to what was observed with M_1G (*261*). Interestingly, Leonard *et al.* also observed successive oxidations with the ribonucleoside, *lin*-benzoinosine. In our investigations, oxidation on the imidazole ring did not occur with either M_1dG, 1,N^2-ε-dG, or any of the propano analogs.

Thus far, all characterized oxidation products of exocyclic adducts occur on tertiary imine carbons on either the exocyclic or imidazole ring. Reduction of the 5,6-double bond on the pyrimido ring of M_1dG (M_1G) yields a secondary carbon at the 6-position, which did not undergo oxidation. Krenitsky *et al.* demonstrated that purine is oxidized by XOR first at the 6-position, and then successively at the 2- and 8 positions. However, AO oxidized purine only at the 8-posititon on the imidazole carbon (*284*). The analogous position on the M_1G analogs is the 2-position, which was not a target for oxidation. This would imply that either the non-planar character of the reduced pyrimido ring or its reduced electron density impacts oxidation on the imidazole ring. AO oxidizes hypoxanthine only at the 2-position (*284*), which implies the 9(10)-oxo group of the exocyclic dG adducts, may also impact substrate orientation in the AO active site.

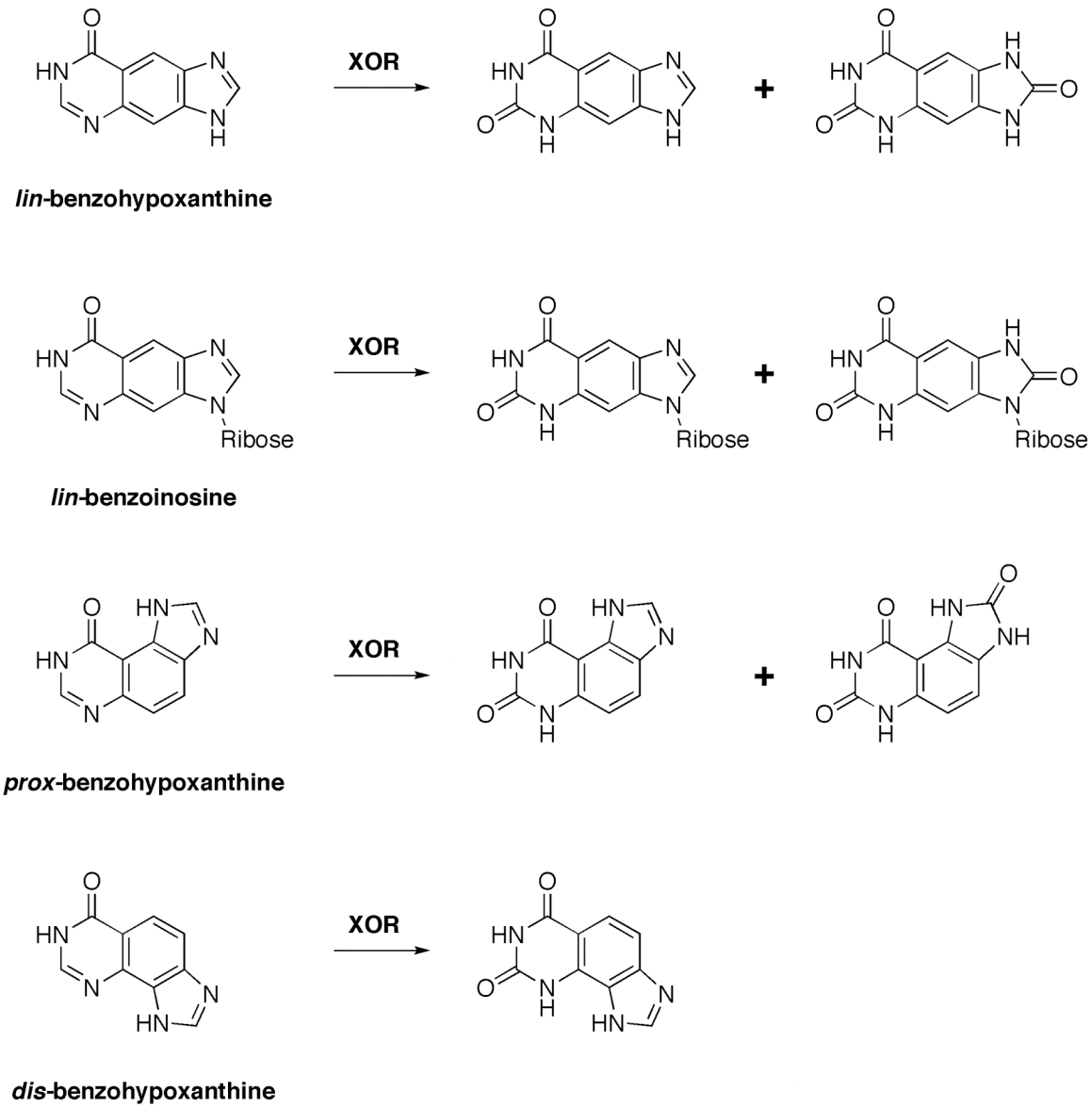

Figure 69. Structures of "stretched-out" 6-oxo-purine analogs synthesized by Leonard *et al.* (*287*) and their conversion to oxidized products by XOR.

The effect of substitutions on the exocyclic ring of propano and etheno dG adducts was investigated. PdG adducts with hydroxyl substituents on the exocyclic ring did not undergo metabolic processing; although, the base adducts were not investigated. The addition of an alkyl substituent on the exocyclic ring of heptanone-1,N^2-ε-Gua did influence metabolism, however. Heptanone-1,N^2-ε-Gua underwent oxidation on the 2-position of imidazole ring, but the deoxynucleoside was unmodified; although, heptanone-1,N^2-ε-dG did not undergo phosphorolysis as seen with the unsubstituted 1,N^2-ε-dG. Several recent reports from the Blair Laboratory suggest substituted etheno adducts of dA, dC and dG are a major class of endogenous adducts derived from products of lipid peroxidation (*49, 50, 198-200, 202, 216, 294*). The repair products of these unsubstituted adducts are unknown. Purine-based therapeutics (aciclovir, penciclovir, zaleplon) and other substituted purine molecules are substrates for oxidation by AO and XOR (*252, 284, 290, 295-297*). Thus, it will be interesting to elucidate the metabolic processing of substituted etheno adducts.

Since endogenously formed exocyclic adducts are all modifications of purine and pyrimidine structures, we targeted our investigation to the cytosolic components of rat liver where XOR and AO are located. It is possible that other enzymes may catalyze metabolism of exocyclic adducts. CYPs and UDP-glucuronosyl transferases (components of the microsomal fraction of rat liver) may have a role in metabolism. Our results with the propano analogs suggest they are stable *in vitro* in cytosol. Propano adducts derived from crotonaldehyde and 4-hydroxy-2-nonenal also have alkyl substituents extended from the exocyclic ring, which may be targeted by different enzymes and alternate routes of metabolic processing.

1,N^2-ε-dG and 1,N^6-ε-dA were phosphorolyzed to the base adducts 1,N^2-ε-Gua and 1,N^6-ε-Ade, respectively, in rat liver cytosol by PNP. Both of these base adducts have been detected in urine from humans and rats (*212, 298, 299*). The elimination of these adducts in urine has generally been attributed to their removal from DNA as base adducts. Interestingly, 1,N^6-ε-dA has also been detected in rat urine (*211*). Based on our metabolism results, 1,N^6-ε-Ade maybe the best target for quantitation in urine samples.

Understanding the *in vitro* routes of metabolic processing should help guide analytical methodologies for the detection of endogenous adducts. Several exocyclic adducts have been characterized as good substrates for oxidative metabolism *in vitro*. The end products of metabolic processing may therefore be a reliable target for assessing the formation of endogenous adducts from biological matrixes *in vivo*.

CHAPTER VII

SUMMARY

Since the discovery of DNA as the heritable genetic material by Avery, and the determination of its structure by Watson and Crick, scientists have been investigating the coding properties of DNA. Chemical agents can modify DNA bases to produce DNA adducts that may alter the choice of incoming nucleotides during replication. In the absence of repair, miscoding leads to permanent changes in the genetic code. Therefore, assessing exposure of DNA bases to genotoxic chemicals may be a diagnostic marker to determine the rate of mutation in human populations.

Correlations between exposure to chemical agents and DNA mutations are well-documented in humans and animals for exogenous chemicals such as B[*a*]P and aflatoxin. Once an exogenous genotoxic chemical has been identified and its environmental sources characterized, a person's risk for mutation is generally related their exposure to these sources. Identifying genomic exposure to endogenously produced chemical agents is complicated by the absence of a universal source of their production. Further complicating this process is the difficulty of detecting specific biologically produced chemicals *in vivo*. Both oxygen radicals and lipid peroxidation products are highly reactive and short-lived, and their direct detection is not feasible. To assess their production *in vivo*, end-products of their reactions can be monitored. Thus, to assess genomic exposure to endogenously produced chemicals DNA adduct formation can be monitored.

Two approaches for the detection of DNA adducts are commonly employed: analysis of adducts in genomic DNA or as repair-products in biological matrixes. Detection of adducts from DNA offers a direct method of analysis, which assesses the amount of DNA damage in a defined tissue. However, this procedure is typically considered invasive because it requires cells or tissue from which to isolate DNA. Analysis of DNA adducts in urine (a biological elimination product) is considered a non-invasive strategy for the analysis of DNA adducts. Urinary analysis is an indirect method since the initial sites of adduct formation and removal is unknown. However, urinary analysis may represent a measure of the total systemic exposure to chemical agents. Furthermore, a non-invasive strategy for the routine analysis of DNA adducts is desirable to minimize cost and labor of sample collection, which offers greater applicability to population-based studies.

The endogenously formed exocyclic adduct M_1dG is derived from reactions of dG with either the lipid peroxidation product, MDA (also a product of prostaglandin synthesis), or the DNA peroxidation product base, propenal. M_1dG is found in genomic DNA of humans and rodents at levels of 1-90 adducts per 10^8 bases. Genetic and biochemical evidence implicates NER in the removal of M_1dG from DNA, which accounts for its appearance in urine as the deoxynucleoside. Analysis of urine collected from healthy humans revealed that M_1dG was eliminated at an average rate of 12 fmol kg^{-1} 24 h^{-1}. The levels of M_1dG in DNA are similar to other endogenously formed DNA adducts such as: 8-oxo-dG, 1,N^6-ε-dA, 1,N^2-ε-dG, and heptanone-1,N^2-ε-dG (*155, 189, 215, 216*). However, M_1dG is eliminated in urine at a much lower level than seen for 8-oxo-dG, 8-oxo-Gua, and 1,N^6-ε-Ade (*155, 156, 211*). (The urinary levels of 1,N^2-ε-dG

and heptanone-1,N^2-ε-dG have not been detected or reported, respectively). Based on this discrepancy, we hypothesized that biological factors (e.g., metabolism, routes of elimination) may limit the direct detection of M_1dG in urine.

Oxidative Metabolism of M_1dG

To test the hypothesis that enzymatic metabolism may limit the direct detection of M_1dG in urine, we devised a series of experiments to investigate the metabolic stability of M_1dG *in vitro* and *in vivo*. M_1dG was found to undergo oxidation *in vitro* in rat liver cytosol and *in vivo* when administered to Sprague Dawley rats. Metabolism occurred on the 6-position of the pyrimido ring to produce 6-oxo-M_1dG rats. Based on experiments with chemical inhibitors and with partially purified enzymes from rat liver, both XOR and AO were shown to catalyze the oxidation of M_1dG. Human liver cytosol incubations with M_1dG produced 6-oxo-M_1dG in a qualitatively similar manner to rat liver cytosol; although, AO appeared to have a greater contribution than XOR in human liver cytosol incubations.

The *in vivo* contribution of XOR to the metabolism of M_1dG was evaluated by pretreating Sprague Dawley rats with allopurinol (a specific, tight binding inhibitor of XOR), followed by administration of M_1dG. Animals receiving allopurinol pretreatment displayed decreased plasma and urinary levels of 6-oxo-M_1dG and increased plasma and urinary levels of M_1dG compared to vehicle control animals. Total inhibition of M_1dG metabolism was not observed in this experiment, which suggested either incomplete inhibition of XOR or the involvement of AO in the production of 6-oxo-M_1dG in the rat.

In the rat, XOR appears to play a significant role in the production of 6-oxo-M_1dG, while AO appears to contribute to a lesser degree.

Metabolism of [^{14}C]M_1dG

The total mass balance and metabolite profile of M_1dG was evaluated *in vivo* by stably incorporating a ^{14}C tracer into M_1dG. [^{14}C]M_1dG was administered to Sprague Dawley rats with or without bile catheters. Urine, feces, and bile were collected following administration of [^{14}C]M_1dG, and the total [^{14}C]recovery was assessed by liquid scintillation counting. Approximately 50% of the radioactivity was collected in urine while the remaining radioactivity was collected in the feces of non-bile-catheterized animals and in the bile of bile-catheterized animals. In urine, approximately 20% of the radioactivity was attributed to 6-oxo-M_1dG and 70% was attributed to M_1dG. In the bile samples, approximately 70% of the radioactivity was attributed to 6-oxo-M_1dG and 20% corresponded to M_1dG. No other significant metabolites were observed in this study; approximately 45% of the administered M_1dG was recovered as 6-oxo-M_1dG. When [^{14}C]6-oxo-M_1dG was administered to Sprague Dawley rats, nearly 70% was recovered in the feces of non-bile catheterized rats, while approximately 55% was recovered in the bile of bile catheterized rats. In all biological samples analyzed, [^{14}C]6-oxo-M_1dG was eliminated unchanged. Together these results demonstrate that 6-oxo-M_1dG is a stable metabolite of M_1dG that does not undergo additional biotransformation reactions, and may represent a significant portion (45%) of the total M_1dG levels.

The amount of M_1dG administered in the ^{14}C mass balance study (0.03 mg per animal) is likely higher than the anticipated daily clearance in humans and rats.

Therefore, we set out to evaluate the *in vivo* metabolism and elimination of M_1dG at lower concentrations. AMS analysis was implemented to enhance the limit of detection. Sprague Dawley rats were dosed with low levels of [^{14}C]M_1dG in separate experiments (2.8 ng, 75 pg, and 0.75 pg per animal). Animals that received 2.8 ng [^{14}C]M_1dG eliminated 50% of the total ^{14}C in urine and 40% of the ^{14}C eliminated in urine corresponded to 6-oxo-M_1dG. A separate cohort of animals received doses of 0.75 pg and 75 pg of [^{14}C]M_1dG. Approximately 50% of the ^{14}C was eliminated in urine and 25% of the urinary radioactivity corresponded to 6-oxo-M_1dG. The 75 pg and 0.75 pg studies were performed at the limit of detection by AMS analysis. Thus, the natural abundance of ^{14}C in biological samples prohibited analysis at lower administration levels. The direct analysis of ^{14}C in fecal samples was not feasible at low administration levels due to the higher carbon background. It was estimated (based on ^{14}C mass balance study) that 50-55% of the [^{14}C]M_1dG administered at concentrations below 3 ng per animal was converted to 6-oxo-M_1dG. This represents a significant conversion of M_1dG to 6-oxo-M_1dG at concentrations that closely approximate the anticipated rate of elimination in rats. Although the metabolism of M_1dG in human populations has not been investigated, the observed conversion of M_1dG to 6-oxo-M_1dG is only 2-fold. Therefore, the oxidation of M_1dG is not likely to limit its detection in urine samples.

Metabolism of M_1G

Based on our observations on the metabolism of M_1dG, we were curious to know if other structurally related exocyclic DNA adducts may also undergo enzymatic oxidation. The free base of M_1dG (M_1G, a putative product of base excision repair) was

evaluated to investigate the effect of deoxyribose on the metabolism of M_1dG. When incubated in rat liver cytosol, M_1G underwent successive oxidations. The first oxidation occurred at the 6-position of the pyrimido ring to produce 6-oxo-M_1G. The second oxidation occurred on the imidazole ring to produce 2,6-dioxo-M_1G. XOR and AO appear to be involved in the production of 6-oxo-M_1G, but only XOR is involved in the production of 2,6-dioxo-M_1G. Comparing the turnover of M_1dG, M_1G, and 6-oxo-M_1G revealed that M_1G and 6-oxo-M_1G were better substrates (approximately 5-fold) than M_1dG. Furthermore, the observed oxidation on the imidazole ring suggested that other exocyclic base adducts may undergo oxidation, with the imidazole ring being a likely site for oxidation.

Metabolism of Other Exocyclic DNA adducts

Unsubstituted etheno adducts are released from DNA by DNA glycosylases, and the products of repair are base adducts, which display structural similarity to M_1G. In particular 1,N^2-ε-Gua varies by one carbon in the exocyclic ring from M_1G. When incubated in rat liver cytosol 1,N^2-ε-Gua underwent oxidation on the imidazole ring to produce 2-oxo-ε-Gua. The deoxynucleoside (1,N^2-ε-dG) did not undergo oxidation in rat liver cytosol. However 1,N^2-ε-dG was subject to phosphorolysis by PNP to produce 1,N^2-ε-Gua, which was then oxidized to 2-oxo-ε-Gua. Other unsubstituted etheno base adducts (1,N^6-ε-Ade, 3,N^4-ε-Cyd) were not subject to oxidation in rat liver cytosol. Although, 1,N^6-ε-dA was subject to phosphorolysis by PNP to yield 1,N^6-ε-Ade.

To investigate the effect of a substituent on the etheno ring the metabolic stability of hepatanone-1,N^2-ε-Gua was investigated. Hepatanone-1,N^2-ε-Gua underwent

oxidation on the imidazole ring to 2-oxo-hepatanone-ε-Gua. The deoxynucleoside (hepatanone-1,N^2-ε-dG) was stable in rat liver cytosol and was neither oxidized nor phosphorolyzed.

The metabolic stability of several propano adducts was evaluated. In all cases (both base and deoxynucleoside adducts) the propano adducts did not undergo metabolic processing. These results suggest that the planarity or electron density of the exocyclic ring may impact either the oxidation or phosphorolysis of substrates in rat liver cytosol. However, molecules with these characteristics may be substrates for other classes of enzymes such as CYPs, not found in cytosolic tissue preparations.

Final Summary

An increasing body of evidence now exists that demonstrates exocyclic DNA adducts are subject to enzymatic oxidation and phosphorolysis reactions (sometimes in tandem). Exocyclic base adducts with planar and unsaturated exocyclic rings are the best substrates for enzymatic oxidation. Base adducts containing substitutions such as deoxyribose on the imidazole ring of M_1dG and a heptanone chain on the etheno ring of heptanone-1,N^2-ε-Gua do not prohibit oxidative metabolism. The enzymes of purine catabolism (XOR, AO, and PNP) are involved in the metabolic processing of exocyclic adducts. Based on *in vivo* metabolism studies at near-physiological concentrations of exogenously administered M_1dG, the metabolic processing of exocyclic adducts is likely to occur at their physiological rate of production in animals and humans. In total, these results demonstrate that exocyclic adducts are subject to metabolic processing (oxidation and phosphorolysis). Furthermore, metabolites of endogenously produced DNA adducts

are likely to be produced *in vivo*, and may provide a new class of biomarkers to assess exposure to endogenous sources DNA damage.

REFERENCES

(1) Pachter, H. M. (1951) *Magic into science, the story of Paracelsus; being the true history of the troubled life, adventures, doctrines, miraculous cures, and prophecies of the most renowned, widely traveled, very learned and pious gentleman, scholar, and most highly experienced and illustrious physicus, the Honorable Philippus Theophrastus Aureolus Bombastus ab Hohenheim, Eremita, called Paracelsus. . .* Henry Schumann, New York.

(2) Hill, J. (1761) *Cautions against the immoderate use of snuff. Founded on the qualities of the tobacco plant; and the effects if must produce when this way taken into the body: and enforced by instances of persons who have perished miserably of diseases, occasaioned or rendered incurable by its use.*, 2nd ed., R. Baldwin, London.

(3) Pott, S. P. (1775) Cancer Scroti, in *Chirurgical observations*, London.

(4) Miller, E. C., and Miller, J. A. (1966) Mechanisms of chemical carcinogenesis: nature of proximate carcinogens and interactions with macromolecules. *Pharmacol. Rev. 18*, 805-838.

(5) Miller, E. C., and Miller, J. A. (1981) Searches for ultimate chemical carcinogens and their reactions with cellular macromolecules. *Cancer 47*, 2327-2345.

(6) Avery, O. T., MacLeod, C. M., and McCarty, M. (1944) Studies on the chemical nature of the substance inducing transformation on pneumococcal types. *J. Exp. Med. 79*, 345-359.

(7) Watson, J. D., and Crick, F. H. (1953) Genetical implications of the structure of deoxyribonucleic acid. *Nature 171*, 964-967.

(8) Watson, J. D., and Crick, F. H. (1953) Molecular structure of nucleic acids; a structure for deoxyribose nucleic acid. *Nature 171*, 737-738.

(9) Szeliga, J., and Dipple, A. (1998) DNA adduct formation by polycyclic aromatic hydrocarbon dihydrodiol epoxides. *Chem. Res. Toxicol. 11*, 1-11.

(10) Lindahl, T. (1993) Instability and decay of the primary structure of DNA. *Nature 362*, 709-715.

(11) Cathcart, R., Schwiers, E., Saul, R. L., and Ames, B. N. (1984) Thymine glycol and thymidine glycol in human and rat urine: a possible assay for oxidative DNA damage. *Proc. Natl. Acad. Sci. U. S. A. 81*, 5633-5637.

(12) Adelman, R., Saul, R. L., and Ames, B. N. (1988) Oxidative damage to DNA: relation to species metabolic rate and life span. *Proc. Natl. Acad. Sci. U. S. A. 85*, 2706-2708.

(13) Li, D. H., and Randerath, K. (1990) Association between diet and age-related DNA modifications (I-compounds) in rat liver and kidney. *Cancer Res. 50*, 3991-3996.

(14) Li, D. H., Xu, D. C., and Randerath, K. (1990) Species and tissue specificities of I-compounds as contrasted with carcinogen adducts in liver, kidney and skin DNA of Sprague-Dawley rats, ICR mice and Syrian hamsters. *Carcinogenesis 11*, 2227-2232.

(15) Nath, R. G., Vulimiri, S. V., and Randerath, K. (1992) Circadian rhythm of covalent modifications in liver DNA. *Biochem. Biophys. Res. Commun. 189*, 545-550.

(16) Randerath, K., Reddy, M. V., and Disher, R. M. (1986) Age- and tissue-related DNA modifications in untreated rats: detection by ^{32}P-postlabeling assay and possible significance for spontaneous tumor induction and aging. *Carcinogenesis 7*, 1615-1617.

(17) Balkwill, F., and Mantovani, A. (2001) Inflammation and cancer: back to Virchow? *Lancet 357*, 539-545.

(18) Coussens, L. M., and Werb, Z. (2002) Inflammation and cancer. *Nature 420*, 860-867.

(19) Crohn, B. B., and Rosenberg, B. (1925) The sigmoidoscopic picture of chronic ulcerative colitis. *Am. J. Med. Sci. 170*, 220-227.

(20) Collins, R. H., Jr., Feldman, M., and Fordtran, J. S. (1987) Colon cancer, dysplasia, and surveillance in patients with ulcerative colitis. A critical review. *N. Engl. J. Med. 316*, 1654-1658.

(21) Ekbom, A., Helmick, C., Zack, M., and Adami, H. O. (1990) Ulcerative colitis and colorectal cancer. A population-based study. *N. Engl. J. Med. 323*, 1228-1233.

(22) Hayashi, P. H., and Zeldis, J. B. (1993) Molecular biology of viral hepatitis and hepatocellular carcinoma. *Compr. Ther. 19*, 188-196.

(23) Peek, R. M., Jr., and Blaser, M. J. (2002) *Helicobacter pylori* and gastrointestinal tract adenocarcinomas. *Nat. Rev. Cancer 2*, 28-37.

(24) Pryor, W. A. (1986) Oxy-radicals and related species: their formation, lifetimes, and reactions. *Annu. Rev. Physiol. 48*, 657-667.

(25) Huie, R. E., and Padmaja, S. (1993) The reaction of NO with superoxide. *Free Radic. Res. Commun. 18*, 195-199.

(26) Halfpenny, E., and Robinson, P. L. (1952) Pernitrous acid. The reaction between hydrogen peroxide and nitrous acid, and the properties of an intermediate product. *J. Chem. Soc.*, 939-946.

(27) Beckman, J. S., Beckman, T. W., Chen, J., Marshall, P. A., and Freeman, B. A. (1990) Apparent hydroxyl radical production by peroxynitrite: implications for endothelial injury from nitric oxide and superoxide. *Proc. Natl. Acad. Sci. U. S. A. 87*, 1620-1624.

(28) Pryor, W. A., and Squadrito, G. L. (1995) The chemistry of peroxynitrite: a product from the reaction of nitric oxide with superoxide. *Am. J. Physiol. 268*, 699-722.

(29) Crow, J. P., Spruell, C., Chen, J., Gunn, C., Ischiropoulos, H., Tsai, M., Smith, C. D., Radi, R., Koppenol, W. H., and Beckman, J. S. (1994) On the pH-dependent yield of hydroxyl radical products from peroxynitrite. *Free Radic. Biol. Med 16*, 331-338.

(30) Marnett, L. J., Riggins, J. N., and West, J. D. (2003) Endogenous generation of reactive oxidants and electrophiles and their reactions with DNA and protein. *J. Clin. Invest. 111*, 583-593.

(31) Margolin, Y., Cloutier, J. F., Shafirovich, V., Geacintov, N. E., and Dedon, P. C. (2006) Paradoxical hotspots for guanine oxidation by a chemical mediator of inflammation. *Nat. Chem. Biol. 2*, 365-366.

(32) Squadrito, G. L., and Pryor, W. A. (2002) Mapping the reaction of peroxynitrite with CO_2: energetics, reactive species, and biological implications. *Chem. Res. Toxicol. 15*, 885-895.

(33) Klaunig, J. E., and Kamendulis, L. M. (2004) The role of oxidative stress in carcinogenesis. *Annu. Rev. Pharmacol. Toxicol. 44*, 239-267.

(34) Schrader, M., and Fahimi, H. D. (2006) Peroxisomes and oxidative stress. *Biochim. Biophys. Acta 1763*, 1755-1766.

(35) Ekstrom, G., and Ingelman-Sundberg, M. (1989) Rat liver microsomal NADPH-supported oxidase activity and lipid peroxidation dependent on ethanol-inducible cytochrome P-450 (P-450IIE1). *Biochem. Pharmacol. 38*, 1313-1319.

(36) Dostalek, M., Brooks, J. D., Hardy, K. D., Milne, G. L., Moore, M. M., Sharma, S., Morrow, J. D., and Guengerich, F. P. (2007) In vivo oxidative damage in rats is associated with barbiturate response but not other cytochrome P450 inducers. *Mol. Pharmacol. 72*, 1419-1424.

(37) Hille, R., and Massey, V. (1981) Studies on the oxidative half-reaction of xanthine oxidase. *J. Biol. Chem. 256*, 9090-9095.

(38) Halliwell, B., and Gutteridge, J. M. (1990) Role of free radicals and catalytic metal ions in human disease: an overview. *Methods Enzymol. 186*, 1-85.

(39) West, J. D., and Marnett, L. J. (2006) Endogenous reactive intermediates as modulators of cell signaling and cell death. *Chem. Res. Toxicol. 19*, 173-94.

(40) Porter, N. A., Caldwell, S. E., and Mills, K. A. (1995) Mechanisms of free radical oxidation of unsaturated lipids. *Lipids 30*, 277-290.

(41) Pryor, W. A., and Stanley, J. P. (1975) Letter: A suggested mechanism for the production of malonaldehyde during the autoxidation of polyunsaturated fatty acids. Nonenzymatic production of prostaglandin endoperoxides during autoxidation. *J. Org. Chem. 40*, 3615-3617.

(42) Diczfalusy, U., Falardeau, P., and Hammarstrom, S. (1977) Conversion of prostaglandin endoperoxides to C17-hydroxy acids catalyzed by human platelet thromboxane synthase. *FEBS Lett. 84*, 271-274.

(43) Hecker, M., and Ullrich, V. (1989) On the mechanism of prostacyclin and thromboxane A_2 biosynthesis. *J. Biol. Chem. 264*, 141-150.

(44) Brash, A. R. (1999) Lipoxygenases: occurrence, functions, catalysis, and acquisition of substrate. *J. Biol. Chem. 274*, 23679-23682.

(45) Blair, I. A. (2001) Lipid hydroperoxide-mediated DNA damage. *Exp. Gerontol. 36*, 1473-1481.

(46) Khan, N. A. (1961) *Pakistan J. Sci. 13*.

(47) Bergström, S. (1946) *Arkiv Kem. 21*.

(48) Lee, S. H., Williams, M. V., Dubois, R. N., and Blair, I. A. (2005) Cyclooxygenase-2-mediated DNA damage. *J. Biol. Chem. 280*, 28337-28346.

(49) Williams, M. V., Lee, S. H., and Blair, I. A. (2005) Liquid chromatography/mass spectrometry analysis of bifunctional electrophiles and DNA adducts from vitamin C mediated decomposition of 15-hydroperoxyeicosatetraenoic acid. *Rapid Commun. Mass Spectrom. 19*, 849-858.

(50) Jian, W., Lee, S. H., Arora, J. S., Silva Elipe, M. V., and Blair, I. A. (2005) Unexpected formation of etheno-2'-deoxyguanosine adducts from 5(S)-hydroperoxyeicosatetraenoic acid: evidence for a bis-hydroperoxide intermediate. *Chem. Res. Toxicol. 18*, 599-610.

(51) Lee, S. H., and Blair, I. A. (2000) Characterization of 4-oxo-2-nonenal as a novel product of lipid peroxidation. *Chem. Res. Toxicol. 13*, 698-702.

(52) Lee, S. H., Oe, T., and Blair, I. A. (2001) Vitamin C-induced decomposition of lipid hydroperoxides to endogenous genotoxins. *Science 292*, 2083-2086.

(53) Schneider, C., Tallman, K. A., Porter, N. A., and Brash, A. R. (2001) Two distinct pathways of formation of 4-hydroxynonenal. Mechanisms of nonenzymatic transformation of the 9- and 13-hydroperoxides of linoleic acid to 4-hydroxyalkenals. *J. Biol. Chem. 276*, 20831-20838.

(54) Pryor, W. A., and Porter, N. A. (1990) Suggested mechanisms for the production of 4-hydroxy-2-nonenal from the autoxidation of polyunsaturated fatty acids. *Free Radical Biol. Med. 8*, 541-543.

(55) Lee, S. H., Oe, T., Arora, J. S., and Blair, I. A. (2005) Analysis of Fe^{II}-mediated decomposition of a linoleic acid-derived lipid hydroperoxide by liquid chromatography/mass spectrometry. *J. Mass Spectrom. 40*, 661-668.

(56) Chung, F. L., Chen, H. J., and Nath, R. G. (1996) Lipid peroxidation as a potential endogenous source for the formation of exocyclic DNA adducts. *Carcinogenesis 17*, 2105-2011.

(57) Uchida, K., Kanematsu, M., Morimitsu, Y., Osawa, T., Noguchi, N., and Niki, E. (1998) Acrolein is a product of lipid peroxidation reaction. Formation of free acrolein and its conjugate with lysine residues in oxidized low density lipoproteins. *J. Biol. Chem. 273*, 16058-16066.

(58) Dedon, P. C., Plastaras, J. P., Rouzer, C. A., and Marnett, L. J. (1998) Indirect mutagenesis by oxidative DNA damage: formation of the pyrimidopurinone adduct of deoxyguanosine by base propenal. *Proc. Natl. Acad. Sci. U.S.A. 95*, 11113-11116.

(59) Dedon, P. C., and Tannenbaum, S. R. (2004) Reactive nitrogen species in the chemical biology of inflammation. *Arch. Biochem. Biophys. 423*, 12-22.

(60) Dedon, P. C. (2007) The chemical toxicology of 2-deoxyribose oxidation in DNA. *Chem. Res. Toxicol. 21*, 206-219.

(61) Rashid, R., Langfinger, D., Wagner, R., Schuchmann, H. P., and von Sonntag, C. (1999) Bleomycin versus OH-radical-induced malonaldehydic-product formation in DNA. *Int. J. Radiat. Biol. 75*, 101-109.

(62) Chen, B., Zhou, X., Taghizadeh, K., Chen, J., Stubbe, J., and Dedon, P. C. (2007) GC/MS methods to quantify the 2-deoxypentos-4-ulose and 3'-phosphoglycolate pathways of 4' oxidation of 2-deoxyribose in DNA: application to DNA damage produced by gamma radiation and bleomycin. *Chem. Res. Toxicol. 20*, 1701-1708.

(63) Breen, A. P., and Murphy, J. A. (1995) Reactions of oxyl radicals with DNA. *Free Radic. Biol. Med. 18*, 1033-1077.

(64) Morrow, J. D., Hill, K. E., Burk, R. F., Nammour, T. M., Badr, K. F., and Roberts, L. J., 2nd. (1990) A series of prostaglandin F_2-like compounds are produced in vivo in humans by a non-cyclooxygenase, free radical-catalyzed mechanism. *Proc. Natl. Acad. Sci. U. S. A. 87*, 9383-9387.

(65) O'Connor, D. E., Mihelich, E. D., and Coleman, M. C. (1981) Isolation and characterization of bicycloendoperoxides derived from methyl linoleate. *J. Am. Chem. Soc. 103*, 223-224.

(66) Musiek, E. S., Yin, H., Milne, G. L., and Morrow, J. D. (2005) Recent advances in the biochemistry and clinical relevance of the isoprostane pathway. *Lipids 40*, 987-994.

(67) Roberts, L. J., II, and Morrow, J. D. (1999) *Isoprostanes as markers of lipid peroxidation in atherosclerosis*, Humana Press, Totowa.

(68) Montine, T. J., Quinn, J., Kaye, J., and Morrow, J. D. (2007) F_2-isoprostanes as biomarkers of late-onset Alzheimer's disease. *J. Mol. Neurosci. 33*, 114-119.

(69) Delanty, N., Reilly, M. P., Pratico, D., Lawson, J. A., McCarthy, J. F., Wood, A. E., Ohnishi, S. T., Fitzgerald, D. J., and FitzGerald, G. A. (1997) 8-epi PGF_2-alpha generation during coronary reperfusion. A potential quantitative marker of oxidant stress in vivo. *Circulation 95*, 2492-2499.

(70) Reilly, M. P., Delanty, N., Roy, L., Rokach, J., Callaghan, P. O., Crean, P., Lawson, J. A., and FitzGerald, G. A. (1997) Increased formation of the isoprostanes IPF_2-α-I and 8-epi-prostaglandin $F_2\alpha$ in acute coronary angioplasty: evidence for oxidant stress during coronary reperfusion in humans. *Circulation 96*, 3314-3320.

(71) Lawson, J. A., Rokach, J., and FitzGerald, G. A. (1999) Isoprostanes: formation, analysis and use as indices of lipid peroxidation in vivo. *J. Biol. Chem. 274*, 24441-24444.

(72) Milne, G. L., and Morrow, J. D. (2006) Isoprostanes and related compounds: update 2006. *Antioxid. Redox Signal. 8*, 1379-1384.

(73) Kadiiska, M. B., Gladen, B. C., Baird, D. D., Germolec, D., Graham, L. B., Parker, C. E., Nyska, A., Wachsman, J. T., Ames, B. N., Basu, S., Brot, N., Fitzgerald, G. A., Floyd, R. A., George, M., Heinecke, J. W., Hatch, G. E., Hensley, K., Lawson, J. A., Marnett, L. J., Morrow, J. D., Murray, D. M., Plastaras, J., Roberts, L. J., 2nd, Rokach, J., Shigenaga, M. K., Sohal, R. S., Sun, J., Tice, R. R., Van Thiel, D. H., Wellner, D., Walter, P. B., Tomer, K. B., Mason, R. P., and Barrett, J. C. (2005) Biomarkers of Oxidative Stress Study II: Are

oxidation products of lipids, proteins, and DNA markers of CCl_4 poisoning? *Free Radic. Biol. Med. 38*, 698-710.

(74) Kadiiska, M. B., Gladen, B. C., Baird, D. D., Graham, L. B., Parker, C. E., Ames, B. N., Basu, S., Fitzgerald, G. A., Lawson, J. A., Marnett, L. J., Morrow, J. D., Murray, D. M., Plastaras, J., Roberts, L. J., 2nd, Rokach, J., Shigenaga, M. K., Sun, J., Walter, P. B., Tomer, K. B., Barrett, J. C., and Mason, R. P. (2005) Biomarkers of oxidative stress study III. Effects of the nonsteroidal anti-inflammatory agents indomethacin and meclofenamic acid on measurements of oxidative products of lipids in CCl_4 poisoning. *Free Radic. Biol. Med. 38*, 711-718.

(75) Sharma, R. A., and Farmer, P. B. (2004) Biological relevance of adduct detection to the chemoprevention of cancer. *Clin. Cancer Res. 10*, 4901-4912.

(76) Kohn, H. I., and Liversedge, M. (1944) On a new aerobic metabolite whose production by brain is inhibited by apomorphine, emetine, ergotamine, epinephrine, and menadione. *J. Pharmacol. 82*, 292-300.

(77) Wilbur, K. M., Bernheim, M. L. C., and Shapiro, O. W. (1949) The thiobarbituric acid reagent as a test for the oxidation of unsaturated fatty acids by various agents. *Arch. Biochem. Biophys. 24*, 305-313.

(78) Patton, S., and Kurtz, G. W. (1951) 2-Thiobarbituric acid as a reagent for detecting mild fat oxidation. *J. Dairy Sci. 34*, 669-674.

(79) Sinnhuber, R. O., Yu, T. C., and Tu, T. C. (1958) Characterization of the red pigment formed in the 2-thiobarbituric acid determination of oxidative rancidity. *Food Res. 23*, 626-633.

(80) Dahle, L. K., Hill, E. G., and Holman, R. T. (1962) The thiobarbituric acid reaction and the autoxidations of polyunsaturated fatty acid methyl esters. *Arch. Biochem. Biophys. 98*, 253-261.

(81) Bothner-By, A. A., and Harris, R. K. (1965) Conformational Preferences in Malondialdehyde and Acetylacetaldehyde Enols Investigated by Nuclear Magnetic Resonance. *J. Org. Chem. 30*, 254-257.

(82) Osman, M. M. (1972) The Acidity of Malondialdehyde and the Stability of its Complexes with Nickel(II) and Copper(II). *Helv. Chim. Acta 55*, 239-244.

(83) Mukai, F. H., and Goldstein, B. D. (1976) Mutagenicity of malonaldehyde, a decomposition product of peroxidized polyunsaturated fatty acids. *Science 191*, 868-869.

(84) Shamberger, R. J., Andreone, T. L., and Willis, C. E. (1974) Antioxidants and cancer. IV. Initiating activity of malonaldehyde as a carcinogen. *J. Natl. Cancer Inst. 53*, 1771-1773.

(85) Shamberger, R. J., Corlett, C. L., Beaman, K. D., and Kasten, B. L. (1979) Antioxidants reduce the mutagenic effect of malonaldehyde and beta-propiolactone. Part IX. Antioxidants and cancer. *Mutat. Res. 66*, 349-355.

(86) Yau, T. M. (1979) Mutagenicity and cytotoxicity of malonaldehyde in mammalian cells. *Mech. Ageing Dev. 11*, 137-144.

(87) Marnett, L. J., and Tuttle, M. A. (1980) Comparison of the mutagenicities of malondialdehyde and the side products formed during its chemical synthesis. *Cancer Res. 40*, 276-282.

(88) Basu, A. K., and Marnett, L. J. (1983) Unequivocal demonstration that malondialdehyde is a mutagen. *Carcinogenesis 4*, 331-333.

(89) Fischer, S. M., Ogle, S., Marnett, L. J., Nesnow, S., and Slaga, T. J. (1983) The lack of initiating and/or promoting activity of sodium malondialdehyde on SENCAR mouse skin. *Cancer Lett. 19*, 61-66.

(90) Spalding, J. W. (1988) Toxicology and carcinogenesis studies of malondialdehyde sodium salt (3-hydroxy-2-propenal, sodium salt) in F344/N rats and B6C3F1 mice, NTP Technical Report 331. *Natl. Toxicol. Program Tech. Rep. Ser. 331*, 5-13.

(91) Basu, A. K., and Marnett, L. J. (1984) Molecular requirements for the mutagenicity of malondialdehyde and related acroleins. *Cancer Res. 44*, 2848-2854.

(92) Brooks, B. R., and Klamerth, O. L. (1968) Interaction of DNA with bifunctional aldehydes. *Eur. J. Biochem. 5*, 178-182.

(93) Reiss, U., Tappel, A. L., and Chio, K. S. (1972) DNA-malonaldehyde reaction: formation of fluorescent products. *Biochem. Biophys. Res. Commun. 48*, 921-926.

(94) Moschel, R. C., and Leonard, N. J. (1976) Fluorescent modification of guanine. Reaction with substituted malondialdehydes. *J. Org. Chem. 41*, 294-300.

(95) Seto, H., Akiyama, K., Okuda, T., Hashimoto, T., Takesue, T., and Ikemura, T. (1981) Structure of a new modified nucleoside formed by guanosine-malonaldehyde reaction. *Chem. Lett.*, 707-708.

(96) Seto, H., Okuda, T., Takesue, T., and Ikemura, T. (1983) Reaction of malondialdehyde with nucleic acid. I. Formation of fluorescent pyrimido[1,2-α]purin-10(3H)-one nucleosides. *Bull. Chem. Soc. Jpn. 56*, 1799-1802.

(97) Marnett, L. J., Basu, A. K., Ohara, S. M., Weller, P. E., Rahman, A. F. M. M., and Oliver, J. P. (1986) Reaction of malondialdehyde with guanine nucleosides - formation of adducts containing oxadiazabicyclononene residues in the base-pairing region. *J. Am. Chem. Soc. 108*, 1348-1350.

(98) Basu, A. K., O'Hara, S. M., Valladier, P., Stone, K., Mols, O., and Marnett, L. J. (1988) Identification of adducts formed by reaction of guanine nucleosides with malondialdehyde and structurally related aldehydes. *Chem. Res. Toxicol. 1*, 53-59.

(99) Nair, V., Turner, G. A., and Offerman, R. J. (1984) Novel adducts from the modification of nucleic-acid bases by malondialdehyde. *J. Am. Chem. Soc. 106*, 3370-3371.

(100) Stone, K., Ksebati, M. B., and Marnett, L. J. (1990) Investigation of the adducts formed by reaction of malondialdehyde with adenosine. *Chem. Res. Toxicol. 3*, 33-38.

(101) Stone, K., Uzieblo, A., and Marnett, L. J. (1990) Studies of the reaction of malondialdehyde with cytosine nucleosides. *Chem. Res. Toxicol. 3*, 467-472.

(102) Chaudhary, A. K., Reddy, G. R., Blair, I. A., and Marnett, L. J. (1996) Characterization of an N^6-oxopropenyl-2'-deoxyadenosine adduct in malondialdehyde-modified DNA using liquid chromatography/electrospray ionization tandem mass spectrometry. *Carcinogenesis 17*, 1167-1170.

(103) Reddy, G. R., and Marnett, L. J. (1996) Mechanism of reaction of β-(aryloxy)-acroleins with nucleosides. *Chem. Res. Toxicol. 9*, 12-15.

(104) Plastaras, J. P., Riggins, J. N., Otteneder, M., and Marnett, L. J. (2000) Reactivity and mutagenicity of endogenous DNA oxopropenylating agents: base propenals, malondialdehyde, and N^{ϵ}-oxopropenyllysine. *Chem. Res. Toxicol. 13*, 1235-1242.

(105) Plastaras, J. P., Dedon, P. C., and Marnett, L. J. (2002) Effects of DNA structure on oxopropenylation by the endogenous mutagens malondialdehyde and base propenal. *Biochemistry 41*, 5033-5042.

(106) Zhou, X., Taghizadeh, K., and Dedon, P. C. (2005) Chemical and biological evidence for base propenals as the major source of the endogenous M_1dG adduct in cellular DNA. *J. Biol. Chem. 280*, 25377-25382.

(107) Jeong, Y. C., and Swenberg, J. A. (2005) Formation of M_1G-dR from endogenous and exogenous ROS-inducing chemicals. *Free Radic. Biol. Med. 39*, 1021-1029.

(108) Reddy, G. R., and Marnett, L. J. (1995) Synthesis of an oligodeoxynucleotide containing the alkaline labile malondialdehyde-deoxyguanosine adduct pyrimido[1,2-α]purin-10(3*H*)-one. *J. Am. Chem. Soc. 117*, 5007-5008.

(109) Riggins, J. N., Daniels, J. S., Rouzer, C. A., and Marnett, L. J. (2004) Kinetic and thermodynamic analysis of the hydrolytic ring-opening of the malondialdehyde-deoxyguanosine adduct, 3-(2'-deoxy-β-D-erythro-pentofuranosyl)- pyrimido[1,2-α]purin-10(3*H*)-one. *J. Am. Chem. Soc. 126*, 8237-8243.

(110) Riggins, J. N., Pratt, D. A., Voehler, M., Daniels, J. S., and Marnett, L. J. (2004) Kinetics and mechanism of the general-acid-catalyzed ring-closure of the malondialdehyde-DNA adduct, N^2-(3-oxo-1-propenyl)deoxyguanosine (N^2OPdG$^-$), to 3-(2'-deoxy-β-D-erythro-pentofuranosyl)pyrimido[1,2-α]purin-10(3*H*)-one (M_1dG). *J. Am. Chem. Soc. 126*, 10571-10581.

(111) Niedernhofer, L. J., Riley, M., Schnetz-Boutaud, N., Sanduwaran, G., Chaudhary, A. K., Reddy, G. R., and Marnett, L. J. (1997) Temperature-dependent formation of a conjugate between tris(hydroxymethyl)aminomethane buffer and the malondialdehyde-DNA adduct pyrimidopurinone. *Chem. Res. Toxicol. 10*, 556-561.

(112) Schnetz-Boutaud, N., Daniels, J. S., Hashim, M. F., Scholl, P., Burrus, T., and Marnett, L. J. (2000) Pyrimido[1,2-α]purin-10(3*H*)-one: a reactive electrophile in the genome. *Chem. Res. Toxicol. 13*, 967-970.

(113) Otteneder, M., Plastaras, J. P., and Marnett, L. J. (2002) Reaction of malondialdehyde-DNA adducts with hydrazines-development of a facile assay for quantification of malondialdehyde equivalents in DNA. *Chem. Res. Toxicol. 15*, 312-318.

(114) Mao, H., Reddy, G. R., Marnett, L. J., and Stone, M. P. (1999) Solution structure of an oligodeoxynucleotide containing the malondialdehyde deoxyguanosine adduct N^2-(3-oxo-1-propenyl)-dG (ring-opened M_1G) positioned in a $(CpG)_3$ frameshift hotspot of the *Salmonella typhimurium* hisD3052 gene. *Biochemistry 38*, 13491-13501.

(115) Mao, H., Schnetz-Boutaud, N. C., Weisenseel, J. P., Marnett, L. J., and Stone, M. P. (1999) Duplex DNA catalyzes the chemical rearrangement of a malondialdehyde deoxyguanosine adduct. *Proc. Natl. Acad. Sci. U. S. A. 96*, 6615-6620.

(116) VanderVeen, L. A., Druckova, A., Riggins, J. N., Sorrells, J. L., Guengerich, F. P., and Marnett, L. J. (2005) Differential DNA recognition and cleavage by EcoRI dependent on the dynamic equilibrium between the two forms of the malondialdehyde-deoxyguanosine adduct. *Biochemistry 44*, 5024-5033.

(117) Szekely, J., Rizzo, C. J., and Marnett, L. J. (2008) Chemical properties of oxopropenyl adducts of purine and pyrimidine nucleosides and their reactivity toward amino acid cross-link formation. *J. Am. Chem. Soc. 130*, 2195-2201.

(118) Basu, A. K., Marnett, L. J., and Romano, L. J. (1984) Dissociation of malondialdehyde mutagenicity in *Salmonella typhimurium* from its ability to induce interstrand DNA cross-links. *Mutat. Res. 129*, 39-46.

(119) Benamira, M., Johnson, K., Chaudhary, A., Bruner, K., Tibbetts, C., and Marnett, L. J. (1995) Induction of mutations by replication of malondialdehyde-modified

M13 DNA in *Escherichia coli*: determination of the extent of DNA modification, genetic requirements for mutagenesis, and types of mutations induced. *Carcinogenesis 16*, 93-99.

(120) Fink, S. P., Reddy, G. R., and Marnett, L. J. (1997) Mutagenicity in *Escherichia coli* of the major DNA adduct derived from the endogenous mutagen malondialdehyde. *Proc. Natl. Acad. Sci. U.S.A. 94*, 8652-8657.

(121) VanderVeen, L. A., Hashim, M. F., Shyr, Y., and Marnett, L. J. (2003) Induction of frameshift and base pair substitution mutations by the major DNA adduct of the endogenous carcinogen malondialdehyde. *Proc. Natl. Acad. Sci. U.S.A. 100*, 14247-14252.

(122) Johnson, K. A., Fink, S. P., and Marnett, L. J. (1997) Repair of propanodeoxyguanosine by nucleotide excision repair in vivo and in vitro. *J. Biol. Chem. 272*, 11434-11438.

(123) Sancar, A. (1996) DNA excision repair. *Annu. Rev. Biochem. 65*, 43-81.

(124) Sancar, A., Lindsey-Boltz, L. A., Unsal-Kacmaz, K., and Linn, S. (2004) Molecular mechanisms of mammalian DNA repair and the DNA damage checkpoints. *Annu. Rev. Biochem. 73*, 39-85.

(125) Reardon, J. T., Bessho, T., Kung, H. C., Bolton, P. H., and Sancar, A. (1997) In vitro repair of oxidative DNA damage by human nucleotide excision repair system: possible explanation for neurodegeneration in xeroderma pigmentosum patients. *Proc. Natl. Acad. Sci. U.S.A. 94*, 9463-9468.

(126) Cleaver, J. E., and Kraemer, K. H. (1995) *Xeroderma Pigmentosum and Cockayne Syndrome*, Vol. III, 7th ed., McGraw-Hill, Inc, New York.

(127) Kensler, T. W., Qian, G. S., Chen, J. G., and Groopman, J. D. (2003) Translational strategies for cancer prevention in liver. *Nat. Rev. Cancer 3*, 321-329.

(128) Eaton, D. L., and Gallagher, E. P. (1994) Mechanisms of aflatoxin carcinogenesis. *Annu. Rev. Pharmacol. Toxicol. 34*, 135-172.

(129) Raney, K. D., Coles, B., Guengerich, F. P., and Harris, T. M. (1992) The *endo*-8,9-epoxide of aflatoxin B_1: a new metabolite. *Chem. Res. Toxicol. 5*, 333-335.

(130) Iyer, R. S., Coles, B. F., Raney, K. D., Their, R., Guengerich, F. P., and Harris, T. M. (1994) DNA adduction by the potent carcinogen aflatoxin B_1: Mechanistic studies. *J. Am. Chem. Soc. 116*, 1603-1609.

(131) Johnson, W. W., and Guengerich, F. P. (1997) Reaction of aflatoxin B_1 *exo*-8,9-epoxide with DNA: kinetic analysis of covalent binding and DNA-induced hydrolysis. *Proc. Natl. Acad. Sci. U. S. A. 94*, 6121-6125.

(132) Raney, V. M., Harris, T. M., and Stone, M. P. (1993) DNA conformation mediates aflatoxin B_1-DNA binding and the formation of guanine N^7 adducts by aflatoxin B_1 8,9-*exo*-epoxide. *Chem. Res. Toxicol. 6*, 64-68.

(133) Bennett, R. A., Essigmann, J. M., and Wogan, G. N. (1981) Excretion of an aflatoxin-guanine adduct in the urine of aflatoxin B_1-treated rats. *Cancer Res. 41*, 650-654.

(134) Groopman, J. D., Hasler, J. A., Trudel, L. J., Pikul, A., Donahue, P. R., and Wogan, G. N. (1992) Molecular dosimetry in rat urine of aflatoxin-N^7-guanine and other aflatoxin metabolites by multiple monoclonal antibody affinity chromatography and immunoaffinity/high performance liquid chromatography. *Cancer Res. 52*, 267-274.

(135) Gan, L. S., Skipper, P. L., Peng, X. C., Groopman, J. D., Chen, J. S., Wogan, G. N., and Tannenbaum, S. R. (1988) Serum albumin adducts in the molecular epidemiology of aflatoxin carcinogenesis: correlation with aflatoxin B_1 intake and urinary excretion of aflatoxin M_1. *Carcinogenesis 9*, 1323-1325.

(136) Groopman, J. D., Hall, A. J., Whittle, H., Hudson, G. J., Wogan, G. N., Montesano, R., and Wild, C. P. (1992) Molecular dosimetry of aflatoxin-N^7-guanine in human urine obtained in The Gambia, West Africa. *Cancer Epidemiol. Biomarkers Prev. 1*, 221-227.

(137) Groopman, J. D., Zhu, J. Q., Donahue, P. R., Pikul, A., Zhang, L. S., Chen, J. S., and Wogan, G. N. (1992) Molecular dosimetry of urinary aflatoxin-DNA adducts in people living in Guangxi Autonomous Region, People's Republic of China. *Cancer Res. 52*, 45-52.

(138) Wild, C. P., Hudson, G. J., Sabbioni, G., Chapot, B., Hall, A. J., Wogan, G. N., Whittle, H., Montesano, R., and Groopman, J. D. (1992) Dietary intake of aflatoxins and the level of albumin-bound aflatoxin in peripheral blood in The Gambia, West Africa. *Cancer Epidemiol. Biomarkers Prev. 1*, 229-234.

(139) Qian, G. S., Ross, R. K., Yu, M. C., Yuan, J. M., Gao, Y. T., Henderson, B. E., Wogan, G. N., and Groopman, J. D. (1994) A follow-up study of urinary markers of aflatoxin exposure and liver cancer risk in Shanghai, People's Republic of China. *Cancer Epidemiol. Biomarkers Prev. 3*, 3-10.

(140) Ross, R. K., Yuan, J. M., Yu, M. C., Wogan, G. N., Qian, G. S., Tu, J. T., Groopman, J. D., Gao, Y. T., and Henderson, B. E. (1992) Urinary aflatoxin biomarkers and risk of hepatocellular carcinoma. *Lancet 339*, 943-946.

(141) Seto, H., Seto, T., Takesue, T., and Ikemura, T. (1986) Reaction of malonaldehyde with nucleic acid. III. Studies of the fluorescent substances released by enzymatic digestion of nucleic acids modified with malonaldehyde. *Chem. Pharm. Bull. 34*, 5079-5085.

(142) Hadley, M., and Draper, H. H. (1990) Isolation of a guanine-malondialdehyde adduct from rat and human urine. *Lipids 25*, 82-85.

(143) Agarwal, S., and Draper, H. H. (1992) Isolation of a malondialdehyde-deoxyguanosine adduct from rat liver DNA. *Free Radical Biol. Med. 13*, 695-699.

(144) Draper, H. H., Agarwal, S., Nelson, D. E., Wee, J. J., Ghoshal, A. K., and Farber, E. (1995) Effects of peroxidative stress and age on the concentration of a deoxyguanosine-malondialdehyde adduct in rat DNA. *Lipids 30*, 959-961.

(145) Jajoo, H. K., Burcham, P. C., Goda, Y., Blair, I. A., and Marnett, L. J. (1992) A thermospray liquid chromatography/mass spectrometry method for analysis of human urine for the major malondialdehyde-guanine adduct. *Chem. Res. Toxicol. 5*, 870-875.

(146) Goda, Y., and Marnett, L. J. (1991) High-performance liquid chromatography with electrochemical detection for determination of the major malondialdehyde-guanine adduct. *Chem. Res. Toxicol. 4*, 520-524.

(147) Chaudhary, A. K., Nokubo, M., Marnett, L. J., and Blair, I. A. (1994) Analysis of the malondialdehyde-2'-deoxyguanosine adduct in rat liver DNA by gas chromatography/electron capture negative chemical ionization mass spectrometry. *Biol. Mass Spectrom. 23*, 457-464.

(148) Chaudhary, A. K., Nokubo, M., Reddy, G. R., Yeola, S. N., Morrow, J. D., Blair, I. A., and Marnett, L. J. (1994) Detection of endogenous malondialdehyde-deoxyguanosine adducts in human liver. *Science 265*, 1580-1582.

(149) Rouzer, C. A., Chaudhary, A. K., Nokubo, M., Ferguson, D. M., Reddy, G. R., Blair, I. A., and Marnett, L. J. (1997) Analysis of the malondialdehyde-2'-deoxyguanosine adduct pyrimidopurinone in human leukocyte DNA by gas chromatography/electron capture/negative chemical ionization/mass spectrometry. *Chem. Res. Toxicol. 10*, 181-188.

(150) Sevilla, C. L., Mahle, N. H., Eliezer, N., Uzieblo, A., O'Hara, S. M., Nokubo, M., Miller, R., Rouzer, C. A., and Marnett, L. J. (1997) Development of monoclonal antibodies to the malondialdehyde-deoxyguanosine adduct, pyrimidopurinone. *Chem. Res. Toxic 10*, 172-180.

(151) Jeong, Y. C., Sangaiah, R., Nakamura, J., Pachkowski, B. F., Ranasinghe, A., Gold, A., Ball, L. M., and Swenberg, J. A. (2005) Analysis of M_1G-dR in DNA by aldehyde reactive probe labeling and liquid chromatography tandem mass spectrometry. *Chem. Res. Toxicol. 18*, 51-60.

(152) Jeong, Y. C., Nakamura, J., Upton, P. B., and Swenberg, J. A. (2005) Pyrimido[1,2-α]-purin-10(3*H*)-one, M_1G, is less prone to artifact than base oxidation. *Nucleic Acids Res. 33*, 6426-6434.

(153) Otteneder, M., Scott Daniels, J., Voehler, M., and Marnett, L. J. (2003) Development of a method for determination of the malondialdehyde-deoxyguanosine adduct in urine using liquid chromatography-tandem mass spectrometry. *Anal. Biochem. 315*, 147-151.

(154) Hoberg, A. M., Otteneder, M., Marnett, L. J., and Poulsen, H. E. (2004) Measurement of the malondialdehyde-2'-deoxyguanosine adduct in human urine by immuno-extraction and liquid chromatography/atmospheric pressure chemical ionization tandem mass spectrometry. *J. Mass Spectrom. 39*, 38-42.

(155) Weimann, A., Belling, D., and Poulsen, H. E. (2001) Measurement of 8-oxo-2'-deoxyguanosine and 8-oxo-2'-deoxyadenosine in DNA and human urine by high performance liquid chromatography-electrospray tandem mass spectrometry. *Free Radical Biol. Med. 30*, 757-764.

(156) Weimann, A., Belling, D., and Poulsen, H. E. (2002) Quantification of 8-oxo-guanine and guanine as the nucleobase, nucleoside and deoxynucleoside forms in human urine by high-performance liquid chromatography-electrospray tandem mass spectrometry. *Nucleic Acids Res. 30*, E71-E78.

(157) Otteneder, M. B., Knutson, C. G., Daniels, J. S., Hashim, M., Crews, B. C., Remmel, R. P., Wang, H., Rizzo, C., and Marnett, L. J. (2006) In vivo oxidative metabolism of a major peroxidation-derived DNA adduct, M_1dG. *Proc. Natl. Acad. Sci. U.S.A. 103*, 6665-6669.

(158) Steenken, S., and Jovanovic, S. V. (1997) How easily oxidizable is DNA? One-electron reduction potentials of adenosine and guanosine radicals in aqueous solution. *J. Am. Chem. Soc. 119*, 617-618.

(159) Burrows, C. J., and Muller, J. G. (1998) Oxidative nucleobase modifications leading to strand scission. *Chem. Rev. 98*, 1109-1151.

(160) Cadet, J., Delatour, T., Douki, T., Gasparutto, D., Pouget, J. P., Ravanat, J. L., and Sauvaigo, S. (1999) Hydroxyl radicals and DNA base damage. *Mutat. Res. 424*, 9-21.

(161) Wagner, J. R., Hu, C. C., and Ames, B. N. (1992) Endogenous oxidative damage of deoxycytidine in DNA. *Proc. Natl. Acad. Sci. U. S. A. 89*, 3380-3384.

(162) Neeley, W. L., and Essigmann, J. M. (2006) Mechanisms of formation, genotoxicity, and mutation of guanine oxidation products. *Chem. Res. Toxicol. 19*, 491-505.

(163) Chung, F. L., Roy, K. R., and Hecht, S. S. (1988) A study of reactions of α,β-unsaturated carbonyl-compounds with deoxyguanosine. *J. Org. Chem. 53*, 14-17.

(164) Chung, F. L., Young, R., and Hecht, S. S. (1984) Formation of cyclic 1,N^2-propanodeoxyguanosine adducts in DNA upon reaction with acrolein or crotonaldehyde. *Cancer Res. 44*, 990-995.

(165) Chung, F. L., and Hecht, S. S. (1983) Formation of cyclic 1,N^2-adducts by reaction of deoxyguanosine with alpha-acetoxy-N-nitrosopyrrolidine, 4-(carbethoxynitrosamino)butanal, or crotonaldehyde. *Cancer Res. 43*, 1230-1235.

(166) Winter, C. K., Segall, H. J., and Haddon, W. F. (1986) Formation of cyclic adducts of deoxyguanosine with the aldehydes *trans*-4-hydroxy-2-hexenal and *trans*-4-hydroxy-2-nonenal *in vitro*. *Cancer Res. 46*, 5682-5686.

(167) Wang, H., Kozekov, I. D., Harris, T. M., and Rizzo, C. J. (2003) Site-specific synthesis and reactivity of oligonucleotides containing stereochemically defined 1,N^2-deoxyguanosine adducts of the lipid peroxidation product trans-4-hydroxynonenal. *J. Am. Chem. Soc. 125*, 5687-5700.

(168) de los Santos, C., Zaliznyak, T., and Johnson, F. (2001) NMR characterization of a DNA duplex containing the major acrolein-derived deoxyguanosine adduct γ-OH-1,N^2-propano-2'-deoxyguanosine. *J. Biol. Chem. 276*, 9077-9082.

(169) Kozekov, I. D., Nechev, L. V., Moseley, M. S., Harris, C. M., Rizzo, C. J., Stone, M. P., and Harris, T. M. (2003) DNA interchain cross-links formed by acrolein and crotonaldehyde. *J. Am. Chem. Soc. 125*, 50-61.

(170) Wang, H., Marnett, L. J., Harris, T. M., and Rizzo, C. J. (2004) A novel synthesis of malondialdehyde adducts of deoxyguanosine, deoxyadenosine, and deoxycytidine. *Chem. Res. Toxicol. 17*, 144-149.

(171) Kim, H. Y., Voehler, M., Harris, T. M., and Stone, M. P. (2002) Detection of an interchain carbinolamine cross-link formed in a CpG sequence by the acrolein DNA adduct gamma-OH-1,N^2-propano-2'-deoxyguanosine. *J. Am. Chem. Soc. 124*, 9324-9325.

(172) Cho, Y. J., Wang, H., Kozekov, I. D., Kurtz, A. J., Jacob, J., Voehler, M., Smith, J., Harris, T. M., Lloyd, R. S., Rizzo, C. J., and Stone, M. P. (2006) Stereospecific formation of interstrand carbinolamine DNA cross-links by crotonaldehyde- and acetaldehyde-derived α-CH_3-γ-OH-1,N^2-propano-2'-deoxyguanosine adducts in the 5'-CpG-3' sequence. *Chem. Res. Toxicol. 19*, 195-208.

(173) Kozekov, I. D., Nechev, L. V., Sanchez, A., Harris, C. M., Lloyd, R. S., and Harris, T. M. (2001) Interchain cross-linking of DNA mediated by the principal adduct of acrolein. *Chem. Res. Toxicol. 14*, 1482-1485.

(174) Hecht, S. S., McIntee, E. J., and Wang, M. (2001) New DNA adducts of crotonaldehyde and acetaldehyde. *Toxicology 166*, 31-36.

(175) Wang, M., McIntee, E. J., Cheng, G., Shi, Y., Villalta, P. W., and Hecht, S. S. (2000) Identification of DNA adducts of acetaldehyde. *Chem. Res. Toxicol. 13*, 1149-1157.

(176) Wang, M., McIntee, E. J., Cheng, G., Shi, Y., Villalta, P. W., and Hecht, S. S. (2001) A Schiff base is a major DNA adduct of crotonaldehyde. *Chem. Res. Toxicol. 14*, 423-430.

(177) Sanchez, A. M., Minko, I. G., Kurtz, A. J., Kanuri, M., Moriya, M., and Lloyd, R. S. (2003) Comparative evaluation of the bioreactivity and mutagenic spectra of acrolein-derived α-HOPdG and γ-HOPdG regioisomeric deoxyguanosine adducts. *Chem. Res. Toxicol. 16*, 1019-1028.

(178) VanderVeen, L. A., Hashim, M. F., Nechev, L. V., Harris, T. M., Harris, C. M., and Marnett, L. J. (2001) Evaluation of the mutagenic potential of the principal DNA adduct of acrolein. *J. Biol. Chem. 276*, 9066-9070.

(179) Fernandes, P. H., Wang, H., Rizzo, C. J., and Lloyd, R. S. (2003) Site-specific mutagenicity of stereochemically defined 1,N^2-deoxyguanosine adducts of trans-4-hydroxynonenal in mammalian cells. *Environ. Mol. Mutagen. 42*, 68-74.

(180) Yang, I. Y., Hossain, M., Miller, H., Khullar, S., Johnson, F., Grollman, A., and Moriya, M. (2001) Responses to the major acrolein-derived deoxyguanosine adduct in Escherichia coli. *J. Biol. Chem. 276*, 9071-9076.

(181) Yang, I. Y., Johnson, F., Grollman, A. P., and Moriya, M. (2002) Genotoxic mechanism for the major acrolein-derived deoxyguanosine adduct in human cells. *Chem. Res. Toxicol. 15*, 160-164.

(182) Barrio, J. R., Secrist, J. A., 3rd, and Leonard, N. J. (1972) Fluorescent adenosine and cytidine derivatives. *Biochem. Biophys. Res. Commun. 46*, 597-604.

(183) Sattsangi, P. D., Leonard, N. J., and Frihart, C. R. (1977) 1,N^2-ethenoguanine and N^2,3-ethenoguanine. Synthesis and comparison of the electronic spectral properties of these linear and angular triheterocycles related to the Y bases. *J. Org. Chem. 42*, 3292-3296.

(184) Secrist, J. A., 3rd, Barrio, J. R., Leonard, N. J., and Weber, G. (1972) Fluorescent modification of adenosine-containing coenzymes. Biological activities and spectroscopic properties. *Biochemistry 11*, 3499-3506.

(185) McCann, J., Simmon, V., Streitwieser, D., and Ames, B. N. (1975) Mutagenicity of chloroacetaldehyde, a possible metabolic product of 1,2-dichloroethane (ethylene dichloride), chloroethanol (ethylene chlorohydrin), vinyl chloride, and cyclophosphamide. *Proc. Natl. Acad. Sci. U. S. A. 72*, 3190-3193.

(186) Guengerich, F. P., Crawford, W. M., Jr., and Watanabe, P. G. (1979) Activation of vinyl chloride to covalently bound metabolites: roles of 2-chloroethylene oxide and 2-chloroacetaldehyde. *Biochemistry 18*, 5177-5182.

(187) Guengerich, F. P. (1992) Roles of the vinyl chloride oxidation products 1-chlorooxirane and 2-chloroacetaldehyde in the in vitro formation of etheno adducts of nucleic acid bases. *Chem. Res. Toxic 5*, 2-5.

(188) Bartsch, H., Barbin, A., Marion, M. J., Nair, J., and Guichard, Y. (1994) Formation, Detection, and Role in Carcinogenesis of Ethenobases in DNA. *Drug Met. Rev. 26*, 349-371.

(189) Nair, J., Barbin, A., Guichard, Y., and Bartsch, H. (1995) 1,N^6-Ethenodeoxyadenosine and 3,N^4-ethenodeoxycytidine in liver DNA from humans and untreated rodents detected by immunoaffinity/^{32}P postlabeling. *Carcinogenesis 16*, 613-617.

(190) Misra, R. R., Chiang, S. Y., and Swenberg, J. A. (1994) A comparison of 2 ultrasensitive methods for measuring 1,N^6-etheno-2'-deoxyadenosine and 3,N^4-etheno-2'-deoxycytidine in cellular DNA. *Carcinogenesis 15*, 1647-1652.

(191) Goldschmidt, B. M., Blazej, T. P., and Van Duuren, B. L. (1968) Reaction of guanosine and deoxyguanosine with blycidaldehyde. *Tetrahedron Lett.*, 1583-1585.

(192) Nair, V., and Offerman, R. J. (1985) Ring-extended products from the reaction of epoxy carbonyl compounds and nucleic acid bases. *J. Org. Chem. 50*, 5627-5631.

(193) Sodum, R. S., and Chung, F. L. (1988) 1,N^2-Ethenodeoxyguanosine as a potential marker for DNA adduct formation by *trans*-4-hydroxy-2-nonenal. *Cancer Res. 48*, 320-323.

(194) el Ghissassi, F., Barbin, A., Nair, J., and Bartsch, H. (1995) Formation of 1,N^6-ethenoadenine and 3,N^4-ethenocytosine by lipid peroxidation products and nucleic acid bases. *Chem. Res. Toxicol. 8*, 278-283.

(195) Douki, T., Odin, F., Caillat, S., Favier, A., and Cadet, J. (2004) Predominance of the 1,N^2-propano 2'-deoxyguanosine adduct among 4-hydroxy-2-nonenal-induced DNA lesions. *Free Radic. Biol. Med. 37*, 62-70.

(196) Lee, S. H., Arora, J. A., Oe, T., and Blair, I. A. (2005) 4-Hydroperoxy-2-nonenal-induced formation of 1,N^2-etheno-2'-deoxyguanosine adducts. *Chem. Res. Toxicol. 18*, 780-786.

(197) Lee, S. H., Oe, T., and Blair, I. A. (2002) 4,5-Epoxy-2(E)-decenal-induced formation of 1,N^6-etheno-2'-deoxyadenosine and 1,N^2-etheno-2'-deoxyguanosine adducts. *Chem. Res. Toxicol. 15*, 300-304.

(198) Lee, S. H., Rindgen, D., Bible, R. H., Jr., Hajdu, E., and Blair, I. A. (2000) Characterization of 2'-deoxyadenosine adducts derived from 4-oxo-2-nonenal, a novel product of lipid peroxidation. *Chem. Res. Toxic 13*, 565-574.

(199) Rindgen, D., Nakajima, M., Wehrli, S., Xu, K., and Blair, I. A. (1999) Covalent modifications to 2'-deoxyguanosine by 4-oxo-2-nonenal, a novel product of lipid peroxidation. *Chem. Res. Toxic 12*, 1195-1204.

(200) Pollack, M., Oe, T., Lee, S. H., Silva Elipe, M. V., Arison, B. H., and Blair, I. A. (2003) Characterization of 2'-deoxycytidine adducts derived from 4-oxo-2-nonenal, a novel lipid peroxidation product. *Chem. Res. Toxicol.*, 893-900.

(201) Kawai, Y., Uchida, K., and Osawa, T. (2004) 2'-Deoxycytidine in free nucleosides and double-stranded DNA as the major target of lipid peroxidation products. *Free Radical Biol. Med. 36*, 529-541.

(202) Lee, S. H., Silva Elipe, M. V., Arora, J. S., and Blair, I. A. (2005) Dioxododecenoic acid: a lipid hydroperoxide-derived bifunctional electrophile responsible for etheno DNA adduct formation. *Chem. Res. Toxicol. 18*, 566-578.

(203) Sodum, R. S., and Chung, F. L. (1991) Stereoselective formation of in vitro nucleic acid adducts by 2,3-epoxy-4-hydroxynonanal. *Cancer Res. 51*, 137-143.

(204) Akasaka, S., and Guengerich, F. P. (1999) Mutagenicity of site-specifically located 1,N^2-ethenoguanine in Chinese hamster ovary cell chromosomal DNA. *Chem. Res. Toxicol. 12*, 501-507.

(205) Langouet, S., Mican, A. N., Muller, M., Fink, S. P., Marnett, L. J., Muhle, S. A., and Guengerich, F. P. (1998) Misincorporation of nucleotides opposite five-membered exocyclic ring guanine derivatives by *Escherichia coli* polymerases *in vitro* and *in vivo*: 1,N^2-ethenoguanine, 5,6,7,9-tetrahydro-9-oxoimidazo[1, 2-α]purine, and 5,6,7,9-tetrahydro-7-hydroxy-9-oxoimidazo[1, 2-α]purine. *Biochemistry 37*, 5184-5193.

(206) Basu, A. K., Wood, M. L., Niedernhofer, L. J., Ramos, L. A., and Essigmann, J. M. (1993) Mutagenic and genotoxic effects of 3 vinyl chloride-induced DNA lesions -1,N^6-ethenoadenine, 3,N^4-ethenocytosine, and 4-amino-5-(imidazol-2-yl)imidazole. *Biochemistry 32*, 12793-12801.

(207) Barbin, A., Bartsch, H., Leconte, P., and Radman, M. (1981) Studies on the miscoding properties of 1,N^6-ethenoadenine and 3,N^4-ethenocytosine, DNA reaction-products of vinyl-chloride metabolites, during *in vitro* DNA-synthesis. *Nucleic Acids Res. 9*, 375-387.

(208) Singer, B., Spengler, S. J., Chavez, F., and Kusmierek, J. T. (1987) The vinyl chloride-derived nucleoside, N^2,3-ethenoguanosine, is a highly efficient mutagen in transcription. *Carcinogenesis 8*, 745-747.

(209) Pollack, M., Yang, I. Y., Kim, H. Y., Blair, I. A., and Moriya, M. (2006) Translesion DNA Synthesis across the heptanone-etheno-2'-deoxycytidine adduct in cells. *Chem. Res. Toxicol. 19*, 1074-1079.

(210) Guengerich, F. P., Persmark, M., and Humphreys, W. G. (1993) Formation of 1,N^2- and N^2,3-ethenoguanine from 2-halooxiranes: isotopic labeling studies and isolation of a hemiaminal derivative of N^2-(2-oxoethyl)guanine. *Chem. Res. Toxicol. 6*, 635-648.

(211) Yen, T. Y., Holt, S., Sangaiah, R., Gold, A., and Swenberg, J. A. (1998) Quantitation of 1,N^6-ethenoadenine in rat urine by immunoaffinity extraction combined with liquid chromatography/electrospray ionization mass spectrometry. *Chem. Res. Toxicol. 11*, 810-815.

(212) Chen, H. J., and Chang, C. M. (2004) Quantification of urinary excretion of 1,N^6-ethenoadenine, a potential biomarker of lipid peroxidation, in humans by stable isotope dilution liquid chromatography-electrospray ionization-tandem mass spectrometry: comparison with gas chromatography-mass spectrometry. *Chem. Res. Toxicol. 17*, 963-971.

(213) Chen, H. J., Hong, C. L., Wu, C. F., and Chiu, W. L. (2003) Effect of cigarette smoking on urinary 3,N^4-ethenocytosine levels measured by gas chromatography/mass spectrometry. *Toxicol. Sci. 76*, 321-327.

(214) Chen, H. J., Wu, C. F., Hong, C. L., and Chang, C. M. (2004) Urinary excretion of 3,N^4-etheno-2'-deoxycytidine in humans as a biomarker of oxidative stress: association with cigarette smoking. *Chem. Res. Toxicol. 17*, 896-903.

(215) Loureiro, A. P., Marques, S. A., Garcia, C. C., Di Mascio, P., and Medeiros, M. H. (2002) Development of an on-line liquid chromatography-electrospray tandem mass spectrometry assay to quantitatively determine 1,N^2-ethenodeoxyguanosine in DNA. *Chem. Res. Toxicol. 15*, 1302-1308.

(216) Williams, M. V., Lee, S. H., Pollack, M., and Blair, I. A. (2006) Endogenous lipid hydroperoxide-mediated DNA-adduct formation in min mice. *J. Biol. Chem. 281*, 10127-10133.

(217) Singer, B., Antoccia, A., Basu, A. K., Dosanjh, M. K., Fraenkel-Conrat, H., Gallagher, P. E., Kusmierek, J. T., Qiu, Z. H., and Rydberg, B. (1992) Both purified human 1,N^6-ethenoadenine-binding protein and purified human 3-methyladenine-DNA glycosylase act on 1,N^6-ethenoadenine and 3-methyladenine. *Proc. Natl. Acad. Sci. U.S.A. 89*, 9386-9390.

(218) Saparbaev, M., Kleibl, K., and Laval, J. (1995) *Escherichia coli*, *Saccharomyces cerevisiae*, rat and human 3-methyladenine DNA glycosylases repair 1,N^6-ethenoadenine when present in DNA. *Nucleic Acids Res. 23*, 3750-3755.

(219) Saparbaev, M., Langouet, S., Privezentzev, C. V., Guengerich, F. P., Cai, H., Elder, R. H., and Laval, J. (2002) 1,N^2-ethenoguanine, a mutagenic DNA adduct, is a primary substrate of *Escherichia coli* mismatch-specific uracil-DNA glycosylase and human alkylpurine-DNA-N-glycosylase. *J. Biol. Chem. 277*, 26987-26993.

(220) Dosanjh, M. K., Chenna, A., Kim, E., Fraenkelconrat, H., Samson, L., and Singer, B. (1994) All 4 known cyclic adducts formed in DNA by the vinyl-chloride metabolite chloroacetaldehyde are released by a human DNA glycosylase. *Proc. Natl. Acad. Sci. U. S. A. 91*, 1024-1028.

(221) Saparbaev, M., and Laval, J. (1998) 3,N^4-ethenocytosine, a highly mutagenic adduct, is a primary substrate for ***Escherichia coli*** double-stranded uracil-DNA glycosylase and human mismatch-specific thymine-DNA glycosylase. *Proc. Natl. Acad. Sci. U.S.A. 95*, 8508-8513.

(222) Hang, B., Chenna, A., Rao, S., and Singer, B. (1996) 1,N^6-Ethenoadenine and 3,N^4-ethenocytosine are excised by separate human DNA glycosylases. *Carcinogenesis 17*, 155-157.

(223) Hang, B., Medina, M., Fraenkel-Conrat, H., and Singer, B. (1998) A 55-kDa protein isolated from human cells shows DNA glycosylase activity toward 3,N^4-ethenocytosine and the G/T mismatch. *Proc. Natl. Acad. Sci. U. S. A. 95*, 13561-13566.

(224) Huffman, J. L., Sundheim, O., and Tainer, J. A. (2005) DNA base damage recognition and removal: New twists and grooves. *Mutat. Res. 577*, 55-76.

(225) Churchwell, M. I., Beland, F. A., and Doerge, D. R. (2002) Quantification of multiple DNA adducts formed through oxidative stress using liquid chromatography and electrospray tandem mass spectrometry. *Chem. Res. Toxicol. 15*, 1295-1301.

(226) Hashim, M. F., Riggins, J. N., Schnetz-Boutaud, N., Voehler, M., Stone, M. P., and Marnett, L. J. (2004) *In vitro* bypass of malondialdehyde-deoxyguanosine adducts: differential base selection during extension by the Klenow fragment of DNA polymerase I is the critical determinant of replication outcome. *Biochemistry 43*, 11828-11835.

(227) VanderVeen, L. A., Hashim, M. F., Shyr, Y., and Marnett, L. J. (2003) Induction of frameshift and base pair substitution mutations by the major DNA adduct of the endogenous carcinogen malondialdehyde. *Proc.Natl.Acad.Sci.USA 100*, 14247-14252.

(228) Elion, G. B., Kovensky, A., and Hitchings, G. H. (1966) Metabolic studies of allopurinol, an inhibitor of xanthine oxidase. *Biochem. Pharmacol. 15*, 863-880.

(229) Roy, S. K., Korzekwa, K. R., Gonzalez, F. J., Moschel, R. C., and Dolan, M. E. (1995) Human liver oxidative metabolism of O^6-benzylguanine. *Biochem. Pharmacol. 50*, 1385-1389.

(230) Schnetz-Boutaud, N. C., Mao, H., Stone, M. P., and Marnett, L. J. (2000) Synthesis of oligonucleotides containing the alkali-labile pyrimidopurinone adduct, M_1G. *Chem. Res. Toxicol. 13*, 90-95.

(231) Guengerich, F. P. (1994) Analysis and Characterization of Enzymes, in *Principles and Methods of Toxicology* (Hayes, A. W., Ed.) pp 1259-1313, Raven Press Ltd., New York, NY.

(232) Ball, E. G. (1939) Xanthine oxidase: purification and properties. *J. Biol. Chem. 128*, 51-67.

(233) Massey, V., Brumby, P. E., and Komai, H. (1969) Studies on milk xanthine oxidase. Some spectral and kinetic properties. *J. Biol. Chem. 244*, 1682-1691.

(234) Rajagapolan, K. V., Fridovich, I., and Handler, P. (1962) Hepatic aldehyde oxidase: I. Purification and properties. *J. Biol. Chem. 237*, 922-928.

(235) Nishino, T., and Tsushima, K. (1981) Purification of highly active milk xanthine oxidase by affinity chromatography on Sepharose 4B/folate gel. *FEBS Lett. 131*, 369-72.

(236) Stell, J. G., Warne, A. J., and Lee-Woolley, C. (1989) Purification of rabbit liver aldehyde oxidase by affinity chromatography on benzamidine sepharose 6B. *J. Chromatogr. 475*, 363-372.

(237) Warne, A. J., and Stell, J. G. (1990) Purification of aldehyde oxidase from liver by affinity chromatography and FPLC. *J. Pharm. Biomed. Anal. 8*, 1015-1019.

(238) Maia, L., and Mira, L. (2002) Xanthine oxidase and aldehyde oxidase: a simple procedure for the simultaneous purification from rat liver. *Arch. Biochem. Biophys. 400*, 48-53.

(239) Stirpe, F., and Della Corte, E. (1969) The regulation of rat liver xanthine oxidase. Conversion in vitro of the enzyme activity from dehydrogenase (type D) to oxidase (type O). *J. Biol. Chem. 244*, 3855-3863.

(240) Della Corte, E., Gozzetti, G., Novello, F., and Stirpe, F. (1969) Properties of the xanthine oxidase from human liver. *Biochim. Biophys. Acta. 191*, 164-166.

(241) Waud, W. R., and Rajagopalan, K. V. (1976) Purification and properties of the NAD+-dependent (type D) and O2-dependent (type O) forms of rat liver xanthine dehydrogenase. *Arch. Biochem. Biophys. 172*, 354-364.

(242) Hunt, J., and Massey, V. (1992) Purification and properties of milk xanthine dehydrogenase. *J. Biol. Chem. 267*, 21479-21485.

(243) Mahler, H. R., Fairhurst, A. S., and Mackler, B. (1955) Studies on Metalloflavoproteins. IV. The Role of the Metal. *J. Am. Chem. Soc. 77*, 1514-1521.

(244) Osada, Y., Tsuchimoto, M., Fukushima, H., Takahashi, K., Kondo, S., Hasegawa, M., and Komoriya, K. (1993) Hypouricemic effect of the novel xanthine oxidase inhibitor, TEI-6720, in rodents. *Eur. J. Pharmacol. 241*, 183-188.

(245) Obach, R. S. (2004) Potent inhibition of human liver aldehyde oxidase by raloxifene. *Drug Metab. Dispos. 32*, 89-97.

(246) Massey, V., Komai, H., Palmer, G., and Elion, G. B. (1970) On the mechanism of inactivation of xanthine oxidase by allopurinol and other pyrazolo[3,4-D]pyrimidines. *J. Biol. Chem. 245*, 2837-2844.

(247) Fowles, S. E., Pratt, S. K., Laroche, J., and Prince, W. T. (1994) Lack of a pharmacokinetic interaction between oral famciclovir and allopurinol in healthy volunteers. *Eur. J. Clin. Pharmacol. 46*, 355-359.

(248) Parkinson, A. (2001) Biotransformation of xenobiotics, in *Casarett & Doull's Toxicology The Basic Science of Poisons* (Klaassen, C. D., Ed.) pp 133-224, McGraw-Hill, United States of America.

(249) Powell, L. W. (1966) Effects of allopurinol on iron storage in the rat. *Ann. Rheum. Dis. 25*, 697-699.

(250) Elion, G. B., and Nelson, D. J. (1974) Ribonucleotides of allopurinol and oxipurinol in rat tissues and their significance in purine metabolism. *Adv. Exp. Med. Biol. 41*, 639-652.

(251) Shuker, D. E., and Farmer, P. B. (1992) Relevance of urinary DNA adducts as markers of carcinogen exposure. *Chem. Res. Toxicol. 5*, 450-460.

(252) Beedham, C. (2002) Molybdenum hydroxylases, in *Enzyme systems that metabolise drugs and other xenobiotics* (Ioannides, C., Ed.) pp 147-187, John Wiley & Sons, Ltd. (UK), Chichester, NY.

(253) Friesen, M. D., Garren, L., Prevost, V., and Shuker, D. E. (1991) Isolation of urinary 3-methyladenine using immunoaffinity columns prior to determination by low-resolution gas chromatography-mass spectrometry. *Chem. Res. Toxicol. 4*, 102-106.

(254) Autrup, H., and Seremet, T. (1986) Excretion of benzo[*a*]pyrene-gua adduct in the urine of benzo[*a*]pyrene-treated rats. *Chem. Biol. Interact. 60*, 217-226.

(255) Bartsch, H., and Nair, J. (2004) Oxidative stress and lipid peroxidation-derived DNA-lesions in inflammation driven carcinogenesis. *Cancer Detect. Prev. 28*, 385-391.

(256) Wang, H., and Rizzo, C. J. (2001) Stereocontrolled syntheses of all four stereoisomeric 1,N^2-deoxyguanosine adducts of the lipid peroxidation product trans-4-hydroxynonenal. *Org. Lett. 3*, 3603-3605.

(257) Hamberg, M., and Samuelsson, B. (1967) Oxygenation of unsaturated fatty acids by the vesicular gland of sheep. *J. Biol. Chem. 242*, 5344-5354.

(258) Niedernhofer, L. J., Daniels, J. S., Rouzer, C. A., Greene, R. E., and Marnett, L. J. (2003) Malondialdehyde, a product of lipid peroxidation, is mutagenic in human cells. *J. Biol. Chem. 278*, 31426-31433.

(259) Szekely, J., Wang, H., Peplowski, K. M., Knutson, C. G., Marnett, L. J., and Rizzo, C. J. (2008) "One-pot" syntheses of malondialdehyde adducts of nucleosides. *Nucleosides Nucleotides Nucleic Acids 27*, 103-109.

(260) Meyer, C., Marek, I., and Normant, J.-F. (1993) (E)- or (Z)-Beta-Iodoacrolein. A Novel Versatile Synthon. *Synlett 1993*, 386-388.

(261) Knutson, C. G., Akingbade, D., Crews, B. C., Voehler, M., Stec, D. F., and Marnett, L. J. (2007) Metabolism *in vitro* and *in vivo* of the DNA base adduct, M_1G. *Chem. Res. Toxicol. 20*, 550-557.

(262) Wada, S., Tsuda, M., Sekine, T., Cha, S. H., Kimura, M., Kanai, Y., and Endou, H. (2000) Rat multispecific organic anion transporter 1 (rOAT1) transports zidovudine, acyclovir, and other antiviral nucleoside analogs. *J. Pharmacol. Exp. Ther. 294*, 844-849.

(263) King, A. E., Ackley, M. A., Cass, C. E., Young, J. D., and Baldwin, S. A. (2006) Nucleoside transporters: from scavengers to novel therapeutic targets. *Trends. Pharmacol. Sci. 27*, 416-425.

(264) Sundaram, M., Yao, S. Y., Ingram, J. C., Berry, Z. A., Abidi, F., Cass, C. E., Baldwin, S. A., and Young, J. D. (2001) Topology of a human equilibrative, nitrobenzylthioinosine (NBMPR)-sensitive nucleoside transporter (hENT1) implicated in the cellular uptake of adenosine and anti-cancer drugs. *J. Biol. Chem. 276*, 45270-45275.

(265) Hamilton, S. R., Yao, S. Y., Ingram, J. C., Hadden, D. A., Ritzel, M. W., Gallagher, M. P., Henderson, P. J., Cass, C. E., Young, J. D., and Baldwin, S. A. (2001) Subcellular distribution and membrane topology of the mammalian concentrative Na^+-nucleoside cotransporter rCNT1. *J. Biol. Chem. 276*, 27981-27988.

(266) Wang, M., and Hecht, S. S. (1997) A cyclic N^7,C-8 guanine adduct of N-nitrosopyrrolidine (NPYR): formation in nucleic acids and excretion in the urine of NPYR-treated rats. *Chem. Res. Toxicol. 10*, 772-778.

(267) Knutson, C. G., Wang, H., Rizzo, C. J., and Marnett, L. J. (2007) Metabolism and elimination of the endogenous DNA adduct, 3-(2-deoxy-β-D-erythropentofuranosyl)-pyrimido[1,2-α]purine-10(3*H*)-one, in the rat. *J. Biol. Chem. 282*, 36257-36264.

(268) Hughey, B. J., Skipper, P. L., Klinkowstein, R. E., Shefer, R. E., Wishnok, J. S., and Tannenbaum, S. R. (2000) Low-energy biomedical GC-AMS system for C-14 and H-3 detection. *Nucl. Inst. and Meth. B 172*, 40-46.

(269) Liberman, R. G., Becker, U. J., and Skipper, P. L. (2006) A gas-multiplication telescope detector for low-energy ions. *Nucl. Instr. Meth. A 565*, 686-690.

(270) Liberman, R. G., Hughey, B. J., Skipper, P. L., Wishnok, J. S., Klinkowstein, R. E., Shefer, R. E., and Tannenbaum, S. R. (2004) The NSI biomedical AMS system at MIT: current status. *Nucl. Inst. and Meth. B 223-24*, 82-86.

(271) Liberman, R. G., Tannenbaum, S. R., Hughey, B. J., Shefer, R. E., Klinkowstein, R. E., Prakash, C., Harriman, S. P., and Skipper, P. L. (2004) An interface for direct analysis of ^{14}C in nonvolatile samples by accelerator mass spectrometry. *Anal. Chem. 76*, 328-334.

(272) Hazra, T. K., Hill, J. W., Izumi, T., and Mitra, S. (2001) Multiple DNA glycosylases for repair of 8-oxoguanine and their potential in vivo functions. *Prog. Nucleic Acid Res. Mol. Biol. 68*, 193-205.

(273) Gallinari, P., and Jiricny, J. (1996) A new class of uracil-DNA glycosylases related to human thymine-DNA glycosylase. *Nature 383*, 735-738.

(274) Oesch, F., Adler, S., Rettelbach, R., and Doerjer, G. (1986) Repair of etheno DNA adducts by N-glycosylases. *IARC Sci. Publ.*, 373-379.

(275) Powell, C. L., Swenberg, J. A., and Rusyn, I. (2005) Expression of base excision DNA repair genes as a biomarker of oxidative DNA damage. *Cancer Lett. 229*, 1-11.

(276) Wood, R. D., Mitchell, M., Sgouros, J., and Lindahl, T. (2001) Human DNA repair genes. *Science 291*, 1284-1289.

(277) Yoshihara, S., and Tatsumi, K. (1986) Kinetic and inhibition studies on reduction of diphenyl sulfoxide by guinea pig liver aldehyde oxidase. *Arch. Biochem. Biophys. 249*, 8-14.

(278) Cho, B. P., Kadlubar, F. F., Culp, S. J., and Evans, F. E. (1990) ^{15}N nuclear magnetic resonance studies on the tautomerism of 8-hydroxy-2'-deoxyguanosine,

8-hydroxyguanosine, and other C_8-substituted guanine nucleosides. *Chem. Res. Toxicol. 3*, 445-452.

(279) Zhang, W., Rieger, R., Iden, C., and Johnson, F. (1995) Synthesis of 3,N^4-etheno, 3,N^4-ethano, and 3-(2-hydroxyethyl) derivatives of 2'-deoxycytidine and their incorporation into oligomeric DNA. *Chem. Res. Toxicol. 8*, 148-156.

(280) Friedkin, M., and Kalckar, H. M. (1950) Desoxyribose-1-phosphate: I. The phosphorolysis and resynthesis of purine desoxyribose nucleoside. *J. Biol. Chem. 184*, 437-448.

(281) Bzowska, A., Kulikowska, E., and Shugar, D. (2000) Purine nucleoside phosphorylases: properties, functions, and clinical aspects. *Pharmacol. Ther. 88*, 349-425.

(282) Fink, S. P., and Marnett, L. J. (2001) The relative contribution of adduct blockage and DNA repair on template utilization during replication of 1,N^2-propanodeoxyguanosine and pyrimido[1,2-α]purin-10(3*H*)-one-adducted M13MB102 genomes. *Mutat. Res. 485*, 209-218.

(283) Fink, S. P., Reddy, G. R., and Marnett, L. J. (1996) Relative contribution of cytosine deamination and error-prone replication to the induction of propanodeoxyguanosine → deoxyadenosine mutations in *Escherichia coli*. *Chem. Res. Toxicol. 9*, 277-283.

(284) Krenitsky, T. A., Neil, S. M., Elion, G. B., and Hitchings, G. H. (1972) A comparison of the specificities of xanthine oxidase and aldehyde oxidase. *Arch. Biochem. Biophys. 150*, 585-599.

(285) Robins, R. K. (1956) Potential purine antagonists. I. Synthesis of some 4,6-substituted pyrazolo[3,4-D]pyrimidines. *J. Am. Chem. Soc. 78*, 784-790.

(286) Robins, R. K., Revankar, G. R., Obrien, D. E., Springer, R. H., Novinson, T., Albert, A., Senga, K., Miller, J. P., and Streeter, D. G. (1985) Purine analog inhibitors of xanthine oxidase - structure activity relationships and proposed binding of the molybdenum cofactor. *J. Heterocycl. Chem. 22*, 601-634.

(287) Leonard, N. J., Sprecker, M. A., and Morrice, A. G. (1976) Defined dimensional changes in enzyme substrates and cofactors. Synthesis of *lin*-benzoadenosine and enzymatic evaluation of derivatives of the benzopurines. *J. Am. Chem. Soc. 98*, 3987-3994.

(288) Moder, K. P., and Leonard, N. J. (1982) Defined dimensional alterations in enzyme substrates - synthesis and enzymatic evaluation of some *lin*-naphthopurines. *J. Am. Chem. Soc. 104*, 2613-2624.

(289) Beedham, C., Bruce, S. E., Critchley, D. J., and Rance, D. J. (1990) 1-substituted phthalazines as probes of the substrate-binding site of mammalian molybdenum hydroxylases. *Biochem. Pharmacol. 39*, 1213-1221.

(290) Rashidi, M. R., Smith, J. A., Clarke, S. E., and Beedham, C. (1997) In vitro oxidation of famciclovir and 6-deoxypenciclovir by aldehyde oxidase from human, guinea pig, rabbit, and rat liver. *Drug Metab. Dispos. 25*, 805-813.

(291) Stubley, C., Stell, J. G., and Mathieson, D. W. (1979) The oxidation of azaheterocycles with mammalian liver aldehyde oxidase. *Xenobiotica 9*, 475-484.

(292) Obach, R. S., Huynh, P., Allen, M. C., and Beedham, C. (2004) Human liver aldehyde oxidase: inhibition by 239 drugs. *J. Clin. Pharmacol. 44*, 7-19.

(293) Beedham, C. (1987) Molybdenum hydroxylases: biological distribution and substrate-inhibitor specificity. *Prog. Med. Chem. 24*, 85-127.

(294) Rindgen, D., Lee, S. H., Nakajima, M., and Blair, I. A. (2000) Formation of a substituted 1,N^6-etheno-2'-deoxyadenosine adduct by lipid hydroperoxide-mediated generation of 4-oxo-2-nonenal. *Chem. Res. Toxicol. 13*, 846-852.

(295) Kawashima, K., Hosoi, K., Naruke, T., Shiba, T., Kitamura, M., and Watabe, T. (1999) Aldehyde oxidase-dependent marked species difference in hepatic metabolism of the sedative-hypnotic, zaleplon, between monkeys and rats. *Drug Metab. Dispos. 27*, 422-428.

(296) Clarke, S. E., Harrell, A. W., and Chenery, R. J. (1995) Role of aldehyde oxidase in the in vitro conversion of famciclovir to penciclovir in human liver. *Drug Metab. Dispos. 23*, 251-254.

(297) Kitamura, S., Sugihara, K., and Ohta, S. (2006) Drug-metabolizing ability of molybdenum hydroxylases. *Drug Metab. Pharmacokinet. 21*, 83-98.

(298) Holt, S., Yen, T. Y., Sangaiah, R., and Swenberg, J. A. (1998) Detection of 1,N^6-ethenoadenine in rat urine after chloroethylene oxide exposure. *Carcinogenesis 19*, 1763-1769.

(299) Chen, H. J., and Chiu, W. L. (2005) Association between cigarette smoking and urinary excretion of 1,N^2-ethenoguanine measured by isotope dilution lIquid chromatography-electrospray ionization/tandem mass spectrometry. *Chem. Res. Toxicol. 18*, 1593-1599.